In vitro and *in vivo* characterization of *Neodiprion abietis* (Hymenoptera: Diprionidae) nucleopolyhedrovirus infection and pathology

by

Beatrixe H. Whittome
B. Sc., University of Victoria, 1996

A Dissertation Submitted in Partial Fulfillment
of the Requirements for the Degree of

DOCTORATE OF PHILOSOPHY

in the Faculty of Science/Department of Biology

In vitro and *in vivo* characterization of *Neodiprion abietis* (Hymenoptera: Diprionidae) nucleopolyhedrovirus infection and pathology

by

Beatrixe H. Whittome
B. Sc., University of Victoria, 1996

Supervisory Committee

Dr. David B. Levin, (Department of Biology)
Supervisor

Dr. Francis Y. M. Choy, (Department of Biology)
Departmental Member

Dr. Richard A. Ring (Department of Biology)
Departmental Member

Dr. Caren C. Helbing (Department of Biochemistry)
Outside Member

Dr. B. Andrew Keddie (Biological Sciences, University of Alberta, Edmonton, Canada)
External Examiner

Supervisory Committee

Dr. David B. Levin, (Department of Biology)
Supervisor

Dr. Francis Y. M. Choy, (Department of Biology)
Departmental Member

Dr. Richard A. Ring (Department of Biology)
Departmental Member

Dr. Caren C. Helbing (Department of Biochemistry)
Outside Member

Dr. B. Andrew Keddie (Biological Sciences, University of Alberta, Edmonton, Canada)
External Examiner

Abstract

This work describes the pathology of the baculovirus native to the balsam fir sawfly, *Neodiprion abietis* nucleopolyhedrovirus (NeabNPV), both *in vitro* and *in vivo*. *In vitro* techniques were initially established through the characterization of *Lambdina fiscellaria lugubrosa* NPV (LafiNPV-W) in *Malacosoma disstria* (forest tent caterpillar) and *Choristoneura fumiferana* (eastern spruce budworm) tissue cultures. The results showed that host cell selection is important for the accurate characterization of viral pathology *M. disstria* cells infected by LafiNPV-W supported a biased production of extracellular viral progeny and aberrant LafiNPV-W occlusion bodies. *C. fumiferana* cells, on the other hand, supported production of both the extracellular and occluded phenotypes. The pathology of NeabNPV was studied *in vitro* using the *C. fumiferana* cell line and three cell lines derived from the closely related red-headed pine sawfly, *N. lecontei*. All three sawfly cell lines were non-permissive to NeabNPV, while *C. fumiferana* was semipermissive and enabled preliminary characterization of early pathology, including

early viral gene transcription. Due to only partial success in characterizing NeabNPV infection *in vitro*, pathology was examined within the native larval host, *N. abietis*. The first step in characterizing NeabNPV infection *in vivo* was to define the morphology and ultrastructure of the gut of uninfected *N. abietis* larvae. The sawfly alimentary canal consisted of cuticle lined foregut and hindgut, which adjoined to an elongated midgut. The epithelial tissue of the midgut was composed of regenerative and digestive columnar cells; the latter possessed a complex ultrastructure that reflexed the cells function in nutrient absorption and digestive enzyme secretion. NeabNPV pathology was only detected in the midgut epithelial cells. A time course of NeabNPV infection enabled the identification of several key cytopathic effects and the correlation of gene expression with specific phases of viral infection. These analyses revealed both differences and similarities between the process of infection and pathology induced by NeabNPV and lepidopteran NPVs and may serve as a different model for baculovirus infection of non-lepidopteran.

Supervisor: Dr. David B. Levin, (Faculty of Science/Department of Biology)

Table of Contents

Supervisory Committee ii
Abstract iii
Table of Contents v
List of Abbreviations viii
List of Abbreviations in Figures x
List of Tables xi
List of Figures xii
Acknowledgments xv
Dedication xvi
Chapter 1 Literature Overview 1
1.1 General Introduction 1
1.2 Taxonomy of Baculoviruses 2
1.3 Historical Perspective 5
1.4 Molecular Biology of Baculoviruses 7
1.5 Host Range and Specificity 12
1.6 *Lambdina fiscellaria lugubrosa* nucleopolyhedrovirus (LafiNPV-W) 12
1.7 *Neodiprion abietis* nucleopolyhedrovirus (NeabNPV) 14
1.8 Insect Gut Morphology 15
1.9 Dissertation Overview 20
Chapter 2 *In vitro* propagation of *Lambdina fiscellaria lugubrosa* nucleopolyhedrovirus in two heterologous host cell lines 23
2.1 Abstract 23
2.2 Introduction 24
2.3 Materials and Methods 26
2.3.1 Virus Stocks 26
2.3.2 DNA Extraction of LafiNPV-W 27
2.3.3 Transfection LafiNPV-W into Md108 cells 28
2.3.4 Passage of Infectious Viral Media 29
2.3.5 Confirmation of Viral Infection 29
2.3.6 PCR Confirmation of Viral DNA 30
2.3.7 Titration of the LafiNPV-W Stock by an End-Point Dilution Method 31

2.3.8 Replication Kinetics of LafiNPV-W and Host Specificity 31
2.3.9 Epifluorescent Characterization of Actin and Nuclear Structure 33
2.3.10 Bioassay of LafiNPV-W in *L. f. somniaria* Larvae 34
2.4 Results 36
2.5 Discussion 51
Chapter 3 *In vitro* propagation and pathogenicity of *N. abietis* nucleopolyhedrovirus in heterologous insect cell lines 56
3.1 Abstract 56
3.2 Introduction 56
3.3 Materials and Methods 59
3.3.1 Virus Stocks: 59
3.3.2 Culturing of the Test Cell Lines: 60
3.3.3 DNA Extraction of NeabNPV: 60
3.3.4 Transfection of NeabNPV into Insect Cells 61
3.3.5 Passage of Infectious Viral Media 62
3.3.6 Confirmation of Viral Infection 62
3.3.7 Epifluorescent Characterization of Actin and Nuclear Structure 65
3.3.8 Titration of NeabNPV Stock by an End-Point Dilution Method 65
3.3.9 Replication Kinetics of LafiNPV-W and Host Specificity 65
3.3.10 RNA Reverse Transcription PCR NeabNPV-infected Cf70 Cells 66
3.4 Results 67
3.5 Discussion 82
Chapter 4 Characterization of the morphology of the *N. abietis* larval gut 88
4.1 Abstract 88
4.2 Introduction 89
4.3 Materials and Methods 94
4.3.1 Larval collection 94
4.3.2 Histological Preparation 95
4.3.3 Light and Transmission Electron Microscopy 96
4.3.4 PCR Amplification, DGGE, and Sequencing of Bacterial *16S* gene ... 96
4.4 Results 99
4.4.1 Overall gut organization 99
4.4.2 The Foregut 101

4.4.3 The Ventricular Caeca 110
4.4.4 The Midgut 110
4.4.5 The Hindgut 123
4.4.6 Gut Microbiota 128
4.5 Discussion 133
Chapter 5 Characterization of the *N. abietis* nucleopolyhedrovirus pathology in the alimentary canal of the native larval host, *N. abietis* 142
5.1 Abstract 142
5.2 Introduction 142
5.3 Materials and Methods 145
5.3.1 Virus Stock 145
5.3.2 Larval infection 145
5.3.3 Determination of Cytopathology 146
5.4 Results 147
5.5 Discussion 155
Chapter 6 Analysis of temporally important transcripts and proteins defining transitional stages in the *N. abietis* nucleopolyhedrovirus life-cycle 165
6.1 Abstract 165
6.2 Introduction 166
6.3 Materials and Methods 170
6.3.1 Virus Stock 170
6.3.2 Larval infection 170
6.3.3 Viral RNA and Protein Isolation 171
6.3.4 RNA Reverse Transcription PCR 172
6.3.5 SDS-PAGE and Western Blot Analysis of GP41 and POLH 172
6.4 Results 174
6.5 Discussion 174
Chapter 7 Summary and Conclusions 183
7.1 Revisiting hymenopteran NPV Pathology 183
7.2 Implications of NeabNPV Pathogenesis on Biocontrol 186
Bibliography 188

List of Abbreviations

AcMNPV	*Autographa californica* multinucleocapsid nucleopolyhedrovirus
ARIF	actin rearrangement inducing factor
bp	base pairs
BV	budded virus
Cf70	*Choristoneura fumiferana* cell line
Cry proteins	delta-endotoxins produced by *Bacillus thuringiensis*
DAPI	4',6-Diamidino-2-phenylindole or Bis-benzimide
DBP	DNA binding protein
ddH_2O	water
DGGE	denaturing gradient gel electrophoresis
DNA	deoxyribonucleic acid
DNAPOL	DNA polymerase
EM	electron microscopy
ER	endoplasmic reticulum
FBS	fetal bovine serum
G-actin	monomeric actin
GV	Granulosis virus
hpi	hours post inoculation
HRF	host range factor
HRP	horse radish peroxidase
kb	kilobase pairs
LafiNPV-E	*Lambdina fiscellaria fiscellaria* nucleopolyhedrosis virus
LafiNPV-O	*Lambdina fiscellaria somniaria* nucleopolyhedrovirus
LafiNPV-W	*Lambdina fiscellaria lugubrosa* nucleopolyhedrovirus
LD_{50}	lethal dose causing 50% mortality
LEF	late expression factor
Md108	*Malacosoma disstra* cell line
MNPV	multiply enveloped or multinucleocapsid nucleopolyhedrovirus
MOI	multiplicity of infection
NCBI	National Center for Biotechnology Information
NeabNPV	*Neodiprion abietis* nucleopolyhedrovirus
NeleNPV	*Neodiprion lecontei* nucleopolyhedrovirus
NL18	*Neodiprion lecontei* cell line
non-hr	non-homologous repeat
NPV	nucleopolyhedrovirus
OB	occlusion bodies (in reference to NPV PIBs and GV granules)

ODV	occlusion derived virion
ORF	open reading frame
P143	viral helicases
PBS	phosphate buffered saline
PBST	phosphate buffered saline with tween
PCNA	proliferating cell nuclear antigen
PCR	polymerase chain reaction
pfu	plaque forming units
PIB	polyhedrin inclusion body
PMRA	Pest Management Regulatory Agency
POLH	polyhedrin, matrix protein
qPCR	quantitative real time polymerase chain reaction
rDNA	ribosomal deoxyribonucleic acid
RDP II	Ribosomal Database Project II
rER	rough endoplasmic reticulum
RNA	ribonucleic acid
rRNA	ribosomal ribonucleic acid
RT (PCR)	reverse transcription (polymerase chain reaction)
SD	standard deviation
SDS	sodium dodecyl sulfate
SDS-PAGE	sodium dodecyl sulfate polyacrylamide gel electrophoresis
Sf9	*Spodoptera frugiperda* cell line
SNPV	singly enveloped or single nucleocapsid nucleopolyhedrovirus
SPSS	statistical package for the social sciences
TBS	tris buffered saline
TBST	tris buffered saline with tween
TBSTM	tris buffered saline with tween and skim milk powder
TEM	transmission electron microscopy
Tn5B1-4	*Trichoplusia ni* cell line
V-CATH	viral cathepsin-like protease
vlf	very late factor
WHL	western hemlock looper

List of Abbreviations in Figures

Arrows	basal cytoplasmic membrane
Arrow heads	mitochondria
B	bacteria
BL	basal lamina
bv	budded virus
C	cytoplasm
C	cuticle
Clx	calyx
CM	circular muscle
E	de novo envelopes
E	epithelium
ec	empty capsids
ER	endoplasmic reticulum
H	hemocoel tissue
L	gut lumen
LCM	lateral cytoplasmic membrane
LM	longitudinal muscle
mnc	multinucleocapsids
MV	microvilli
Mx	virogenic stromal matrix
N	nucleus
nc	nucleocapsids
nm	nuclear membrane
nu	nucleoli
P	polyhedra
R	regenerative cells
rz	ring zone
S	secretory vesicle
T	Tracheoles
V	virion
V	vesicle
V	ventricular caeca
ve	virion envelope
VS	virogenic stroma

List of Tables

Table 2-1. Observed traits of mock and LafiNPV-W infected *M. disstria* and *C. fumiferana* cells. 40

Table 2-2. Cox proportional hazard analysis of mock-infected and LafiNPV-W infected *Lambdina fiscellaria somniaria* larvae. 52

Table 3-1. Primers used in reverse transcription PCR of RNA extracted from NeabNPV-infected Cf70 cells. 68

Table 3-2. Observed traits of mock, NeabNPV, and LafiNPV-W infected *N. lecontei* and *C. fumiferana* cells. 77

Table 4-1. NCBI Blast-n results and Ribosomal Database Project II comparison values for *16S* RNA gene sequences. 129

Table 5-1. Determination of the reduction of microvilli and nuclear hypertrophy based on mean values of the proportional surface area of the cytopathic effect. 149

Table 5-2. Analysis of significant of cytopathic effects observed over a 72 hour period of NeabNPV infection of *N. abietis* larvae. 151

List of Figures

Figure 2-1. Light micrographs of mock and LafiNPV-W infected *Choristoneura fumiferana* and *Malacosoma disstria* cell cultures. 37

Figure 2-2. Epifluorescent micrographs of mock and LafiNPV-W infected *C. fumiferana* and *M. disstria* cells at 24 hours post-inoculation. 38

Figure 2-3. Agarose gel electrophoresis of LafiNPV-W *polh* PCR products. 41

Figure 2-4. Replication kinetics of LafiNPV-W infection in various host cell lines over a 72 hour period. 43

Figure 2-5. Electron micrographs of LafiNPV infected Md108 cells. 45

Figure 2-6. Electron micrographs of LafiNPV infected Cf70 cells. 47

Figure 2-7. Kaplan-Meyer Survival Curve (A) and probit analysis of dose-mortality (B) of mock-infected and LafiNPV-W infected *L. f. somniaria* larvae. 50

Figure 3-1. Light micrographs of NL18 cultures, after which transfection or infection with NeabNPV. 69

Figure 3-2. Light micrographs of Cf70 cultures, after transfection or infection with NeabNPV. 70

Figure 3-3. Gel electrophoresis of PCR products of the NeabNPV polyhedrin (*polh*) gene amplified from NL18 (A) and Cf70 (B) cultures. 72

Figure 3-4. Southern blot analysis of NeabNPV infected Cf70 culture. 73

Figure 3-5. Epifluorescent micrographs of mock, NeabNPV, and LafiNPV-W infected *N. lecontei* cells at 24 hours post-inoculation. 75

Figure 3-6. Epifluorescent micrographs of mock, NeabNPV, and LafiNPV-W infected *C. fumiferana* cells at 24 hours post-inoculation. 76

Figure 3-7. Replication kinetics of NeabNPV in Cf70 cells. 79

Figure 3-8. RT-PCR amplicons of host (*28S*), immediate early (*Neab24* and *Neab52*), and early NeabNPV (*dnapol*, *lef-1*, and *le-f2*) genes transcribed in Cf70 cells. 81

Figure 4-1. Schematic of *Neodiprion abietis* larval gut 100

Figure 4-2. Light (A and B) and transmission electron (C) micrographs of the crop epithelia and surrounding connective tissue of *N. abietis* larvae. 103

Figure 4-3. Light (A and B) and transmission electron (C) micrographs of the valve-like structure and surrounding connective tissue of *N. abietis* larvae..... 105

Figure 4-4. Light (A and B) and transmission electron (C and D) micrographs of the proventriculus and the surrounding developed musculature of *N. abietis* larvae. 109

Figure 4-5. Light (A-C) and transmission electron (D) micrographs of the ventricular caeca and surrounding connective tissue of *N. abietis* larvae..... 113

Figure 4-6. Light (A-F) micrographs of the midgut epithelia and the surrounding connective tissue of *N. abietis* larvae..... 117

Figure 4-7. Transmission electron (A-F) micrographs of the midgut epithelia of *N. abietis* larvae..... 121

Figure 4-8. Light (A and B) micrographs of the pylorus-like structure and surrounding connective tissue of *N. abietis* larvae..... 125

Figure 4-9. Light (A-B) and transmission electron (C) micrographs of the ileum and the surrounding connective tissue of *N. abietis* larvae. 127

Figure 4-10. Phylogenetic analysis of the *16S* rRNA gene from bacteria isolated from insect guts..... 132

Figure 5-1. Reduction of midgut epithelial cell microvillar surface area and increase in size of nuclei during NeabNPV infection of *N. abietis* larvae..... 150

Figure 5-2. Accumulation of cytopathic effects exhibited in midgut epithelial cells infected with NeabNPV. 152

Figure 5-3. Light micrographs of *N. abietis* midgut epithelia infected with NeabNPV at 2 (A) and 5 (B) hpi..... 153

Figure 5-4. Light (A) and electron transmission (B) micrographs of *N. abietis* midgut epithelia infected with NeabNPV at 8 hpi. 154

Figure 5-5. Light (A) and electron transmission (B) micrographs of *N. abietis* midgut epithelia infected with NeabNPV at 12 hpi. 156

Figure 5-6. Light (A) and electron transmission (B) micrographs of *N. abietis* midgut epithelia infected with NeabNPV at 24 hpi. 157

Figure 5-7. Light (A) and electron transmission (B) micrographs of *N. abietis* midgut epithelia infected with NeabNPV at 48 hpi. 158

Figure 5-8. Light (A) and electron transmission (B) micrographs of *N. abietis* midgut epithelia infected with NeabNPV at 72 hpi. 159

Figure 6-1. Quantification of NeabNPV DNA copy number in mid-guts of NeabNPV-infected *N. abietis* larvae..... 168

Figure 6-2. RT-PCR of selected NeabNPV genes with RNA extracted from mid-guts of NeabNPV-infected N. abietis larvae..... 169

Figure 6-3. RT-PCR analysis of *vlf-1* and *polh* gene expression in NeabNPV-infected *N. abietis* larvae, harvested at various time points post inoculation..... 175

Figure 6-4. Western blot analysis of NeabNPV GP41 (A) and POLH (B & C) expression. 177

Acknowledgments

The support and help of many individuals are gratefully acknowledged. Firstly, I thank Dr. David Levin for providing the opportunity to conduct this research, giving sage advice and lending his constant optimism and support. I am grateful for the instruction, friendship and support that I have received from members of the Center for Biomedical Research (formerly, the Center for Environmental Health), and in particular my peers in the Levin lab: Jiahne Huang, Sarah Barber, Giovana Valadares de Amorim, Roberto Alberto, Simon Duffy, Christina Thorne, David Harrison, Carlo Carere, Dan Sanderson, and Elisa Becker. Valued assistance was provided by John Fraser (LafiNPV transfection), Mandy Miller (LafiNPV replication kinetics), and Emilie Bosquet (NeabNPV light microscope imaging). I am particularly grateful for the mentoring and advice giving by: Dr. Chaman Singla and Brent Gowen (electron microscopy), Dr. Robert Burke (confocal and epifluorescent microscopy), Tom Gore and Heather Down (advanced imaging), Dr. Louise Page (histology), Dr. Richard Ring (entomological anatomy), Dr. Terry Pearson (immunology and proteins), and Dr. Imre Otvos (viral bioassays).

I thank Dr. Christopher J. Lucarotti, Grant White, and their Canadian Forest Services staff for aid with larval collection and their hospitality in Newfoundland. I also thank Dr. Lucarotti for his advice of NeabNPV infection and coordination of the NeabNPV project. I am grateful for the insect cells lines and culturing advice provided by Guido Caputo and Barb Cook (Canadian Forest Service, Sault St. Marie), as well as the *Lambdina* larvae provided by Dr. Imre Otvos and Nicholas Condor (Canadian Forest Sevice, Victoria). I would like to extend a special thank you to Dr. Delano James and David Lye (Canadian Food Inspection Agency) and Dr. Terry Holmes (Canadian Forest Services) for use of their electron microscopes during the shutdown at UVic.

I would like to extend my appreciation to my supervisory and examining committee for their advice and time. I am gratified by the administrative assistance provided by Eleanore Floyd (Graduate Student Secretary), as well as Pauline Tymchuk and Valentina Sutcliffe. Funding was provided by the Canadian Forest Service (CFS), National Science and Engineering Research Council (NSERC), and the BioControl Network of Canada.

Dedication

I would like to dedicate this work to my husband, Kristopher R. M. Waygood, for all his loving support, and our family.

Chapter 1 Literature Overview

1.1 General Introduction

Viruses are submicroscopic obligate intracellular parasites of the prokaryotic or eukaryotic cells that they infect. Typically, viruses are composed of a proteinaceous shell that protects their fragile nucleic acid genomes and may be wrapped in membranous envelopes (Cann, 1997). Paramount to the success and spread of viruses are the use of the genes encoded within their genetic material and their use of the host's metabolic and translational machinery. Viral genomes are composed of either DNA or RNA, which may be either single or double stranded. The largest viral genomes are double-stranded DNA molecules, encoding all the necessary genes that allow the viruses to overcome their host's defences and replicate.

Several families of viruses contain members that infect either arthropods or vertebrates: Reoviridae, Rhabdoviridae, Poxviridae, Iridoviridae, Parvoviridae, and Picornaviridae. Only viruses of the families Ascoviridiae, Baculoviridae, and Nimoviridae are restricted to arthropods. Mounting evidence suggests that baculoviruses are restricted to dipteran, lepidopteran and hymenopteran hosts (Herniou *et al.*, 2001; Herniou *et al.*, 2003; Lauzon *et al.*, 2004). Earlier literature, however, reported that baculoviruses were infectious to coleopteran, thysanuran, and trichopteran insects, as well as some crustaceans (Federici, 1997). Traditionally, baculoviruses are named after the host species from which they are derived, followed by the viral genera. Although greater than 600 species of insects are susceptible hosts to baculovirus infections, the exact number of virus species is unknown since some viruses are able to infect multiple insect species.

Two genera of baculoviruses exist: the Nucleopolyhedroviruses (NPV) and the Granuloviruses (GV). Several common processes occur in their pathogenicity, but key events define the two genera. Nucleocapsids of both GVs and NPVs are actively transported to the nucleus along actin fibres (Charlton & Volkman, 1991). The nucleocapsids of GVs align vertically at nuclear pores, and the genome is injected into the nucleoplasm (Summers, 1971). Nucleocapsids of NPVs, in contrast, are translocated into the nucleus, wherein they are uncoated. Both GVs and NPVs induce cytopathic effects that are characterized by an enlargement of the nucleoli and hypertrophy of the nucleus. NPVs replicate within the virogenic stroma that forms in the nucleus, while GVs replicate in the virogenic stroma that develops in the mixture of the cytoplasm and nucleoplasm, upon the disruption of the nuclear membrane.

1.2 Taxonomy of Baculoviruses

Viruses of the Baculoviridae family have circular supercoiled double-stranded DNA genomes that range in size from 81.8 kilobases (kb), such as the NPV derived from *Neodiprion lecontei* (Lauzon *et al.*, 2004), to 178.8 kb, as found in the *Xestia c-nigrum* GV (Hayakawa *et al.*, 1999). Previously the Baculoviridae were divided into two subfamiles: Eubaculovirinae and Nudibaculovirinae. The family is currently broken into two genera, which now excludes the non-occluded viruses. As mentioned above, baculoviruses are named after the host species from which they were first isolated, followed by the viral genus (NPV or GV). An abbreviation system, taking the first two letters from each of the host's genus and species (4 letters total) and followed by the viral genus, is also used to define baculovirus species.

Thirty-three baculovirus genomes have been completely sequenced and are available through the GenBank database of the National Center for Biotechnology Information (NCBI, U.S. National Library of Medicine), including two unpublished direct submissions: GenBank Accession numbers NC008035 and NC007767. Baculoviruses infecting three orders of insects (Lepidoptera, Hymenoptera, and Diptera) are represented. Of the 33 sequences genomes, there are 21 lepidopteran NPVs, 8 lepidopteran GVs, 3 hymenopteran NPVs, and a dipteran NPV (Escasa *et al.*, 2006; Jehle *et al.*, 2006). Complete genome phylogeny, in conjunction with gene content and gene order phylogenies, indicate that there are three distinct clades of lepidopteran-derived baculoviruses; GV, Group I-NPV, and Group II-NPV (Herniou *et al.*, 2001; Herniou *et al.*, 2003). The dipteran and hymenopteran baculoviruses are representative of more ancestral viruses and belong within new taxonomical groupings (Duffy *et al.*, 2006; Jehle *et al.*, 2006). A new proposal for reclassification suggests that the current taxa of baculoviruses be rearranged into 4 genera. This system would group the baculoviruses based on host origin as opposed to just morphological traits (Jehle *et al.*, 2006). These genera would consist of the lepidopteran NPVs (Alphabaculovirus), lepidopteran GVs (Betabaculovirus), the hymenopteran NPVs (Gammabaculovirus) and the dipteran NPV (Deltabaculovirus).

Granuloviruses are distinguished from NPVs based on the previously mentioned differences in their cytopathologies, as well as the composition and structure of their occlusion bodies. Granules tend to be smaller than the analogous polyhedra , ranging in size from 0.13-0.5 μm in diameter and contain a single nucleocapsid per granule (Ackermann & Smirnoff, 1983); while NPV polyhedra are multiply embedded and range

in size from 0.15-15 μm (Jehle *et al.*, 2006). Three types of GVs currently exist and are classified based on different tissue trophisms (Federici, 1997). Type 1 GVs infect midgut epithelium and fat body only. Type 2 GVs are capable of systemic infection and parallel the pathology exhibited by singly enveloped nucleopolyhedroviruses (SNPV). The third type of GV exhibits pathology similar to the hymenopteran derived NPVs, with tissue trophism being limited to the midgut epithelia.

Group I and II NPVs are distinguished by the type of peplomer proteins on the budded virus (BV) or extracellular phenotype of progeny virions (Federici, 1997). Group I NPVs contain GP64 proteins within the envelope of the BV and are represented by such viruses as the prototype *Autographa californica* multinucleocapsid nucleopolyhedrovirus (AcMNPV). Group II NPVs express Fusion protein (f-protein), which allows the entry of extracellular progeny into secondary tissues, and are represented by such NPVs as *Lymantria dispar* MNPV (Lung *et al.*, 2002; Pearson *et al.*, 2000). Both groups of NPVs contain species that exhibit either the singly enveloped (SNPV) or multiply enveloped (MNPV) phenotype of occluded virions, each of which has evolved specialized strategies for infection (Washburn *et al.*, 2003). SNPVs initiate primary infection rapidly and require the production of progeny virions to cause systemic infection. MNPVs exhibit an alternative strategy, wherein they initiate infection of primary tissues later than SNPVs and repackage nucleocapsids from ODVs. The repacking of nucleocapsids requires the expression of structural proteins of the BV, but not the completion of viral DNA synthesis (Washburn *et al.*, 2003). The occlusion process also differs between SNPVs and MNPVs. Polyhedra of the SNPV variant are small, ranging in size from 0.15-2 μm, and contain numerous singly enveloped capsids. The MNPV polyhedra are larger (0.5-5

μm) and contain few virions, although they have approximately an equal number of nucleocapsids (Ackermann & Smirnoff, 1983).

1.3 Historical Perspective

In 1527, the Italian poet and bishop, Marco Girolano Vida, gave the first European description of baculovirus infection (Benz, 1986); although the disease was probably known ever since the silkworm was brought to Europe from China. True scientific research on baculovirus diseases was limited until techniques and instruments had advanced sufficiently to allow for virus detection. In the middle of the 19th century, the first description of polyhedra, visible under the compound microscope, was given as strongly refractive crystal-like corpuscles within cells of silkworms (Benz, 1986). It was not until the late 1800s that J. Bolle determined that polyhedra dissociate in strong acids and alkaline solution, while they are insoluble in water, glycerol and ethanol. Bolle continued to advance the knowledge of baculoviruses when, in 1906, he showed that polyhedra fed to silkworms cause disease. At the same time, von Prowazek discovered the supernatant of hemolymph was also infective. Unfortunately, von Prowazek's results were discounted and it was not until he had shown that the virus was filterable through a Berkefeld candle that researchers started to look for the causal agent of infection other than polyhedra (Benz, 1986). The two virion phenotypes were not linked until much later.

Support for the filterable-virus theory came from Paillot (1924), when he reported that "granules", likely naked virus particles, could be visualized by dark-field microscopy. Paillot observed that these particles were less than 0.1μm in diameter, had vigorous Brownian motion, and formed a shining ring-like structure within the nucleus. Using

modern dark-field and phase contrast microscopes, these same characteristics of nucleocapsids are observed (Benz, 1963). Further support came from the successful multiplication of baculovirus in tissue culture by Trager (1935). Using culturing techniques, virus multiplication and the formation of polyhedra could be visualized and were shown to be progressive stages of the baculovirus lifecycle.

After several years of research on the dissociation of polyhedra in alkaline solution, Gratia *et al.* (1945) performed micro-chemical analysis and discovered that no RNA was present in polyhedra, but DNA represented 0.84% of the organic material. Oswald Avery (1944) had already shown that DNA carried genetic information. This knowledge, combined with the analysis of Gratia *et al.* (1945), allowed Bergold (1947) to classify the causal agent of infection as a virus. Over several years, Bergold used electron microscopy to elucidate and develop a theory for the lifecycle of baculoviruses. Concurrent with Bergold's studies, Hughes (1953) investigated infected silkworm tissues by electron microscopy and observed that virions initially formed in the virogenic stroma, an electron dense mass centered in the nucleus, and were later enveloped before being surrounded by the polyhedrin matrix. Bergold's lifecycle theory prompted research in several areas of baculovirology, including: *in vivo* and *in vitro* replication studies, histopathology, molecular characterization, and host specificity (Benz, 1986).

Understanding of the biology of baculoviruses has advanced greatly over the past three decades due to the use of molecular techniques and modern equipment. Restriction endonuclease patterns allowed for the initial comparison of viral genomes and approximation of their size (Maruniak *et al.*, 1984; McIntosh & Ignoffo, 1986; Smith & Summers, 1978), while the complete sequencing of a baculovirus genomes, first

published nearly 20 years later (Ayres *et al.*, 1994), gave insights into gene content and baculovirus evolution (Herniou *et al.*, 2001; Herniou *et al.*, 2003). Also, studies of viral gene expression, common throughout the late 1970s to present time, demonstrate the regulated expression of viral gene products through a temporal cascade and the specialized tissue trophism of various taxonomic baculovirus groups (Herniou *et al.*, 2004; Washburn *et al.*, 2003).

1.4 Molecular Biology of Baculoviruses

Sequence analysis, molecular characterization, and studies on the pathology of model viruses have led to a basic understanding of their lifecycles. The following descriptions of a lepidopteran baculovirus pathology, AcMNPV, are representative of a model lifecycle, although information obtained from other lepidopteran NPVs has been used to augment studies of AcMNPV.

An NPV infection begins with the ingestion of polyhedra, also known as polyhedrin inclusion bodies (PIBs) or occlusion bodies (OBs), by the larval host. Once in the midgut lumen, the polyhedra dissociate due to the alkaline nature of the insect's gastric fluids, along with the proteolytic enzymes contained therein. The released virions, termed occlusion derived virions (ODVs), migrate through the host's peritrophic membrane and attach to the microvilli of the midgut epithelia. There are two generally accepted theories about the mechanisms used by virions to bypass the peritrophic membrane. These mechanisms are dependent on the morphology of the individual insect species. Insects with fibrous and porous peritrophic membranes, such as *Orgyia pseudotsugata*, allow particles smaller than 800 nm to pass through their membrane (Granados & Williams, 1986; Williams & Faulkner, 1997). Baculovirus virions are generally 40-50 nm in

diameter and 250-400 nm in length (Federici, 1997); therefore virions theoretically encounter little inhibition to their migration through the peritrophic membrane of such insects. Other insects, such as *Trichoplusia ni*, have multi-layered and channelled peritrophic membranes, which inhibit virions from passing through easily to the midgut epithelia (Adang & Spence, 1981; Federici, 1997). Viruses infecting insects with this type of membrane contain specialized enzymes, enhancins, within their polyhedrin matrix (Derksen & Granados, 1988). When the polyhedra dissociate, these enzymes are released and proteolytically digest the mucin component of the peritrophic membrane. The holes created within the membrane allow the virions to pass through and gain access to the epithelium beneath. Studies by Washburn *et al.* (1995) suggested that the peritrophic membrane may not be an obstacle for some lepidopteran derived NPVs since the membrane is shed during the molting process, which permits virions to interact with the midgut epithelium directly.

Entry into the cell is believed to occur by direct fusion of the virion envelope and the plasma membrane of the midgut epithelial cells (Granados & Lawler, 1981; Summers, 1971). Although binding studies indicate the presence of cell receptors and their corresponding viral ligand (Granados & Lawler, 1981), neither has been identified. Virions may either enter into the microvilli of the epithelial cell or migrate through the brush-border and enter at the apical surface (Williams & Faulkner, 1997). After entry, actin molecules transport the nucleocapsid into the nucleus (Charlton & Volkman, 1991, 1993), where they are uncoated upon translocation through the nuclear pores. The viral genome replicates within the nucleus and two distinct forms of the virus progeny are produced: a budded or non-occluded form and the occluded form.

Budded virions spread the infection to neighbouring tissues. The nucleocapsids egress through the nuclear membrane, with the aid of GP41 (Olszewski & Miller, 1997), thereby acquiring an envelope and migrate to the plasmalemma. Before the virions reach the plasma membrane, the nuclear envelope is lost. Little information is available about this process. The virions bud through the plasma membrane, obtaining an envelope with the peplomers that allow for fusion into new cells (Blissard & Rohrmann, 1990; Blissard & Wenz, 1992). Transmission electron micrographs of the budded virions show a single envelope, with peplomers that give the virus polarity, and demonstrate the lack of any nuclear membrane.

The tissues in which the occluded virus are produced seem to be dependent on the host organism. Most NPV-infected lepidopteran larvae lack polyhedra in their midgut epithelia, but show abundant production thereof in secondarily infected tissues (Williams & Faulkner, 1997). In other lepidopterans, polyhedra production in the primary infected tissue is rare and sparse. Baculoviruses have likely evolved a strategy of rapid systemic spread since epithelial cells are sloughed off and replaced during ecdysis (Flipsen *et al.*, 1995) and by host defence mechanisms. Baculoviruses that infect other families of insects show a distinctly different pathology, *in vivo*. The *Culex nigripalpus* nucleopolyhedrovirus produces extensive pathology in the midgut epithelial cells, particularly of the gastric caeca and posterior stomach (Moser *et al.*, 2001). These researchers found no other tissue infection indicative of virus spread.

All the events that occur within the nucleus occur in a precisely regulated, temporal cascade: immediate early, early, late, and very late. The first genes expressed are the immediate early proteins and their mRNA is detectable within 30 minutes after

inoculation, *in vitro* (Carstens *et al.*, 2002; Kovacs *et al.*, 1991). However, *in vivo*, ODVs may still be found in the cytoplasm at 2 hours post inoculation (Granados & Williams, 2000), indicating that the timing between *per os* and *in vitro* pathogenesis may differ. The immediate early proteins are transregulators and transcription factors of early and late genes or enzymes, which are necessary for the progression of the infectious cycle. By definition, immediate early genes are transcribed in the absence of any viral gene products or machinery and are dependent on the host RNA polymerase II (Federici, 1997). Early phase gene products include DNA replication enzymes and their expression leads directly to viral DNA synthesis. Other early gene products include the transcriptional machinery used in late gene expression. The late phase commences within 6 hours post inoculation (hpi) and leads to the synthesis of proteins involved in the packaging of viral DNA progeny and the production of budded virus (Granados & Williams, 1986). The very late phase is characterized by the expression of structural proteins involved in virion occlusion and enzymes, which aid in cell lysis and virus dispersion. Each of these events is dependent on viral gene products of the preceding stage (Lu & Miller, 1995a).

There are eleven key viral proteins which function in the viral DNA replication: DNAPOL, P143, LEF-1, IE-1, LEF-2, LEF-3, P35, IE-2, PE-38, LEF-7 and HCF-1 (Lu *et al.*, 1997a). The first three proteins (DNAPOL, P143, and LEF-1) make up the replisome, while IE-1, LEF-2 and LEF-3 interact with the DNA-replisome complex (Hefferon & Miller, 2002). The remaining proteins are accessory factors that promote replication in a species-specific manner and may contribute to host range (Hefferon, 2003; Lu & Miller, 1996; Todd *et al.*, 1996). The genome is replicated using cis-acting

elements, most commonly in the form of non-homologous repeat (non-hr) origins of replication, although homologous repeat regions have also been shown to act as origins of replication for plasmids, during transient replication assays (Huang & Levin, 2001). Replication continues until 18 hpi when the very late stage of infection commences.

Structural proteins that make up the viral nucleocapsids are expressed in the late stage. These include the major capsids proteins (VP39, P80, and P24), the capsids end protein (PP78/83) and the basic DNA-binding protein (P6.9). Other structural proteins are localized to envelope and depend on the phenotype of the progeny virion. BVs have GP64/fusion protein, while the ODV envelope is composed of E18, E27, E35, and E56 (Blissard, 1996). The envelope proteins bind and interact with the tegument protein, GP41, which localizes between the capsids and the envelope. Not until the very late stage are the structural proteins for the occluded virus produced, along with enzymes that aid in the dispersion of the polyhedra into the environment. The late and very late genes are preferentially expressed during the appropriate stages due to the presence of viral specific promoters that rely on late expression factors (LEFs) and very late expression factors (VLFs).

Some of the most important genes, which allow for host specificity and the completion of the infectious cycle, are the anti-apoptotic genes. The host organisms have evolved, as part of their defence mechanisms, an inducible programmed cell death pathway (apoptosis) that is designed as a protective measure against pathogens or substances that threaten its well being. Viruses, in general, have adapted such that they can overcome their hosts' programmed cell death response and optimize their own propagation. They do this by using proteins that are able to inhibit or delay apoptosis. These viral proteins,

which have been created either by convergent evolution or by the capture of host sequences encoding entire proteins or individual functional domains, interfere with the host response by targeting strategic points in defence pathways (O'Brien, 1998; Roulston *et al.*, 1999). Most often, the apoptotic mechanisms that viruses exploit are inherent in normal cellular regulation.

1.5 Host Range and Specificity

In vivo, baculoviruses are generally very host-specific, capable of infecting either a single species or a few closely related species. *In vitro,* however, baculovirus host range is much broader. The ability of a baculovirus to enter host cells and tissues, replicate, and then release viable viral progeny, defines the host-range of the virus. For most baculoviruses, entry into a cell is limited by the surrounding environment, such as strong acids that denature virions or physical barriers that are impenetrable. In pH neutral, laboratory-cultured systems, baculoviruses have been shown to enter non-permissive insect cells and mammalian cells (Boyce & Bucher, 1996; Carbonell & Miller, 1987), suggesting that the receptor utilized during endocytosis is conserved and common amongst several phyla or that cells may actively uptake the virus particles by mechanisms such as phagocytosis.

1.6 *Lambdina fiscellaria lugubrosa* nucleopolyhedrovirus (LafiNPV-W)

The Western Hemlock Looper (WHL), *Lambdina fiscellaria lugubrosa* (Hulst) (Lepidoptera: Geometridae), is one of the most destructive defoliators of conifers in British Columbia, Canada. WHL is native to North America and is found most commonly along the coast, although infestations also occur in the interior wet belt regions of British Columbia and the north-western United States. The larvae feed

wastefully, beginning at the base of the needles, and usually cut the needles off before completely consuming them (Parfett *et al.*, 1995). New and old foliage, as well as new buds and shoots, are destroyed by larval feeding behaviour, resulting in tree mortality within 1 year. The preferential host of WHL larvae are western hemlock (*Tsuga heterophylla* (Raf.) Sarg.), however, several other host trees are defoliated, including: western red cedar, Douglas fir and several true fir and spruce species (Parfett *et al.*, 1995).

Larvae hatch from eggs in late May/ early June and begin feeding on new foliage. As the larvae mature they disperse throughout the tree, feeding upon foliage of any age. Larvae pupate in August/September within the crevices of bark and under debris. Pupation lasts from 10 to 14 days, thereafter the adults emerge and mate until early October. Females lay their eggs on moss, lichens, and bark, which provided shelter for the overwintering eggs. (Erickson, 1984)

Fourteen distinct WHL outbreak periods have occurred between 1911 and 1994 within British Columbia (Turnquist, 1991). WHL outbreaks commonly last for 2-4 years and are balanced by a 6-10 year period of low population densities. An ongoing infestation has been recorded in Washington state, USA. The epizootic peaked in 2002, with 35,000 acres of severe defoliation, and had mostly subsided in 2005. Along with the recent damage from a bark-beetle outbreak, the direct damage of WHL defoliation has resulted in large areas of tree mortality, which threatens to cripple the surrounding forestry industry (Washington State Department of Natural Resources, 2006, http://www.dnr.wa.gov/htdocs/rp/forhealth/2005highlights/fhwhlinter.html).

Currently, the only registered pest control agents, against WHL, are the chemical insecticides fenitrothion and tebufenozide (National Forestry Database Program). The Cry1B, Cry1C, Cry1D, and Cry1E delta-endotoxin, from *Bacillus thuringiensis* (Bt), have been investigated for their insecticidal activity in larvae of the eastern hemlock looper, *Lambdina fiscellaria fiscellaria*, a closely related looper located in the eastern provinces of Canada . *L. f. fiscellaria* larvae showed no response to the Cry1B but were highly susceptible to Cry1E, while Cry1C and Cry1D toxins had moderate effects on the larvae. Susceptibility *L. f. lugubrosa* larvae to Dipel and Forey formulas of Bt was determined by Koot (1994) and the two subspecies of *L. fiscellaria* showed similar mortality to the Cry1 endotoxins. The limitations of these biological insecticides, particularly their effects on valued non-target species and the increasing resistance in pests, necessitates the development of new control agents such as native baculoviruses.

1.7 *Neodiprion abietis* nucleopolyhedrovirus (NeabNPV)

The Balsam Fir Sawfly (BFS), *Neodiprion abietis* Harris (Hymenoptera: Diprionidae) is a native species of Canada and the United States (Li *et al.*, 2003). *N. abietis* was first documented by Struble (1957), as the White-Fir Sawfly, which he described as being complex of 5 distinct populations from the western and eastern coasts of North America. BFS larvae selectively fed and propagated on western white fir, eastern balsam fir, and eastern black and white spruce. Although some entomologists still group the species as a complex, recent literature focuses on the eastern North American population that defoliates balsam fir (*Abies balsamea* Mill) (Moreau *et al.*, 2005).

N. abietis larvae emerge in early-summer and feed preferentially on foliage that is 1-2 years old. The larvae are gregarious and large populations can be found on branches as

they vigorously and wastefully feed, accumulating biomass until their 5th and 6th instar - for males and females, respectively- after which they pupate. The adults emerge in late summer to mate, after which the females lay their eggs in the current year's foliage, using a "saw-like" ovipositor to make slits in the edge of the needle. The eggs overwinter and the new cycle begins the follow summer.

Outbreak populations of *N. abietis* can damage trees to such a state that they display reduced growth and are very susceptible to infections by secondary pathogens (Li *et al.*, 2003). Outbreaks are common and typically last an average of two to four years before the population collapses by natural means (Piene *et al.*, 2001; Moreau, 2006). In Atlantic Canada, particularly western Newfoundland, an unprecedented outbreak of *N. abietis* has lasted from 1991 to present and threatens valued timber stands that support the local economy. The added threat of migration into a protected national park (Chris Lucarotti, Canadian Forest Services - Atlantic Forestry Center, personal communication) has prompted the control of *N. abietis* populations by a naturally-occurring pathogen, the *N. abietis* nucleopolyhedrovirus (NeabNPV). Along with several collaborators, C. Lucarotti has sought to register the virus under the name Abietiv for biological control purposes.

1.8 Insect Gut Morphology

Most knowledge about the digestive system of hymenopteran insects comes from studies of apocritan larvae and adults (Arab & Caetano, 2001; da Cruz-Landim & Cavalcante, 2003; Davies, 1977; Davies & King, 1977a, b; Terra *et al.*, 1996). A few studies have focused on the endosymbiotic bacteria of various ant species, although detailed gut morphology is lacking. The most comprehensive investigation of sawfly anatomy was performed and review by Maxwell (1955), in which the gut was studied for

the purpose of taxonomic identification and only a macro-morphological description was given. The following description of gut morphology is an accumulation of knowledge of the general insect gut structure.

The largest organ found in many insects is the alimentary canal, or gut. Insect guts are diverse and show modification in both structure and function, such that the processing of food is optimized (Billingsley & Lehane, 1996; Nation, 2002; Wigglesworth, 1972). Insects have adapted to obtain food from many sources, although some are more specialized feeders than others (Arab & Caetano, 2001; Boursaux-Eude & Gross, 2000; Li *et al.*, 2005; Santos *et al.*, 2004; Sauer *et al.*, 2002; Schroder *et al.*, 1996; van Borm *et al.*, 2002a; van Borm *et al.*, 2002b). The generalized scavenger, representing the most primitive feeding behaviour, has evolved into specialized phytophagous or carnivorous feeders. Commonly, solid-food feeders, such as phytophagous insects, have a straight tubular gut, similar in length to their body. Convoluted and elongated guts present difficult obstacles for the passage of solid foods, possibly leading to the co-evolution between food source and gut structure (Billingsley & Lehane, 1996; Nation, 2002; Wigglesworth, 1972). Many insects with straight guts have an abundant food source, such as plants, and are able to feed frequently, voiding partially digested food in their frass without risk of starvation.

Irrespective of insect species and food source, a basic gut, which is divided into three major regions – the foregut, the midgut, and the hindgut – has been retained throughout insect evolution (Wigglesworth, 1972). In solid-food feeders, the initial mechanical breakdown of ingested material occurs at the mandibles in the buccal cavity. The food bolus passes through the pharynx, oesophagus and crop before it is ground by the

muscular proventriculus of the foregut. During development, the foregut arises from the invagination of the ectodermal tissue and differentiates into a circular layer of epithelial cells, which secrete a cuticular lining along their apical end (Chapman, 1985). The lining, composed of both chitin and proteins, varies in thickness and sclerotization with respect to the position within the foregut; the proventriculus is the most heavily sclerotized and consists of a hard exocuticle. The foregut epithelial cells are typically flattened squamous cells, which neither secrete digestive enzymes nor absorb free nutrients.

The midgut is the primary site for the secretion of digestive enzymes and absorption of nutrients. In many insects, the gastric or ventricular caeca define the anterior end of the midgut at the fore-midgut junction, although they may also be located along the length of the midgut in some species (Chapman, 1985). The caeca, especially those at the anterior of the midgut, play an important role in nutrient absorption due the establishment of the endo-ectoperitrophic countercurrent flow of fluid contents within the midgut (Berridge, 1970). In contrast to the epithelia of the foregut, the midgut epithelial cells lack the attached cuticular lining and instead secrete a chitin-protein-mucin matrix, the peritrophic membrane, which encompasses the food bolus and protects the fragile surfaces of cells from abrasive food particles (Chapman, 1985).

The types of cells located in the midgut vary depending on the insect species, and the midgut may be composed of all the cell types or only a subset of them. Four general cell types have been identified: columnar epithelial cells, regenerative cells, endocrine cells, and goblet cells (Billingsley & Lehane, 1996; Nation, 2002; Sehnal & Zitnan, 1996; Wigglesworth, 1972). Columnar cells, the most numerous type in the midgut, are

responsible for the secretion of digestive enzymes and nutrient absorption. These cells have microvilli, also termed a brush-border, on their apical end that aids in the absorption of nutrients from the gut lumen (Nation, 2002). The lateral membranes between cells are relatively straight in most insects and are usually linked by septate and gap junctions at the apical end of the cells, forming an impermeable layer. The basal membrane of columnar cells is highly invaginated, providing a large surface area for the transfer of nutrients to the hemocoel. A basal laminae, composed of fibres and granules embedded in a matrix of connective tissue, acts as an additional support structure for the epithelial cells, as well as a protective barrier to the hemocoel (Chapman, 1985; Nation, 2002). Due to the extensive metabolic functions exhibited by columnar epithelium, an enrichment in the quantity of mitochondria and secretory vesicles is often apparent, as well as an enlargement of the rough endoplasmic reticulum and Golgi apparatus.

Regenerative cells are important for the replacement of worn out and sloughed off midgut cells. Regenerative cells are usually very small and can be found in various numbers and sites of the midgut (Nation, 2002). Dipteran and lepidopteran regenerative cells lie at the base of mature cells, randomly distributed throughout the midgut, while orthopteran and odonatan regenerative cells nest together in small clusters within the basal lamina, along the midgut length. The regenerative cells of coleopteran insects protrude through the muscles layer, at the apex of crypts and caeca. The maturation process from regenerative cell into a differentiated columnar epithelium is gradual, often taking 40-120 hours as seen in Coleoptera (Nation, 2002).

The third midgut cell type, endocrine cells, are characterized by cells that may have dense core granules and cytoplasm that does not retain histological stain well. These

cells may be either of the "open type", extending their apical ends to the gut lumen, or of the "closed type", which have no luminal contact (Sehnal & Zitnan, 1996). Endocrine cells are usually found as singly, although some taxa have pairs or small groups of these cells. Endocrine cells are often interlinked with the enteric nervous system and co-jointly control gut movement, production of digestive fluids, and the regenerative rate of midgut epithelium (Dockray, 1988; Sehnal & Zitnan, 1996).

The final midgut cell type, goblet cell, has a large central cavity that is shaped like a goblet, after which the cells were named. The membrane facing into the cavity is lined with microvilli, and the microvilli of the lateral sides of the cell curving in towards the cell center, interdigitating to form an apex along the gut lumen (Nation, 2002). This membrane contains proton-ATPase pumps that are responsible for the exchange of hydrogen ions (H+) for potassium within the cavity. The exchange of the two ions creates a transmembrane voltage that can reach 240mV and results in a pH gradient, between the cavity and cytosol, which may exceed 4 pH units (Nation, 2002). Goblet cells are interspersed amongst the columnar epithelium and have only been reported in Lepidoptera, Ephemenoptera, Plecoptera, and Trichoptera. Hennigan *et al.* (1993) have shown that goblet cells play an important role in amino acid absorption through a cationic-dependent exchange mechanism.

The hindgut is the last region of the insect gut. Similar to the foregut, the hindgut is lined by a cuticular layer, although it is mostly unsclerotized and has large pores that allow for the absorption of water, ions, and remaining free nutrients. There are three distinct regions of the hindgut: the pylorus, the ileum, and the rectum. The pylorus defines the junction between the midgut and hindgut. Malpighian tubules, the excretory

organ of insects, empty into the pyloric region. The main function of the pylorus is the passage of waste material from the midgut and Malpighian tubules to the ileum. A series of thick longitudinal and circular muscles line the pyloric region and create a sphincter that pushes material through the gut with the aid of small sclerotized denticles. The ileum and rectum are chiefly responsible for the absorption of water and important salts from the urine and faecal matter. Water conservation is of prime importance to most terrestrial insects and its recovery results in a dry frass. This function is performed by specialized columnar cells that aggregate to form fold or pad-like structures amongst otherwise flat, unspecialized epithelium. The columnar cells have microvilli, a large quantity of mitochondria, and a highly invaginated basal membrane. In addition to the absorptive function of ileum-fold and rectal-pad cells, the thickened plate of the cuticle overlay results in the formation of the faecal pellets.

1.9 Dissertation Overview

In chapter 2, the nucleopolyhedrovirus native *to Lambdina fiscellaria lugubrosa* is characterized, using an *in vitro* propagation system. Viral pathology and replication are investigated in two permissive cell lines derived from foreign lepidopteran insects, *Malacosoma disstria* and *Choristoneura fumiferana*. The oral infectivity of LafiNPV-W, cultured in each cell culture, is also examined. These experiments were used to establish protocols suitable for the *in vitro* characterization of *Neodiprion abietis* NPV (NeabNPV) and determination of the permissibility of the host cell culture, Cf70.

Chapter 3 focuses on the first ever *in vitro* characterization of a hymenopteran-derived nucleopolyhedrovirus, NeabNPV. Several cell lines, derived from a closely related *Neodiprion* species, were studied for their permissiveness to the virus, as well as the

aforementioned *C. fumiferana* cell line, which was found to be semi-permissiveness for NeabNPV. Cf70 cells infected with NeabNPV were characterized by light and epifluorescent microscopy, southern hybridization for replication kinetics, and transcriptional analysis of early genes.

The morphology and ultrastructure of the uninfected *N. abietis* larval gut is examined in chapter 4. The hymenopteran gut has been studied in bees, wasps and ants, particularly in adult insects. In contrast, only one brief macro-morphological investigation of sawfly guts has been reported (Maxwell, 1955).

Due to the inability to fully characterize NeabNPV *in vitro*, a time course assay was conducted to investigate NeabNPV pathology *in vivo* in *N. abietis* larvae. A direct comparison of uninfected and virally-infected larval midgut tissue was made to understand the pathogenesis of NeabNPV. The results from this investigation are presented in chapter 5. Midgut epithelia of larvae, obtained from the *in vivo* time course assay, were analyzed for pathogenesis at 1, 2, 5, 8, 12, 24, 48, and 72 hours post inoculation. Cytopathic effects (nuclear hypertrophy and change in microvillar surface area) and viral structures (virogenic stroma, virion maturation, and occlusion body formation) were determined at each time point.

In order to correlate the histopathology with the molecular events of NeabNPV infection and expand upon the findings of Duffy (2006), transcriptional analyses of *vlf-1* and *polh* and protein expression studies of GP41 and POLH were performed for samples ranging from 0.5 up to 96 hours post inoculation (Chapter 6). Transcriptional analyses were performed using cDNA obtained from total RNA extracted from larvae whose viral DNA content fit within the NeabNPV replication kinetics curve, as previously

determined by Duffy (2006). Finally, total protein was extracted and separated by SDS-PAGE. Time course samples were probed with anti-GP41 (viral tegument protein) and anti-POLH antibodies to determine the onset of protein synthesis for late and very late phases of infection, respectively.

Chapter 2 *In vitro* propagation of *Lambdina fiscellaria lugubrosa* nucleopolyhedrovirus in two heterologous host cell lines

2.1 Abstract

Infections in two heterologous host cell lines (Md108 and Cf70) by the nucleopolyhedrovirus of *Lambdina fiscellaria lugubrosa* (Lepidoptera: Geometridae), LafiNPV-W, have been characterized. Cytopathic effects characteristic of NPV infection, including rounding of the cells, nuclear hypertrophy, and polyhedra production, were observed in both cell lines. Viral titres were slightly higher in Md108 cells compared to titres obtained from Cf70 cells ($5.8x10^7$ versus $3.1x10^7$ infectious units ml^{-1}, respectively). Replication kinetics of LafiNPV-W in the two cultures were similar, but earlier onset of replication and lower yield of intracellular viral progeny were observed in the Md108 cells. Actin rearrangements occurred within 24 hour post inoculation (hpi) in both cell lines, resulting in the loss of cytoplasmic extensions and focal adhesions. Hypertrophy, measured by an increase in nuclear size, and redistribution of heterochromatin/euchromatin were detected by DAPI staining. Large quantities of virions and nucleocapsids were visualized by electron microscopy at 48 hours. The ultrastructure of the polyhedra from the two cultures revealed significant differences in the assembly and embedding of virions into the POLH matrix. Cf70 cultures produced polyhedra with numerous singly embedded virions, while the highly crystalline occlusion bodies of Md108 cultures were either empty, with nucleocapsids packed in the intranuclear spaces between them, or contained few virions that lacked their *de novo* envelope. Bioassays, with polyhedra derived from the two cultures, resulted in significantly different mortality rates. Inefficient embedding of virions into Md108 propagated polyhedra resulted in to decreased virulence *per os*. While the infectious

process in the two different cell lines was very similar, polyhedra maturation was markedly different suggesting that host factors may influence nucleocapsid occlusion and therefore *per os* virulence.

2.2 Introduction

The nucleopolyhedrovirus isolated from the western hemlock looper (LafiNPV-W) is a multiply enveloped, multiply embedded virus, of approximately 146 kb in size (R. Alberto and D. Levin, personal communication). *In vivo* the polyhedra, produced in *Lambdina fiscellaria fiscellaria* (Guen.), are 1.5 to 3.0 μm in diameter and show no characteristic angles or shape (Cunningham, 1970b). Nucleopolyhedroviruses (LafiNPV-E and LafiNPV-O) isolated from the closely related Eastern Hemlock Looper, *Lambdina fiscellaria fiscellaria* (Guen.), and the Western Oak Looper, Lambdina *fiscellaria somniaria* (Hulst), each showed two variant polyhedra morphologies, *in vivo*. One type of polyhedra was cuboidal with virions of the same dimensions as those produced within the usual icosahedral polyhedra. Typically, cuboidal polyhedra tended have similar properties as icosahedral polyhedra, other than shape, though some cells infected with LafiNPV-E exhibited cuboidal polyhedra nearly double in size, 4.0 to 6.0 μm in diameter (Cunningham, 1970b). Mixtures of cuboidal and icosahedral polyhedra have never been observed within the same nucleus.

When Cunningham (1970a) examined polyhedra cross-sectionally, no difference in the number or size of virions embedded with polyhedra of different size or shape were found. The viral genome was proposed to control the inclusion body size and shape, even though no variant strains of the virus could be isolated. Nucleopolyhedrovirus polyhedra isolated from each of the closely related species (LafiNPV-W, LafiNPV-E and LafiNPV-O) were

equally infectious compared to the heterologous hosts of the other subspecies (Cunningham, 1970a; Levin *et al.*, 1997).

Baculovirus host specificity is usually very high, as different viruses optimally infect either a single species or a few closely related ones. Host range is limited by the ability of the virus to replicate and release new virulent particles within the host (McClintock *et al.*, 1986; McClintock *et al.*, 1991; Morris & Miller, 1992). Permissive cells fully support viral DNA replication and production of viable progeny, as evident by *in vitro* studies using cultured insect cells. Some cells support limited replication and produce little or no viable progeny (semi-permissive), while others support neither viral DNA replication nor the production of viable progeny (non-permissive). Virus-host interactions blocked at the transcription and translation levels are likely the cause of aborted infections within semi- and non-permissive cells (Castro *et al.*, 1997; Huang *et al.*, 1999; McClintock *et al.*, 1986).

In this study, we demonstrate that LafiNPV-W is able to infect two cell lines derived from heterologous lepidopteran hosts. Sohi and Cunningham (1972) found that LafiNPV-O, which has a host range similar to LafiNPV-W, was infectious to a cultured line of cells from the forest tent caterpillar, *Malacosoma disstria* (Md108). We have found that a cell line derived from Eastern Spruce Budworm, *Choristoneura fumiferana* (Cf70), is also susceptible to LafiNPV-W. While the pathology produced by LafiNPV-W is nearly identical in Md108 and Cf70 cells, polyhedra produced in Md108 cells lack proper nucleocapsid occlusion compared to the polyhedra produced in Cf70 cells, which are full of mature virions.

2.3 Materials and Methods

2.3.1 Virus Stocks

The *Lambdina fiscellaria lugubrosa* nucleopolyhedrovirus (LafiNPV-W), was obtained from Dr. I. S. Otvos, (Natural Resources Canada, Canadian Forest Services, Pacific Forestry Center, Victoria, British Columbia, Canada), as a suspension of $1x10^9$ PIBs ml^{-1}. The LafiNPV-W polyedra were derived from infected *Lambdina fiscellaria fiscellaria* larvae.

Four insect cell lines were screened for their permissibility to the LafiNPV-W. These cultures included the *Malacosoma disstria* cell line (Md108) that Sohi and Cunningham (1972) found to be permissive to the nucleopolyhedrovirus of *L. f. somniaria* (LafiNPV-O), a *C. fumiferana* cell line (Cf70), the *Spodoptera frugiperda* cell line (Sf9) that is a commonly used and permissive host to the model *Autographa californica* multicapsid nucleopolyhedrovirus, and a hymenopteran cell line derived from *Neodiprion lecontei* (NL18).

The Md108, Cf70 and NL18 cell lines were obtained from Dr. S. Sohi of the Canadian Forest Services (Sault St. Marie, Ontario). Md108 cells were propagated with Grace's Insect Media (GibcoBRL, Inc.), supplemented with 0.25% Bacto Tryptose Broth (Difco, Inc.) and 15% heat-inactivated Fetal Bovine Serum (FBS), USDA certified (GibcoBRL) and subcultured using Trypsin-EDTA (0.1% Trypsin, 1.06 mM EDTA) in Rinaldini's Balanced Salt Solution. The cells were incubated in the trypsin solution for 3-5 minutes. The cells were then centrifuged at 400x g and passed 1:5 into new flasks. The Cf70 and NL18 cell lines were subcultured in the same manner as the Md108 cells, except the media was supplemented with only 10% FBS. Sf9 cells were purchased from

PharMingen Corp. (San Diego, CA.) and were cultured in accordance to procedures described by O'Reilly *et al.* (O'Reilly *et al.*, 1992) in Grace's Insect Medium supplemented with 3.33 g L-1 TC yeastolate, 3. 33 g L-1 lactalbumin hydrolysate and 10% FBS. SF9 cells were subcultured using mechanical force and passed 1:6 into new flasks.

2.3.2 DNA Extraction of LafiNPV-W

Polyhedra of LafiNPV-W were purified from infected Eastern Hemlock Looper larvae, and concentrated to 1 x 10^9 polyhedra ml^{-1}. DNA was extracted from a 5 ml sample (5 x 10^9 polyhedra), using the standard organic extraction procedure published by O'Reilly (O'Reilly *et al.*, 1992). LafiNPV-W polyhedra were resuspended in 0.4% sodium dodecyl sulphate (SDS) and incubated from one hour, gently shaking. The suspension was centrifuged at 3000 xg for 30 minutes, after which the supernatant was discarded and the pellet was rinsed twice with distilled water with centrifugation at 3000 xg for 10 minutes between washes. The polyhedra were dissolved in 0.1 M sodium carbonate and 0.04 M sodium thioglycolate over 10 minutes, before the undissolved occlusion bodies were removed by centrifugation at 2000 xg for 5 minutes at 4 °C. The supernatant, containing the released occlusion derived virions (ODVs), was collected and centrifuged at 15 000 xg for 30 minutes at 4 °C. The pelleted ODVs were resuspended in 5 volumes of TE buffer (pH 7.5) (10 mM Tris-HCl, 1mM EDTA). Proteinase K (Amersham-Pharmacia Inc.) (0.1 mg ml^{-1}) and sodium lauryl sarcosine (2%) were added to the resuspension, which was then incubated overnight in a circulating water bath at 50 °C. An equal volume of DNAzol (Molecular Research Centre) was added to the sample and incubated, shaking, for 20 minutes at room temperature. The sample was incubated at -80

°C, following the addition of ice cold ethanol (20%) and mixing by inversion. A DNA pellet was obtained by centrifuging the solution at 15 000 xg for 30 minutes at 4 °C. The DNA was resuspended in 50 µl of sterile, distilled water, then 10 volumes of ice cold ethanol was added to precipitate the DNA. After centrifuging (15 000 xg for 30 minutes at 4 °C) the sample, the DNA pellet was dried and resuspended in 10mM Tris-HCl (pH 7.5). The concentration of DNA was determined by spectrophotometry.

2.3.3 Transfection LafiNPV-W into Md108 cells

Md108 and Cf70 cells (5 x 10^6) were plated separately into each well of two six-well plates. The cells were incubated overnight in serum-containing media, to ensure no contamination had occurred during the passage and allowing for cell recovery and adhesion to the plate surface. On each plate, wells were designated A through F. In each treatment, well A served as the untreated control and well D was the control with transfection reagent only. Wells B and C were each transfected with 1 µg LafiNPV-W DNA, while wells E and F were each transfected with 2 µg LafiNPV-W DNA. When using the Cellfectin transfection, a 1:3 ratio (µg DNA: µl reagent) was used for wells B and E, while a 1:6 ratio was utilized in wells C and F. Well D (the negative control) was transfected with an equivalent amount of transfection reagent without DNA as well F. Transfections were performed following the procedures of the manufacturer's manual. All transfections were incubated until either cytopathic effects were observed, by light microscopy, or the untreated controls died in order to show that the transfection reagent was not toxic.

2.3.4 Passage of Infectious Viral Media

The viral-laden media from the transfection experiments was removed from each well (upon observation of cytopathic effects) and passed, at a 1:1 ratio with fresh complete media, onto freshly plated Md108 or Cf70 cells, in a well of a new six-well plate. When similar cytopathic effects were observed (rounding up of cells, hypertrophied nuclei, and lysed cells), the new infectious media was passed and overlain onto fresh cultures in TC-25 cm^2 flasks. The process was continued by passing the viral laden media at 10% for up to 12 serially passages of the virus. Virus titres were determined at the 4^{th} and 6^{th} passages of LafiNPV-W, for both the Md108 and Cf70 cultures (see Section 2.3.7)

2.3.5 Confirmation of Viral Infection

The presence of propagating virus in cells was confirmed by: light microscopy, transmission electron microscopy, and amplification of the polyhedrin gene (*polh*) by polymerase chain reaction.

2.3.5.1 Light Microscopy

Characteristic cells exhibiting the cytopathic effects of infected cells were photographed. Cells were viewed on a Zeiss Axiovert microscope at 200X magnification. Representative cells of infected and uninfected Md108 and Cf70 cultures were chosen and photographed using standard Kodak T-max 100 black and white film in an Olympus PM6 camera, at 100X magnification. Negatives were digitalized using a Polaroid SprintScan35 scanner and Polaroid PolaColor Insight software (v.4.5.1). Scale bars were added to the digital images using Adobe Photoshop 5.

2.3.5.2 Electron Microscopy

Cells were fixed in TC-25cm^2 flasks (Sarstedt) using 4% gluteraldehyde in a 0.1 M sodium cacodylate buffer. Post-fixation was also performed in the tissue culture flask, with a 2% osmium tetroxide in 0.1 M sodium cacodylate buffer. Fixed cells were mechanically harvested with rubber policemen, centrifuged at 400 x g and resuspended in a 5x volume of 10% agar. The agar block containing the fixed cells was sliced into small cubes. The sample cubes were dehydrated, using increasing concentrations of ethanol and propylene oxide, and then incubated in a 1:1 propylene oxide and Epon resin solution, at room temperature overnight. The Epon penetrated samples were then embedded within Epon resin and incubated at 65°C for 48 hours. The resulting blocks were sectioned and samples were view with a Hitachi H7000 Transmission Electron microscope, using a 75 kV beam. Electron micrographs were imaged on Kodak 4489 Electron microscope film and processed with Kodak D19 Developer and Rapid Fix. The images were digitalized by scanning the negatives with Polaroid SprintScan45 Scanner and Polaroid PolaColor Insight software (v.4.5.1). Scale bars were added to the digital images using Adobe Photoshop 5.

2.3.6 *PCR Confirmation of Viral DNA*

Three separate inoculated cultures for each cell line, Md108 and Cf70, were used to determine the presence of viral DNA. LafiNPV-W laden media was separated from each cell culture by initially centrifuging the cell suspensions at 400 x g for 5 minutes. The extracellular virus was isolated by an additional centrifugation at 10,000 x g for 20 minutes. Viral DNA was extracted using standard organic extraction protocols (O'Reilly *et al.*, 1992). Total extracted DNA (500 ng) was used in a PCR that specifically amplified the LafiNPV-W polyhedrin gene (*polh*). Total extracted DNA from uninfected

cultures (500 ng) were used as a negative control, in addition to a no template control. LafiNPV-W forward and reverse primers were designated p001F (5'–GCGTGAACGGCGACGTCG–3') and p756R (5-ATGACCGG GCATCCACC–3'), respectively. Taq DNA polymerase was used in a reaction with an initial denaturation period of 4 minutes at 94 °C, followed by 35 cycles of denaturation (30 seconds, 94 °C), annealing (45 seconds, 55 °C), and elongation (45 seconds, 72 °C) periods. Half of the reaction volume was loaded onto a 0.8% agarose gel buffered with TBE (0.09 M Tris, 0.09 M boric acid, 0.002 M EDTA) and stained with ethidium bromide (0.25 $\mu g\ ml^{-1}$). The amplification products were imaged using an Eagle-eye II UV Transluminator System (Stratagene) with EagleSight Software (v.3.2). The gel image was cropped using Adobe Photoshop (v5.0.2).

2.3.7 Titration of the LafiNPV-W Stock by an End-Point Dilution Method

Once polyhedra were visible with the nuclei, 72 hours post infection (hpi), a sample of media was taken for titre determination. The virus stock was diluted in tenfold increments, from $1x10^{-3}$ to $1x10^{-9}$. For each dilution, 200 µl of virus were added to 1.8 ml of a $1x10^{5}$ cell ml^{-1} solution. Each dilution of the virus/cells was added to a single row of a 96-well plate, with each well containing 100ul of the cell/virus solution. The infected cells were incubated for 10 days, and scored daily for cytopathic effects and PIB production. The 50% end-point was calculated using the Reed and Muensch formula (Reed & Muench, 1938).

2.3.8 Replication Kinetics of LafiNPV-W and Host Specificity

Md108, Cf70, NL18, and SF9 cells were tested to determine their susceptibility to LafiNPV-W. For each type of culture, cells ($1x10^{5}$) were plated in 25 cm^{2} tissue culture

flasks, incubated overnight to test for contamination and to allow for cell recovery. At time zero (0), seven sets of cultures per cell type were inoculated with a MOI of 5 and incubated for six hours. The viral-laden media was removed and cells were washed twice before fresh complete media was added. At the 16-hour interval post infection, cells from the first plate were harvested. Subsequent samples were harvested at 20, 24, 28, 32, 48 and 72 hpi. A mock-infected plate of cells was used as the time zero (control) reference. Once all the samples were harvested, the cells were pelleted and total DNA was extracted. Using spectrophotometry, the concentration of each DNA extract was calculated. Based on the sample with lowest yield of extracted DNA, three micrograms (3 μg) of total DNA at each time interval was applied to a nylon membrane, via a dot blot apparatus (BioRAD), then hybridized with radio-labelled probe. The original DNA extracted from PIBs (i.e. for the transfection) was used as positive control markers, and blotted in 1, 5, 10, 50, and 100 ng amounts. Genomic LafiNPV-W DNA used as a template for amplifying (α-^{32}P)-dCTP radio-labelled probes, which were then hybridized to the membrane. Images of the Southern dot blot were obtained using the Molecular Dynamics Storm 860 Scanning system with ImageQuant 5 Software. The experiment was repeated twice and the intensity of values of the hybridized probes were measured, using ImageQuant 5 Software, and then were averaged.

Cell lines, which showed permissibility to the virus, were photographed to depict the cytopathology that occurred. Cells were viewed on a Zeiss Axiovert microscope at 200x magnification. Representative cells were chosen and photographed using standard Kodak T-max 100 black and white film in an Olympus PM6 camera.

2.3.9 Epifluorescent Characterization of Actin and Nuclear Structure

Md108 or Cf70 cells (2×10^3) were plated into each well of an eight chambered slide and cells in 6 of the wells were inoculated 24 hours prior to fixation, at an MOI of 10. Uninfected and LafiNPV-W infected Md108 and Cf70 cultures were fixed using 500 µl fresh 4% paraformaldehyde in phosphate buffered saline (pH 7.5) (PBS), for 15 minutes at room temperature. After rinsing in 500 µl PBS, the cultures were post fixed using 500 µl of 0.1% Tween 20 in PBS for 10 minutes at room temperature, then rinse again with 500 µl PBS.

The actin structures of fixed cultures were labelled with rhodamine-conjugated phalloidin (Molecular Probes, Inc., Cat. No. R-415). PBS was removed from the cultures and 100 µl of 5 U μl^{-1} rhodamine-phalloidin was added to each well. The cultures were incubated in the solution for one hour, at room temperature, in the dark. Following labelling, the cultures were rinsed twice with 500 µl PBS. Prior to dismantling the chamber slide, 100 µl of 250 ng ml^{-1} bis-benzimide in PBS was applied to the cultures at room temperature, in the dark, for 15 minutes, followed by two rinses twice with 500 µl PBS. Chambers were removed from the slides, which were subsequently mounted using a glycerol-PBS mounting media, containing 0.625% n-propyl gallate. Actin structures were view under a Zeiss Universal Compound Upright Epifluorescent Microscope with Zeiss filter set 15 (FITC). Bis-benzimide (DAPI) staining nuclei were visualized using a Zeiss filter set 02 (UV) and images were saved using a CCD digital video capturing system and ScionImage Beta 3b software (National Institutes of Health, USA). Separate images were taken for each fluorescent probe. Overlaid images were composed by a screening technique, using Adobe PhotoShop 5.0. Cultures were

analyzed to determine the effects the virus had on the labelled structures. Four parameters of viral induced effects were examined: 1) changes to filopodia, 2) changes to focal adhesions, 3) changes to nucleus size, and 4) changes to DNA structure (euchromatin vs. heterochromatin).

Phalloidin stained actin structures were manually counted for each cell of each treatment. Filopodia and focal adhesions were analyzed since no stress fibres and lamellipodia were detectable in the preparations. Bis-benzimide staining allow for the determination of the nucleus size and the intensity of fluorescence, representing the proportion of euchromatin and heterochromatin. ScionImage software was used to measure the diameter of the nucleus and the average intensity of fluorescence for the entire nuclear region. Kruskal-Wallis non-parametric analyses were calculated using GraphPad Instat 3.05 software.

2.3.10 Bioassay of LafiNPV-W in *L. f. somniaria* Larvae

Freshly moulted, second instar larvae of the western oak looper, *L. f. somniaria*, were infected with LafiNPV-W polyhedrin inclusion bodies (PIBs) derived from orally inoculated eastern hemlock looper, *L. f. fiscellaria*, larvae or either of the two insect cell cultures, Md108 or Cf70. Inoculation of the larvae was performed using the diet plug methodology, modified by Li and Otvos (Li & Otvos, 1999b). An artificial diet, tested for laboratory rearing of the closely related subspecies *L. f. fiscellaria* (Li & Otvos, 1999a), was prepared and formed into plugs of approximately 1 mm diameter and 3 mm length.

Eight treatment solutions were prepared: 1) distilled deionized sterile water, 2) filter sterilized insect cell culture media, 3) $5x10^6$ larval derived PIBs ml^{-1}, 4) $5x10^5$ larval

derived PIBs ml^{-1}, 5) $5x10^4$ larval derived PIBs ml^{-1}, 6) $5x10^5$ Md108 cell culture derived PIBs ml^{-1}, 7) $5x10^5$ Cf70 cell culture derived PIBs ml^{-1}, and 8) $5x10^4$ Cf70 cell culture derived PIBs ml^{-1}. Concentrations of polyhedra derived from Eastern Hemlock Looper larvae were prepared based on the LD50 determined in foliage contamination bioassays (Morris, 1962). All other PIB concentrations were determined by visual counts with a hemocytometer at 100x magnification. Solutions without PIBs were used as negative controls for the virus, while solutions containing larval derived PIBs were used as positive controls. The prepared diet plugs were placed individually into wells of a 24 well tissue-culture plate and were inoculated with 1µl of a sample or control solution listed above. The solution was allowed to absorb into the diet plug before larvae were added. The loopers were left in culture plates for up to 72 hours to allow for the complete consumption of the inoculated plug. Larvae that did not consume the entire diet plug were selected for the experiment only if they had consumed 75% of the plug; otherwise they were excluded. Larvae were monitored twice daily in this first 72 hours to detect when the diet was eaten and then they were transferred to individual P100 plastic solo cups that contained fresh diet and a sprig of Douglas-fir, *Pseudotsuga menziesii* (Levin *et al.*, 1997). The cups were capped with PL1 plastic Solo lids and transferred to a growth chamber with a photoperiod of 16:8 (Light:Dark) hours, 22 °C (±1 °C), 55-60% RH. After the initial week, larvae were reared strictly on fresh sprigs of Douglas-fir, which were changed twice a week.

Three replicas (2x 25 individual and 1x 26 individuals) for each treatment were prepared, yielding a total of 608 individuals. Each larva was examined 6 days per week until death or pupation occurred, upon which the time and visual health/disease was

recorded. The experiment lasted for 88 days at which time the final individual pupated. Treatments were analysed, using SPSS v 12, for mortality curves by Probit and Kaplan-Meyer analysis. The significance in mortality between treatments was determined using the Cox regression model for proportional hazards.

2.4 Results

Md108 and Cf70 were found to be fully permissive to LafiNPV-W infection, producing typical cytopathic effects such as hypertrophied nuclei, virogenic stroma, and polyhedra (Figure 2-1). Varying sizes and shapes of polyhedra were found in each culture, including the icosahedral (2-3.5 μm) and cuboidal (4.5-10 μm) types described by Cunningham (Cunningham, 1970b, 1971). Polyhedra were first visible at 48 hours within 10-15% of the cell population in each culture. In Md108 cultures, approximately 80% of cells exhibited polyhedra by 120 hours post inoculation (hpi), with 55% of the nuclei producing the smaller icosahedral polyhedral phenotype and 45% producing the larger cuboidal type. LafiNPV-W disease progression was very similar in Cf70 cultures, with 85% of the cells producing polyhedra by 120 hpi, 67% of which were icosahedral and 33% of which were cuboidal. Cells typically lysed within the following 24 hours.

Virus titres were determined in both cell lines after 72 hours post inoculation (hpi). Md108 infected cultures produced a LafiNPV-W titre of 5.8×10^7 infectious units ml^{-1}, while Cf70 cells produced a titre of 3.1×10^7 infectious units ml^{-1}, an approximate 120- and 60-fold increase in budded virus from the 5×10^5 inoculation titre, respectively. No further increase in virus titre was detected with higher multiplicities of infection in either culture (data not shown).

Cf70 cells Md108 cells

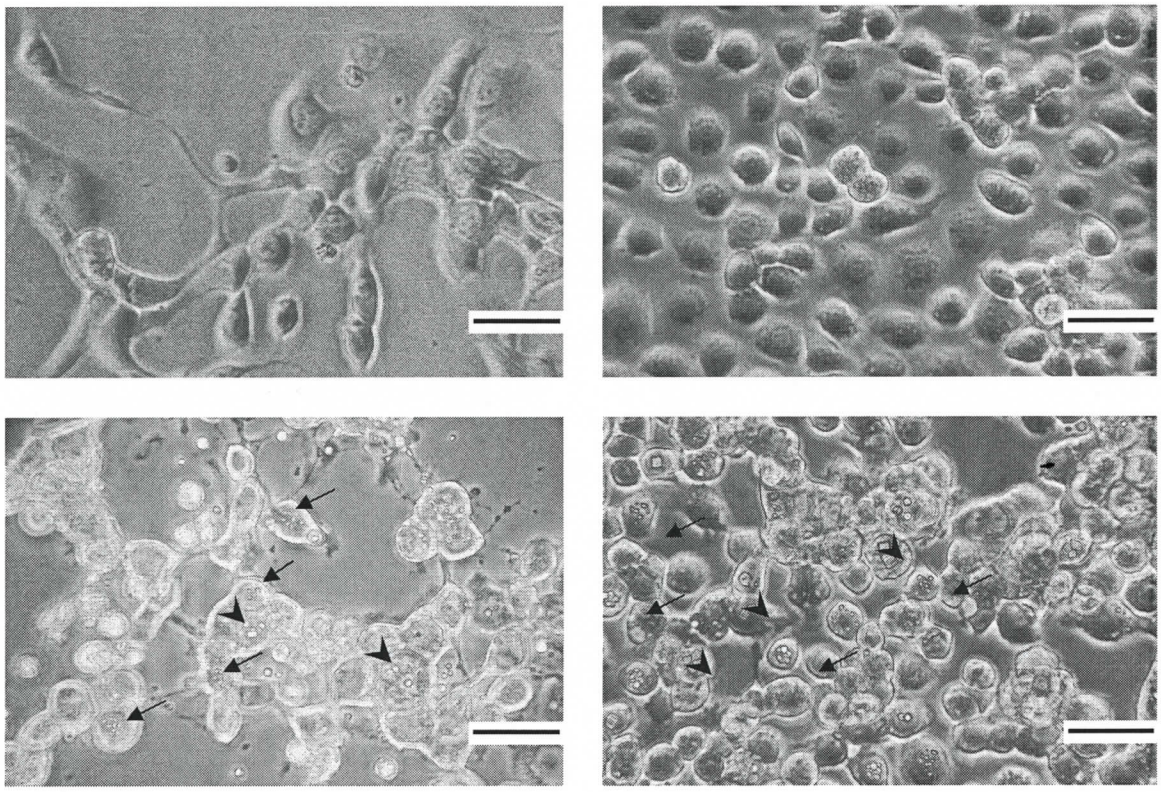

Figure 2-1. Light micrographs of mock and LafiNPV-W infected *Choristoneura fumiferana* and *Malacosoma disstria* cell cultures.

Cultures were imaged using phase contrast on a Zeiss Universal Compound Microscope, at 48 hour post inoculation. Images **A** & **C** show differences in cytopathology between mock and LafiNPV-W infected Cf70 cells, respectively. Images **B** (mock) and **D** (LafiNPV-W infection) show similar cytopathic effects for Md108 cells. Arrows indicate icosahedral polyhedra, while arrow heads indicate cuboidal polyhedra.

Scale bars = 40 μm.

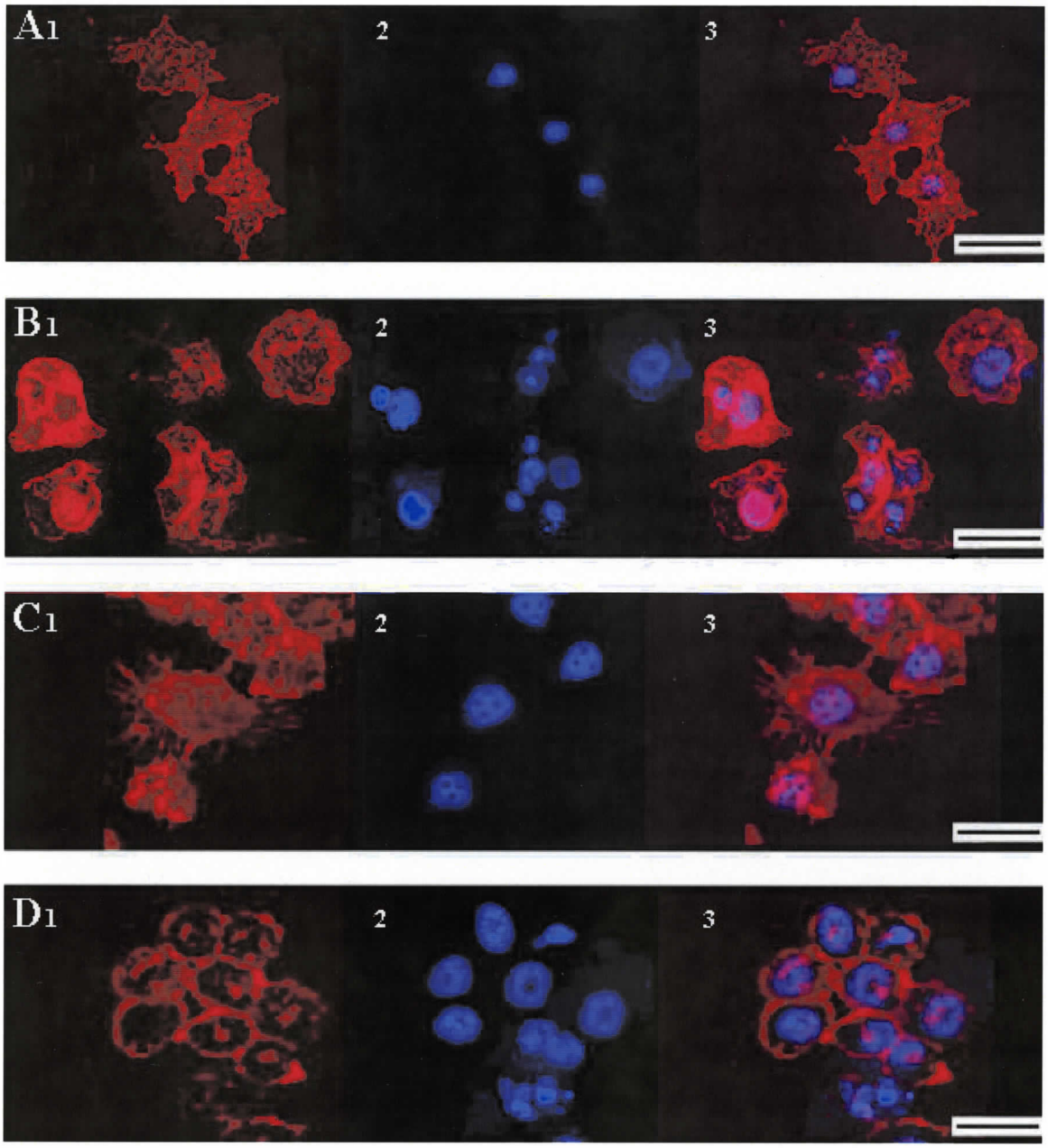

Figure 2-2. Epifluorescent micrographs of mock and LafiNPV-W infected *C. fumiferana* and *M. disstria* cells at 24 hours post-inoculation.

Mock infected (**A & C**) and LafiNPV-W infected (**B & D**) Cf70 and Md108 cultures, respectively, were imaged at 24 hours post inoculation using a Zeiss Universal Epifluorescent Upright microscope. Actin cytoskeletons (first image of each plate (#**1**)) were stained with Rhodamine-phalloidin and nuclei (second image of each plate (#**2**)) were labelled with DAPI. The third image of each plate (#**3**) represents an overlay of the labelled nuclei upon the cytoskeleton. Scale bars = 40 μm.

Actin rearrangements and changes in nuclear size were examined to provide supporting evidence of LafiNPV-W infection in both cell lines, since no antibodies against viral proteins were available. At 24 hpi, both cell lines showed distinct changes to their actin cytoskeleton (Figure 2-2). The cells rounded, leading to the loss of cytoplasmic extensions (filopodia), and they lost their ability to adhere to the culture substrate, as evident by the loss of focal adhesions. When compared to mock infected cells at the same time post-inoculation, a 10-fold decrease in the number of filopodia and focal adhesions was observed in LafiNPV-W infected cultures. No significant difference was detected between mock-infected cultures with respect to actin structure and nuclear morphology (Table 2-1). Nuclear size, used to measure the extent of nuclear hypertrophy, was significantly increased in both LafiNPV-W infected cultures. Infected cell nuclei tended to be 1.5-2 times as large in diameter as those of mock infected cells in either cell-line. A visible difference in chromatin structure was evident by DAPI staining of the nuclei. Mock-infected cells showed a characteristic pattern of euchromatin and heterochromatin, while LafiNPV-W infected cells exhibited regions of intense DAPI staining, indicating a concentration of condensed double-stranded DNA (heterochromatin-like structures). A quantitative measure of nuclear density, however, failed to detect a significant difference between mock and infected cells, likely due to the limitation of the ScionImage Beta 3b software in averaging the pixel intensity (data not shown).

PCR analysis was used to confirm the infectivity of LafiNPV-W in the two cell lines (Figure 2-3). Both the viral laden media and inoculated cells of LafiNPV-W infected Md108 and Cf70 cultures were positive for viral DNA based on the amplification of the

Table 2-1. Observed traits of mock and LafiNPV-W infected *M. disstria* and *C. fumiferana* cells.

Cultures were incubated for 24 hours, then cellular structures were imaged and measured using ScionImage software. Kruskal-Wallis analysis was performed for each data set.

Observed Traits	Group	Number of cells analysed	Mean	Median	Min.	Max.	P-value of uninfected and infected of same cell line	P-value of like treatments between cell lines
Number of Filopodia*	Md108 uninfected	18	49.93	30	14	64		
	Md108 LafiNPV-W	22	1.85	1	0	9	<0.001	
	Cf70 uninfected	17	43.77	27	12	60		>0.05
	Cf70 LafiNPV-W	13	1.74	1	0	9	<0.001	>0.05
Number of Focal adhesions**	Md108 uninfected	18	52.5	31	18	67		
	Md108 LafiNPV-W	22	2.05	2.5	0	15	<0.001	
	Cf70 uninfected	17	44	24	19	53		>0.05
	Cf70 LafiNPV-W	13	1.36	0	0	8	<0.001	>0.05
Nuclear size †£	Md108 uninfected	15	0.54	0.55	0.48	0.6		
	Md108 LafiNPV-W	23	0.71	0.73	0.46	0.92	<0.001	
	Cf70 uninfected	17	0.56	0.55	0.49	0.63		>0.05
	Cf70 LafiNPV-W	16	0.77	0.83	0.37	1.1	<0.001	>0.05

*Kruskal-Wallis Statistic KW = 33.374 (corrected for ties)
**Kruskal-Wallis Statistic KW = 36.310 (corrected for ties)
†Kruskal-Wallis Statistic KW = 22.214 (corrected for ties)
£ Nuclear size measured in inches from 72 pixels/inch digital images

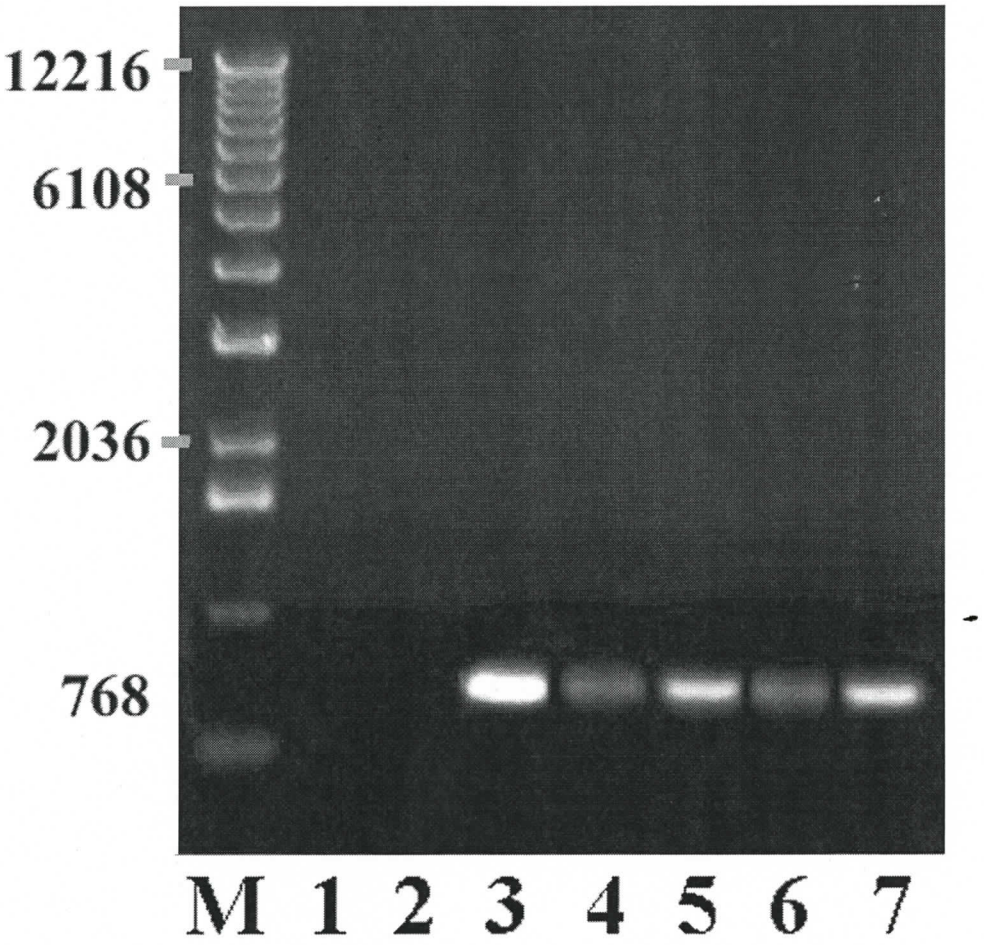

Figure 2-3. Agarose gel electrophoresis of LafiNPV-W *polh* PCR products. Agarose (1%) gel, buffered with TBE, depicting the PCR products of the amplified polyhedrin gene. Template DNA was extracted from: 1) uninfected Md108 cells, 2) uninfected Cf70 cells, 3) polyhedra derived from *Lambdina fiscellaria fiscellaria* larvae, 4) LafiNPV-W infected Md108 cells, 5) viral laden media of LafiNPV-W infected Md108 culture, 6) LafiNPV-W infected Cf70 cells, 7) viral laden media of LafiNPV-W infected Cf70 culture. M) 1kb molecular weight markers.

polyhedrin gene PCR product. Greater amplification of viral DNA was found in the viral laden media, consistent with the extraction of a relatively purer sample of virus from media compared to that extracted from cells which also contained host DNA.

Southern hybridization of DNA extracted from LafiNPV-W infected Md108, Cf70, Sf9, and NL18 cells cultures (Figure 2-4) at various times post-inoculation showed that Md108 and Cf70 cultures fully supported viral DNA replication. The amount of LafiNPV-W DNA detected in Sf9 cells was constant throughout the time course, while a decrease in the virus quantity was observed after 32 hours in NL18 cells. A viral specific increase in DNA, indicative of DNA replication, was observed in Md108 cultures, with the first detectable increase over background levels observed at 24 hpi. Replication was evident until 60 hpi, and then the amount of viral DNA plateaued with no further observed increase. In Cf70 cells, viral DNA replication commenced at approximately 24 hpi and continued until 72 hours when a maximum amount of DNA was detected.

Electron micrographs of LafiNPV-W infected Md108 cells showed a distinct virogenic stroma with many nucleocapsids at the periphery of the nucleus (Figure 2-5). During the late phase of infection, nucleocapsids were observed budding through the nuclear membrane into the cytoplasm. Typically the nucleocapsids budded as a single entity, although small bundles within a single membraned structure were observed infrequently. At the very late phase of infection, nucleocapsids were observed in bundles ranging from 2-20 and enveloped into virions with a *de novo* bilayered membrane. Although large quantities of mature singly enveloped virions were produced in this cell line, few of them were embedded into the large cuboidal polyhedra that were observed. The crystalline

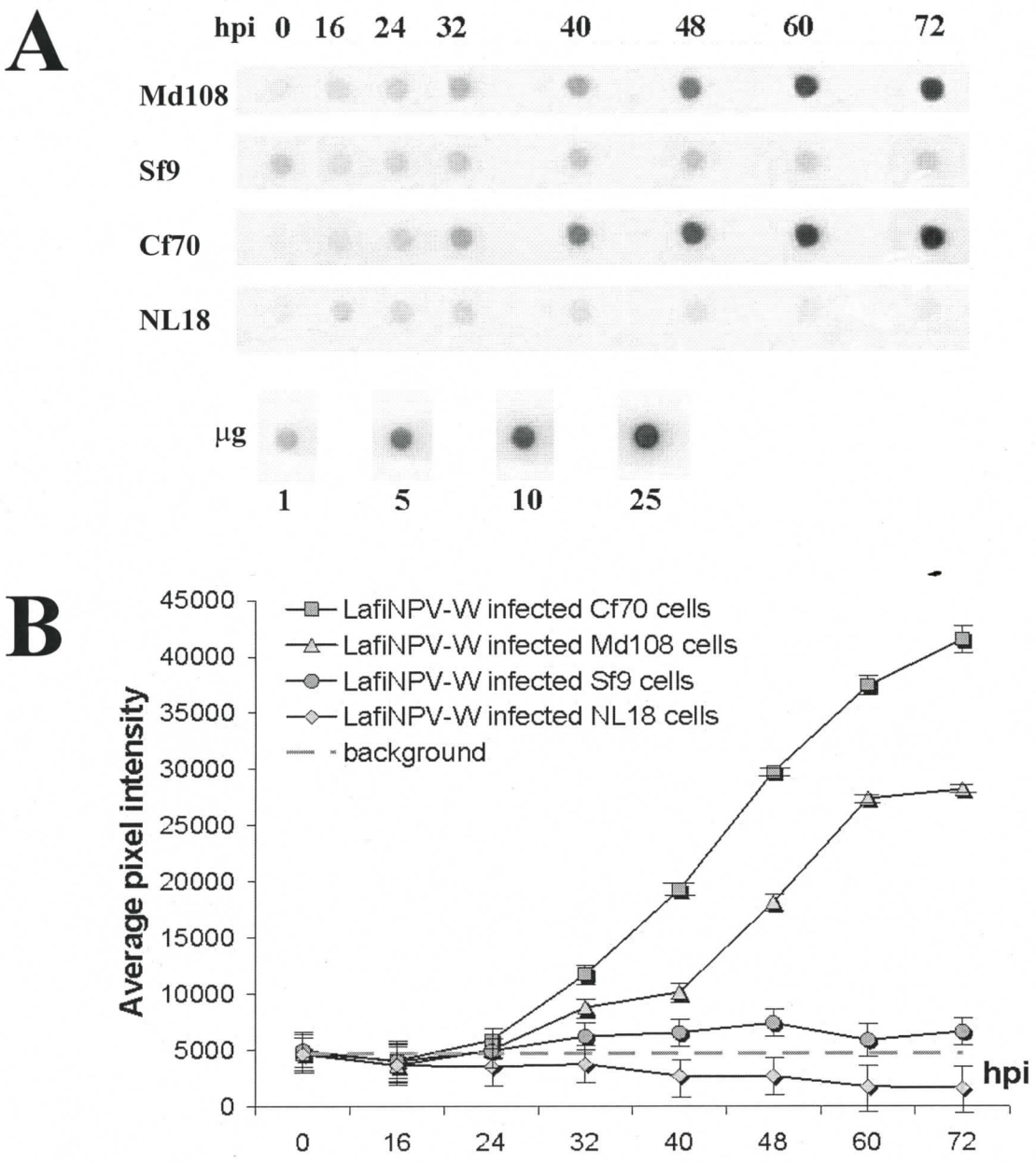

Figure 2-4. Replication kinetics of LafiNPV-W infection in various host cell lines over a 72 hour period.

A) Dot blot hybridization and **B)** replication kinetics of LafiNPV-W infected cell lines. Md108, Sf9, Cf70 and NL18 cell cultures were harvested at 0, 16, 24, 32, 40,48, 60, and 72 hours post inoculation (hpi). Hybridization intensities at each time point were plotted to determine the *in vitro* replication kinetics of LafiNPV-W infection in Md108 (▲), Sf9 (●), Cf70 (□), and NL18 (♦) cell lines.

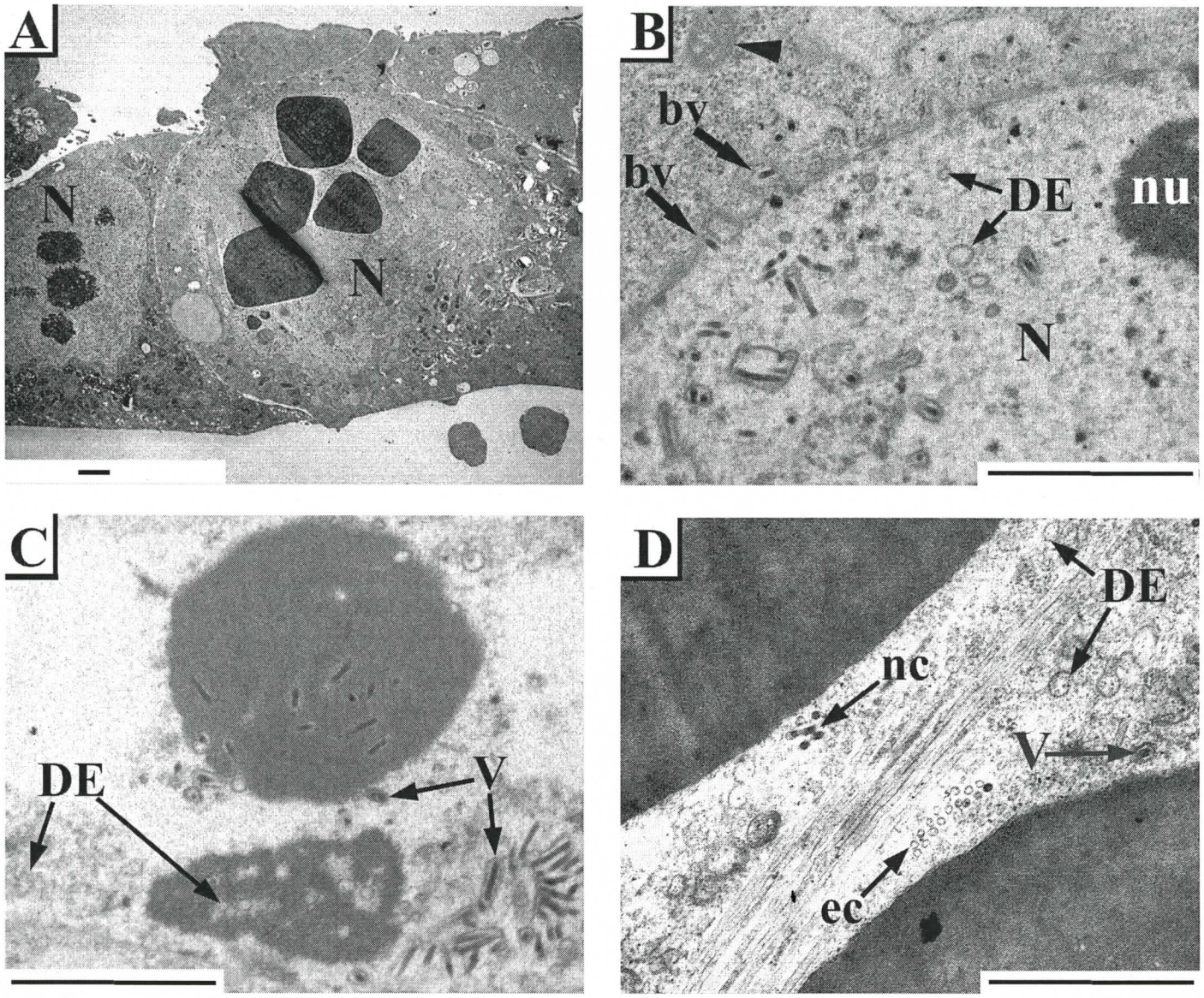
A
N
N
B
by
by
DE
nu
N
C
DE
V
D
DE
nc
V
ec

Figure 2-5. Electron micrographs of LafiNPV infected Md108 cells.

A) Whole cells with nuclei (N) containing icosahedral or cuboidal polyhedra at 72 hpi. **B**) Nucleus (N) of infected Md108 cell at 48 hpi, showing virions budding (bv) into cytoplasm. **C**) Virions (V) embedded within maturing isocahedral polyhedra and within peristromal space at 72 hpi. **D**) Virions (V), nucleocapsids (nc), *de novo* envelope (DE), and empty capsids (ec) associated with maturing cuboidal polyhedra at 72 hpi. Arrow head indicates mitochondria; nu, nucleolus. Scale bars represent 1 micron.

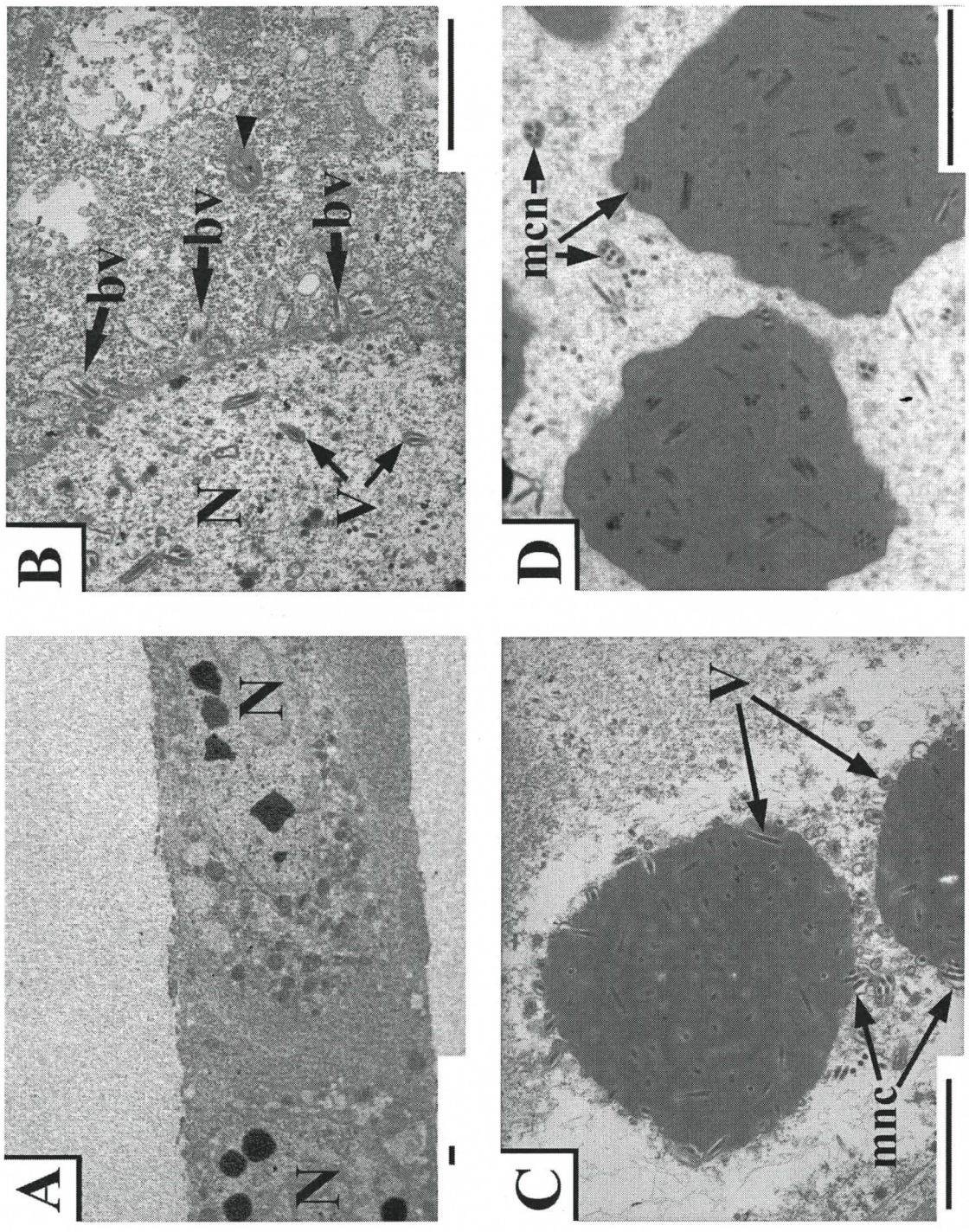
A
N
N
-
B
bv
bv
bv
N
V
V
C
V
mnc
D
mcn

Figure 2-6. Electron micrographs of LafiNPV infected Cf70 cells.

A) Whole cells with nuclei (N) containing icosahedral or cuboidal polyhedra at 72 hpi. **B**) Nucleus (N) of infected Cf70 cell at 48 hpi, showing virions budding (bv) into cytoplasm. **C**) Multinucleocapsids (mnc) and singly enveloped virions (V) embedded within maturing isocahedral polyhedra at 72 hpi. **D**) Multinucleocapsids (mnc) localized within the peristromal space and embedded within maturing cuboidal polyhedra at 72 hpi. Arrow head indicates mitochondria. Scale bars represent 1 micron.

structure of the polyhedrin matrix was highly organized and the occlusion bodies had smooth edges. Immature virions could be seen in the intranuclear spaces between the polyhedra, along with several empty-nucleocapsid structures lacking the electron dense core that are indicative of viral DNA. Although icosahedral polyhedra produced in Md108 cells exhibited embedded nucleocapsids within the polyhedrin matrix, they were few in number and many appeared to lack the bilayered envelope of mature virions.

The ultrastructural properties of Md108 derived polyhedra were different from those of derived from Cf70 cultures (Figure 2-6). LafiNPV-W PIBs produced in Cf70 cells contained a bilayered membrane, surrounding singly- or multiply enveloped nucleocapsids, which were embedded into both the cuboidal and icosahedral polyhedra. The polyhedrin matrix was less organized than those derived in the Md108 culture. At late phases within the viral life cycle, non-occluded virions were observed with a single membrane and could be seen budding from the nucleus. These virions were multiply and singly enveloped and exhibited the typical nucleocapsid structure. Once outside the nuclear membrane, budded viruses were released from vesicle-like structure into the cytoplasm. These virions maintained the envelope acquired within the nucleus.

Based on the differences in polyhedra structure, the virulence of the viruses derived from the two cell cultures was investigated through the use of bioassays. The mortality of *L. f. somniaria* inoculated with polyhedra derived from *L. f. fiscellaria* larvae ($5x10^4$-$5x10^6$ polyhedra ml^{-1}) was compared to the mortality induced by inoculation with polyhedra derived from Md108 ($5x10^5$ polyhedra ml^{-1}) and Cf70 cultures ($5x10^4$-$5x10^5$ polyhedra ml^{-1}). One hundred percent mortality was observed when larvae were inoculated with $5x10^6$ and $5x10^5$ polyhedra ml^{-1} of larval derived virus, and occurred

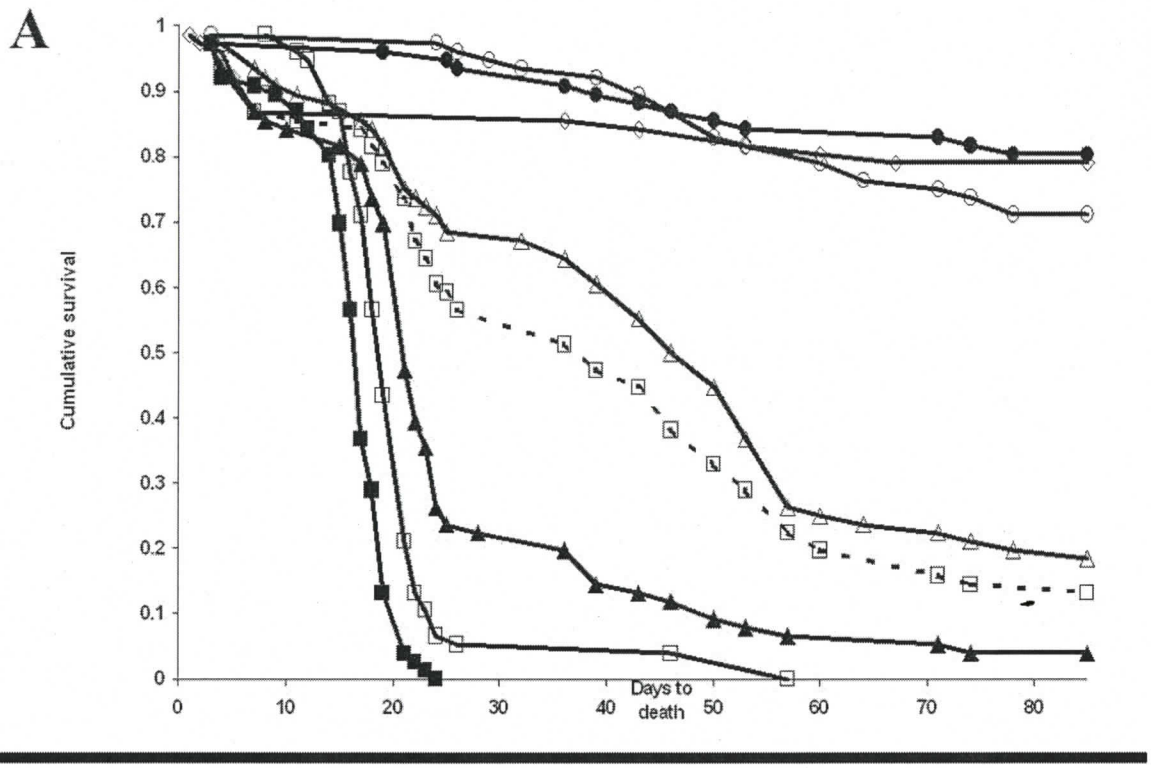
A
Cumulative survival
1
0.9
0.8
0.7
0.6
0.5
0.4
0.3
0.2
0.1
0
0
10
20
30
40
Days to death
50
60
70
80

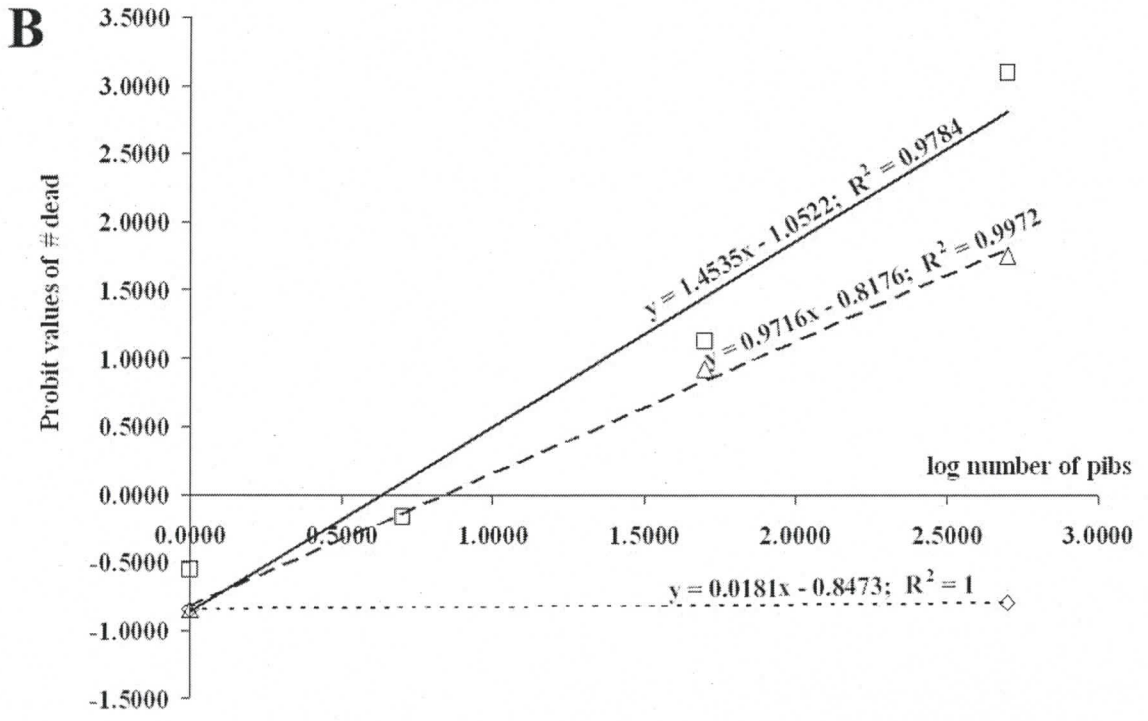
B
Probit values of # dead
3.5000
3.0000
2.5000
2.0000
1.5000
1.0000
0.5000
0.0000
-0.5000
-1.0000
-1.5000
0.0000
0.5000
1.0000
1.5000
2.0000
2.5000
3.0000
log number of pibs
y = 1.4535x - 1.0522; R² = 0.9784
y = 0.9716x - 0.8176; R² = 0.9972
y = 0.0181x - 0.8473; R² = 1

Figure 2-7. Kaplan-Meyer Survival Curve (A) and probit analysis of dose-mortality (B) of mock-infected and LafiNPV-W infected *L. f. somniaria* larvae.

Seventy-six larvae, in three replica sets, were inoculated *per os* for each treatments: three concentrations of polyhedra derived from *L. f. fiscellaria* larvae (larval), two concentrations of polyhedra obtained from the Md108 cell culture, or three concentrations of polyhedra obtained from the Cf70 cell culture. Legend (A): □ with dotted line =$5x10^4$ larval polyhedra ml^{-1}; □ with solid line =$5x10^5$ larval polyhedra ml^{-1}; ■ with solid line =$5x10^6$ larval polyhedra ml^{-1} ; ▲ with solid line =$5x10^5$ Cf70 polyhedra ml^{-1}; Δ with solid line =$5x10^4$ Cf70 polyhedra ml^{-1} ; ◊ with solid line =$5x10^5$ Md108 polyhedra ml^{-1}; • with solid line = no polyhedra, media only; ○ with solid line = no polyhedra, water only. Legend (B): □ larval polyhedra; Δ Cf50 polyhedra; ◊ Md108 polyhedra.

within 24 and 57 days post inoculation, respectively (Figure 2-7). At an inoculation dose of $5x10^4$ larval derived polyhedra ml^{-1}, 86% mortality was observed, which is comparable to the 82% mortality observed in larvae inoculated with $5x10^4$ Cf70 culture derived polyhedra ml^{-1}. There was no little difference in the mortalities of uninfected larvae (20%) and those infected with polyhedra derived from Md108 cells (23%). Probit (Figure 2-7) and Cox's proportional hazard (Table 2-2) analysis revealed that larval derived polyhedra were the most virulent, although infection from Cf70 derived polyhedra was also very lethal. The Cox proportional hazard rating, B value (Table 2-2), for Md108-derived occluded virus was lower than that of the untreated control group, which exhibited 28% mortality from inoculation with distilled water. These data support the ultrastructural findings that revealed the malformation of polyhedra from this source.

2.5 Discussion

Suspectibility of host insect larvae, or insect cell lines, to NPV infections has been characterized in many studies (Battu, 1986; Bonning *et al.*, 1995; Castro *et al.*, 1997; Huang *et al.*, 1999; Morris & Miller, 1993; Sohi & Cunningham, 1972; Tompkins *et al.*, 1981). A permissive host supports the efficient replication of viral DNA and the production/assembly of viable viral progeny, which allows for a broad range of pathologies. Some hosts have limited tissue tropisms or only a portion of their cell population that is susceptible to infection (Castro *et al.*, 1997; Washburn *et al.*, 2003), while other hosts are susceptible to an entire systemic infection (Castro *et al.*, 1997; Herz *et al.*, 2003). Hosts that support limited viral DNA replication with little to no infectious progeny are called semi-permissive, while hosts that fail to support viral DNA replication are non-permissive.

Table 2-2. Cox proportional hazard analysis of mock-infected and LafiNPV-W infected *Lambdina fiscellaria somniaria* larvae.

Larvae were feed polyhedra derived from *Lambdina fiscellaria fiscellaria* larvae, Md108 cell culture, or Cf70 cell culture and percent mortality and time to death were measured.

Variables in the Equation			
	Hazard Ratio	Standard Error	Significance
Between all Treatments			0.000
Media only	-0.395	0.335	0.238
Larval derived PIBs, 5000/larva	3.561	0.264	0.000
Larval derived PIBs, 500/larva	2.916	0.254	0.000
Larval derived PIBs, 50/larva	1.733	0.248	0.000
Md108 culture produced PIBs, 500/larva	-0.269	0.329	0.412
Cf70 culture produced PIBs, 500/larva	2.389	0.249	0.000
Cf70 culture produced PIBs, 50/larva	1.525	0.249	0.000

Two cell lines, isolated from *M. disstria* and *C. fumiferana*, were evaluated for their susceptibility to LafiNPV-W and were found to be fully permissive to the virus based on cytopathic effects, replication of viral DNA, and production of infectious progeny. Cell lines from *N. lecontei* and *S. frugiperda* were non-permissive to LafiNPV-W and no further characterization beyond the observed replication kinetics was performed.

The distinguishing differences between the two permissive cultures were the degree of susceptibility to infection and the assembly of infectious progeny into polyhedra. Both cell lines displayed characteristics typical of a productive infection, including nuclear hypertrophy and the presence of polyhedrin inclusion bodies (PIBs). The replication kinetics of the virus was similar in both cell lines, with DNA replication commencing marginally earlier in Md108 cells and stopping nearly 8 hours before the maximally yield was achieved in Cf70 cells. By 72 hpi, a greater amount of viral DNA was detected in Cf70 cells than Md108 cells, initially suggesting that virus replication was more efficient in former culture. However, when the higher titre of budded virus from Md108 cells is taken into account, the two cultures replicated LafiNPV-W with similar efficiency.

Pathology effecting cellular structures such as the actin cytoskeleton and nuclear morphology was studied to help determine the timing of infection within the two cultures. Both cultures exhibited rearrangements of their actin cytoskeletons during the infectious process. By 24 hpi LafiNPV-W infected Md108 and Cf70 cultures exhibited a loss of filopodia as the cells rounded and significantly reduction in the quantity of focal adhesions. Electron micrographs of virions budding from the nucleus suggest that temporally the virus is still in the replicative phase of infection in Cf70, supporting the findings of actin rearrangement. In *Autographa californica* nucleopolyhedrovirus

infection, actin transcripts are significantly reduced between 12-18 hpi, which corresponds to the onset of the late phase of the life-cycle, and suggests that rearrangement of the cytoskeleton is no longer required to support infection.

A significant increase in nuclear size of both infected cell lines was detected by DAPI labelling. The mixture of heterochromatin and euchromatin was altered leading to a more uniform staining of DNA throughout the nucleus. These results support the replication kinetics and electron micrographs, which show large quantities of virions being produced, since DAPI stains transcriptionally inactive DNA by binding within the minor groove.

The oral infectivity of the two different culture-derived LafiNPV-W polyhedra were significantly different in *L. f. somniaria* larvae. Electron microscopy of polyhedra cross-sections showed that many of the Md108 occlusion bodies lack embedded virions, resulting in low mortality of inoculated larvae. In contrast, polyhedra produced in Cf70 culture had numerous singly embedded virions and the mortality of larvae inoculated with these polyhedra was marginally, but not significantly lower than mortality observed from larval derived polyhedra. Along with interactions between viral proteins, host factors have been shown to influence the shape and size of the polyhedra assembled (Eason *et al.*, 1998), and possibly the process of embedding virions into the protein matrix. Larval derived polyhedra from *L. f. fiscellaria* have multiply embedded virions within their polyhedra (Cunningham, 1970a, b, 1971; Morris, 1962, 1964), which may explain the increased time and lower mortality from the singly embedded polyhedra that were propagated in Cf70 cells. Singly embedded nucleocapsids enter primary midgut tissue and replicate before establishing secondary sites of infection, while multiply

embedded nucleocapsids can be shuttled through the primary infected tissue and initiate secondary sites of infection before replication is completed (Morris & Miller, 1993; Washburn *et al.*, 2003). The delay in initiating infection at secondary foci allows for host responses that remove infected cells by encapsulation or sloughing of midgut epithelium (Washburn *et al.*, 2003), putatively reducing mortality.

Host factors are important in influencing every stage of the viral life-cycle. Restrictions to the successive viral phases inhibit disease progression and viral spread: blockage of early viral transcription prevents the replication the viral genome and allows cellular immune responses, such as apoptosis, can prevent lethal infections (Du & Thiem, 1997b). The inability of the virus to regulate host factors, such as Hsc70, may prevent the assembly of capsids (Nobiron *et al.*, 2003). Even at the very late stages of infection, after host transcription and protein synthesis have been shutdown, host factors are important for the proper assembly of occluded virus. These influences illustrate the need for careful selection of hosts in studying the infectious process and responses of host and virus.

Chapter 3 *In vitro* propagation and pathogenicity of *N. abietis* nucleopolyhedrovirus in heterologous insect cell lines

3.1 Abstract

This chapter documents the first published report of the propagation of *N. abietis* in an *in vitro* system. Several cell lines were examined for their ability to support a productive NeabNPV infection, but only a cell line derived from *Choristoneura fumiferana* (Cf70) was semipermissive to the virus. All other cultures were nonpermissive. Cytopathic effects were observed in Cf70 cells after transfection with NeabNPV DNA or infection of NeabNPV virions. Cytopathic effects included nuclear hypertrophy, rounding of the cells, and detachment from the substrate. NeabNPV was detected in both media and cells from infected cultures after several serial passages of the virus, by polymerase chain reaction (PCR) and Southern hybridization. Significant alterations to the actin cytoskeleton were observed, as well as an enlargement of nuclear size and changes to the euchromatin-heterochromatin content. Replication kinetics indicated that NeabNPV DNA was synthesized in Cf70 cultures, and transcriptional analysis by reverse transcription (RT) PCR determined that some key NeabNPV early genes (*Neab24* and *Neab52*) and replicative genes (*dnapol*, *lef-1*, and *lef-2*) were transcribed. NeabNPV infection, however, was aborted at the late phase of infection since no transcripts or peptides of the very late phase could be detected..

3.2 Introduction

The majority of knowledge about hymenopteran NPVs comes from ecological studies (Bird, 1955; Li, 2005; Moreau *et al.*, 2005) and sequence data (Duffy *et al.*, 2006; Garcia-Maruniak *et al.*, 2004; Lauzon *et al.*, 2006; Lauzon *et al.*, 2004). The NeabNPV

genome is one of the smallest baculoviruses sequenced to data, consisting of 84264 bp with a G-C content of 33.5% (Duffy *et al.*, 2006). Based on sequence analysis, ninety-three open reading frames (ORFs) are predicted, however no orthologues of known early expressed genes were found (Duffy, 2006). Along with the unusual nature of the predicted gene-expression, NeabNPV has 11 ORFs that are unique. These characteristics, along with the lack of knowledge about host-cell interactions, support the need for research into hymenopteran NPV pathology.

Traditionally, baculoviruses have been characterized by *in vitro* studies to determine their replication kinetics and pathology. The prototype NPV, *Autographa californica* (AcMNPV), has been studied extensively *in vitro*. Permissive cell lines, such as those originating from *Spodoptera frugiperda* (Sf9 and Sf21) and *Trichoplusia ni* (Tn5B1-4) (Bonning *et al.*, 1995), have been used to determine the function of essential viral genes (Bonning *et al.*, 1995; Gomi *et al.*, 1997; Hefferon & Miller, 2002; Lu & Miller, 1995b; Todd *et al.*, 1995) and the temporal expression of host and viral transcripts during infection (Morris & Miller, 1992, 1993; Ooi & Miller, 1988).

Expression of virally encoded genes occurs in a temporal cascade. Early genes of lepidopteran NPVs are transcribed upon entry of the viral DNA into the nucleus, which occurs prior to the onset of DNA replication (Hefferon & Miller, 2002). The products of early genes function as replicative and transcriptional machinery and regulators (Mikhailov & Rohrmann, 2002). Late genes are expressed following viral DNA replication and encode for structural proteins and transactivators of very late genes (Yang & Miller, 1998a, 1999). Expression of very late genes yields products involved in the

occlusion of the virions, which were assembled in the late phase, and virulence factors that aid in the dispersal of the virus.

A set of eighteen genes necessary to support DNA replication and progression to the late and very late phases of infection, were proposed by Todd *et al.* (1995) based on transient expression assays. Lu and Miller (1995) defined the roles of these 18 late expression factor (LEF) with respect to DNA replication and transcription. Nine of the LEFs are directly involved in viral replication; six genes are essential (*p143*, *dnapol*, *ie-1*, *lef-1*, *lef-2*, and *lef-3*) and three are stimulatory (*ie-2*, *p35* and *lef-7*). The other nine LEFs directly support the expression of late and very late genes (Lu & Miller, 1995b). A novel virally encoded RNA polymerase complex that transcribes late and very late genes is a hetero-tetramer, consisting of LEF-4, LEF-8, LEF-9, and P47 (Gross & Shuman, 1998). The remaining genes (*lef-5*, *lef-6*, *lef-10*, *lef-11*, and *pp31*) either act as transcription factors or function to stabilize late gene transcripts (Lu & Miller, 1995b). A tenth gene (*lef-12*) essential for late gene transcription was later discovered (Rapp *et al.*, 1998), increasing the number of genes necessary for supporting late gene expression to nineteen.

Prior to the cultivation of the *Neodiprion abietis* nucleopolyhedrovirus (NeabNPV) in the cultures studied in this experiment, an attempt was made to establish a cell culture derived from *N. abietis* larval midgut tissue. Although the tissue was successful isolated, natural gut flora with resistance to ampicillin and kanamycin, inhibited the culturing process. The differentiated state of the midgut tissue resulted in few epithelial cells that survived past the first three days post excision. These suriviving cells were quickly overcome by the antibiotic resistant bacteria. In addition, the observations that many of the midgut epithelial cells have free floating bacteria within their cytoplasm (see Chapter

4) and the quick demise of the tissue after use of antibiotics to control luminal floral populations may suggest that these bacteria have evolved a symbiotic relationship with the midgut epithelial cells and may play an important role in their survival.

This chapter presents the first known study of a hymenopteran NPV (NeabNPV) in an *in vitro* system. Few cell lines of derived from hymenopteran insects are available, necessitating the used of cultures from a closely related Diprionid, *Neodiprion lecontei*, and a lepidopteran (*Choristoneura fumiferana*) inhabiting the same geographic regions. Three *N. lecontei* (NL10, NL18, and NL28) and one *C. fumiferana* cell lines were investigated for their permissibility to NeabNPV. Only the lepidopteran cell line was semipermissive.

3.3 Materials and Methods

3.3.1 Virus Stocks:

The *Neodiprion abietis* nucleopolyhedrovirus (NeabNPV) was obtained from Dr. C. Lucarotti (Natural Resources Canada, Canadian Forest Services, Atlantic Forestry Center, Fredricton, New Brunswick, Canada) as a suspension of 5 X 10^9 polyhedra ml^{-1} in water. The virus was isolated from *N. abietis* larvae collected in 1997 between Stephenville and Corner Brook, Newfoundland, Canada. NeabNPV polyhedra were purified from field-collected NeabNPV-infected *N. abietis* larvae, according to the procedure outlined by Moreau *et al.* (2005) and is briefly described as follows. NeabNPV infected *N. abietis* larvae, frozen at -20°C, were homogenized in a 0.3% sodium dodecyl sulfate (SDS) solution. The homogenate was filtered twice through a 1 mm^2 plastic mesh and the resulting filtrate was collected. Any unfilterable insect matter was re-homogenized and refiltered until a clear filtrate was obtained. The filtered resuspension, containing

polyhedra, was centrifuged at 9000 x g for 15 minutes. The pellet of NeabNPV polyhedra was resuspended in 0.3% SDS, then re-centrifuged and resuspended until a clear supernatant was obtained. The final NeabNPV-polyhedra pellet was resuspended in water. Polyhedra were counted on a hemocytometer, and then concentrated to 5 X 10^9 polyhedra ml^{-1} (Moreau *et al.*, 2005).

Budded virus of the *Lambdina fiscellaria lugubrosa* nucleopolyhedrovirus (LafiNPV-W) was cultured as described in Chapter 2. This virus was used as a negative and positive control for determining actin rearrangement and changes to nuclear morphology in NeabNPV infected NL18 and Cf70 cultures, respectively (see Section 3.3.7).

3.3.2 Culturing of the Test Cell Lines:

Four insect cell lines were screened for their permissibility to the NeabNPV. These cultures included three embryonic tissue-culture isolates derived from a closely related hymenopteran *Neodiprion lecontei* (NL10, NL18, NL28), and a ovarian derived *Choristoneura fumiferana* cell line (Cf70), whose permissibility to a foreign NPV was investigated in Chapter 2.

The Cf70 and *N. lecontei* cell lines were obtained from Dr. S. Sohi of the Canadian Forest Services (Sault St. Marie, Ontario). The Cf70 and *N. lecontei* cell lines were propagated as described in Chapter 2 Section 2.3.2, with the additional *N. lecontei* cell lines being treated in the same manner as the NL18 cultures.

3.3.3 DNA Extraction of NeabNPV:

Purified NeabNPV DNA was obtained from Simon Duffy (University of Victoria, Victoria, BC, Canada). DNA was extracted from NeabNPV PIBs s described by Duffy *et al.* (2006). Briefly, a portion of the NeabNPV polyhedral suspension obtained from Dr.

C. Lucarotti was centrifuged at 15000 x g. The pellet was washed with sterile water and centrifuged at 15000 x g for 5 minutes at 20°C. The wash step was repeated three times. The final pellet was resuspended in 0.4% SDS and mixed for one hour at room temperature. The suspension was further washed and centrifuged at 15000 x g for 10 minutes at 20°C three times, then incubated in dissociation buffer (0.1M sodium carbonate; 0.04M sodium thioglycolate; pH 10.8) for 20 minutes. Insect debris and polyhedra were separated from the released virions by centrifugation at 2000 x g for 5 minutes at 4°C. The polyhedra and insect debris pellets were resuspended in fresh dissociation buffer and centrifuged until a pellet was no longer obtained. The supernatants were pooled and centrifuged at 15000 x g for 30 minutes at 4°C. The pelleted virions were resuspended in Tris-HCl (pH 7.5) and incubated for 16 hours at 50°C after the addition of proteinase K (Invitrogen) (0.01 mg ml^{-1}) and N-lauryl sarcosyl (2%). DNAzol (Invitrogen) was added to the proteased NeabNPV solution and DNA was extracted following the standard protocol of the manufacturer. DNA concentration was measured by absorbance at 260nm and the purity by the ratio of absorbance at 260nm to 280nm. Extracted DNA was used for transfection experiments and as positive NeabNPV DNA controls.

3.3.4 Transfection of NeabNPV into Insect Cells

NL10, NL18, NL28, and Cf70 cells (5 x 10^6) were plated separately into each well of four six-well plates. Cultures were incubated overnight in serum-containing media to ensure no contamination had occurred and to allow for cell recovery. All cell lines were transfected using Cellfectin transfection reagent (Invitrogen) as described in Chapter 2 Section 2.3.4 with the exception that Md108 cells were substituted for the *N. lecontei*

cells and NeabNPV DNA was used to transfect the cells as opposed to LafiNPV-W. All transfections were incubated at 27 °C until either cytopathic effects were observed, by light microscopy, or the untreated controls senesced.

3.3.5 Passage of Infectious Viral Media

Identical procedures were followed, as described in Chapter 2, Section 2.3.5, for the passage of viral laden media. Transfection media was removed from the each well and passed with fresh complete media onto freshly-plated cells. When cytopathic effects were observed, the new infectious media was harvested and overlain onto fresh cultures in TC-25 cm^2 flasks. The process was continued by passing 10% of the viral laden media for up to 6 serially passages. As a control, viral laden media was removed from cells within 12 hours post inoculation and fresh media was added. Cells that continued to exhibit cytopathic effects were analyzed by DNA methods and microscopic techniques. No further experiments were performed with cells that recovered and grew normally.

3.3.6 Confirmation of Viral Infection

Four methods were employed to confirm the presence of propagating virus: light and transmission electron microscopy, PCR amplification of the NeabNPV polyhedrin (*polh*) gene, and Southern hybridization of genomic NeabNPV.

3.3.6.1 Light Microscopy

NL18 and Cf70 cultures were monitored over several days for cells exhibiting characteristic cytopathic effects, using a Zeiss Axiovert microscope with at 200x magnification. Representative cells of the infected and uninfected NL18 and Cf70 cultures were selected and photographed using standard Kodak T-max 100 black and white film in an Olympus PM6 camera, at 100x magnification. Negatives were

digitalized using a Polaroid SprintScan35 scanner and Polaroid PolaColor Insight software (v.4.5.1). Scale bars were added to the digital images using Adobe Photoshop 5.

3.3.6.2 PCR Confirmation of Viral DNA

NeabNPV laden media was separated from NL18 and Cf70 cells by centrifuging the harvested cultures at 400 x g for 5 minutes, for both the transfected samples and cultures infected with the third passage of the virus. The extracellular virus was isolated by an additional centrifugation at 10,000 x g for 20 minutes. Viral DNA was extracted using standard organic extraction protocols (O'Reilly *et al.*, 1992). Total extracted DNA (50 ng) was used as a template for the amplification of the NeabNPV polyhedrin gene (*polh*) by PCR. NeabNPV *polh* forward and reverse primers were designed from sequence data obtained from a NeabNPV Hind III restriction nuclease Z fragment (5'–CAAACTCC GAAATCTACCCG–3') and p756R (5'–CCGTTTGTTAATGGACCAGG–3'), respectively (Young, 2002). Taq DNA polymerase (Invitrogen) was used following the manufacturer's protocols and under reaction conditions of an initial denaturation period of 4 minutes at 94 °C, followed by 35 cycles of denaturation (30 seconds, 94 °C), annealing (45 seconds, 55 °C), and elongation (45 seconds, 72 °C) periods. Half of the reaction volume was loaded onto a 0.8% agarose gel buffered with TBE (0.09 M Tris, 0.09 M boric acid, 0.002 M EDTA) and stained with ethidium bromide (0.25 ug ml^{-1}). The PCR products were imaged using an Eagle-eye II UV Transluminator System (Stratagene) with EagleSight Software (v.3.2). The gel image was cropped using Adobe Photoshop (v5.0.2).

3.3.6.3 Southern Hybridization of NeabNPV DNA in Cf70 Cultures

DNA from cells and infectious media of the fourth viral passage was extracted following the same method as in Section 2.3.8. Two micrograms (2 μg) of total DNA was applied to a nylon membrane, via a dot blot apparatus (BioRAD, Inc), then hybridized with a radio-labelled NeabNPV probe. Genomic NeabNPV DNA, originally extracted from PIBs (Section 3.3.3), was used as positive control markers (10 ng blotted) and also as the template for randomly amplifying the (α-^{32}P)-dCTP radio-labelled probes, which were then hybridized (0.75 M sodium chloride, 0.075 M sodium citrate, 0.5% SDS, 0.1% Ficoll 400, 0.1% polyvinylpyrrolidone, 0.1% bovine serum albumin, 1mg ml^{-1} sonicated salmon sperm DNA) to the membrane-bound DNA of cellular and media extracts at 56°C, overnight. Hybridization was followed by three 20-minute incubations in wash buffer (0.15 M sodium chloride, 0.015 M sodium citrate, and 0.1% SDS). Images of the Southern dot blot were obtained using the Molecular Dynamics Storm 860 Scanning system with ImageQuant 5 Software.

3.3.6.4 Electron Microscopy

Cf70 cells were fixed in 25 cm^2 tissue culture flasks (Sarstedt) with 4% gluteraldehyde in a 0.1 M sodium cacodylate buffer. Post-fixation was undertaken in the flask with 2% osmium tetroxide in 0.1 M sodium cacodylate buffer, prior to mechanically harvesting the cells, centrifuging at 400 x g and resuspending in a 5x volume of 10% agar. The agar blocks of samples were cubed and dehydrated, using increasing concentrations of ethanol and propylene oxide, then incubated in a 1:1 propylene oxide and Epon resin solution, at room temperature overnight. The Epon penetrated samples were then embedded within Epon resin and incubated at 65°C for 48 hours. The resulting blocks were sectioned on a

Reichart ultra-microtome and 70 nm sections were stained with uranyl acetate (5%) and lead citrate (5%) before viewing on a Hitachi H7000 Transmission Electron microscope, using a 75 kV beam. Electron micrographs were imaged on Kodak 4489 Electron microscope film and digitalized by scanning the negatives with a Polariod SprintScan45 Scanner and Polaroid PolaColor Insight software (v.4.5.1). Scale bars were added to the digital images using Adobe Photoshop 5.

3.3.7 Epifluorescent Characterization of Actin and Nuclear Structure

Due to the lack of available NeabNPV specific antibodies, the pathological effects of NeabNPV on actin and nuclear structures within NL18 and Cf70 cells were examined. Each cell line was either mock-infected or infected with either NeabNPV or LafiNPV-W according to the procedure described in Chapter 2 Section 2.3.9.

3.3.8 Titration of NeabNPV Stock by an End-Point Dilution Method

NeabNPV stock was titred in CF70 cells following the procedure listed in Chapter 2 Section 2.3.7. The cultures were observed until nuclear hypertrophy was visualized and the mock infected control cultures died. The 50% end-point was calculated using the Reed and Muensch formula.

3.3.9 Replication Kinetics of LafiNPV-W and Host Specificity

The replication kinetics of NeabNPV in Cf70 cells was determined using the methodology described in Chapter 2 Section 2.3.8. Cultures were harvested from 0-120 hpi, at 6 hour intervals. Once all the samples were harvested, the cells were pelleted and total DNA was extracted using TRIzol (Invitrogen), following the manufacturer's instructions. Using spectrophotometry, the concentration of each DNA extract was calculated. Based on the sample with lowest yield of extracted DNA, two micrograms (2

μg) of total DNA from each time interval was applied to a nylon membrane, using a dot blot apparatus (BioRAD), then hybridized with a (α-^{32}P)-dCTP-radio-labelled NeabNPV probe, overnight at 56°C, according to the procedures mentioned in Section 2.3.8. Membranes were washed for three-20 minute periods in 0.15 M sodium chloride, 0.015 M sodium citrate, and 0.1% SDS. Images of the Southern dot blot were obtained using the Molecular Dynamics Storm 860 Scanning system with ImageQuant 5 Software.

3.3.10 RNA Reverse Transcription PCR NeabNPV-infected Cf70 Cells

RNA was extracted from samples obtained from the replication kinetics (Section 3.3.8) using TRIzol (Invitrogen) and following the manufacturer's procedures. The samples were treated with 3 U of DNAse (Invitrogen) in PCR buffer solution (20 mM Tris-Cl, pH 8.4; 50 mM KCl; 2 mM $MgCl_2$) for 15 minutes at room temperature. The reaction was terminated by the addition of EDTA (2.5 mM) and incubated at 65°C for 10 minutes. Synthesis of the first strand of the cDNA was performed by incubating 500 ng DNAse-treated total RNA with 200 U Superscript II Reverse Transcriptase in 20 μl reaction mixture (50 mM KCl; 25 mM Tris-HCl, pH 8.3; 500 μM dNTP; 10 μM DTT; 10 U RNAse Inhibitor) at 25°C for 10 minutes. The reaction was then incubated at 42°C for 50 minutes and inactivated by an additional incubation at 70°C for 15 minutes.

PCR amplification was undertaken on cDNA templates of mock-infected Cf70 cells, along with 6, 12, and 18 hpi time-point samples, using NeabNPV specific primers (Table 3-1). Amplification reactions yielded products 150-250 base pairs (bp) in length and were representative of temporal standards for immediate early (*Neab24* and *Neab52*), early (*dnapol*, *lef-1*, and *lef-2*), late (*gp41* and *vlf-1*) and very late (*p74* and *polh*) genes. NeabNPV genomic DNA, extracted from PIBs, was used as the positive control template,

while a nuclease-free-water negative control was included in each PCR set. Amplification of the *28S* rRNA host gene ensured the integrity of the cDNA. Templates were diluted 10-fold and amplified with Platinum Taq DNA polymerase (Invitrogen), following the manufacturer's protocol. Reaction conditions included a hot-start cycle of 95°C (9 minutes), followed by 45 cycles of 95°C (30 seconds), 55°C (60 seconds), and 72°C (90 seconds). All products were resolved by electrophoresis in 2% agarose gel and stained with SYBR Green (Molecular Probes). Each PCR reaction was repeated three times for cDNAs extracted from three different tissue culture samples at each time point.

3.4 Results

N. lecontei cell line isolates, NL10 and NL28, showed little cytopathic effects from the transfection of NeabNPV. NL10 cells rounded slightly but the culture continued to grow as per the untreated control. NL28 cells rounded, detached from the culturing substrate, and lysed within 6 days post transfection. The untreated and Cellfectin-reagent treated NL28 cultures grew to 100% confluency. Passage of media from transfected NL28 cells resulted in similar cytopathic effects within 12 hours. However, upon removal of the spent media and replacement with fresh complete media, the NeabNPV-infected NL28 cells recovered and grew to 100% confluency. The cytopathic effects were likely due to necrosis since changes to media pH and nutrient depletion caused similar effects in untreated cultures. NL10 and NL28 cells were not used for further experiments.

Table 3-1. Primers used in reverse transcription PCR of RNA extracted from NeabNPV-infected Cf70 cells.

Target Gene	Amplicon size	Forward Primer Sequence (5' to 3')*	Reverse Primer Sequence (5' to 3')*
28S rDNA	153 bp	AAAGATCGAATGGGGAGATTCATC	CGTCCTACTAGGGGAGAAGTGCAC
Neab ORF24	195 bp	GCCCACGGCGTAGTGTGTTGT	GGGCCATGATATGTCGGCA
Neab ORF52	195 bp	CGCGTTTTGAACGTCATCGTCA	ACGGTTTTTCTTTCGTATGCGTTCT
lef-1	223 bp	GCGATGCAACCGACGACGATA	TTGTATTGCGCTTCGTCAATTTTG
le-f2	259 bp	ATGGATAAATGCAAATACGTCAAAA	CGGCGGTCCTTGTTGTTGATC
dnapol	218 bp	CAGCGCACAGTGGACGTGGTT	GCCGTTTGGGAAATTGTTGCA
gp41	206 bp	TCCATTCCGTTGAGCGCAAAA	TCGCGCTCTTGTTCGATTATCC
p74	320 bp	GAATTCGCACCACCGAAGCCACCGT	CTGCAGGGCGGTTGCCCATTCA
vlf-1	216 bp	GGGGTGTACGAATTCGCCATC	CAAAATTTCTTTCCGTCAAAACGTT
polh	176 bp	GCAGGTTATCAAACCTCGGCC	GGACCCGTTCGTGGGTCCAAC

*Primer sequences reported by Duffy (2006)

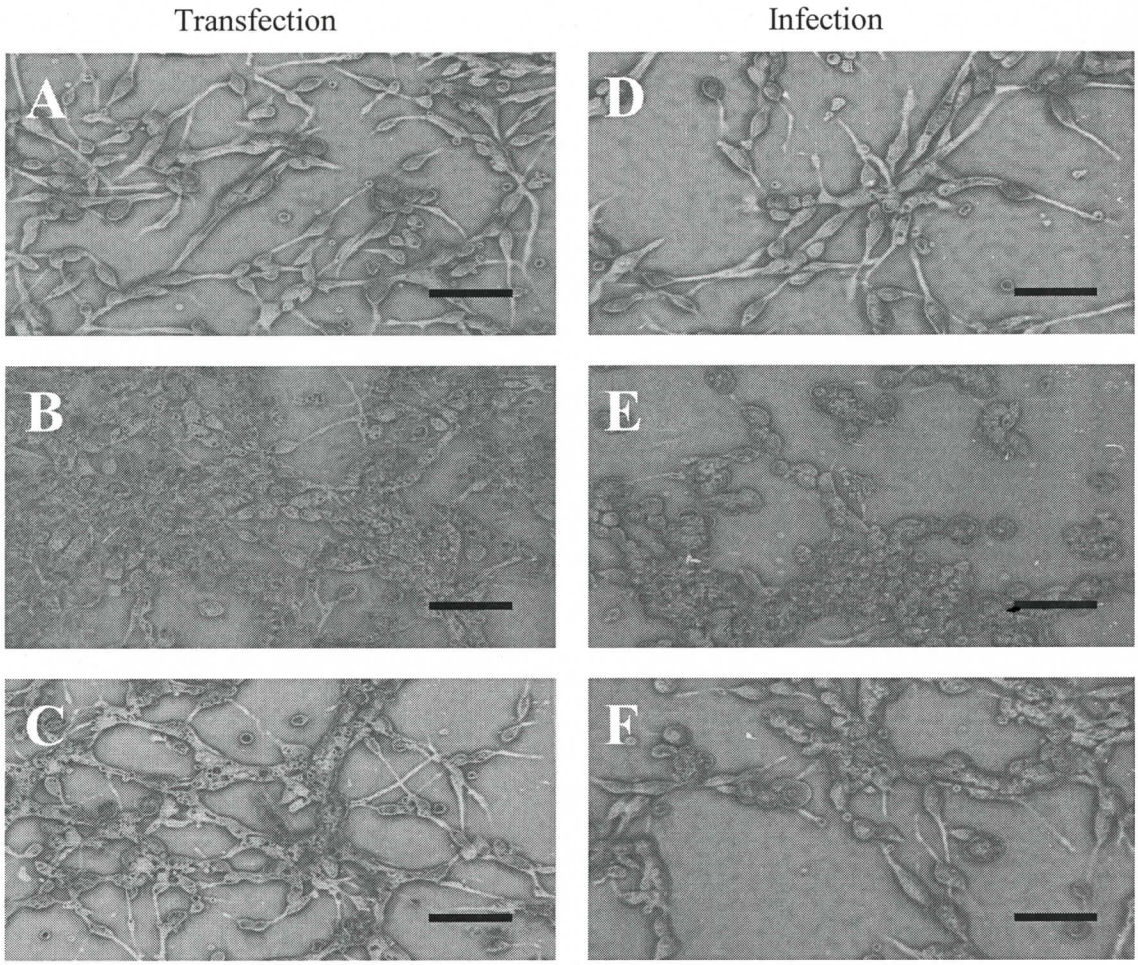

Figure 3-1. Light micrographs of NL18 cultures, after which transfection or infection with NeabNPV.

A) Untreated NL18 control cell of transfection; B) NeabNPV transfected NL18 cells, Day 4; C) NeabNPV transfected NL18 cells, Day 6; D) Mock-infected NL18 cells; E) NeabNPV infected NL18 cells, Day 4; F) NeabNPV infected NL18 cells, Day 6. Scale bars = 40 microns

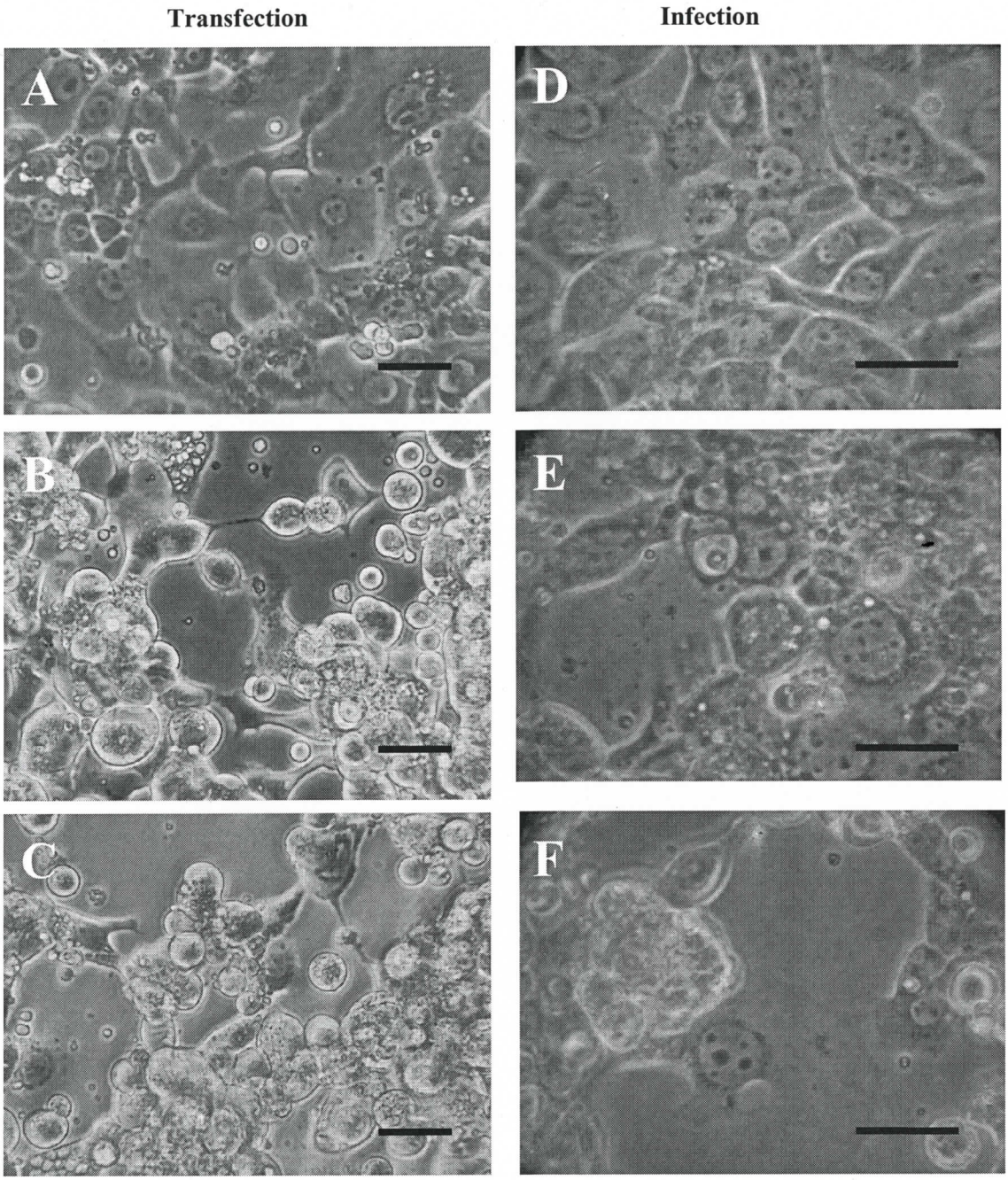

Figure 3-2. Light micrographs of Cf70 cultures, after transfection or infection with NeabNPV.

A) Untreated CF70 control cells of transfection; B) NeabNPV transfected CF70 cells, Day 4; C) NeabNPV transfected CF70 cells, Day 6; D) Mock-infected CF70 cells; E) NeabNPV infected CF70 cells, Day 4; F) NeabNPV infected CF70 cells, Day 6. Scale bars = 40 microns

The third *N. lecontei* (NL18) and the *Choristoneura fumiferana* (Cf70) cell lines exhibited similar cytopathic effects to the NL28 cells from transfection with NeabNPV. Within four days post transfection, the cells of both cultures rounded, aggregated together and detached from the substrate (Figure 3-1 A-C and Figure 3-2 A-C), and by day 6 the cells had vesicles and started to lyse. Cytopathic effects were observed for 3 subsequent passages (Figure 3-1 D-F and Figure 3-2 D-F) of the infectious media onto fresh NL18 and Cf70 cultures, even when the spent media was replace by fresh complete media after a 12 hpi incubation period . After the third passage of the infectious media, cytopathic effects took longer to appear in NL18 cells and by the sixth passage no effects were observed. Cf70 cells continued to exhibit cytopathic effects, including nuclear and cellular hypertrophy, until the sixth passage.

PCR amplification products of the NeabNPV *polh* gene were detected in total DNA extracted from both media and cells of transfected NL18 and Cf70 cultures (Figure 3-3). The infected Cf70 cultures, at the third viral passage, also yielded *polh* PCR amplicons from both cellular and extracellular DNA extracts, while *polh* amplicons were only detected in cellular extracts of the infected NL18 culture, at the same viral passage.

Southern hybridization of NeabNPV infected NL18 and Cf70 cultures revealed similar findings. Cellular and media extracts of Cf70 cultures hybridized with the radio-labelled NeabNPV-genomic probe at pass 4 of the viral laden media (Figure 3-4). No viral DNA was detected from NL18 cultures at pass 4 of the virus (blot not shown).

Transmission electron microscopy failed to reveal any viral structures in NeabNPV infected Cf70 cells, such as virogenic stroma, virions or polyhedra. Nuclei were rounded and small vesicles were abundant within the cytosol. The chromatin condensed into

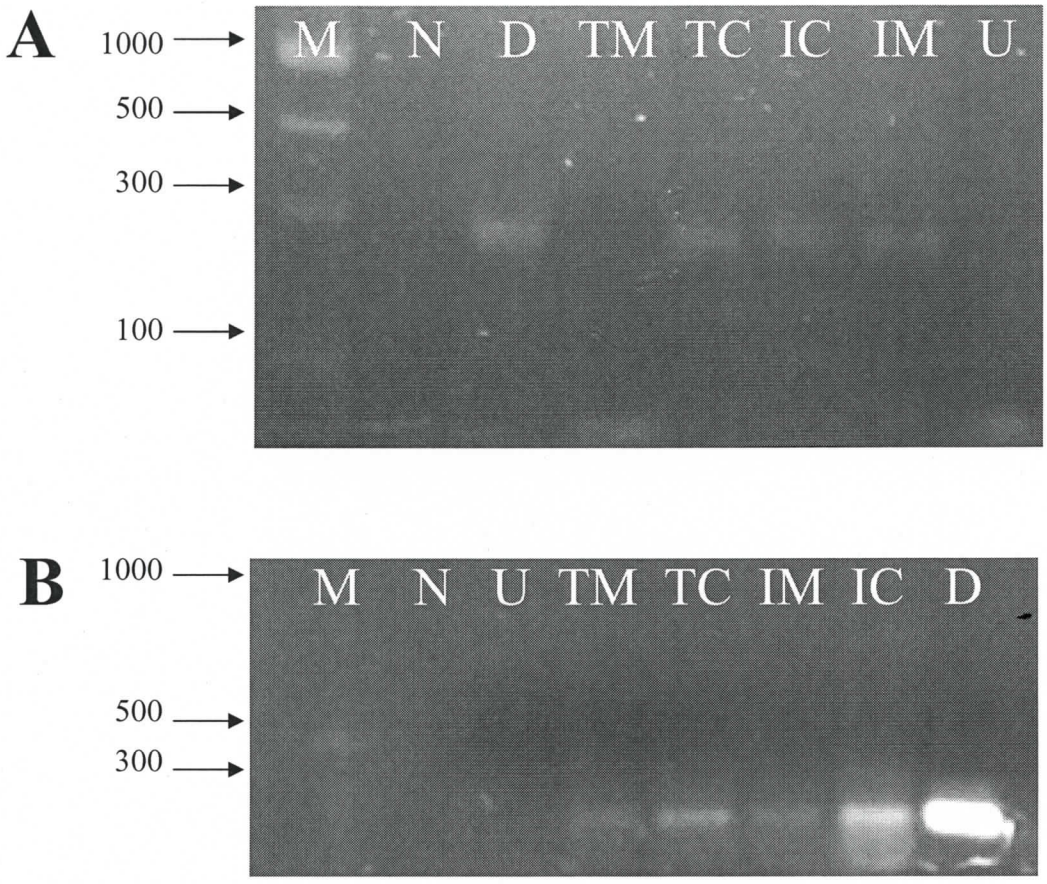

Figure 3-3. Gel electrophoresis of PCR products of the NeabNPV polyhedrin (*polh*) gene amplified from NL18 (A) and Cf70 (B) cultures.

D, NeabNPV DNA extracted from polyhedra; IC, total DNA extracted from infected cells; IM, total DNA extracted from the media of infected cells; M, molecular weight marker; N, no template control; TC, total DNA extracted from transfected cells; TM, total DNA extracted from the media of transfected cells; U, total DNA extracted from uninfected cells

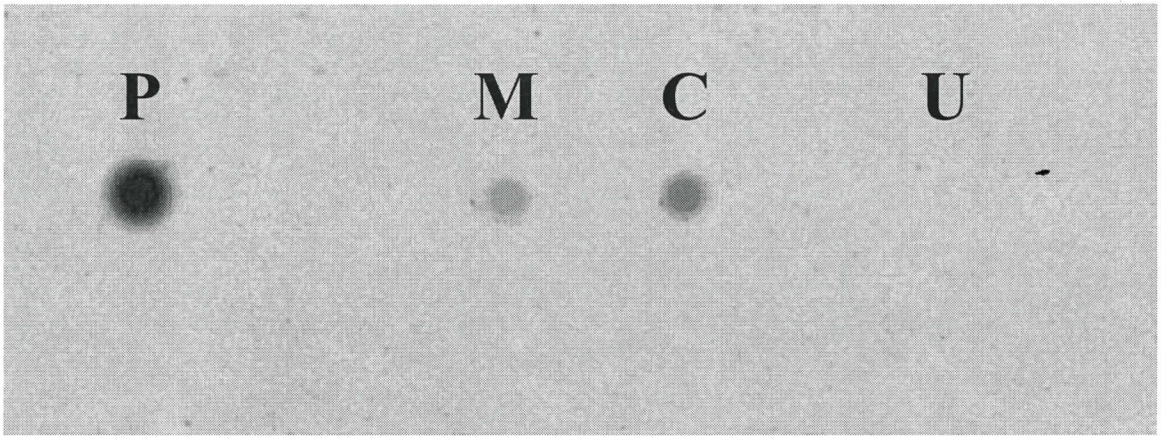

Figure 3-4. Southern blot analysis of NeabNPV infected Cf70 culture.
P, 10 ng of NeabNPV DNA extracted from larval derived polyhedra; M, total DNA extracted from media of infected Cf70 cells inoculated with fourth passage NeabNPV; C, total DNA extracted from infected Cf70 cells inoculated with fourth passage NeabNPV; U, total DNA extracted from uninfected Cf70 cells.

electron dense patches, which were localized to the nuclear periphery (micrographs not shown).

Cytopathic effects induced by NeabNPV infection were further investigated in NL18 and Cf70 cell lines. The NPV of *Lambdina fiscellaria fiscellaria* (LafiNPV-W) was used as a negative and positive control for measuring changes induced by NeabNPV infection in the two test cell lines, respectively. These cells were previously shown to be non- (NL18) and full (Cf70) permissive to LafiNPV-W by host specificity and replication kinetics assays (Chapter 2).

The number of focal adhesions and filopodia were measured by labelling permeated and formaldehyde-fixed cultures with rhodamine-phalloidin, while nuclear size and euchromatin/heterochromatin distribution were determined from DAPI-labelled DNA (Figure 3-5 and Table 3-2). No significant differences between mock- and NeabNPV-infected NL18 cells were observed with regards to any of the investigated traits (Figure 3-5 and Table 3-2). The negative control, LafiNPV-W infected NL18 cells, exhibited more changes to actin structure than NeabNPV-infected cells did. The mean number of focal adhesions decreased in LafiNPV-W infected NL18 cells (3.62 focal adhesions per cell), but increased in the NeabNPV infected culture (11.3 focal adhesions per cell), when compared to the untreated control sample (8.95 focal adhesions per cell). A similar trend was observed for the number of filopodia, which were decreased significantly in LafiNPV-W infected NL18 cells (0.37 filopodia per cell) and marginally in NeabNPV infected culture (2.5 filopodia per cell) compared to the untreated sample (2.68 filopodia per cell). No significant difference was observed in nuclear size between any of the

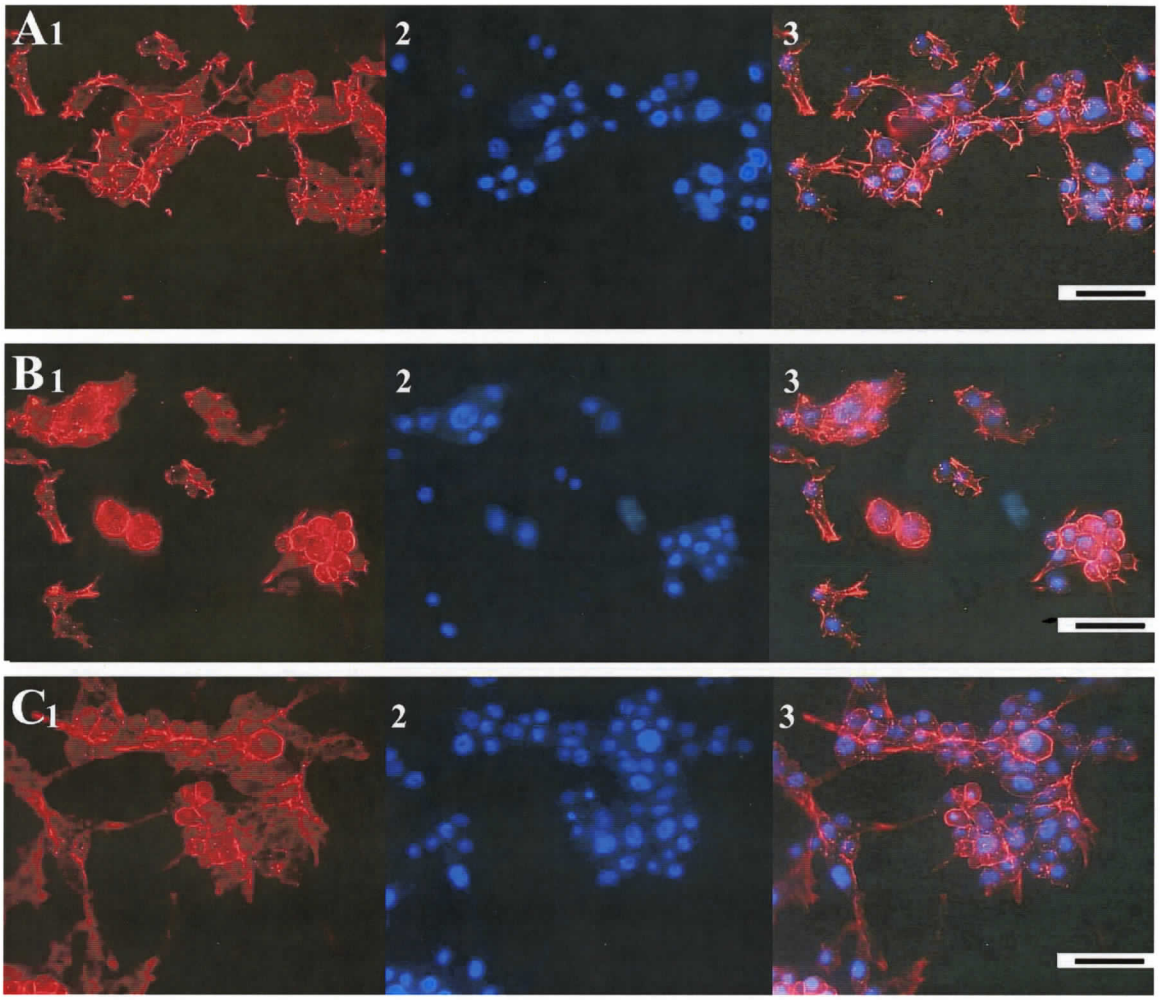

Figure 3-5. Epifluorescent micrographs of mock, NeabNPV, and LafiNPV-W infected *N. lecontei* cells at 24 hours post-inoculation.

Mock infected (A), NeabNPV infected (B) ,and LafiNPV-W infected (C) NL18 cultures, respectively, were imaged at 24 hours post inoculation using a Zeiss Universal Epifluorescent Upright microscope. Actin cytoskeletons (first image of each plate) were stained with Rhodamine-phalloidin and nuclei (second image of each plate) were labelled with DAPI. The third image of each plate represents an overlay of the labelled nuclei upon the cytoskeleton. Scale bars = 40 μm.

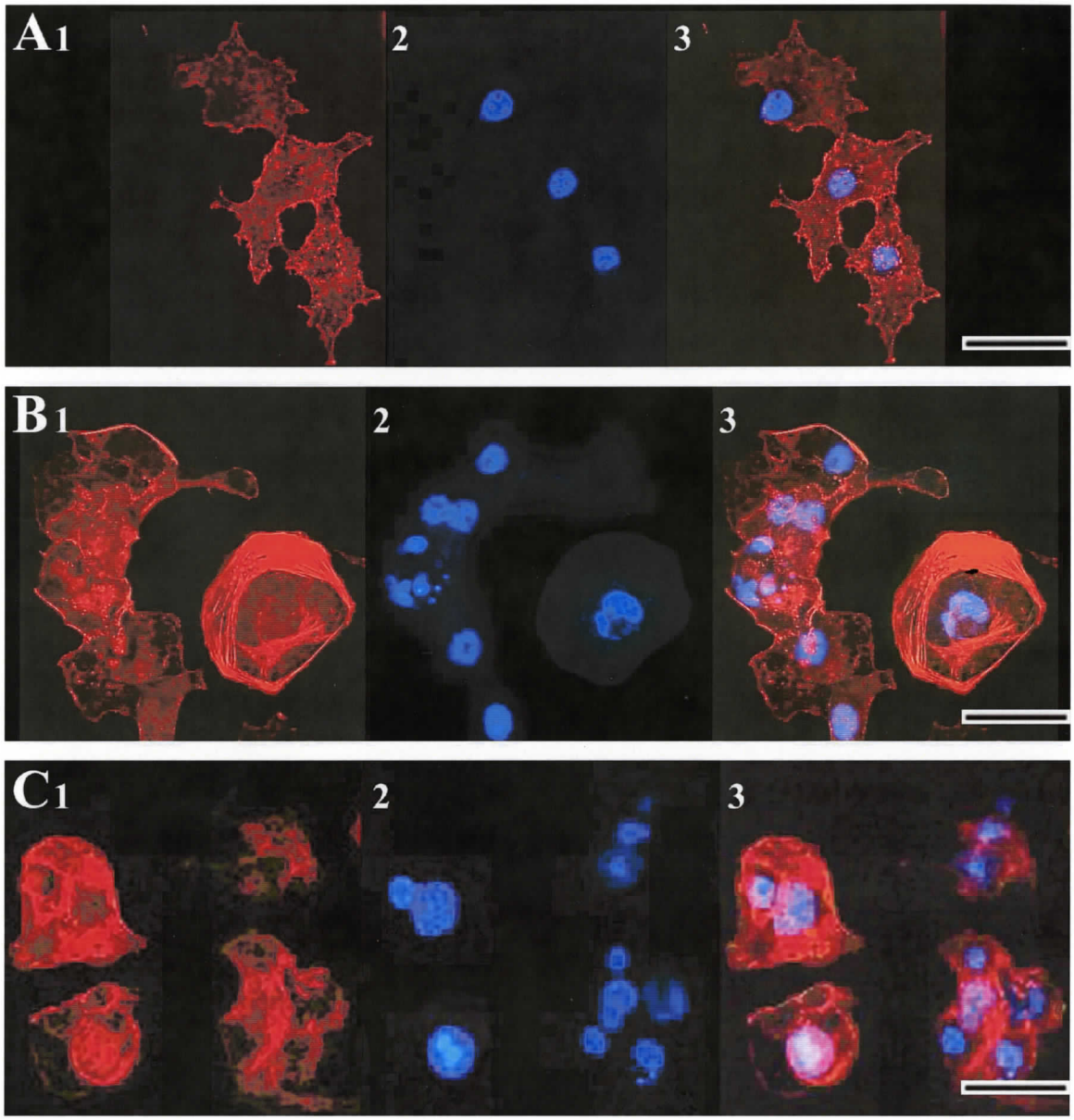

Figure 3-6. Epifluorescent micrographs of mock, NeabNPV, and LafiNPV-W infected *C. fumiferana* cells at 24 hours post-inoculation.

Mock infected (A), NeabNPV infected (B) ,and LafiNPV-W infected (C) Cf70 cultures, respectively, were imaged at 24 hours post inoculation using a Zeiss Universal Epifluorescent Upright microscope. Actin cytoskeletons (first image of each plate) were stained with Rhodamine-phalloidin and nuclei (second image of each plate) were labelled with DAPI. The third image of each plate represents an overlay of the labelled nuclei upon the cytoskeleton. Scale bar = 40 μm.

.

Table 3-2. Observed traits of mock, NeabNPV, and LafiNPV-W infected *N. lecontei* and *C. fumiferana* cells.

Cultures were incubated for 24 hours prior to cellular structures being imaged and measured using ScionImage software. Dunn's multiple comparison tests was performed for each data set.

Observed traits	Group	Number of points analysed	Mean	Median	Minimum	Maximum	*P-value of uninfected and infected	*P-value of viral treatments
Focal Adhesions	CF70 Uninfected	34.00	24.59	24	19	33	<0.001	>0.05
	CF70 NeabNPV	42.00	4.00	3	0	15	<0.001	
	CF70 LafiNPV-W	39.00	1.62	0	0	8		
	NL18 Uninfected	37.00	8.95	8	3	21	>0.05	<0.001
	NL18 NeabNPV	40.00	11.30	7	3	30	<0.001	
	NL18 LafiNPV-W	60.00	3.62	3	0	8		
Filopodia	CF70 Uninfected	34.00	27.76	27	12	60	<0.001	>0.05
	CF70 NeabNPV	42.00	1.76	1	0	9	<0.001	
	CF70 LafiNPV-W	42.00	6.50	1	0	56		
	NL18 Uninfected	37.00	2.68	2	0	14	>0.05	<0.001
	NL18 NeabNPV	40.00	2.50	2	0	6	<0.001	
	NL18 LafiNPV-W	60.00	0.37	0	0	4		
Nuclear Size†	CF70 Uninfected	51.00	0.55	0.55	0.49	0.63	<0.001	>0.05
	CF70 NeabNPV	52.00	0.70	0.73	0.40	0.92	<0.001	
	CF70 LafiNPV-W	48.00	0.73	0.69	0.22	1.11		
	NL18 Uninfected	68.00	0.30	0.29	0.13	0.53	>0.05	>0.05
	NL18 NeabNPV	40.00	0.33	0.29	0.23	0.60	>0.05	
	NL18 LafiNPV-W	78.00	0.28	0.27	0.11	0.48		

† Nuclear size measured in inches from 72 pixels/inch digital images at 200x magnification

* Dunn's Multiple Comparisons Test

treatments for NL18 cells. All nuclei stained uniformly with DAPI, therefore observation of the distribution of euchromatin and heterochromatin was not possible.

Infection of Cf70 cells by NeabNPV and LafiNPV-W induced significant changes to both actin structure phenotypes (Figure 3-6, Table 3-2) with large reductions of both the number of focal adhesions (NeabNPV 4.0 focal adhesions per cell; LafiNPV-W 1.62 focal adhesions per cell) and filopodia (NeabNPV 1.76 filopodia per cell; LafiNPV-W 6.50 filopodia per cell). The size of the nucleus increased significantly upon infection by either virus. The staining pattern of DAPI changed from an equal mix of euchromatin and heterochromatin (Figure 3-6) to either weak staining throughout the nucleus with concentrated spots at the nuclear periphery or intense staining at the center of the nucleus. Clusters of very small nuclei or fragmenting nuclei were observed in NeabNPV-infected cells, indicating either overlapping cells or possibly apoptosis. The exact nature of these nuclei was not determined. There was no significant difference observed between the two virally treated cultures for any of the traits investigated, indicating that pathology was progressing in a similar manner.

Based on the inability to detect viral DNA from cells or media, at the fourth passage of the virus, and the insignificant changes to actin structures and nuclear morphology, the NL18 cell line was not used to determine replication kinetics or to amplify viral transcripts. A titre of 6.6×10^5 plaque forming units (pfu) ml^{-1} of spent media was obtained, such that Cf70 cells could be inoculated at a 5x multiplicity of infection (MOI) for the replication kinetics assay. NeabNPV-infected cells were harvested every 6 hours as the LafiNPV-W replication kinetics assay indicated that DNA synthesis did not occur until later time points (Chapter 2) and the cytopathic effects observed in NeabNPV-

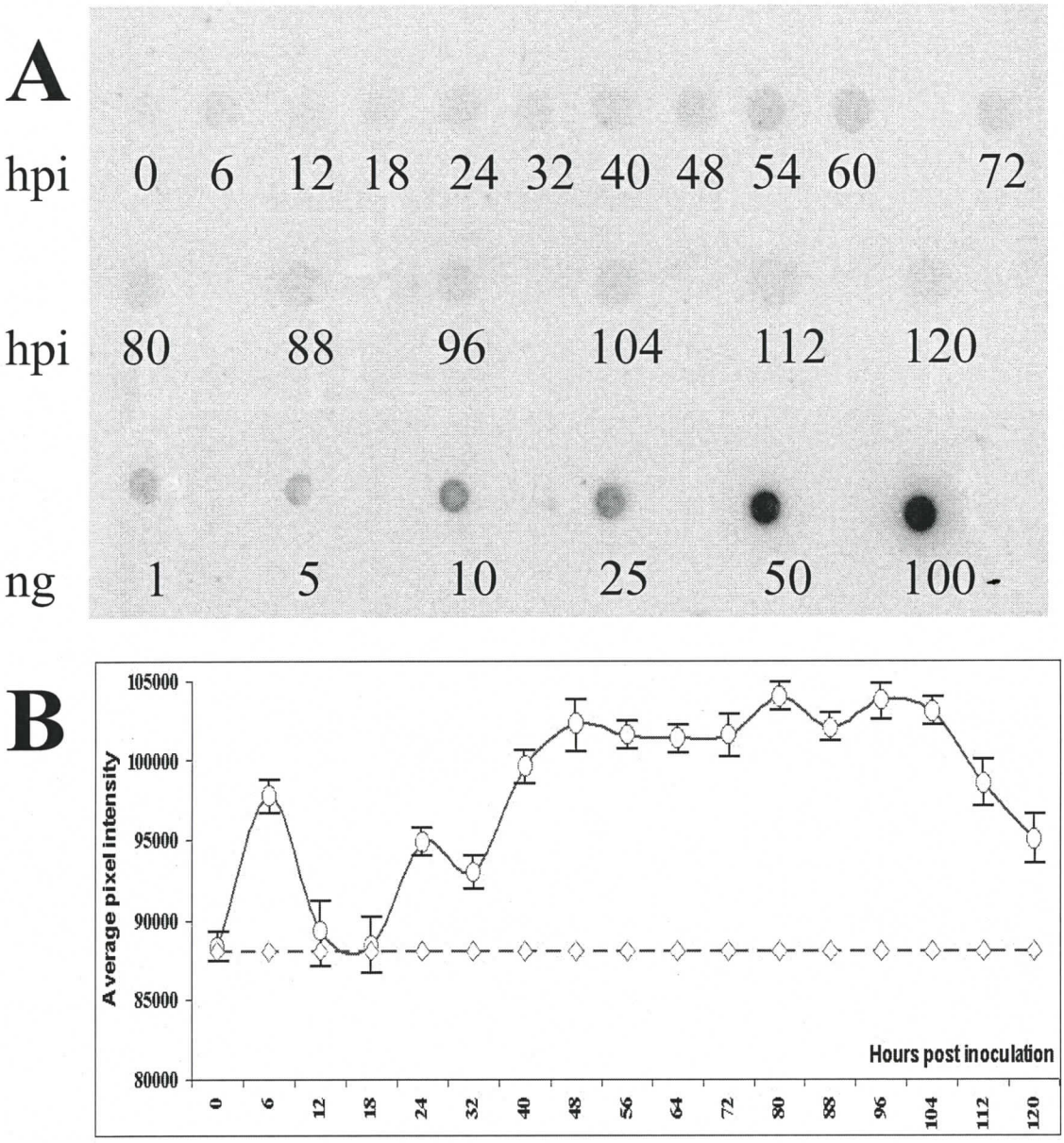

Figure 3-7. Replication kinetics of NeabNPV in Cf70 cells.

Cultures were harvested at 6 hour intervals between 0 and 24 hpi and at 8 hours intervals after 24 hpi, until120 hpi. A) Southern hybridization analysis of NeabNPV infected Cf70 cells. Genomic NeabNPV DNA, extracted from *N. abietis* larval derived polyhedra, was used as positive controls of hybridization and quantity indicators. B) Graphical representation of the replication kinetics of NeabNPV based on nanogram quantities of NeabNPV DNA, which were calculated from hybridization intensities, and plotted time points. ○ = NeabNPV infected Cf70 cells; ◊ = uninfected Cf70 cells (background)

infected Cf70 cells seemed to mimic those of CF70 cells infected with LafiNPV-W. An increased amount of NeabNPV DNA was observed within the first 6 hours of infection (Figure 3-7), thereafter the quantity fell to nearly the background level observed in cells infected and harvested at time zero (0). Another sharp increase in the amount of NeabNPV DNA detected was observed at 24 hours hpi, followed again by a reduction in the quantity of DNA detected. The nearly 24-hour cycle of increasing and decreasing quantities of NeabNPV DNA continued until 48 hpi, when a pseudo-steady state level was established and remained at this level until 104 hpi. Between 104 and 120 hpi, the amount of detectable NeabNPV DNA had reduced to half the amount established at 48 hpi.

Finally, viral transcripts were analyzed by Reverse Transcription PCR (RT-PCR) of time points within the initial 18 hour period. Primers for two putative immediate-early (*Neab24* and *Neab52*), three delayed-early (*lef-1*, *lef-2* and *dnapol*), two late (*vlf-1* and *gp41*), and two very late genes (*polh* and *p74*) were used to determine a temporal time-line of viral gene transcription. RT-PCR amplicons were observed for the putatively immediate-early and delayed early genes at 6 hpi (Figure 3-8). Late and very late gene transcripts were not observed, nor were any RT-PCR products detected beyond 6 hpi.

Unexpected amplicons were observed for *lef-1*, and *lef-2*. These amplicons were not observed in the no template control but were observed in the mock infected samples. The presence of RT-PCR products in mock infected samples suggests that some host-specific RNAs contained sequences with homology to the primers and were amplified under the conditions used.

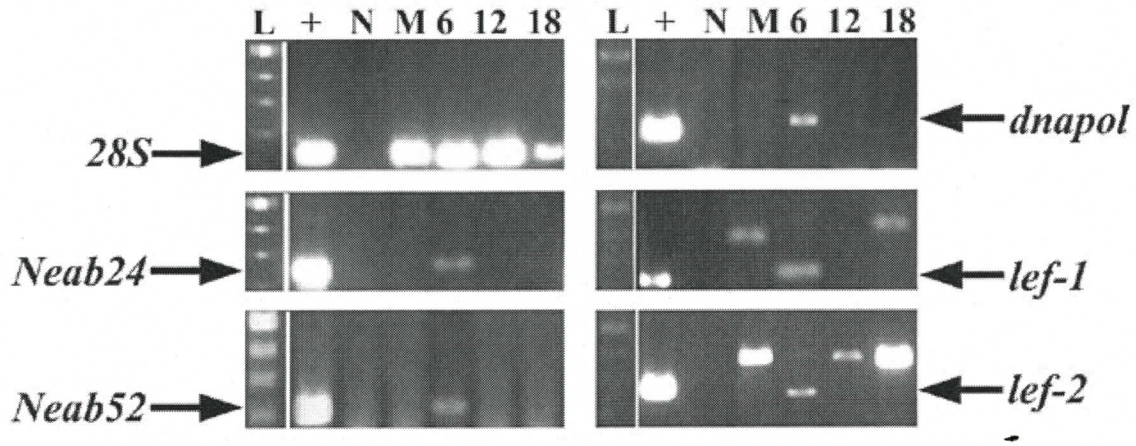

Figure 3-8. RT-PCR amplicons of host (*28S*), immediate early (*Neab24* and *Neab52*), and early NeabNPV (*dnapol*, *lef-1*, and *le-f2*) genes transcribed in Cf70 cells. RT-PCR was undertaken to detect transcripts of NeabNPV immediate early genes, characterized by Simon Duffy (2006), and early genes orthologous to known lepidopteran NPV genes. Lanes C, NeabNPV DNA extracted from *N. abietis* larval derived polyhedra; N, no template control; 1, mock infected Cf70 cells; 2, NeabNPV infected Cf70 cells at 6 hpi; 3, NeabNPV infected Cf70 cells at 12 hpi; 4, NeabNPV infected Cf70 cells at 18 hpi. M, molecular weight markers (500, 400, 300, 200 bp). Arrows indicated the expected amplicon size for each primer set.

3.5 Discussion

Several cell lines derived from *N. lecontei* were nonpermissive to NeabNPV, although some cytopathic effects were observed in NL18 cells. NPV infection in other nonpermissive cell lines has resulted in varying cytopathic effects. *Anticarsia gemmatalis* NPV infection of a *Bombyx mori* cell line, BM-5, resulted in early classic cytopathic effects, including nuclear hypertrophy, but thereafter led to the induction of apoptosis-like morphology (Castro *et al.*, 1997). In contrast, no clear pathology was observed when *B. mori* NPV infection was initiated in *Spodoptera frugiperda* (Sf9) cells, allowing the culture to continue proliferating normally (Katou *et al.*, 2001). These varying degrees of nonpermissibility were observed when comparing the effects of NeabNPV on the different *N. lecontei* cell lines. Cytopathic effects exhibited by NL18 cells were more similar to the effects observed by Castro *et al.* (1997), while NL10 and NL28 cultures showed little effects and continued to proliferate in a manner similar to Sf9 cells infected with BmNPV.

Cf70 cells exhibited the greatest degree of permissibility, showing actin rearrangement, low-levels of DNA replication and transcription of viral genes up to and including some of the delayed early viral replication genes. The cytopathic effects and pathology observed were in accordance with the expected limits of a semi-permissive cell line (Castro *et al.*, 1997; Huang *et al.*, 1999; McClintock *et al.*, 1986; Morris & Miller, 1993; Simón *et al.*, 2004). Actin rearrangement occurs early in the viral life-cycle. The first evidence of this rearrangement occurs within 0.5 hpi, when virions enter into the host cell and induce actin cable formation (Charlton & Volkman, 1993). This process is independent of protein synthesis and transportation of nucleocapsids to the nucleus

occurs as pre-existing actin monomers are bound and nucleated by viral proteins P39 and P78/83 (Charlton & Volkman, 1991; Lanier & Volkman, 1998; Machesky *et al.*, 2001). Thereafter, monomeric actin (G-actin) localizes to the nucleus with the aid of virally encoded proteins (in AcMNPV: *Ac102, Ac152,* and *he65*) that are expressed early in infection (Ohkawa *et al.*, 2002). Localization of actin to the nucleus is important for the proper formation of nucleocapsids and has been shown to associate with nucleocapsid proteins (P39 and P78/83) at the virogenic stroma (Charlton & Volkman, 1991; Ohkawa & Volkman, 1999). During nuclear localization of G-actin, rearrangement and breakdown of actin cables and the cytoskeleton occurs. Actin aggregates at the cell membrane early in infection (3-7 hpi), continuing until 48 hpi, due to the sequestering action of the viral actin rearrangement inducing factor (ARIF-1) (Roncarati & Knebel-Morsdorf, 1997). ARIF-1induced actin rearrangement appears to be a prerequisite for the breakdown of early cables and the actin network late in infection (Dreschers *et al.*, 2001) and may play an important role in the formation and dispersal of polyhedra, although the mechanisms of this rearrangement and contribution to each phase of infection are still speculative. Breakdown of the actin network and suppression of actin synthesis are both required during the very late phase of infection (Volkman *et al.*, 1996; Wei & Volkman, 1992) as polyhedrin (POLH) synthesis and assembly of polyhedra are delayed and inhibited upon over expression of actin. Finally, virally encoded cathepsin-like protease (V-CATH) has been shown to associate with budded virus of AcMNPV and lead to the destruction of the actin cytoskeleton, which possibly aids in the release of virions from infected cells during late phases of infection (Lanier *et al.*, 1996).

Actin cables forming during early infection are extremely unstable and have only been viewed in phalloidin-stabilized, unfixed cells lending support to the inability to detect these structures in NeabNPV infected Cf70 cells at 24 hours. The identification by N-terminal peptide sequencing of the NeabNPV P39 proteins (Young, 2002) and homologues of the *Ac152* (Duffy *et al.*, 2006), along with the observed rearrangement of actin in NeabNPV infected Cf70 cells suggests that actin may play an important role in the translocation of NeabNPV nucleocapsids to the nucleus and virion morphogenesis. These processes have been observed in six other NPVs (Kasman & Volkman, 2000), suggesting that interactions with host actin is a common characteristic among baculoviruses. Accumulation of actin at the cell membrane of NeabNPV infected Cf70 cultures suggests that actin rearrangement has occurred, possibly due to an orthologue of AcMNPV ARIF-1 and that degradation by a budded virus associated viral cathepsin has not occurred. The lack of degradation is expected since sequence data (Duffy *et al.*, 2006) and observations of tissue trophism (Bird, 1955) suggest that sawfly NPVs do not form an extracellular virion phenotype. In addition transcriptional analysis suggests that NeabNPV infection is arrested at the end of the replicative phase, possibly extending into the late phase of infection due to the isolation and identification of the nucleocapsid protein, P39. Therefore, breakdown of the actin cytoskeleton would not be expected.

The permissibility of insect cells helps define the viral host range. Cell lines that are semi- and non-permissive (non-productive) to AcMNPV infection exhibit classical cytopathic effects of early infection, but succumb to host defences, such as apoptosis and/or global protein synthesis shutdown, during late stages of infection (Du & Thiem, 1997b; Ishikawa *et al.*, 2004; McClintock *et al.*, 1986; Morris & Miller, 1992, 1993; Ooi

& Miller, 1988). The degree of host permissibility is dependent on the level and pattern of viral gene expression, with some non-productive cell lines continuing to produce viral transcripts of early to very late genes, but at levels well below those obtained from permissive cells (Morris & Miller, 1993). Typically, non-productive infections fail to replicate DNA and viral progeny due to insufficient quantities of essential viral proteins or a block in translating viral transcripts.

Semipermissive cell lines typically allow for replication of viral DNA but fail to yield viral progeny. Although possibly delayed, transcription proceeds in a manner similar to permissive cells, but declines during the late and very late phases of infection (Castro *et al.*, 1997; Huang *et al.*, 1999; McClintock *et al.*, 1986). Several studies have suggested that a subset of the population is permissive and will complete the infectious process (Katou *et al.*, 2001; Morris & Miller, 1993), resulting in the detection of transcripts of late and very late genes. The major restriction to infection appears to result from limited transcription of immediate early genes at the transcriptional level (Katou *et al.*, 2001; Levin *et al.*, 1997).

Another block to infection is the global shutdown of protein synthesis. This process has been shown to be independent of apoptosis (Du & Thiem, 1997b) and can be rescued by the addition of factors that alter host-virus interaction, such as host-specific helicases (Croizier *et al.*, 1994), viral encoded host range factors (HRF-1) (Du & Thiem, 1997a; Ishikawa *et al.*, 2004), and small RNA species (Mazzacano *et al.*, 1999). Protein synthesis shutdown occurs late in infection, allowing for viral DNA synthesis but preventing the assembly of viral progeny.

NeabNPV infection of Cf70 cells resulted in hypertrophy of nuclei and rounding of cells, classic cytopathic effects of early NPV infection. The intensity of the hybridized radiolabelled NeabNPV DNA probe was shown to increase above background levels within the initial 6 hpi period and reached a maximal level within 48 hours, then declined. This suggested that viral replication had commenced within the first time point and continued to 48 hpi. Other NPV infections in semipermissive cell lines have shown similar patterns of increasing and declining DNA synthesis (McClintock *et al.*, 1986).

Finally transcripts of delayed early genes were detected within 6 hpi but were no longer detectable at 12 hpi when late expression was predicted to occur. A transcript of *gp41* was detected at 6 hpi (data not shown) but this result was not reproducible. This finding, along with the identification of P39 of NeabNPV infected Cf70 cultures by N-terminal peptide sequencing (Young, 2002) and genomic analysis (Duffy *et al.*, 2006), suggest that some late genes were expressed. All evidence indicates that Cf70 cells were semipermissive to NeabNPV and infection progressed to the late phase of infection.

In conclusion, NeabNPV infection of several cell lines was investigated. The virus was shown to be non-productive in cells derived from a closely related sawfly, *N. lecontei* (NL10, NL18, and NL28) and was semi-productive in a culture of the lepidopteran *C. fumiferana* (Cf70). Light microscopy revealed nuclear hypertrophy and rounding of cells, cytopathic effects observed in early infection. Actin rearrangement, an important process in viral infection, was observed and resulted in the loss of filopodia and focal adhesions. Hypertrophy of the nucleus was confirmed by staining with DAPI, a fluorophore that intercalates in the minor groove of DNA, while Southern hybridization revealed that NeabNPV DNA synthesis initiated at 6 hpi. The increase in DNA quantity

plateaued at 48 hpi and indicated that a maximal level of DNA synthesis had occurred. RT-PCR analyses also suggest that transcription of some NeabNPV genes essential for replication occurred by 6 hpi. This study documents the first known *in vitro* propagation of a hymenopteran baculovirus and gives insights into the pathology of NeabNPV.

Chapter 4

Characterization of the morphology of the *N. abietis* larval gut

4.1 Abstract

The morphology and ultrastructure of the larval alimentary canal of *Neodiprion abietis* were examined by conventional light and electron microscopy. The digestive tract was excised from 3rd - 5th instar larvae, embedded in resin, and 70 nm and 500 nm sections were obtained. The *N. abietis* gut consisted of a long straight tube that was divided into three basic regions: the foregut, midgut and hindgut. The excised foregut was further divided into a crop, valve, and proventriculus, all of which were lined with a cuticle. Laterally elongated cuboidal epithelial cells marked the junction between the foregut and midgut. This tissue partitioned into several caeca (up to 15) that extended both anteriorly and posteriorly, and invaginated into the midgut epithelium. The midgut was the longest and broadest part of the gut. A multi-layered peritrophic membrane was observed throughout the midgut and segmented the lumen into endo- and ectoperitrophic spaces. Two types of epithelial cells were observed in the midgut: digestive and regenerative. The digestive columnar epithelium had a complex ultrastructure, which was consistent with their function in secreting digestive enzymes and absorbing nutrients. The hindgut was the final region examined and consisted of the pylorus and ileum regions. Rectal tissue was not characterized as this region was removed upon excision of the alimentary canal. Thick pad-like folds, composed of irregularly spaced columnar epithelium, were observed in the pylorus, while the epithelia of the ileum reverted to the cells that resembled the squamal, cuticle-lined epithelia of the foregut. Bacteria were located in the lumen of all three major regions of the alimentary canal, as well as intracellularly in midgut columnar epithelial cells. The bacteria were analysed by culture-independent *16S*

ribosomal DNA (rDNA) amplification, using two primer sets to the V6-V8 and V4 regions. Denaturing Gradient Gel Electrophoresis (DGGE) revealed 6 DNA products, which were directly sequenced. BLAST-n analysis and comparison-rank searches of the Ribosomal Database Project II (RDP II) database revealed 4 predicted bacteria, one of which was similar to Alphaproteobacteria. The other three sequences aligned with Gammaproteobacteria. Phylogenetic analysis by Maximum Parsimony and Neighbour Joining supported these findings and suggest that *Rahnella*, *Yersinia*, *Enterobacter*, and *Caulobacter*-like species inhabit the *N. abietis* larval gut.

4.2 Introduction

The insect gut is a complex and highly structured organ. Gut function and morphology are dependent on several factors: the stage of development, the feeding behaviour of each developmental stage, the food source, and the environment that the insect inhabits (Chapman, 1985; Nation, 2002; Wigglesworth, 1972). Irrespective of the diversity of structures that can be found in the guts of insects, a basic evolutionarily pattern of foregut, midgut, and hindgut has been preserved. The foregut typically functions as a storage site and transportation route for the ingested food. The midgut specializes in the production of digestive enzymes and the absorption of nutrients. The final region, the hindgut, regulates the reabsorption of water and ions, while disposing of waste products from excretion and digestion (Chapman, 1985; Nation, 2002).

The first comparative review of hymenopteran guts was performed by Bordas, who investigated the macro-morphology of guts from selected insects of every family in the Hymenoptera (Bordas, 1895). Sixty years later, Maxwell compared the internal anatomy of 132 different larval species from eleven families of North American and European

sawflies within the Symphyta (Maxwell, 1955). In her review, Maxwell examined larval structures with respect to defining taxonomic groups. The major anatomical characteristics useful for establishing evolutionary relationships amongst and between groups were the salivary glands and the Malpighian tubules. Other anatomic features were also noted, particularly the diverticula, fat bodies and midguts. The family Diprionidae was classified as intermediate-advanced sawflies, because they have multiple Malpighian tubules (as many as 28) that enter the gut individually at the junction between the midgut and hindgut (Maxwell, 1955). Each tubule extends anteriorly, for approximately one-eighth of the gut length before looping posteriorly and binding perirectally. In her study of the Symphyta, Maxwell found that the number of tubules could vary between 3 and more than 100, with three different arrangement types: "primitive" with a small number (3-20) of tubules entering the gut separately; "intermediate-advanced" with many tubules (>20) entering the gut individually; and "advanced" with one or more common collecting stalks of branching tubules that entered the gut. The Diprionidae are also distinguished as a family, based on their paired oesophageal-diverticula, while other sawfly families can be distinquish from their pharyngeal diverticula, ventricular caeca, or ventral abdominal eversible glands. The diprion diverticula or pouches act as reservoirs for plant resins and are termed pitch sacs. Finally, Maxwell noted that the anterior midguts of *N. swainei*, *N. abietis*, and *N. lecontei* are all marked by six deep longitudinal folds. These folded regions have various degrees of transverse striations that continue until the fourth abdominal segment, where two or three rows of protruding crypt cells are observed (Maxwell, 1955). The midguts, from the middle to posterior region, are smooth, becoming heavily striated along the regions

where the Malpighian tubules extend anteriorly. The striations are transverse and continue until the hindgut junction. Maxwell compared the morphology of the sawfly guts on a macroscopic level and even to the present day little is known about larval-gut cell-types or their ultrastructure in these insects.

The majority of known gut-ultrastructure comes from studies of larval lepidopterans, adult stages of ants (Formicidae), bees (Apidae), parasitic wasps (Pteromalidae), and mosquitoes (Diptera) (Arab & Caetano, 2001; Billingsley & Lehane, 1996; Cioffi, 1979; da Cruz-Landim & Cavalcante, 2003; Davies, 1977; Davies & King, 1977a, b; Dubreuil, 2004; Egert *et al.*, 2005; Flower & Filshie, 1976; Gartner, 1970, 1987; Gemetchu, 1974; Gul *et al.*, 2001; Hakim *et al.*, 2001; Hecker, 1977; Herrera-Alvarez *et al.*, 2000; Hung *et al.*, 2000; Kocan *et al.*, 1987; Levy *et al.*, 2004; Lipovsek *et al.*, 2004; Martin & Chiu, 2003; Murakami & Shiotsuki, 2001; Takahashi *et al.*, 1988; Tang & Ward, 1998; Trinadha Babu *et al.*, 1989; Villaro *et al.*, 1999). Many of these studies have detailed the midgut region due to its significance in digestion and nutrient absorption, leading to a lack of information about fore- and hindgut ultrastructure.

The best characterized hymenopteran midgut, with regards to ultrastructure, was studied in the larvae of the parasitic wasp, *Nasonia vitripennis* (Davies, 1977; Davies & King, 1977a, b). The authors investigated the effects of age and diet on the epithelial ultrastructure and described the composition of gut tissues. The midgut consists of a uniform single cell epithelial layer that is closely associated with tracheal, regenerative, and muscle cells. The associated cells tend to be restricted to the basal lamina, though some tracheal projection were seen extending to the basal region of the epithelium. The midgut epithelial cells are subdivided into 4 distinct intracellular regions:

1. the apical region that consists of a dense microvillar border,
2. the sub-microvillar zone, which has numerous mitochondria and randomly placed smooth endoplasmic reticulum (ER),
3. the central region, where the nucleus is located,
4. and the basal region that is characterized by deep infolds of the basal plasmalemma and compartmentalized mitochondria (Davies, 1977; Davies & King, 1977a, b).

Studies of other insect species have described similar gut ultrastructure, however, differences have been noted in the clustering and number of regenerative cells (Hecker, 1977), the types of cells that make up the epithelial tissue (Hung *et al.*, 2000; Levy *et al.*, 2004), and variations to the organelles within the intracellular regions (Arab & Caetano, 2001; Gul *et al.*, 2001).

Another aspect of insect gut morphology is the characterization of indigenous microbiota. Microbes in the gut represent microbial-host interactions that range from pathogenic to obligate mutualism. Studies that define the composition of microbial communities in the digestive system have primarily been performed using termites, tsetse flies, and cockroaches (Dillon & Charnley, 2002). Recent interest in endosymbioses, such as those exhibited by *Wolbachia, Buchnera,* and *Wigglesworthia* bacteria, has increased our knowledge about the integration of microbes with their insect hosts.

Currently, the most studied insect gut microbial communities are termite symbionts (Bignell, 2000; Breznak, 2000; Brune, 1998). Details of the functional roles of gut microbes have been studied in few other insects. Insect gut microbes are often located in specialized regions and structures within the gut. In the termite midgut, the microbial

communities are typically sparse and tend to localize between the microvilli of the epithelial cells (Breznak & Pankratz, 1977). The majority of the termite microbiota are found in paunch structures of the hindgut, where densities can reach 10^{11} cells per ml of gastric fluid (Breznak & Pankratz, 1977). The microorganisms may attach to surfaces such as spines, colonize the gut wall, or course freely in the lumen (Bignell, 2000). Depending on the taxonomical grouping of the termite and its food source, the functional role of the microbes may range from fermentation and hydrogen production to nitrogen recycling and carbon elimination (Bauer *et al.*, 2000; Bignell, 2000; Brauman *et al.*, 2001; Breznak & Pankratz, 1977; Brune, 1998).

Unlike the termites, recent studies of gut-microbiota from *Tetraponera, Solenopsis,* and *Camponotus spp.* (Hymenoptera: Formicidae) have revealed that bacteria are primarily localized in the midgut (Li *et al.*, 2005; Sauer *et al.*, 2002; Shannon *et al.*, 2001; van Borm *et al.*, 2002a). Many of these microbes have been analysed by *16S* rDNA sequence-analysis and many species of symbionts have been identified. A novel endosymbiont, Candidatus *Blochmannia floridanus*, was characterized and found in specialized bacteriocytes that are dispersed throughout the midgut epithelium of *Camponotus floridanus* (Sauer *et al.*, 2002). Transmission electron microscopy reveals that these bacteria floated freely within the host cell cytoplasm, a unique feature as compared to other known endosymbionts such as *Buchnera spp.* characterized in aphids (Boursaux-Eude & Gross, 2000).

This study documents the gut morphology and ultrastructure of *N. abietis* larvae. The larval gut was separated into three regions: foregut, midgut and hindgut. The crop was composed of a thin layer of squamous epithelia that is lined by a thin layer of cuticle and

leads into a stomodaeal valve and a fully developed proventriculus. The midgut was the longest part of the larval gut and consists of two cell types: digestive columnar epithelial cells and regenerative cells. The columnar cells harboured elongated rod-like bacteria that float freely within the epithelial cytosol. Bacteria were also localized to the gut lumen. The columnar epithelium formed fold-like structures at the junction between the midgut and hindgut. This region lacked a cuticular lining but still exhibited a shallow microvillar border. The ileum region of the hindgut was characterized by irregularly shaped squamal epithelia. A cuticular lining, thicker than found in the foregut, covered these epithelial cells. The microbiota within the sawfly gut was studied for the first time by culture independent methods. *16S* ribosomal DNA (rDNA), extracted from excised larval guts, was amplified by polymerase chain reaction (PCR), separated by Denaturing Gradient Gel Electrophoresis (DGGE), and revealed 6 distinct DNA products. BLAST-n analysis and comparison rank searches of the Ribosomal Database Project II sequences identified sequences with similarity to Alpha- and Gammaproteobacteria. Maximum Parsimony and Neighbour Joining analysis confirmed these findings.

4.3 Materials and Methods

4.3.1 Larval collection

Balsam fir (*Abies balsamae*) branches, containing *N. abietis* larvae, were collected from the leading edge of the epizootic located at Old Man's Pond, Newfoundland, Canada, in July of 2003 and 2004. Larvae were maintained on balsam fir in paper bags at 4 °C for 48 hours before being harvested for a 12-15 hour starvation period. Head capsule widths of healthy larvae were measured using a dissecting microscopy with a calibrated objective. Mid-stadium larvae with head-capsule widths between 0.96 to 1.5 mm, which

corresponds to 3rd to 5th instar larvae (Carroll, 1962), were transferred to sterile microcentrifuge tube. The larvae were allowed to imbibe a solution of 10% pasteurized honey, and then incubated on fresh balsam fir sprigs, for 72 hours at room temperature, to monitor for signs of NeabNPV infection.

4.3.2 Histological Preparation

Larvae harvested for morphological and ultrastructural characterization of the gut were submerged in fixative (2.5% gluteraldehyde, 0.1 M sucrose, 0.05M sodium cacodylate buffer). The heads and tails were removed at the head capsule and eighth proleg, respectively, and the gut was pulled from the hemocoel, using forceps. Excised guts exceeding 8 mm were bisected and transferred into 10 volumes of fresh fixative and incubated overnight at 4 °C. The gut samples were rinsed for 15 minutes at room temperature (RT) in 0.1 M sucrose/0.05M sodium cacodylate buffer, followed by two additional rinses for 15 minutes each in 0.05 M sucrose/0.05M sodium cacodylate buffer and 0.05M sodium cacodylate buffer, respectively. The samples were then post-fixed (1% osmium tetroxide, 0.05M sodium cacodylate buffer) for 1 hour. Two 15-minute rinses in 0.05M sodium cacodylate buffer were followed by two 10 minute washes in distilled deionized water. Samples were incubated overnight at 4 °C in 4% uranyl acetate in water. Two additional 10-minute washes in water were followed by a dehydration series in increasing concentrations of acetone (30%, 50%, 70%, 80%, and 90%), each for 15 minutes. The samples were dehydrated twice in 100% acetone for 30 minutes, before being infiltrated with 2:1 solution of acetone to Epon-araldite (5 g Epon, 5 g araldite, 12 g DDSA, 500ul DMP-30), for 2 hours. The samples were transferred into a fresh 1:1 solution of acetone and Epon-araldite, overnight, and then into a 1:2 solution of acetone

and Epon-araldite for 2 hours. The final infiltration step was performed using Epon-araldite resin, and then the samples were embedded into fresh resin and incubated at 60 °C for 48 hours.

4.3.3 Light and Transmission Electron Microscopy

Embedded samples were sectioned with a Leica Ultra-cut microtome to thin (500 nm) and ultra-thin (70 nm) thicknesses using a Diatom Histo and Diamond knife, respectively. Thin sections were stained with Richardson Stain (1% azure blue, 1% borax, 1% methylene blue) and visualized on a Zeiss Universal upright compound microscope. Light micrographs were taken with a Spot CCD camera and Spot Software.

Ultra-thin sections were stained with uranyl acetate (5%) and lead citrate (5%), before viewing on a Hitachi H7000 Transmission Electron microscope, using a 75 kV beam. Electron micrographs were captured on Kodak 4489 Electron microscope film and digitalized by scanning the negatives with a Polaroid SprintScan45 Scanner and Polaroid PolaColor Insight software (v.4.5.1). Scale bars were added to the digital images using Adobe Photoshop 5.

4.3.4 PCR Amplification, DGGE, and Sequencing of Bacterial *16S* gene

Larvae harvested for molecular characterization of sawfly-gut bacteria were surface sterilized by a 60-second wash in 5% bleach, followed by a 60-second rinse in DEPC-treated water (0.1% diethyl pyrocarbonate). Larvae were submerged in sterile phosphate buffered saline (PBS, pH 7.4). The heads and tails were excised immediate posterior of the head capsule and immediately anterior to the eighth proleg, respectively. The cuticle was secured and the gut was pulled from the body cavity. The excised gut was transferred to fresh PBS and the peritrophic membrane was pulled from the gut lumen,

using forceps, along with any food bolus. The gut tissue was immediately placed into RNAlater (Ambion Inc.) and stored at –20 °C.

The gut tissue was centrifuged and the RNAlater was filtered through a Microcon 10 (Millipore Inc.) to collect released DNA, RNA and proteins. One millilitre of TRIzol (Invitrogen, Life Sciences) was added to the pelleted gut tissue and concentrated retentate. RNA, DNA and protein were extracted following the manufacturer's protocols. The RNA and protein fractions, as well as some of the DNA, were used as uninfected controls for studying the pathology of the naturally occurring nucleopolyhedrovirus, NeabNPV (see Chapter 6).

An aliquot of the extracted DNA was given to Dr. Rob Graham (Natural Resources Canada, Canadian Forest Services, Atlantic Forestry Centre, Fredericton, New Brunswick) for amplification with G-C clamp primers and electrophoresis on a denature gradient gel (DGGE). Two primer sets were used to ensure amplification of the targeted bacterial *16S* rDNA. Primers p984f-GC (5'-CGCCCGGGGCGCGCCCCGGGCGGGGC GGGGGCACGGGGGGAACGCGCCGAACCTTAC-3') and p1401r (5'-GCGTGTGTA CAAGACCC-3') (Frederick & Caesar, 2000; Nòbel *et al.*, 1996) were used to amplify the V6 to V8 regions of the *16S* rDNA (320 bp length). Primers p515f-GC (5'- CGCCC GGGGCGCGCCCCGGGCGGGGCGGGGGCACGGGGGGCCAGCAGCCGCGGTAA -3') and p806r (5'GGACTACCAGGGTATCTAAT-3') (Relman, 1993) were used to amplify the variable V4 region of *16S* rDNA (200 bp length). PCR mixtures of 50 µl volume contained reaction buffer (10 mM Tris-HCl pH 8.3 at 25°C, 50 mM KCl, 1.5 mM $MgCl_2$, 0.001% gelatin), 10 μM each of dATP, dTTP, dCTP and dGTP, 0.1 μM of each primer, 1 unit Taq polymerase (Qiagen) and approximately 10 ng insect genomic DNA

template. PCR was undertaken using a Mastercycler EP thermal cycler (Eppendorf), with the following settings: (i) 94°C for 5 min, 1 cycle; (ii) 94°C for 30 sec, 52°C for 30 sec, 72°C for 45 sec, 40 cycles; (iii) 72°C for 5 min, 1 cycle. On completion of PCR, 10% of the reaction was loaded on a 1% agarose gel and electrophoresed in 1 x TBE (0.09 M Tris, 0.09 M boric acid, 0.002 M EDTA) for 2 hrs at 60 V. The gel was stained with ethidium bromide and visualised using UV illumination.

PCR products (50% of the reaction) were separated by DGGE using the DCode system (BioRad) according to the manufacturer's instructions. Gels consisted of 1 mm thick 6% polyacrylamide with a denaturing gradient of 30-70 % (100 % denaturant corresponds to 7 M urea and 40 % vol/vol deionized formamide) and 1 x TAE buffer (0.09 M Tris, 2.2% w/v glacial acetic acid, 0.004 M EDTA). Electrophoresis was performed at 60°C and 80 V in 1 x TAE running buffer for 16 hours. Gels were stained with SYBR Gold nucleic acid stain (Invitrogen) for 30 minutes and images captured *via* UV analysis. DNA bands were excised with a sterile razor blade and placed in 100 µl of sterile distilled H_2O. The samples were placed at 94°C for 5 minutes to elute the DNA from the polyacrylamide and stored at 4°C overnight. Five microlitres of the supernatant were used as template to reamplify the individual DNA bands. The PCR conditions were the same as above, but only 30 cycles of amplification were undertaken. The PCR products were gel purified using the QIAquick Gel Extraction Kit (Qiagen), and samples stored at -20°C ready for sequencing. Sequencing was sent to Ontario Genomics Innovation Centre, where ABI 3730 DNA Analyzer (BigDye 3.1) was used. Phylogenetic and molecular evolutionary analyses were conducted using MEGA version 3.1 (Kumar *et al.*, 2004).

4.4 Results

4.4.1 Overall gut organization

The length of excised alimentary canals ranged from 1.0 to 1.2 cm. Serial sectioning of fixed, embedded guts revealed three distinct regions: foregut, midgut, and hindgut (Figure 4-1). The foregut was further divided into the crop, a valve-like structure, and the proventriculus and comprised approximately 22% of the total length of the excised gut. The diverticula and oesophagus were not observed as these structures were anterior to the dissected tissue. The diverticula of *N. abietis* larvae provide storage for plant resins and are commonly known as pitch sacs (Chris Lucarotti, personal communication). The ventricular or cardiac caeca marked the junction of the foregut and midgut. This tissue subdivided into numerous tubules (up to 12 were observed) that extend both anteriorly and posteriorly for approximately 0.4 mm (3.5% of the gut length). The caeca invaginated into the midgut epithelia, the length of which comprised the majority (~ 63%) of the alimentary canal. The final region observed in the excised gut was the hindgut, which totalled approximately 15% of the gut length. A pylorus-like structure was observed at the junction between the midgut and hindgut.

Malpighian tubules were observed randomly beside this tissue but were not observed branching from the midgut and hindgut epithelia. The fragile nature of the Malpighian tubules likely led to their removal from the alimentary canal by mechanical tearing and damage during histological preparation. The excised hindgut extended only to a tissue defined as the ileum, as the rectum was posterior to the dissection point at the eighth proleg.

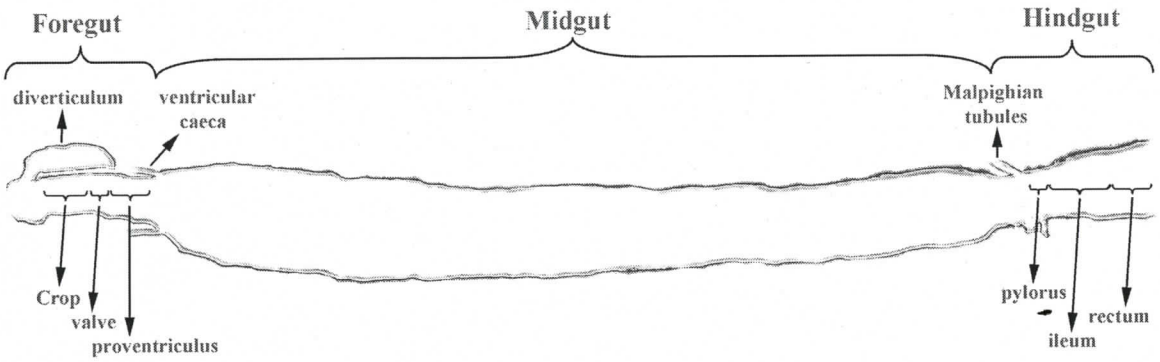

Figure 4-1. Schematic of *Neodiprion abietis* larval gut .

Larval gut excised posterior to the head capsule and anterior to the 8th proleg. Three regions comprise the gut of the sawfly larvae: the foregut, midgut, and hindgut. Each region can be further divided into important regions for digestion..

4.4.2 The Foregut

The crop was one of the narrowest regions of the alimentary canal observed in these preparations, measuring approximately 300 μm in diameter (Figure 4-2 A). A single layer of irregularly shaped squamal epithelia was observed in this tissue. The cells were elongated with large central nuclei, which contained 2-3 large nucleoli and several small darkly stained regions (Figure 4-2 B and C). Well-organized rough endoplasmic reticula (rER) were observed within the cells, as well as a sparse amount of mitochondria. A thin layer of cuticle covered the cells and separated the tissue from the contents of the gut lumen. The cuticle contained two layers, an electron dense outer layer that was approximately 10 nm thick and a fibrous layer that ranged in thickness from 200 to 800 nm. The basal membrane of the epithelia was flush with the basal lamina, which contained an inner layer of circular muscles and a discontinuous outer layer of longitudinal muscles. Both rod-shaped and coccoid bacteria were observed in the crop lumen and associated with both the ingested plant tissue and cuticle lining.

A valve-like structure was observed posterior to the crop. This structure consisted of six folds of squamal epithelium that pinched together due to a continuous layer of circular muscles and connective tissue (Figure 4-3 A and B). The valve was relatively short in length, spanning approximately 400 μm. The epithelial cells appeared similar to those found in the crop and were also lined by a cuticular layer (Figure 4-3 C). A large central nucleus, containing 2-4 nucleoli, was surrounded by multiple mitochondria and free ribosomes. The basal membrane was often invaginated and lay adjacent to a granular basal lamina. The circular muscles were often separated from the epithelial layer, especially where the epithelia folded into the gut lumen. Two layers of cuticle similar to

A

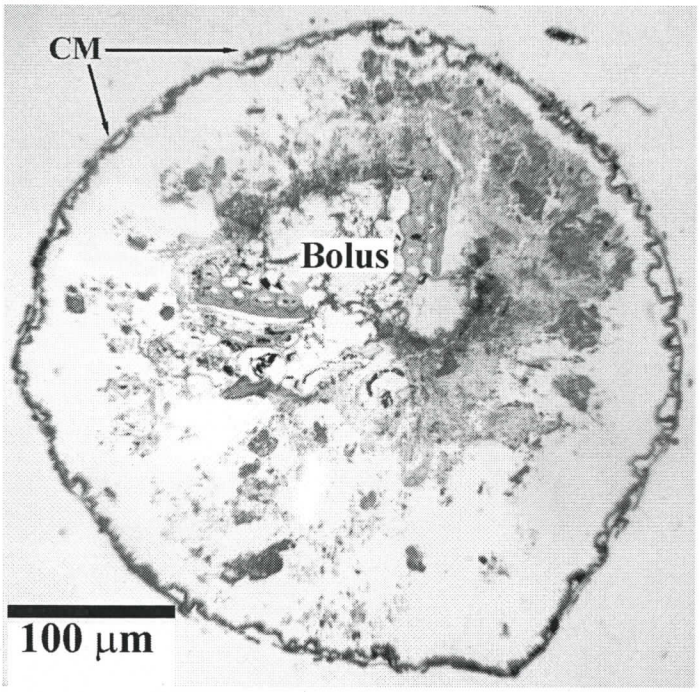

B

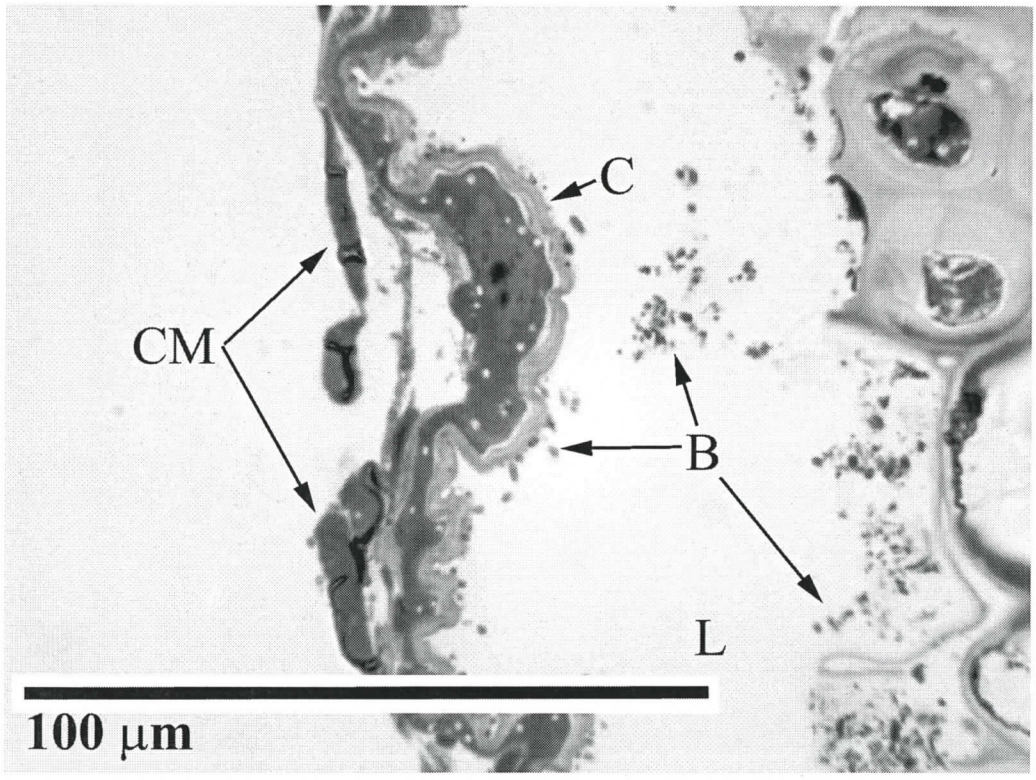

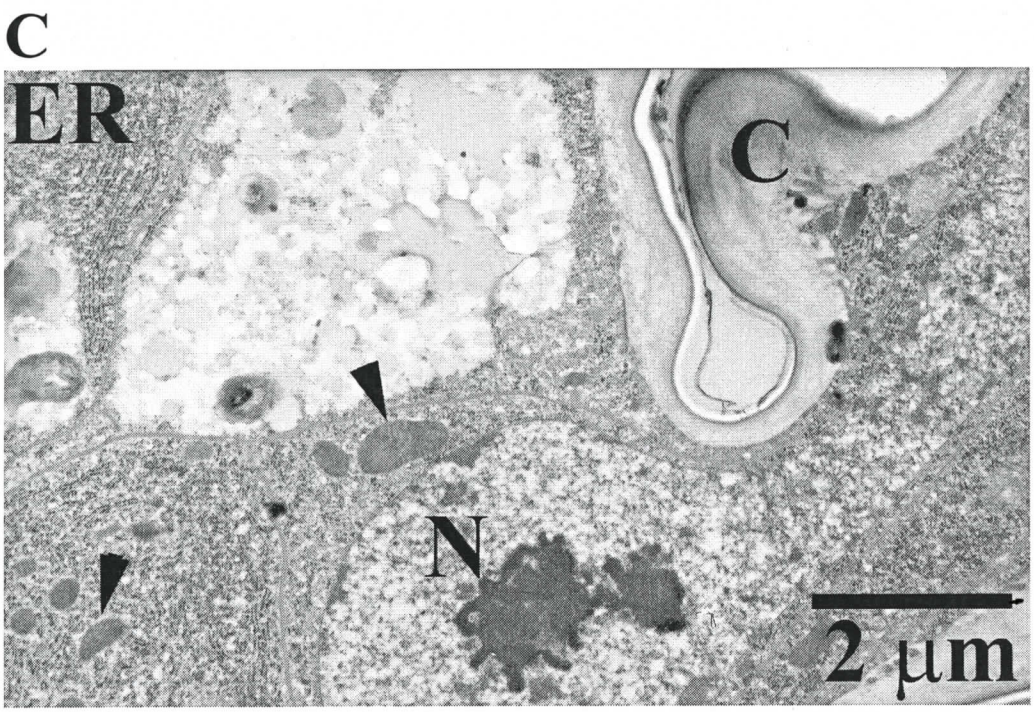

Figure 4-2. Light (A and B) and transmission electron (C) micrographs of the crop epithelia and surrounding connective tissue of *N. abietis* larvae.

The epithelial layer consisted of irregularly shaped squamal cells that were lined by a cuticle. Dispersed circular muscles lay basally to the epithelium and were connected by a thin basal lamina. C, cuticle; CM, circular muscles; ER, endoplasmic reticulum; B, bacteria; L, gut lumen; N, nucleus; Arrow heads indicate mitochondria.

A

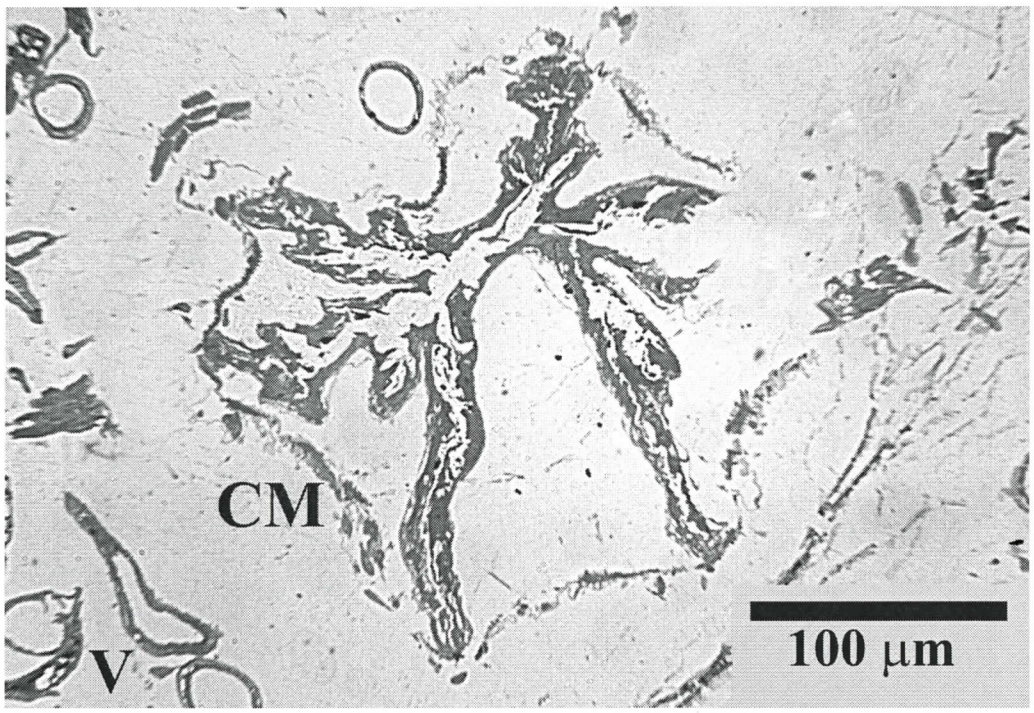

B

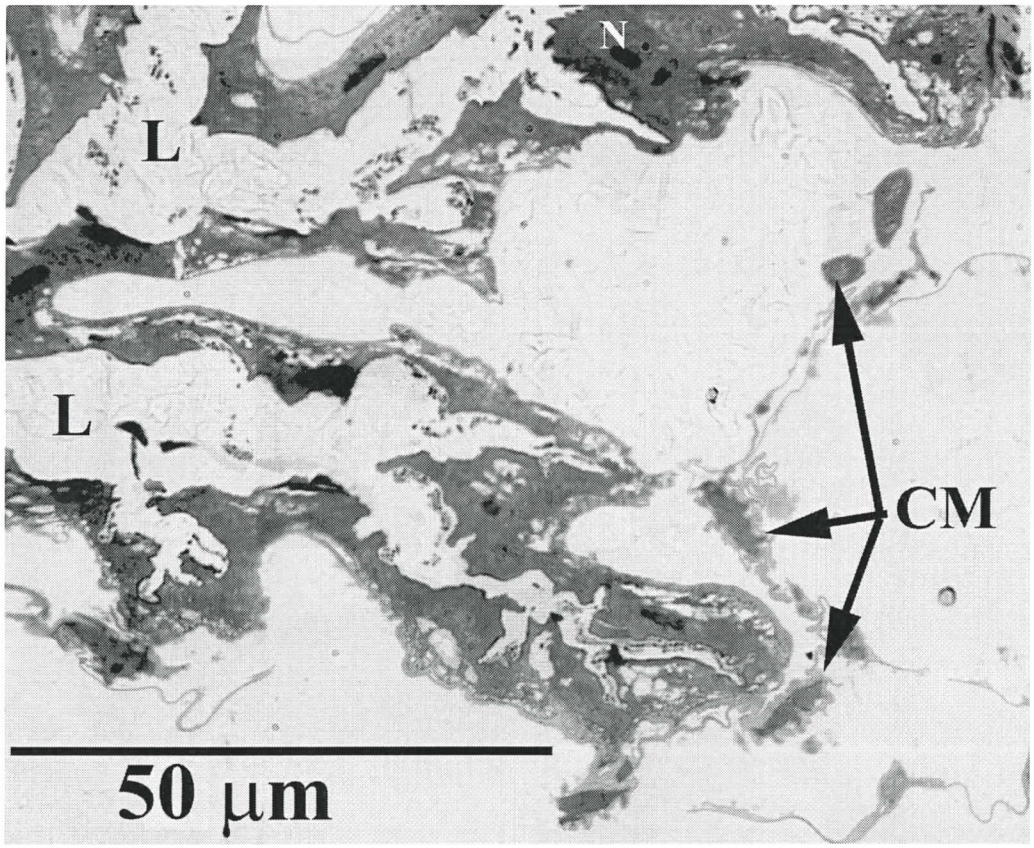

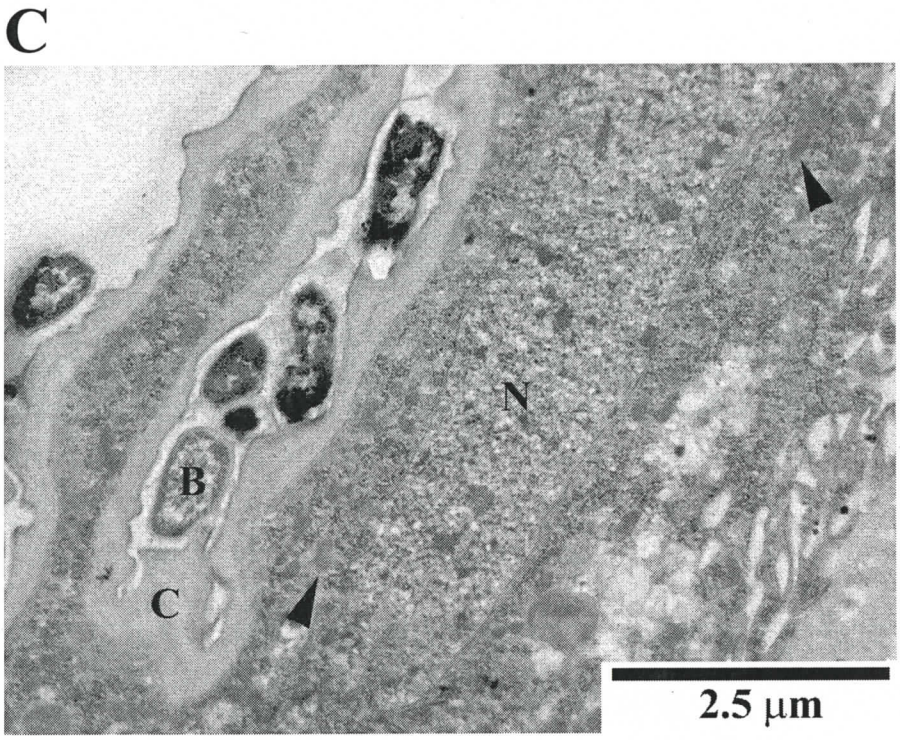

Figure 4-3. Light (A and B) and transmission electron (C) micrographs of the valve-like structure and surrounding connective tissue of *N. abietis* larvae.

The epithelial layer consisted of irregularly shaped squamal cells that were lined by a bilayered cuticle. Large circular muscles lay basally to the epithelium and were connected by the basal lamina to form a continuous layer. B, bacteria; C, cuticle; CM, circular muscles; L, gut lumen; N, nucleus; V, ventricular caeca; Arrow heads indicate mitochondria.

that found in the crop were observed. The bacteria observed in the crop were also observed within the lumen of the valve and were commonly located in the small recesses created by the epithelium.

The proventriculus was the longest structure observed in the foregut, ranging from 1.02 to 1.24 mm in length and comprising approximately 10% of the total length of the excised gut. This structure was heavily sclerotized and exhibited 6 teeth that increased in size in a posterior direction (Figure 4-4 A). The epithelial layer was again composed of irregularly shaped squamal cells that exhibited no microvilli (Figure 4-4 B-D). Few mitochondria were detected in this region of the foregut epithelium, but more rER and free ribosomes were observed compared to the squamal cells of the crop and valve. The nuclei were the prominent organelle of the epithelial cells and typically had one large nucleolus. The cuticular lining increased progressively in thickness toward the posterior of the foregut. Similar to the cuticle of the crop and valve, two distinct regions were observed: a thin electron dense outer layer and a thick fibrous inner layer. The inner layer ranged in thickness from 300 nm (Figure 4-4 D) to over 5 μm and appeared to be composed of several layers (Figure 4-4 B and C). Three to six layers of circular muscle were observed throughout the proventriculus and were contained within a fibrous layer of connective tissue. Longitudinal muscles surrounded the circular muscle layers and were often observed in bundles. Ultrastructural examination of the muscle cells revealed an abundance of actin-myosin filaments, many large mitochondria, and large nuclei that were located asymmetrically (Figure 4-4 D). The proventriculus was the last organ observed in the foregut and connected with the ventricular caeca that marked the junction between the foregut and midgut.

A

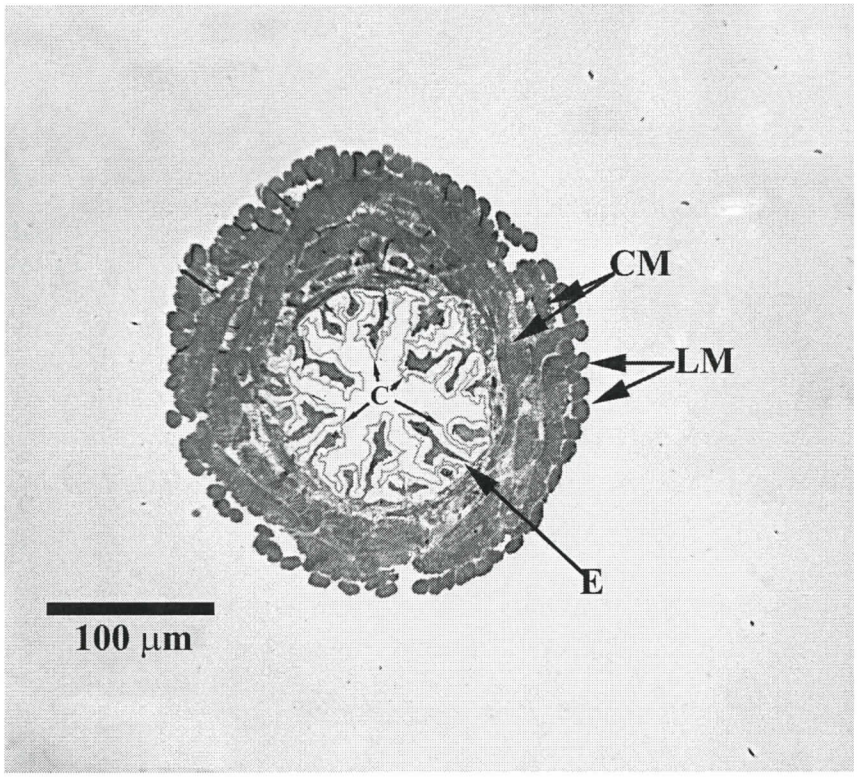

B

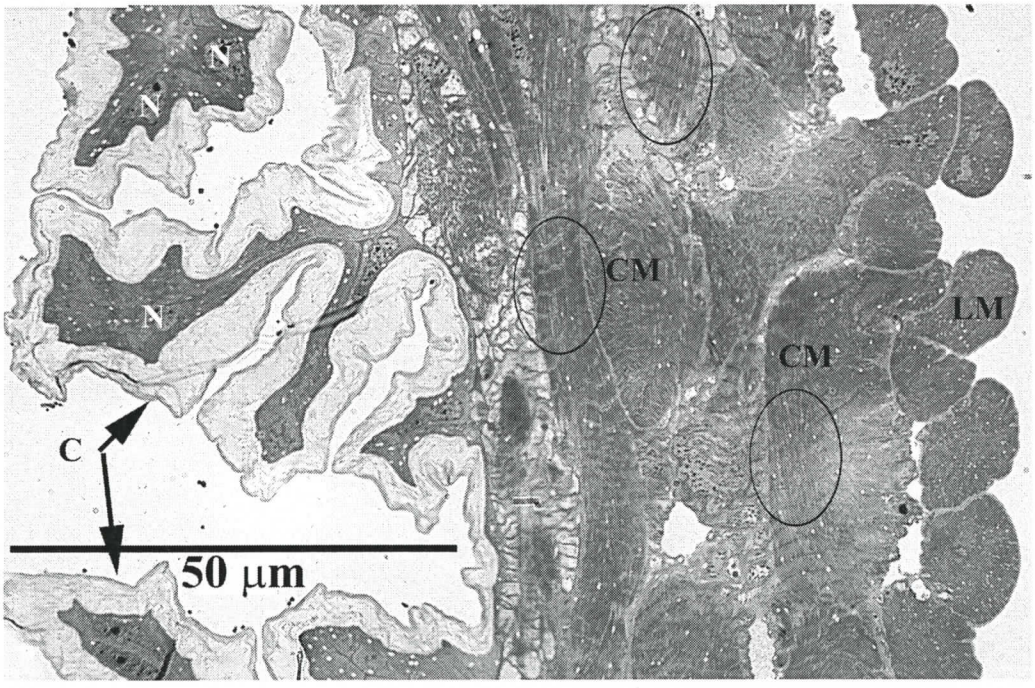

C

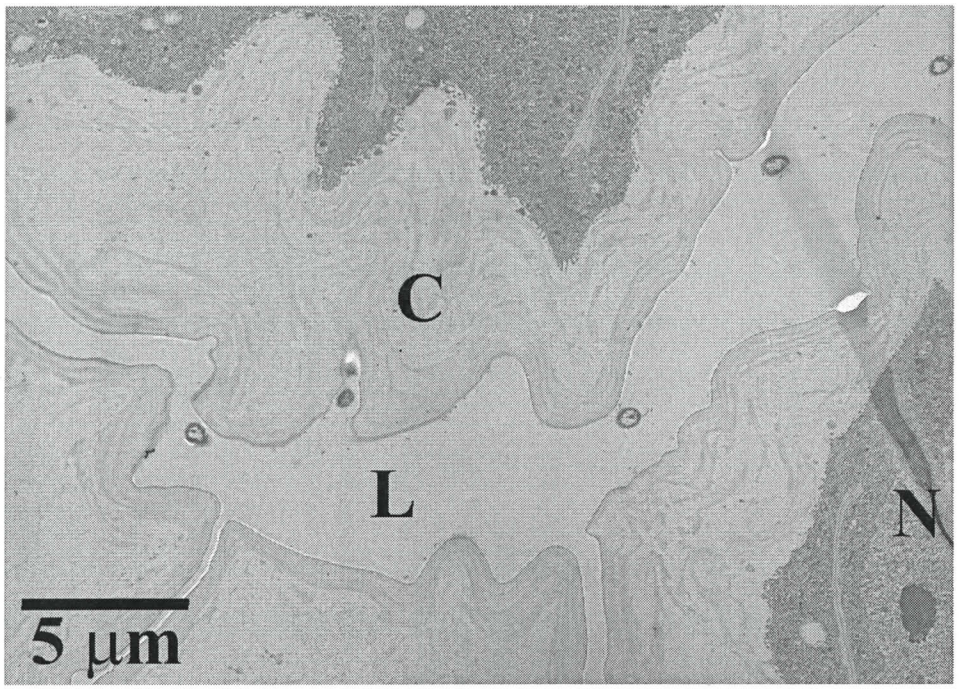

D

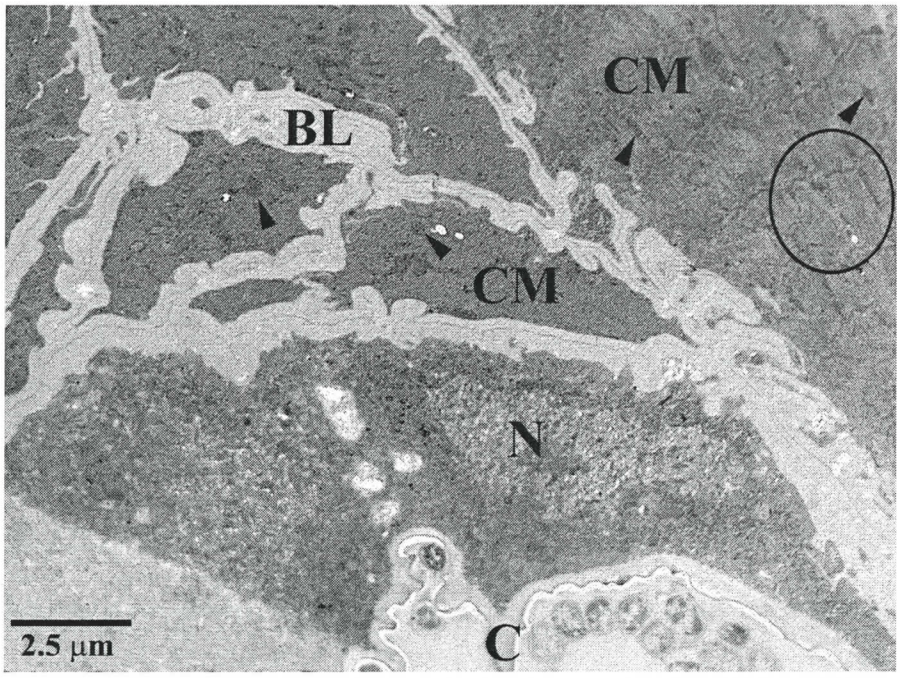

Figure 4-4. Light (A and B) and transmission electron (C and D) micrographs of the proventriculus and the surrounding developed musculature of *N. abietis* larvae. The epithelial layer consisted of irregularly shaped squamal cells that were lined by a heavily sclerotized bilayer of cuticle. Large circular muscles lay basally to the epithelium and were connected by the basal lamina to form a continuous layer. BL, basal lamina; C, cuticle; CM, circular muscles; E, epithelium; L, gut lumen; LM, longitudinal muscle; N, nucleus; Arrow heads indicate mitochondria; Circled regions highlight actin-myosin fibers. Scale bars as depicted on each micrograph.

4.4.3 The Ventricular Caeca

Ventricular caeca were numerous (up to 15 detected) and extended both anteriorly and posteriorly within the hemocoel. Caeca epithelial tissues were characterized by elongated cuboidal epithelium, with a sparse microvillar border and an invaginated basal membrane (Figure 4-5 A-C). These cells have elongated nuclei with one prominent nucleolus. Copious mitochondria were observed, in addition to many electron light vesicles (Figure 4-5 D). Free ribosomes and rER were readily apparent, while Golgi complexes were scarcely observed. This tissue lacked the circular and longitudinal muscular characteristic of other gut regions. Peritrophic membranes were also not observed.

4.4.4 The Midgut

The midgut epithelium constituted the major portion of the entire gut (58.9% of the gut length) and had the largest luminal region (ranging from 600 to 900 μm in diameter). A peritrophic membrane, often multilayered, contained both granular and fibrous material (Figure 4-6 A, E, and F). Rod-shaped bacteria were located within the endoperitrophic (luminal) and ectoperitrophic (between the epithelium and peritrophic membrane) spaces. Bacteria located within the midgut epithelial cells were elongated rods that floated freely within the host cell cytosol (Figure 4-6 C, D, and Figure 4-7 B). A discontinuous layer of inner circular muscles and outer longitudinal muscles were contained within the multi-layered basal laminas between the hemocoel and the midgut epithelia (Figure 4-6 A-F, and Figure 4-7 C). Tracheal cells were also embedded within the basal lamina while tracheolae intercalated within the invaginations of the epithelial basal membrane. Regenerative cells were observed along the basal region of the epithelia in nidi of 2 to 8

A

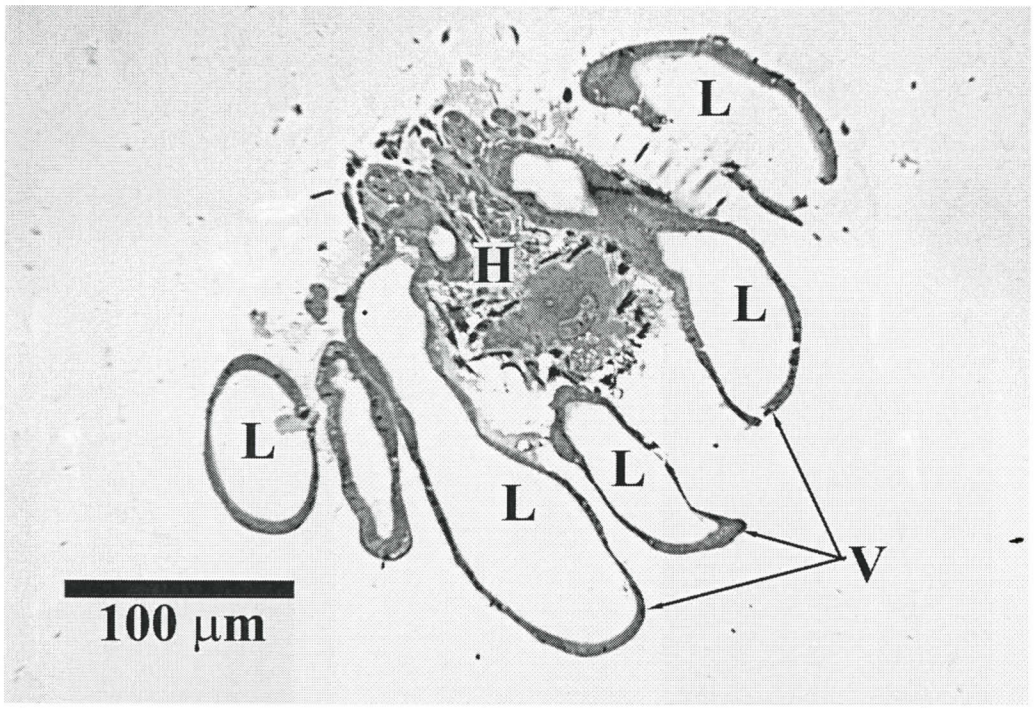

B

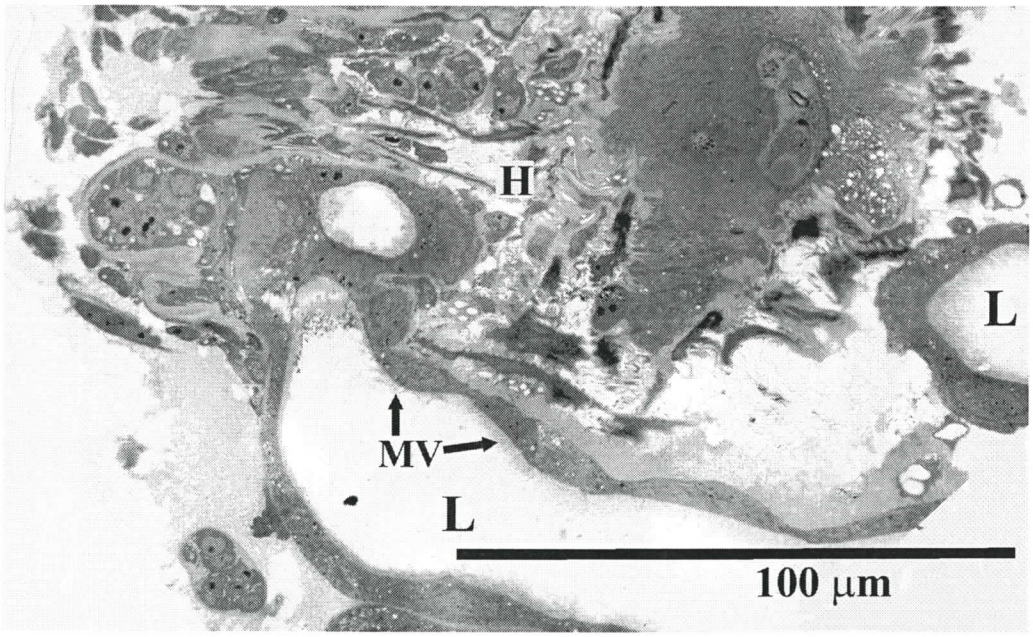

C

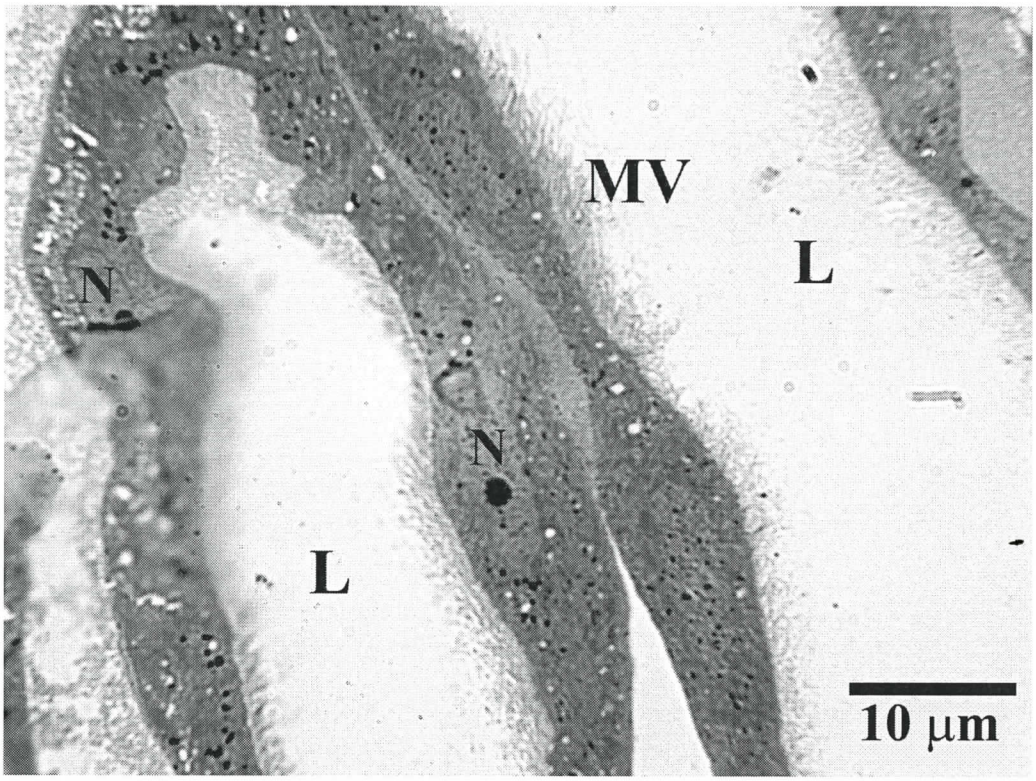

D

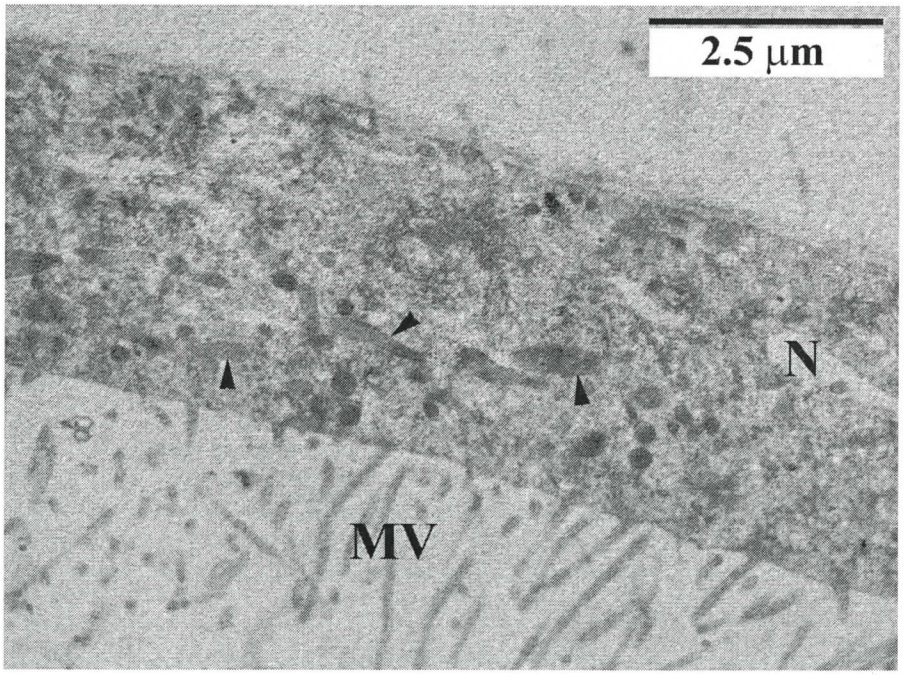

Figure 4-5. Light (A-C) and transmission electron (D) micrographs of the ventricular caeca and surrounding connective tissue of *N. abietis* larvae. The epithelial layer consisted of elongated cuboidal cells that have a spare microvillar border. The caeca lack the hemocoelic musculature of the foregut and instead have a densely packed hemocoelic region (A & B) composed of predicted hemocytes and tracheolar cells. H, hemocoel tissue L, gut lumen; N, nucleus; MV, microvilli; V, ventricular caeca; Arrow heads indicate mitochondria. Scale bars as depicted on each micrograph.

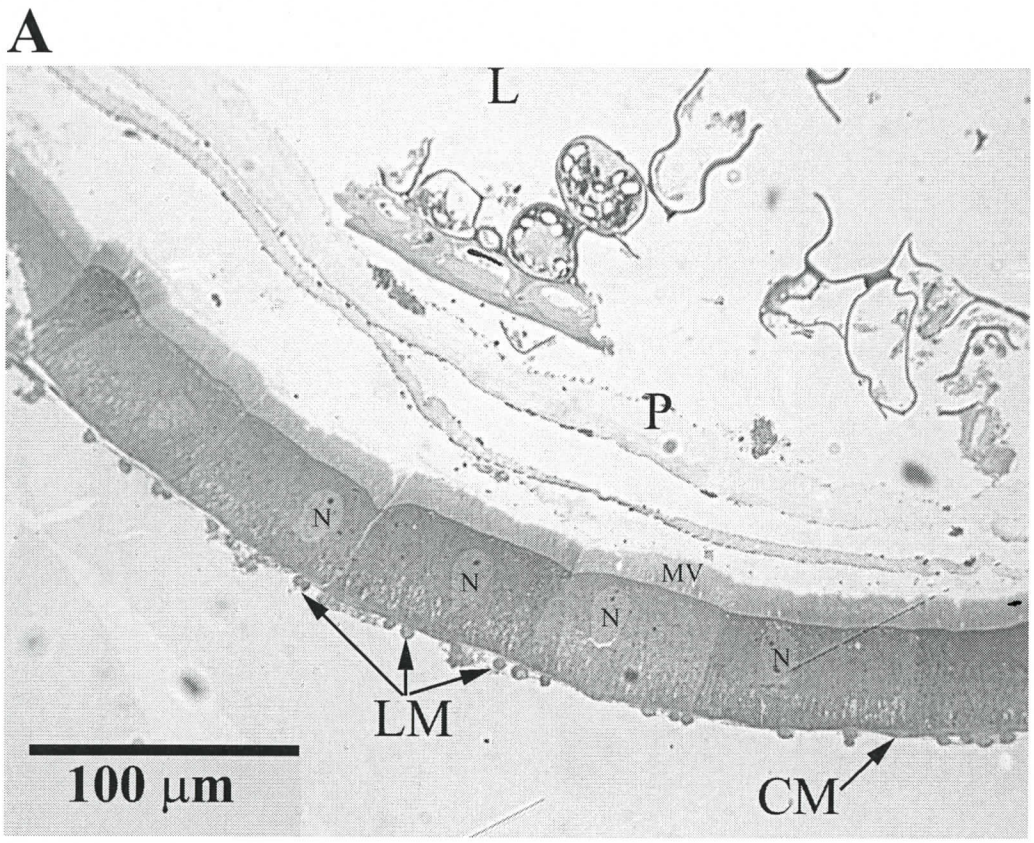
A
L
P
N
N
N
N
MV
LM
CM
100 μm

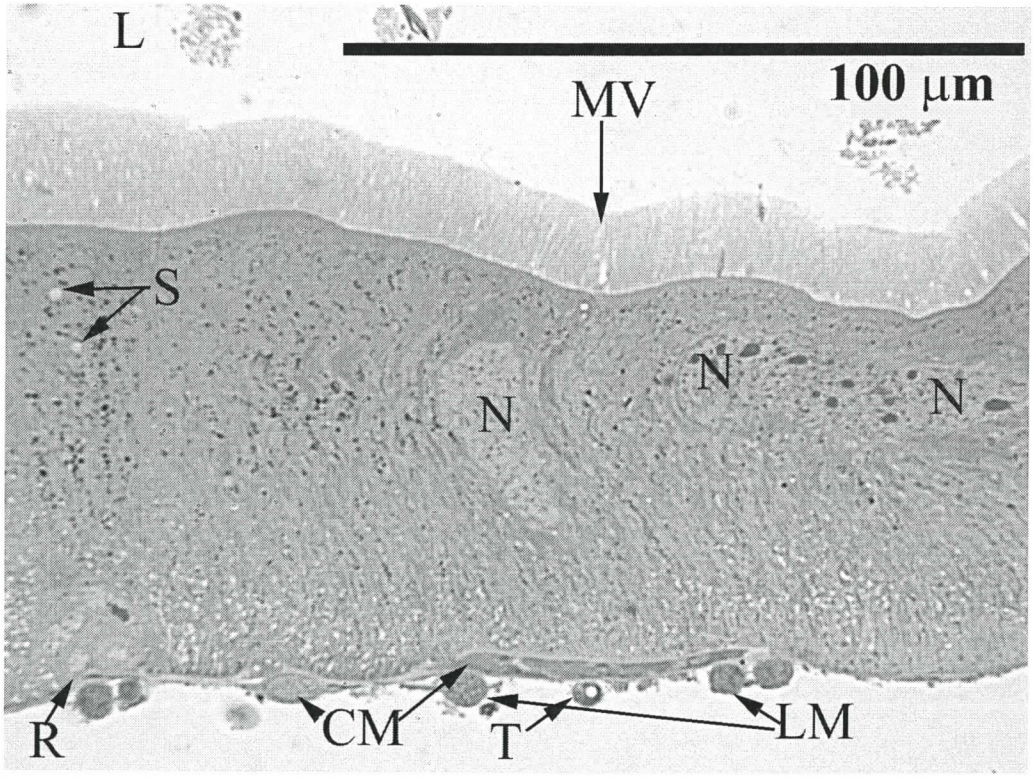
B
L
100 μm
MV
S
N
N
N
R
CM
T
LM

C

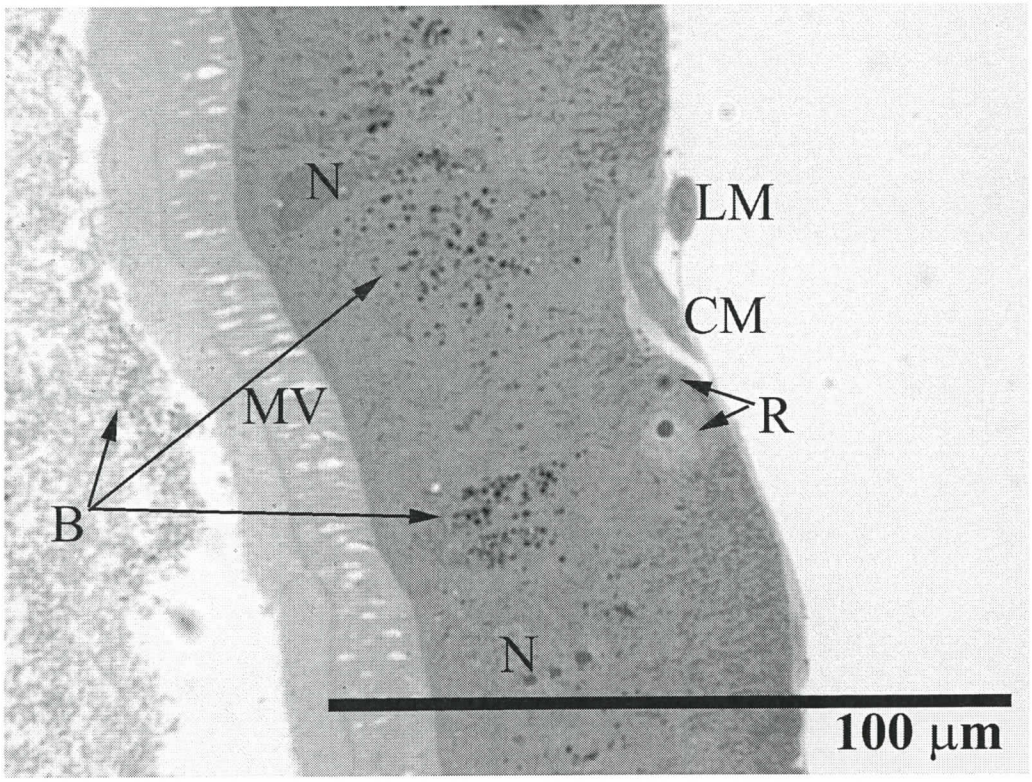

D

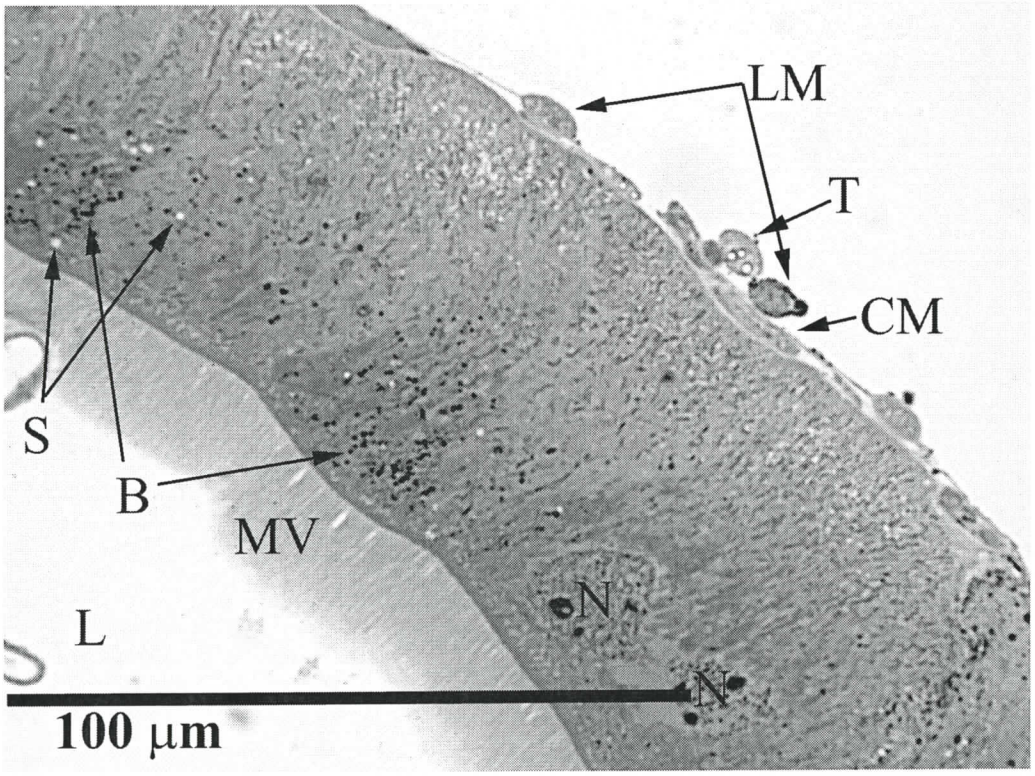

E

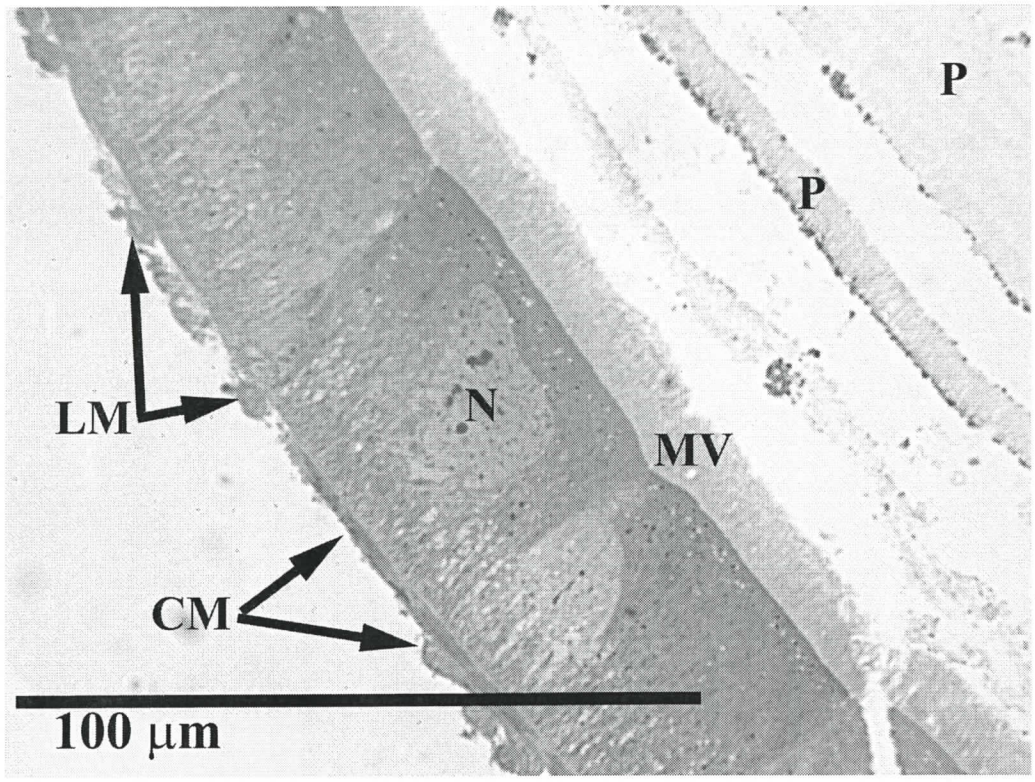

F

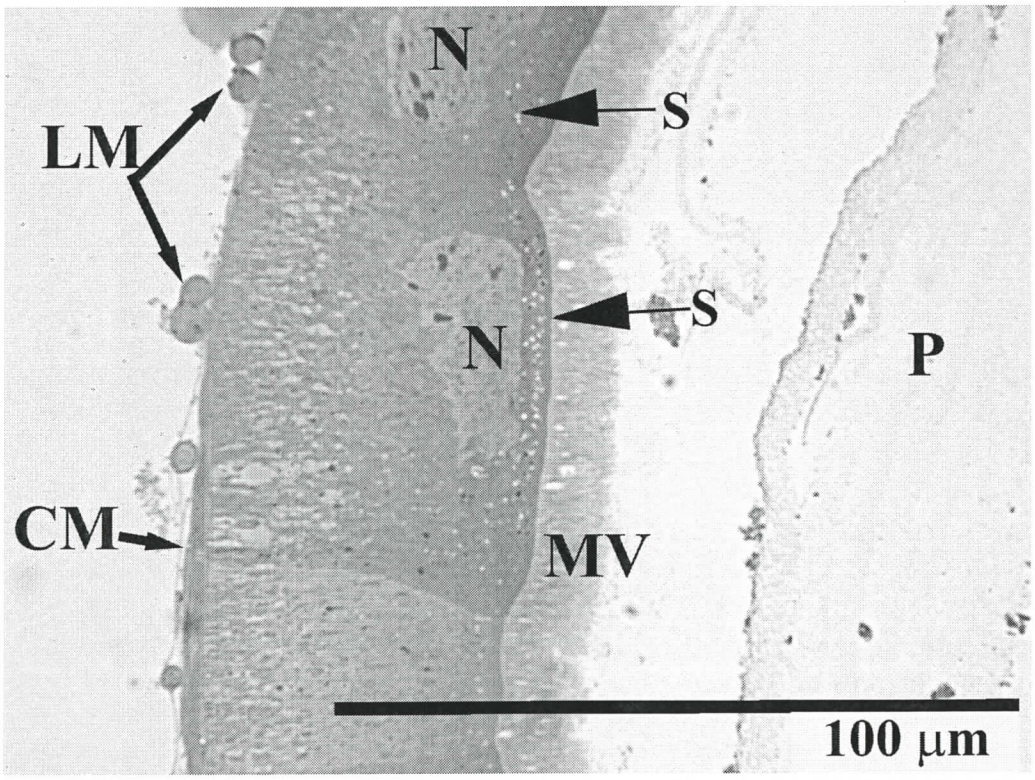

Figure 4-6. Light (A-F) micrographs of the midgut epithelia and the surrounding connective tissue of *N. abietis* larvae.

The epithelial layer consisted of columnar cells that had dense microvillar borders. Circular and longitudinal muscles and tracheolae lay basally to the epithelium and were contained within the basal lamina. Regenerative cells were located in nidi that lay basal to the midgut epithelial cells and luminal to the basal lamina. Lumen bacteria lay within the endo and ecto-peritrophic space, while intracellular bacteria localized to the apical region of the epithelial cells. A multilayered peritrophic membrane was visible along the entire length of the midgut epithelium. B, bacteria; BL, basal lamina; CM, circular muscles; ER, endoplasmic reticulum; L, gut lumen; LCM, lateral cytoplasmic membrane; LM, longitudinal muscle; N, nucleus; nu, nucleolus; MV, microvilli; P, peritrophic membrane; R, regenerative cells S, secretory vesicles; T; tracheolae; Arrow heads (►) indicate mitochondria; Arrows (→) indicate basal cell membrane (micrograph I). Scale bars as depicted on each micrograph.

A

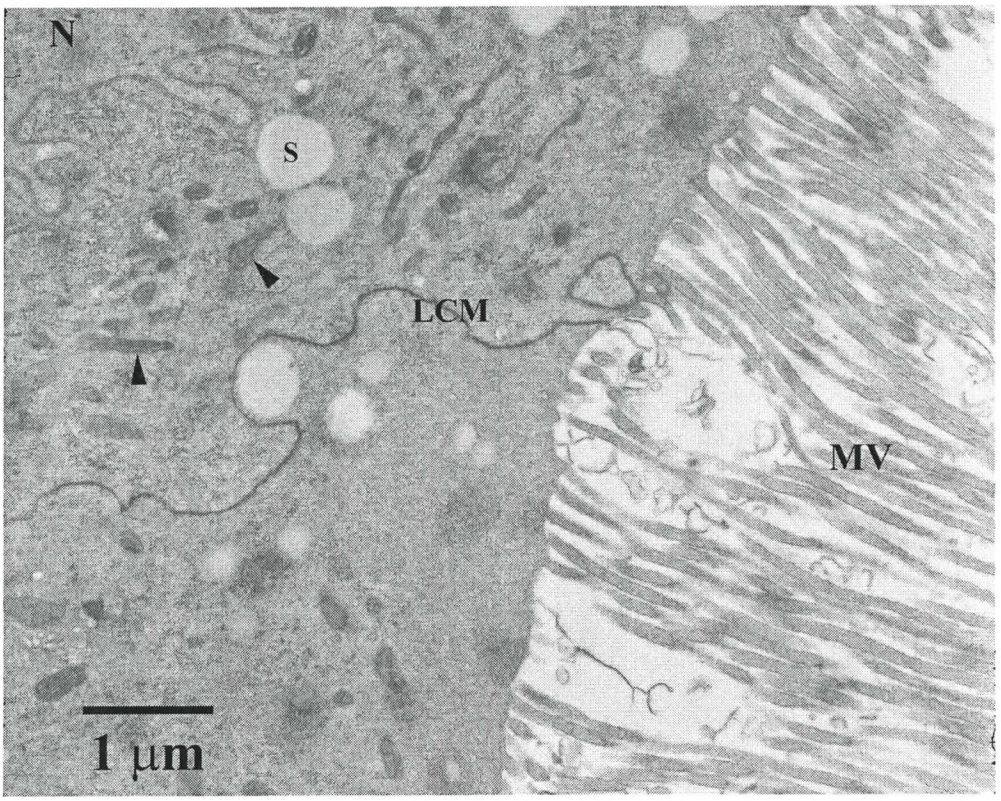

B

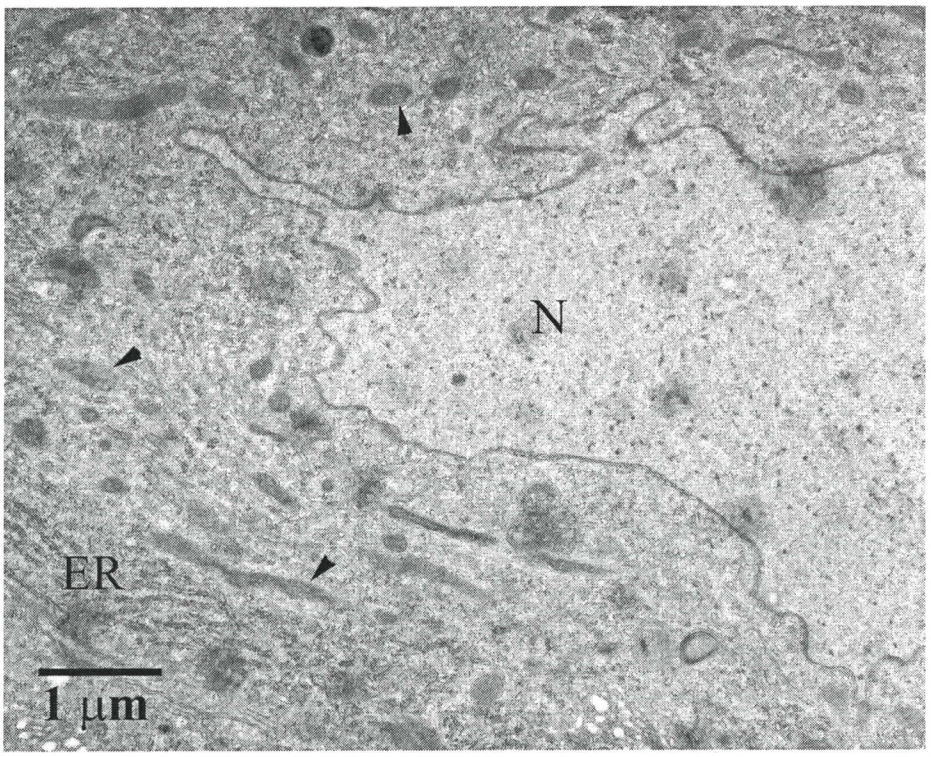

C

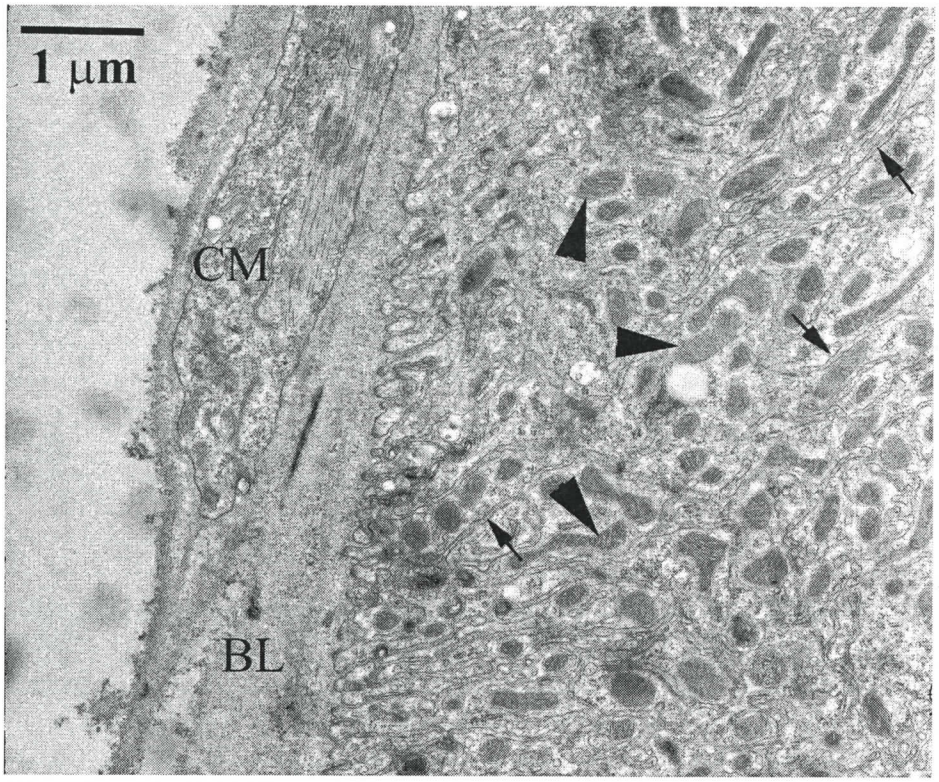

D

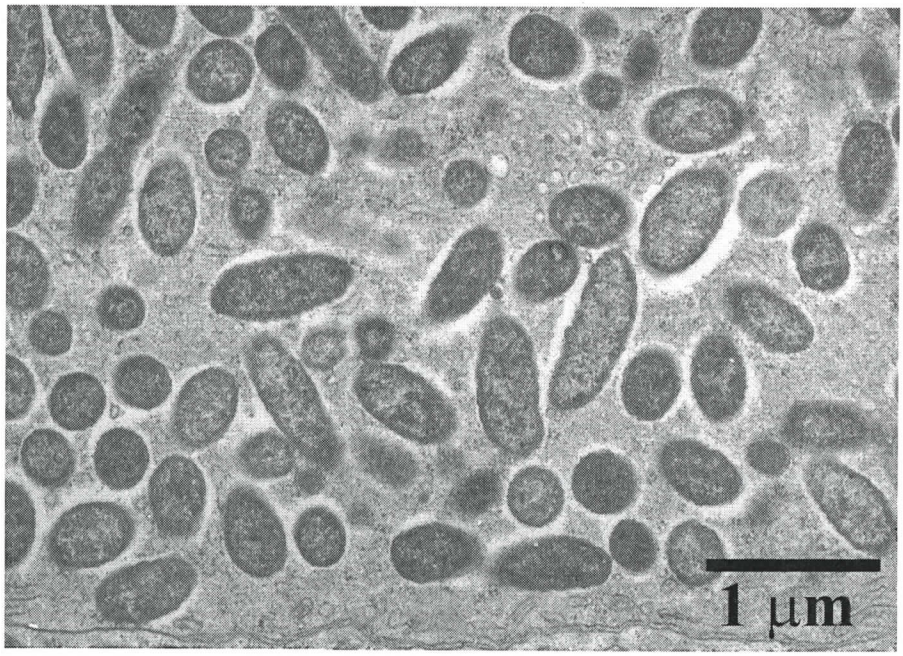

E

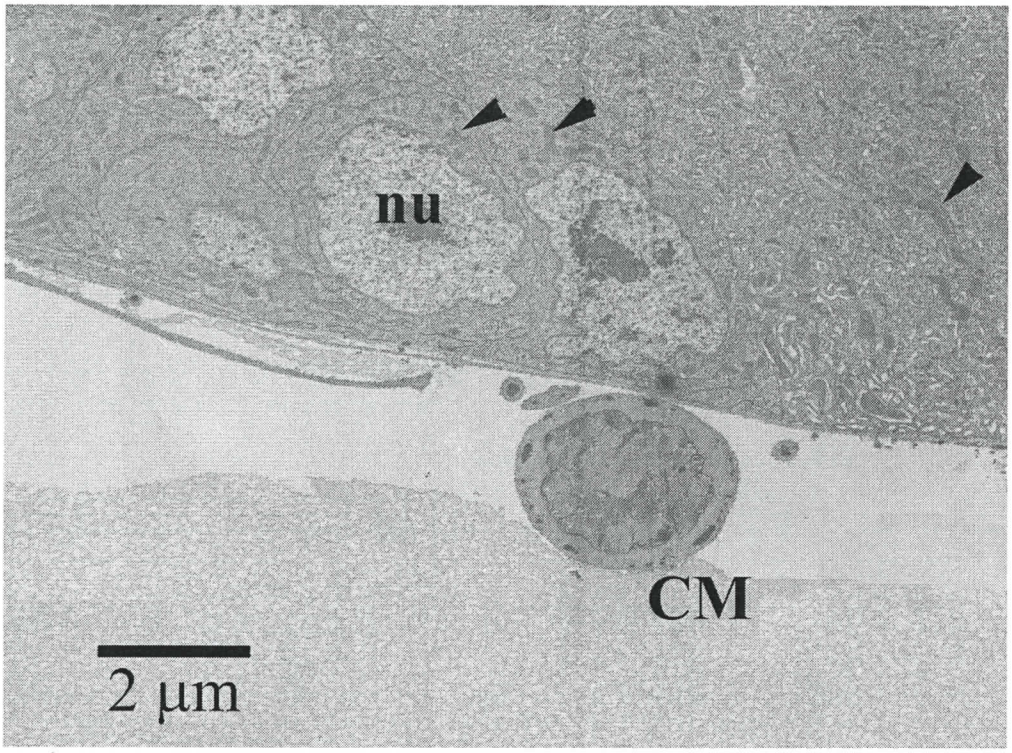

F

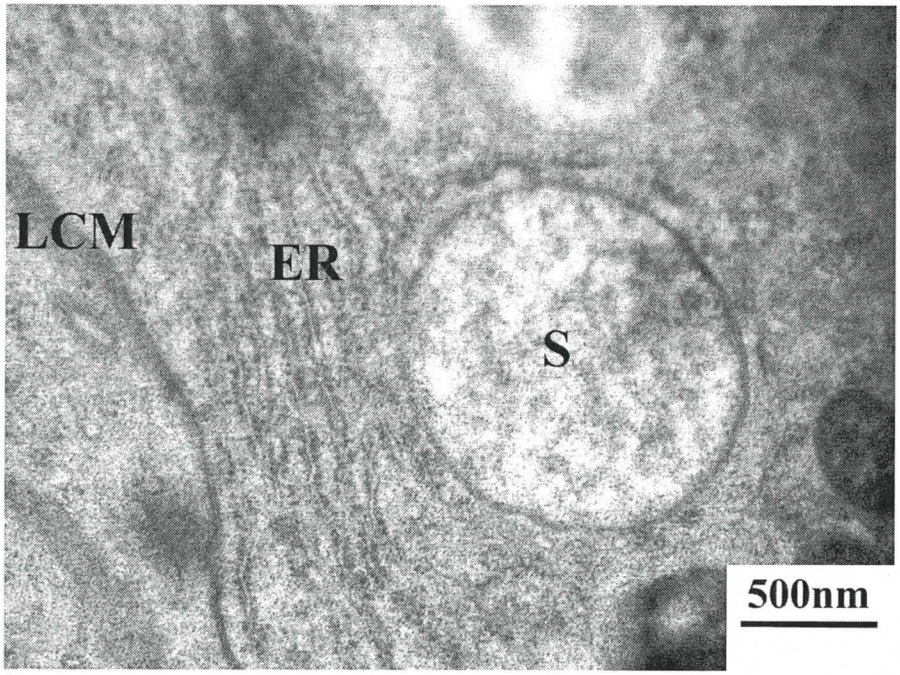

Figure 4-7. Transmission electron (A-F) micrographs of the midgut epithelia of *N. abietis* larvae.

The epithelial layer consisted of columnar cells that had dense microvillar borders (A). The epithelial cells exhibited a complex ultrastructure, including many mitochrondria, well defined ERs and an asymmetric nuclei (B). The basal membrane of the epithelia was highly invaginated and often compartmentalized the copious amount of mitochondria (C). Intracellular bacteria (D) localized to the apical region of the epithelial cells. Regenerative cells (E) were located in nidi that lay basal to the midgut epithelial cells and luminal to the basal lamina. B, bacteria; BL, basal lamina; CM, circular muscles; ER, endoplasmic reticulum; L, gut lumen; LCM, lateral cytoplasmic membrane; LM, longitudinal muscle; N, nucleus; nu, nucleolus; MV, microvilli; P, peritrophic membrane; R, regenerative cells S, secretory vesicles; T, tracheolae; Arrow heads (►) indicate mitochondria; Arrows (→) indicate basal cell membrane (micrograph I). Scale bars as depicted on each micrograph.

cells. These cells had a large nucleus that encompassed nearly 80% of the cross-sectional surface area. The nuclei contained a large nucleolus and several other small electron dense patches. Few organelles were observed other than a sparse quantity of mitochondria

Transmission electron microscopy revealed the complex ultrastructure of the midgut epithelial cells. The apical region was characterized by a dense layer of microvilli, which measured approximately 50 nm in diameter and 15 μm in length (~20% of the cell depth) (Figure 4-7 A). Submicrovillar, the cytoplasm was devoid of any organelles except the occasional secretory vesicle. Below this zone, mitochondria were abundant, as were the intracellular bacteria. Secretory vesicles typically accumulated in the apical region. Large, elongated, and circular nuclei were centrally located and constituted nearly one quarter (1/4) of the cell surface area (Figure 4-7 B). Well organized rER and Golgi complex were observed lateral to the nucleus, as well as large numbers of free ribosomes. Secretory vesicles were observed neighbouring the Golgi complex (Figure 4-7 F). Mitochondria were less concentrated in the central region but became densely packed in the basal region of the epithelial cells. Invagination of the basal membrane compartmentalized mitochondria within the basal cell region (Figure 4-7 C). Basal membrane invaginations often extended to one quarter of the cell depth, nearing the nucleus. The ultrastructure of midgut epithelial cells was consistent throughout the majority of the midgut length, except within the posterior region where cells exhibited an accumulation of lipid vesicles.

4.4.5 The Hindgut

In the pylorus region, the epithelia were composed of irregularly shaped columnar cells that had a dense microvillar border (Figure 4-8 A and B). The lumal area was greatly reduced compared to the midgut lumen and approximating half the size of the crop. Large numbers of tracheal cells and longitudinal muscles were observed adjacent to the epithelia; however the basal lamina connecting these cells was thin. Malpighian tubules were also observed in the hemocoel but not integrating into the gut lumen (not shown). Epithelial cells exhibited an ultrastructure that was similarly complex as the midgut epithelium. Cells had large numbers of mitochondria and a prominent Golgi complex. Nuclei were generally small and centrally located. The most distinct difference in ultrastructure was the presence of large numbers of vesicles at the basal membrane, which was deeply invaginated. Many cells contained lipid filled vesicles.

The final region examined of the excised larval gut was the ileum. This tissue resembled the foregut, having irregularly shaped squamal epithelia that were lined by a cuticular layer (Figure 4-9 A-C). Unlike the foregut, the hindgut epithelial layer was characterized by a high degree of folding. A nearly continuous layer of circular muscle was observed at the basal end of the epithelia, while in the center of the lumen, an unknown structure was found. The cells of the unknown structure resembled those of the epithelial layer and contained the same cuticular lining. Ultrastructural examination showed cells that had a large central nucleus and cytoplasm that extended laterally. Two to five nucleoli were typically observed within the nuclei, as well as many small electron dense patches at the nuclear periphery. Vesicles were often observed within the cytosol, particularly within the basal region and located close to the nucleus. Abundant quantities

A

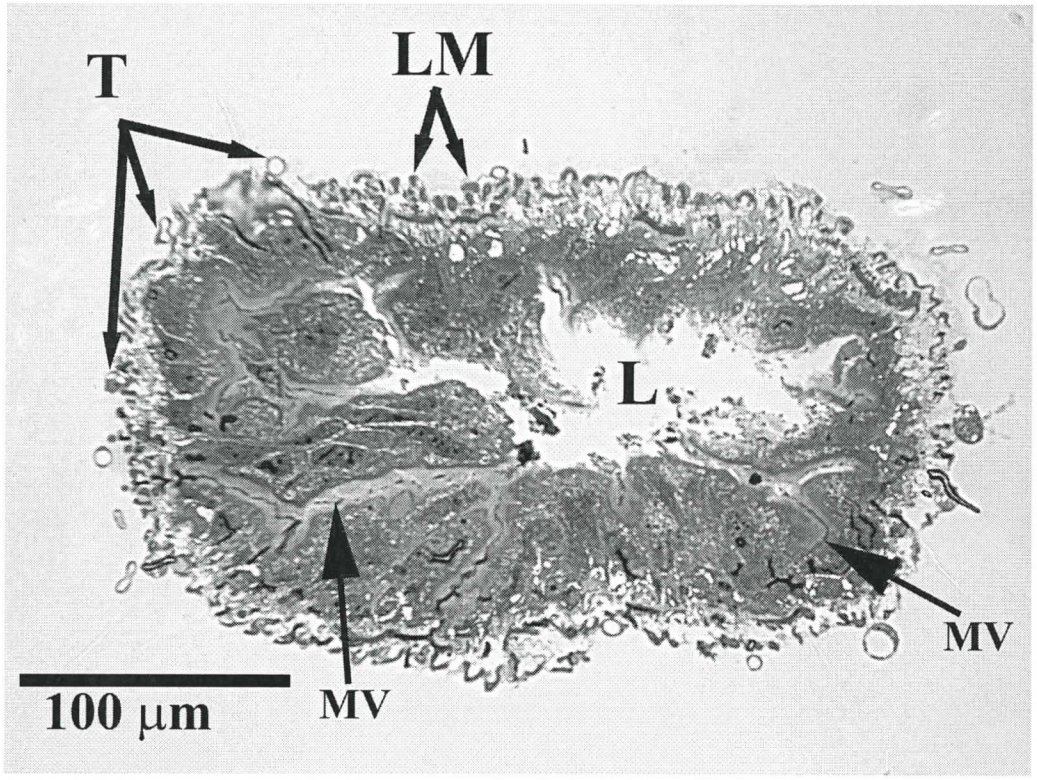

B

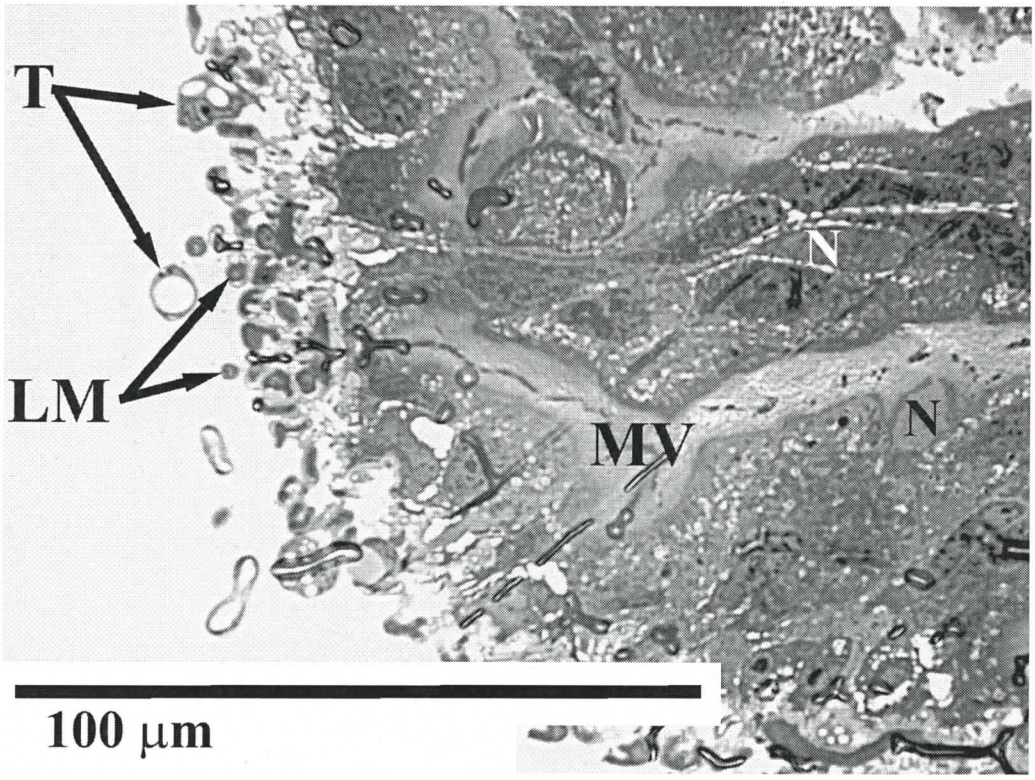

Figure 4-8. Light (A and B) micrographs of the pylorus-like structure and surrounding connective tissue of *N. abietis* larvae.

The epithelial layer consisted of irregularly shaped columnar cells that had a dense microvillar border and formed thick pad-like folds. Abundant longitudinal muscles and tracheolae lay basally to the epithelium within the basal lamina to formed a continuous layer. L, gut lumen; LM, longitudinal muscle; N, nucleus; MV, microvilli; T, tracheolae. Scale bars as depicted on each micrograph.

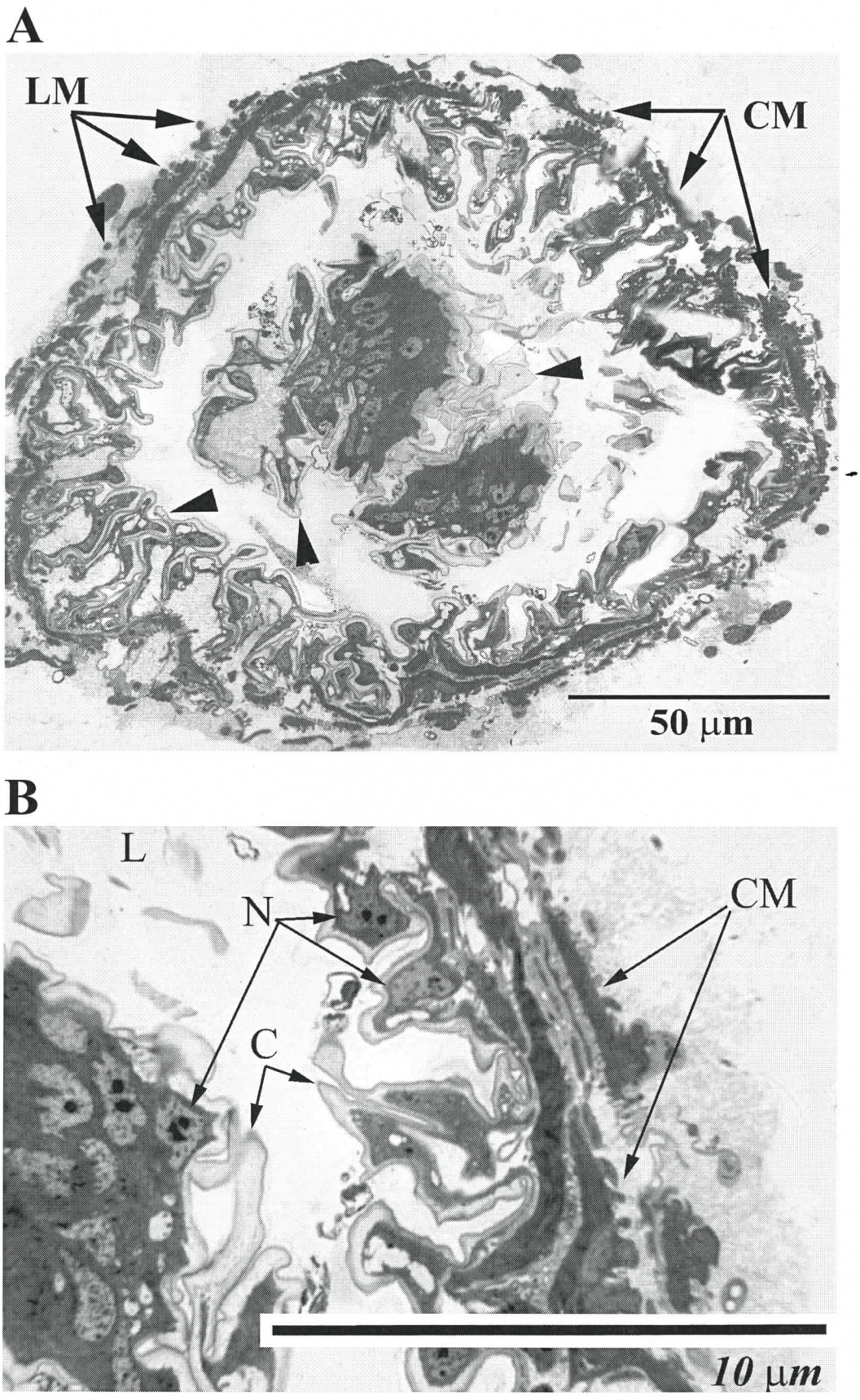
A
LM
CM
50 μm
B
L
N
CM
C
10 μm

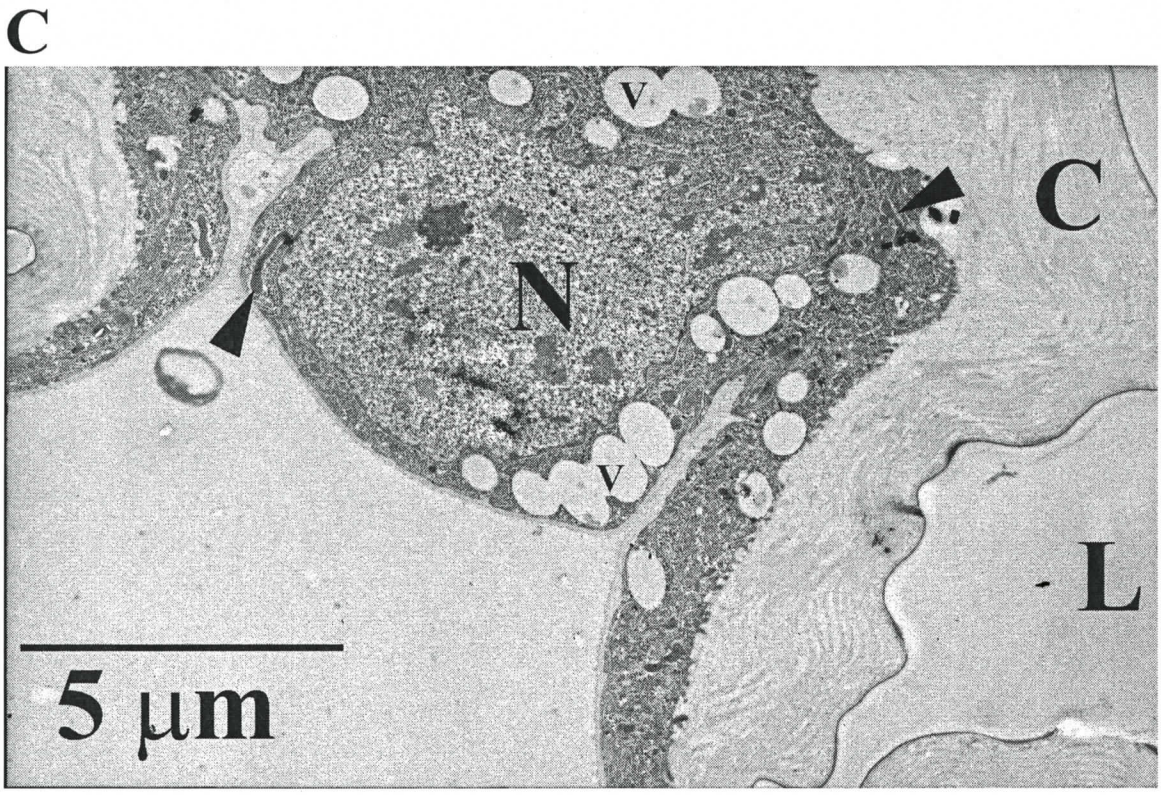

Figure 4-9. Light (A-B) and transmission electron (C) micrographs of the ileum and the surrounding connective tissue of *N. abietis* larvae.

The epithelial layer consisted of irregularly shaped squamal cells that were lined cuticle layer. Large circular muscles lay basally to the epithelium and were connected by the basal lamina to form a continuous layer. C, cuticle; CM, circular muscles; L, gut lumen; LM, longitudinal muscle; N, nucleus; V, vesicles; Arrow heads indicate cuticle (micrograph A) or mitochondria (micrograph C) . Scale bars as depicted on each micrograph.

of mitochondria and free ribosomes were observed throughout the cytosol but few other organelles were observed. The cuticle was composed of two layers, similar to the cuticle observed in the foregut, but the lining was twice as thick as the foregut cuticle and very fibrous. Coccoid and rod- shaped bacteria were found between the luminal folds of the epithelial layer, in closely proximity to the cuticular lining.

4.4.6 Gut Microbiota

The identity of gut inhabiting bacteria was investigated by culture independent techniques. *16S* rDNA was amplified from total extracted DNA of the *N. abietis* larval-gut using 2 sets of primers. Denature gradient gel electrophoresis separated four *16S* rDNA fragments when using the p984f-GC/p1401r set (Sequences 1-4), and two fragments after amplification from the p515f-GC/p806r primer set (Sequences 5-6). BLAST-n analysis and similarity rank comparisons to the Ribosome Database Projects II sequences resulted in four possible bacteria types: *Rahnella sp.* (Sequence #1), *Yersinia sp.* (Sequence #2-4), Enterobacteriaceae sp (Sequence #5), and an Alphaproteobacteria (Sequence #6).

Phylogenetic analysis confirmed the predicted identities of the first four bacteria and showed their close relationship to other known insect-gut microbes in the Enterobacteriaceae family of Gammaproteobacteria. Maximum Parsimony and Neighbor Joining analyses suggest that bacterium #1 was a *Rahnella aquatilis* subspecies. Although both analyses supported the finding that bacteria #2-4 belong to the genus *Yersinia*, their degree of relatedness to *Yersinia aleksiciae* varied (Table 4-1 and Figure 4-10 A&B).

Table 4-1. NCBI Blast-n results and Ribosomal Database Project II comparison values for *16S* RNA gene sequences. DNA, extracted from *N. abietis* larval-midguts, was amplified by PCR and separated by DGGE. The separated products were purified and sequenced, then compared to *16S* sequences in GenBank† and the Ribosomal Database Project II (RDP II)*.

DGGE fragment (primer set)	Predicted Identity	Blast-n Match Accession No. (% identity)	RDP II (% identity)
#1 (p984f-p1401r)	*Rahnella* sp.	U90758 (99%), DQ440548 (97%)	S000438772 (96.5%), S000653581 (96.5%)
#2 (p984f-p1401r)	*Yersinia* sp.	AJ627599 (99%), AJ627600 (99%)	S000539482 (94.6%), S000539483 (94.6%)
#3 (p984f-p1401r)	*Yersinia* sp.	AJ627599 (99%), AJ627600 (99%)	S000539482 (95.3%), S000539483 (95.3%)
#4 (p984f-p1401r)	*Yersinia* sp.	AJ627599 (99%), AJ627600 (99%)	S000539482 (100%), S000539483 (100%)
#5 (p515f-p806r)	Enterobacteriaceae sp.	AY859722 (97%) U93263 (97%) DQ440548 (97%)	S000015297 (100%), S000440651 (100%), S000497099 (100%)
#6 (p515f-p806r)	Uncultured Alphaproteobacterium	AJ459874 (100%) DQ163946 (100%)	S000093253 (100%) S000600168 (100%)

† NCBI Blast website: http://www.ncbi.nlm.nih.gov/BLAST

* RDP II website: http://rdp.cme.msu.edu/seqmatch/seqmatch_intro.jsp

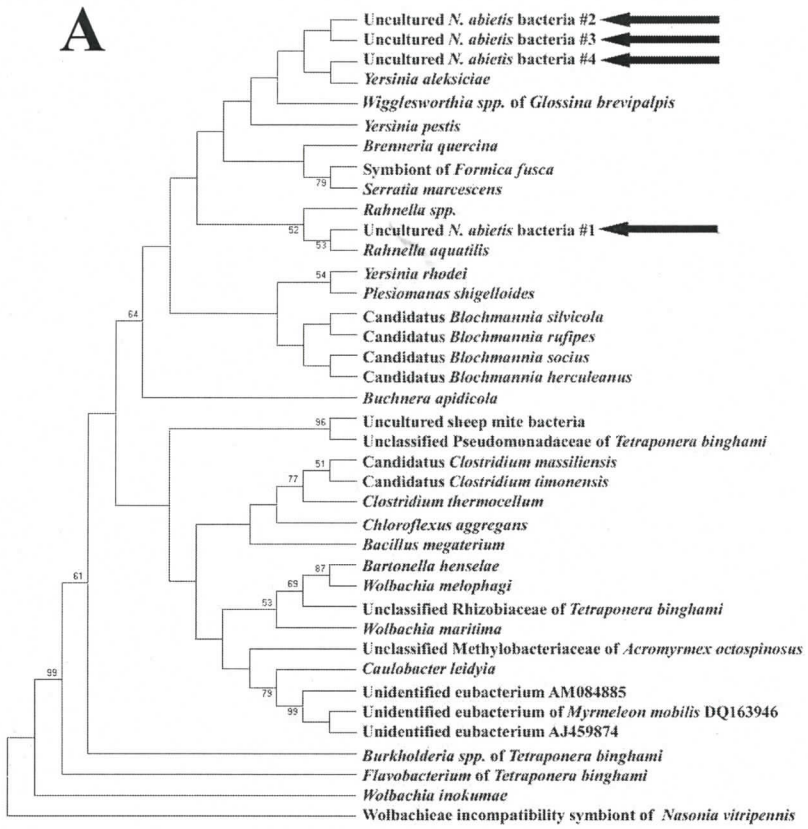
A
Uncultured N. abietis bacteria #2
Uncultured N. abietis bacteria #3
Uncultured N. abietis bacteria #4
Yersinia aleksiciae
Wigglesworthia spp. of Glossina brevipalpis
Yersinia pestis
Brenneria quercina
Symbiont of Formica fusca
Serratia marcescens
Rahnella spp.
Uncultured N. abietis bacteria #1
Rahnella aquatilis
Yersinia rhodei
Plesiomanas shigelloides
Candidatus Blochmannia silvicola
Candidatus Blochmannia rufipes
Candidatus Blochmannia socius
Candidatus Blochmannia herculeanus
Buchnera apidicola
Uncultured sheep mite bacteria
Unclassified Pseudomonadaceae of Tetraponera binghami
Candidatus Clostridium massiliensis
Candidatus Clostridium timonensis
Clostridium thermocellum
Chloroflexus aggregans
Bacillus megaterium
Bartonella henselae
Wolbachia melophagi
Unclassified Rhizobiaceae of Tetraponera binghami
Wolbachia maritima
Unclassified Methylobacteriaceae of Acromyrmex octospinosus
Caulobacter leidyia
Unidentified eubacterium AM084885
Unidentified eubacterium of Myrmeleon mobilis DQ163946
Unidentified eubacterium AJ459874
Burkholderia spp. of Tetraponera binghami
Flavobacterium of Tetraponera binghami
Wolbachia inokumae
Wolbachieae incompatibility symbiont of Nasonia vitripennis

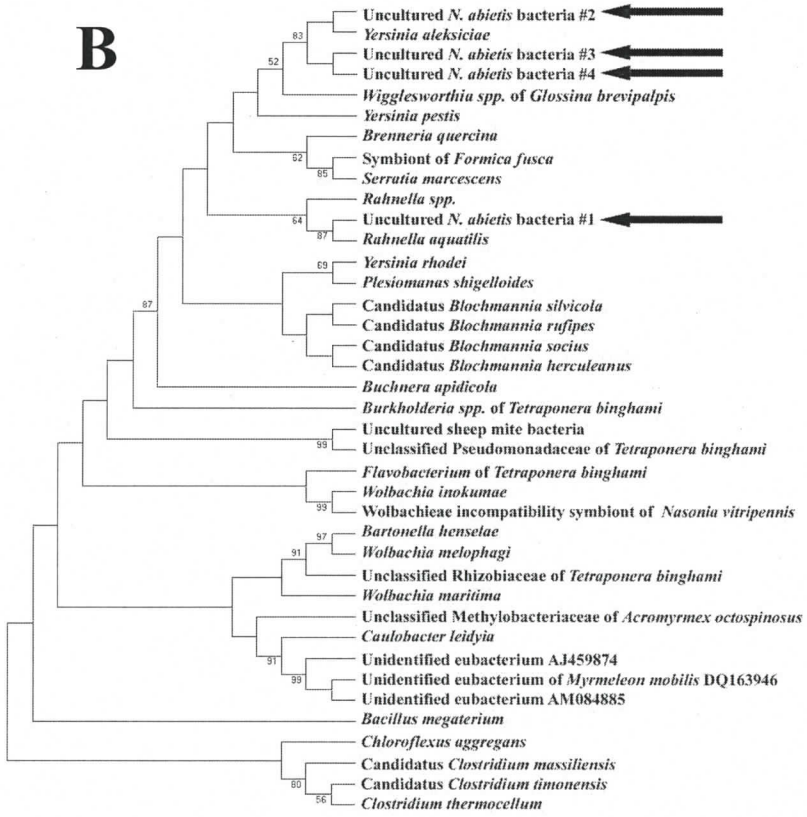
B
Uncultured N. abietis bacteria #2
Yersinia aleksiciae
Uncultured N. abietis bacteria #3
Uncultured N. abietis bacteria #4
Wigglesworthia spp. of Glossina brevipalpis
Yersinia pestis
Brenneria quercina
Symbiont of Formica fusca
Serratia marcescens
Rahnella spp.
Uncultured N. abietis bacteria #1
Rahnella aquatilis
Yersinia rhodei
Plesiomanas shigelloides
Candidatus Blochmannia silvicola
Candidatus Blochmannia rufipes
Candidatus Blochmannia socius
Candidatus Blochmannia herculeanus
Buchnera apidicola
Burkholderia spp. of Tetraponera binghami
Uncultured sheep mite bacteria
Unclassified Pseudomonadaceae of Tetraponera binghami
Flavobacterium of Tetraponera binghami
Wolbachia inokumae
Wolbachieae incompatibility symbiont of Nasonia vitripennis
Bartonella henselae
Wolbachia melophagi
Unclassified Rhizobiaceae of Tetraponera binghami
Wolbachia maritima
Unclassified Methylobacteriaceae of Acromyrmex octospinosus
Caulobacter leidyia
Unidentified eubacterium AJ459874
Unidentified eubacterium of Myrmeleon mobilis DQ163946
Unidentified eubacterium AM084885
Bacillus megaterium
Chloroflexus aggregans
Candidatus Clostridium massiliensis
Candidatus Clostridium timonensis
Clostridium thermocellum

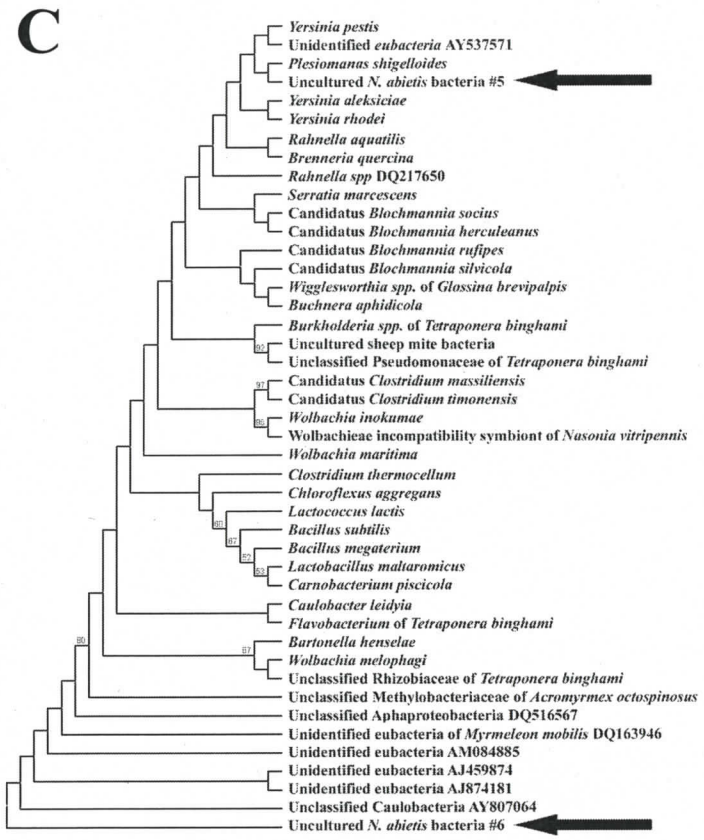
C
Yersinia pestis
Unidentified eubacteria AY537571
Plesiomanas shigelloides
Uncultured N. abietis bacteria #5
Yersinia aleksiciae
Yersinia rhodei
Rahnella aquatilis
Brenneria quercina
Rahnella spp DQ217650
Serratia marcescens
Candidatus Blochmannia socius
Candidatus Blochmannia herculeanus
Candidatus Blochmannia rufipes
Candidatus Blochmannia silvicola
Wigglesworthia spp. of Glossina brevipalpis
Buchnera aphidicola
Burkholderia spp. of Tetraponera binghami
Uncultured sheep mite bacteria
Unclassified Pseudomonaceae of Tetraponera binghami
Candidatus Clostridium massiliensis
Candidatus Clostridium timonensis
Wolbachia inokumae
Wolbachieae incompatibility symbiont of Nasonia vitripennis
Wolbachia maritima
Clostridium thermocellum
Chloroflexus aggregans
Lactococcus lactis
Bacillus subtilis
Bacillus megaterium
Lactobacillus maltaromicus
Carnobacterium piscicola
Caulobacter leidyia
Flavobacterium of Tetraponera binghami
Bartonella henselae
Wolbachia melophagi
Unclassified Rhizobiaceae of Tetraponera binghami
Unclassified Methylobacteriaceae of Acromyrmex octospinosus
Unclassified Aphaproteobacteria DQ516567
Unidentified eubacteria of Myrmeleon mobilis DQ163946
Unidentified eubacteria AM084885
Unidentified eubacteria AJ459874
Unidentified eubacteria AJ874181
Unclassified Caulobacteria AY807064
Uncultured N. abietis bacteria #6

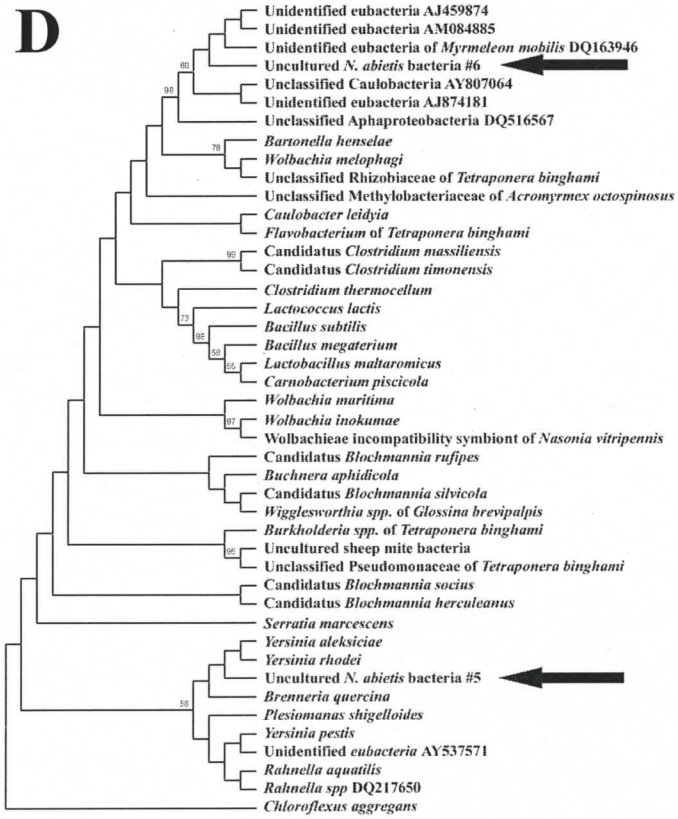
D
Unidentified eubacteria AJ459874
Unidentified eubacteria AM084885
Unidentified eubacteria of Myrmeleon mobilis DQ163946
Uncultured N. abietis bacteria #6
Unclassified Caulobacteria AY807064
Unidentified eubacteria AJ874181
Unclassified Aphaproteobacteria DQ516567
Bartonella henselae
Wolbachia melophagi
Unclassified Rhizobiaceae of Tetraponera binghami
Unclassified Methylobacteriaceae of Acromyrmex octospinosus
Caulobacter leidyia
Flavobacterium of Tetraponera binghami
Candidatus Clostridium massiliensis
Candidatus Clostridium timonensis
Clostridium thermocellum
Lactococcus lactis
Bacillus subtilis
Bacillus megaterium
Lactobacillus maltaromicus
Carnobacterium piscicola
Wolbachia maritima
Wolbachia inokumae
Wolbachieae incompatibility symbiont of Nasonia vitripennis
Candidatus Blochmannia rufipes
Buchnera aphidicola
Candidatus Blochmannia silvicola
Wigglesworthia spp. of Glossina brevipalpis
Burkholderia spp. of Tetraponera binghami
Uncultured sheep mite bacteria
Unclassified Pseudomonaceae of Tetraponera binghami
Candidatus Blochmannia socius
Candidatus Blochmannia herculeanus
Serratia marcescens
Yersinia aleksiciae
Yersinia rhodei
Uncultured N. abietis bacteria #5
Brenneria quercina
Plesiomanas shigelloides
Yersinia pestis
Unidentified eubacteria AY537571
Rahnella aquatilis
Rahnella spp DQ217650
Chloroflexus aggregans

Figure 4-10. Phylogenetic analysis of the *16S* rRNA gene from bacteria isolated from insect guts.

Maximum parsimony (A and C) and Neighbour joining trees (B and D) were determined using the Mega 3.1 program with 1000 bootstrap repetitions. Sequences of *16S* rDNA from the microbiota of *N. abietis* larval guts are depicted by arrows. Bacterial isolates 1-4 (from primer set p984f-GC/p1401r) are represented in Trees A and B, while isolate 5 and 6 (primer set p515f /p806r) are represented in Trees C and D.

The identity of bacterium #5 was not determined because results from Maximum Parsimony and Neighbor Joining analysis were inconsistent (Figure 4-10 C&D). This difficulty in confirming identity may be a result of the small amplicon size. However, bacterium #6, which was amplified with the same primer set, clearly clustered with the Alphaproteobacteriaceae. Maximum Parsimony analysis suggested that bacterium #5 belonged to the genus *Caulobacter*. New primer sets amplifying larger gene segments, would help to resolve the identity of these bacteria.

4.5 Discussion

The morphology and ultrastructure observed in the alimentary canal of larval *N. abietis* are common to many other insect larvae, although few contain all the same structures. The crop epithelium of *Drosophila auraria* consists of a single layer of thin epithelial cells whose apex is covered with cuticle (Dimitriadis & Papamanoli, 1992). These epithelial cells contain small amounts of rough endoplasmic reticulum, Golgi complexes and secretory granules. The crop epithelia of *N. abietis* have similar ultrastructure, but the Golgi complex and secretory vesicles were not observed. The crop is a storage medium for undigested food and digestive enzymes are probably provided by cells of the salivary glands and fluid that passes forward from the midgut (Chapman, 1985; Dimitriadis & Papamanoli, 1992), eliminating the need for secretion from crop epithelial cells and passage through the impermeable cuticle layer. Folding and unfolding of the crop is dependent on the amount of food contained within the organ. The tissue observed in *N. abietis* was unfolded as large amounts of plant food were present therein.

The presence of food retained in the crop is likely due to the actions of the stomodaeal or cardiac valve. Many insects have this structure, which limits the passage of food from

the crop into the midgut. Few insects, however, retain both the valve and proventriculus (Chapman, 1985). Epithelial cells of the valve have been studied in the phlebotomine sandfly, *Lutzomyia longipalpis*, and transmission electron microscopy showed an enrichment of mitochondria and pit-like structures that are probably secretory in nature (Tang & Ward, 1998). Secretory vesicles were not observed in the sawfly foregut epithelial cells, but there is no functional reason to expect these vesicles in the valve as the nature of this organ is to limit the passage of food.

Most of the mechanical digestion of food is performed by the grinding action of the proventriculus. This organ is typically found in insects feeding on solid foods (Nation, 2002) and is characterized by heavily sclerotized teeth and well developed circular musculature. Six main folds run longitudinally through the epithelia. In termites and cockroaches, the proventriculus is arranged into three regions: the stomodaeal valve, a pulvillar area, and the dental area (Miller & Fisk, 1971; Noirot & Noirot-Timothee, 1969). In larval odonatans and some adult coleopterans, the symmetry of the proventriculus is tetraradial (Chapman, 1985). Little information is available with regards to the ultrastructure of the foregut and most studies of the proventriculus have examined the internal anatomy of the organ. Therefore a comparison of the ultrastructure of the *N. abietis* larval proventriculus with the organ in other insects could not be made.

The ventricular caeca are important structures in the absorption of digested nutrients. A countercurrent flow between the endo- and ectoperitrophic spaces pushes nutrients to the anterior region of the gut as food passes posteriorly (Chapman, 1985; Nation, 2002; Wigglesworth, 1972). Due to this flow, the ultrastructure exhibited by caeca epithelial cells is not surprising. The presence of large quantities of mitochondria and free

ribosomes, as well as a well developed rER, all support the function of these cells in nutrient absorption (Nation, 2002). Invagination of the basal membrane and microvilli increase the surface are of the cuboidal epithelial cells, allowing for efficient transfer of nutrients from the lumen to the hemocoel.

The midgut is the best characterized region of the insect gut in general. The complex ultrastructure of these cells is in accordance with their role in the secretion of digestive enzymes and absorption of nutrients. The best characterized hymenopteran midgut, with regards to ultrastructural properties, is the parasitic wasp, *Nasonia vitripennis* (Walk.) (Davies, 1977; Davies & King, 1977a, b). This midgut epithelium consists of regenerative and digestive cells, and is bordered by tracheal cells and muscles along the basal laminae. The digestive cells show similar ultrastructure to those observed in the *N. abietis* midgut: a dense microvillar border is apical to a zone of mitochondria, well-organized rER, Golgi complex, and nucleus in the central region, and a basal region characterized by deep infolds of the cell membrane that frequently compartmentalizes mitochondria. The regenerative cells of *N. vitripennis* were singly located basal to the digestive cells and contained a large nucleus with a sparse cytoplasm. Regenerative cells in *N. abietis* had similar morphology, except that they occurred in nidi, which are more similar to the regenerative patches found in the ant, *Solenopsis saevissima* (Arab & Caetano, 2001).

Other studies of midgut structures have described two different cell types that were not observed in *N. abietis* (Arab & Caetano, 2001; da Cruz-Landim & Cavalcante, 2003; Gul *et al.*, 2001; Hecker, 1977; Hung *et al.*, 2000; Levy *et al.*, 2004; Neves *et al.*, 2000). Goblet cells are found in lepidopteran and ephemenopteran insects (Arab & Caetano,

2001; Gul *et al.*, 2001), as well as a single description in the Oriental fruit fly, *Bactrocera dorsalis* (Hung *et al.*, 2000). These cells are responsible for the exchange of potassium and hydrogen ions across the midgut epithelium, which creates a basic lumen environment and plays an important role in amino acid absorption (Billingsley & Lehane, 1996; Hennigan *et al.*, 1993). The second epithelial type, endocrine cells, has been documented in dipteran, lepidopteran and apocritan insects (Gul *et al.*, 2001; Hung *et al.*, 2000; Neves *et al.*, 2000). These cells have cytoplasm that does not retain histological stains well and are locate along the basal region of the epithelium. Frequently cytoplasmic projections are observed extending up between the digestive cells to the gut lumen.

The hindgut tissues of *N. abietis* are similar to those described in other insects (Murakami & Shiotsuki, 2001; Villaro *et al.*, 1999). The pylorus of *Drosophila spp.* and *Formica nigricans* consist of epithelial cells that are cuboidal and has a microvillar border. This structure typically forms a valve due to the thick pad-like folds that restrict food passage, instead of having valve-like invagination (Chapman, 1985). The ileum is responsible for the absorption of water and ions. The more fibrous cuticle that lines this tissue may facilitate absorption, as compared to the cuticle of the foregut. The extensive folding of the hindgut provides additional surface area by which absorption may occur (Chapman, 1985; Nation, 2002; Wigglesworth, 1972).

Microscopic analysis revealed bacteria in the lumen of both the midgut and hindgut of *N. abietis* larvae. Due to the uncultured nature of these bacteria it is impossible to state whether the microbes are indigenous or transient. Bacteria of similar structure have been described in the *Hofmannoophila pseudospretella* (Lepidoptera) midgut (Shannon *et al.*,

2001) and the *Tetraponera binghami* (Hymenoptera) hindgut pouch (van Borm *et al.*, 2002b). Ultrastructural similarities exist between the *N. abietis* intracellular microbes and Candidatus *Blochmannia spp.* detected in bacteriocytes of the *Camponotus* genus of ants. Both bacteria are located free-floating in the cytoplasm of the host midgut epithelial cells, a characteristic that has to date only been described for Candidatus *Blochmannia* microbes (Dillon & Charnley, 2002; Sauer *et al.*, 2002). In the *Camponotus* ants, the intracellular bacteria are localized to the midgut bacteriocytes and the ova of mature adults. The bacteriocytes intercalate between normal digestive cells and do not have a microvillar border (Boursaux-Eude & Gross, 2000). In contrast, the intracellular bacteria of *N. abietis* are located in midgut epithelial cells, as the microvillar border is readily apparent. These bacteria may represent a new species that are important for providing essential nutrients to their host.

Many of the *16S* bacterial sequences obtained from the gut of *N. abietis* are common insect-gut-dwelling species, similar to species identified in other sawfly gut tissues: *Pristiphora geniculata, Acantholyda erythrocephala* and *Pikonema alaskensis* (Dr. Rob Graham, Atlantic Forestry Center, personal communication). The first five sequences represent bacteria that belong to the Gammaproteobacteria, specifically those in the Enterobacteriaceae family of Gram-negative, anaerobic, rod-shaped microbes. *Rahnella aquatilis* and *Yersinia aleksiciae* have not been described as insect gut microbes, but *R. aquatilis* has been isolated from both the fowl-tick, *Argas persicus* (Montasser, 2005), and the intestinal contents of snails in Germany (Brenner *et al.*, 1998). Also, uncultured *Rahnella spp.* were reported in GenBank (Accession # U84730) as isolates of the microbial gut flora from coleopterans *Phaleria sp.* and *Latreille sp.* (Tenebrionidae).

Rahnella spp. are commonly isolated from plant roots and foliage (Hashidoko *et al.*, 2002; Izumi *et al.*, 2006), indicating that this bacteria may have originally been acquired through the sawflies diet. *Rahnella aquatilis* has been shown to ferment several polysaccharides, including cellobiose (Brenner *et al.*, 1998). Recently, *Rahnella spp* have been demonstrated as strong nitrogen fixers (Brenner *et al.*, 1998; Izumi *et al.*, 2006), a characteristic that would be important for nitrogen recycling in nutrient poor diets and promote the retention of this bacterium within sawfly gut as a symbiont.

Species of *Yersinia* have been isolated from other insect guts (Ulrich *et al.*, 1981); therefore it is not surprising that bacteria from the same genus were found in the gut flora of *N. abietis.* No beneficial characteristics have been attributed to *Yersinia.* Their ubiquitous presence in soils and detritus suggest that this bacterium is more likely to be a transient microbe ingested with food matter, rather than a permanent flora of the sawfly gut.

16S-sequence analysis of bacterium #5 and subsequent phylogenetic comparisons to other Gammaproteobacteria resulted in an ambiguous identification. Maximum Parsimony indicated that the closest relative to the *N. abietis* bacteria was *Plesiomanas shigelloides*, while Neighbor Joining analysis suggested that *Y. rhodei* was more closely related. BLAST-n searches of the 16S ribosomal sequence commonly aligned *Serratia* spp. with high degrees of identity (97%). *16S* sequences from these genera, *Yersinia, Rahnella,* and *Serratia,* have been shown to cluster closely together in a Group B of Enterobacteriaceae, with the main signature nucleotides located between positions 590-649 (Sproer *et al.*, 1999). The p515f-p806r primer set amplifies the variable V4 region of 16S rDNA between base pairs 627 and 807, resulting in only a 22 bp overlap of the

signature nucleotides. Without greater variability of the sequence data of bacterium #5, a positive identity is difficult and the bacterium can only be classified as an Enterobacteriaceae.

Finally 16S-sequence analysis indicated that bacterium #6 was a member of the Alphaproteobacteria, showing high similarity to the uncultured bacteria of insect larvae and soil (GenBank AJ459874, DQ163946, and AM084885; Table 4-1, Figure 4-10 C and D). An uncultured Caulobacter (GenBank AY807064) aligned within the unidentified Alphaproteobacteria, supported by a 98% bootstrap value, suggesting that the *N. abietis* bacterium #6 may be Caulobacter-like. If this bacterium is a Caulobacter, the microbe may play an important role in nutrient acquisition since Caulobacteria have been shown to acquire phosphorus from nutrient poor environments (Gonin *et al.*, 2000). Caulobacteria have typically been isolated from aquatic environments, but a few isolates have been reported from the intestinal contents of a millipede (Abraham *et al.*, 1999) and the predaceous mite *Tetranychus urticae* (Hoy & Jeyaprakash, 2005).

The diversity of *N. abietis* gut-microbiota is relatively simple compared to the variety of microbes observed in termite and cockroach guts (Cruden & Markovetz, 1984; Hongoh *et al.*, 2003). Over 270 bacterial phylotypes have been detected in the gut of the lower termite *Reticulitermes speratus* and were classified into 9 of the 20 phyla of Eubacteria (Hongoh *et al.*, 2003). In contrast, only 4 phylotypes were detected in *N. abietis* and were classified within a single eubacterial phylum (Proteobacteria). Low bacterial diverisity has been reported in other insect guts, but the flora is typically composed of species from multiple bacterial phyla. The bacterial communuity characterized from the gut of the gypsy moth, *Lymantria dispar* (Lepidoptera), depends

on the insect's diet, and the bacterial diversity ranges from 15 phylotypes at its most complex to 7 phylotypes at its simplest (Broderick *et al.*, 2004). A total of 13 microbial genera were identified from larvae feeding on all diet sources and were classified within the Actinobacteria, the Bacteroidetes/Chlorobi group, Firmicutes and Proteobacteria. Similar results were obtained from cultured isolates and 16S sequence analysis of microbes detected within the midgut of *Culex quinquefasciatus* (Order Diptera), where bacteria from 13 genera were identified (Pidiyar *et al.*, 2004). The majority of bacteria belonged to the Gammaproteobacteria class (60% of cultured and 46% of culture-independent), while Actinobacteria and Firmicutes constituted the remainder of the bacterial types.

While diet plays a key role in the acquisition of bacterial flora observed in insect guts, morphology is also a significant factor affecting the diversity of the gut microbiota. Many termites and cockroaches have a complex and convoluted gut (Brune & Friedrich, 2000; Wigglesworth, 1972) that has evolved to allow the retention of bacteria in specialized fermentation structures. Insects possessing simple and straight alimentary canals, such as the Diprionidae, Lepidoptera, and many Diptera, generally have a lower diversity of gut microbes (Dillon & Dillon, 2003). Due to the selective diet of *N. abietis* and the simple morphology of its gut, the low level of bacterial diversity is expected.

In summary, the gut morphology and ultrastructure of *N. abietis* larvae has been described. This represents the first fine-detail study of most of a diprionid sawfly gut. The foregut has three regions that aid in the storage and breakdown of food, and the ultrastructure of this tissue reflects its function in these processes. A cuticle lines cells that have simple ultrastructural properties, creating an impenetrable region. The midgut

is composed of three main structures: a peritrophic membrane, ventricular caeca and the midgut epithelia. Secretion of digestive enzymes and absorption of nutrients necessitate the complex ultrastructure exhibited by these cells. Finally, the hindgut consists of two regions, a sphincter created by pad-like folds of the epithelial layer and the ileum, which is highly folded to create abundant surface area for water and ion absorption. The gut microbiota of *N. abietis* larvae are located in the gut lumen of the foregut, midgut and hindgut. Intracellular bacteria were also detected in the digestive epithelial cells of the midgut tissue. Four types of bacteria were identified, based on *16S* rDNA gene sequencing and phylogenetic comparisons to known insect gut microbiota. Two of the isolates were defined as a *Rahnella sp.* and *Yersinia sp.*, based on their closest relatives *Rahnella aquatilis* and *Yersinia aleksiciae*, respectively. The other two isolates we have determined to be of the Enterobacteriaceae and Caulobacteriaceae families. Further analysis will help determine an identity to the species level and if these bacteria play a role in digestive biology of the sawfly.

Chapter 5 Characterization of the *N. abietis* nucleopolyhedrovirus pathology in the alimentary canal of the native larval host, *N. abietis*

5.1 Abstract

Microscopic examination of NeabNPV infected *N. abietis* larvae, from 1-72 hours post inoculation (hpi), revealed distinct phases of cytopathology, most of which were in strong agreement with NeabNPV DNA replication kinetics and transcriptional analyses previously performed. While viral entry and translocation to the nucleus were not observed, cytopathic effects, characterized by cellular and nuclear hypertrophy and the presence of a virogenic stroma, were observed within 5 hpi. Nucleocapsid assembly was detected within the intrastromal spaces by 8 hpi and continued until 24 hpi. Localization of virions to the peristromal ring-zone were observed within 12 hpi, however polyhedra formation did not occur until 12 hours later. During the very late phases of infection, the virogenic stroma condensed and polyhedra matured gradually. The early initiation of each phase of NeabNPV infection, as compared with those of AcMNPV, suggests that baculoviruses with limited trophism undergo rapid progression of the infectious cycle before host defences are activated.

5.2 Introduction

Baculovirus infection and pathology are well characterized for viruses that infect lepidopteran hosts, and is best characterized for the *Autographa* californica nucleopolyhedrovirus (AcMNPV) (Trudeau *et al.*, 2001). The bias in information about lepidopteran nucleopolyhedroviruses has occurred for three reasons: 1) *in vitro* culturing systems for lepidopteran NPVs have allowed for characterization of the infection cycle and pathology in a controlled environment, 2) *in vitro* culture systems are not available

for non-lepidopteran NPVs, and 3) non-lepidopteran NPVs have a monorganotrophic pathology that lacks the second phenotypic form of virions, budded virus.

The model baculovirus pathology *in vivo*, characterized from extensive studies of lepidopteran NPV infections, begins with the ingestion of occlusion bodies (OBs). Once in the midgut lumen, the alkaline fluids and digestive enzyme of the host dissolve the OBs. This process occurs rapidly and releases the embedded occlusion derived virions (ODV), which migrate through the peritrophic membrane to the microvilli of the digestive columnar cells. ODV attachment of AcMNPV to the microvilli of *Trichoplusia ni* midgut cells has been reported has early as 15 minutes (Granados & Lawler, 1981). Factors released from the dissolved OBs, termed enhancins, alter the integrity and elasticity of the peritrophic membrane and allow for passage of the ODVs (Derksen & Granados, 1988).

Once at the microvillar membrane, direct fusion of the viral envelope and cytoplasmic membrane occurs. Little is known about the fusion process, other than a cellular ligand or receptor is involved. This site is easily saturated and protease activity is able to cleave the ligand from the cell, inhibiting viral entry (Granados & Lawler, 1981). After entry, nucleocapsids are translocated to the nucleus using F-actin cables. Each nucleocapsid is associated with a single actin cable via the VP39 and P78/83 proteins, and the number of cables is directly proportional to the multiplicity of infection (Charlton & Volkman, 1993; Kasman & Volkman, 2000; Lanier & Volkman, 1998).

Uncoating of the nucleocapsid occurs within the nucleus, allowing for the rapid transcription of immediate early genes. As the viral replicative machinery is expressed, host chromatin condenses and marginates along the inner nuclear membrane. At the onset

of viral DNA replication, approximately 6 hpi, the virogenic stroma forms as a loose granular network dispersed throughout the nucleoplasm (Williams & Faulkner, 1997). As late gene expression occurs, progeny nucleocapsids appear within the stromal network, ca. 10 hpi. By 16-18 hpi, when very late gene expression commences, the virogenic stroma condenses into a dense matrix within the central region of the nucleus (Williams & Faulkner, 1997). Progressive nuclear hypertrophy and condensation of the virogenic stroma result in the formation of the peristromal ring-zone (Benz, 1986). Nucleocapsids are enveloped within the ring-zone, to become virions, and are subsequently embedded in the polyhedrin matrix. During the final maturation of polyhedra, a *de novo* membrane is attached to the outer surfaces of the developing occlusion bodies (Whitt & Manning, 1988). This structure is composed mostly of carbohydrates and phosphoproteins.

Similar events were reported in the pathology of NPVs derived from three hymenopteran insects, *Diprion hercyniae, Gilpinia hercyniae,* and *Neodiprion americanus banksianae* (Bird, 1952; Bird & Whalen, 1954). The first observed cytopathic effects were swelling of the nucleus and nucleoli. Chromatin coagulation and the formation of rod-shaped particles were followed by the gradual maturation of polyhedra. Although neither the timing post-inoculation nor the phase of infection were reported, the pathology induced by these hymenopteran NPVs appear to be similar to those of lepidopteran baculoviruses.

This chapter details the pathology of the *Neodiprion abietis* nucleopolyhedrovirus (NeabNPV), *in vivo.* Although the pathology of three other hymenopteran NPVs have been reported, the accumulation of information and improved techniques available today

have allowed for an in-depth characterization of the NeabNPV infection process.

5.3 Materials and Methods

5.3.1 Virus Stock

The nucleopolyhedrovirus of *Neodiprion abietis* (NeabNPV) was collected from infected *N. abietis* larvae in Western Newfoundland in 1997. Polyhedra of the virus were obtained from Dr. C. Lucarotti (Natural Resources Canada, Canadian Forest Services, Atlantic Forestry Center, Fredricton, New Brunswick, Canada) as a 5 X 10^9 polyhedra ml^{-1} suspension in water, which had been purified as per Moreau *et al.* (2005). A description of the purification is found in Chapter 3, Section 3.3.1 Materials and Methods.

5.3.2 Larval infection

N. abietis larvae were collected on balsam fir (*Abies balsamea*) branches at the Old Man's Pond region (Corner Brook), Western Newfoundland, Canada, in July of 2003. The larvae and branches were maintained in paper bags in a walk-in 4 °C refrigerator, until they were harvested. Larval head capsules were measured, according to the procedure described by Carroll (1962) and only third to fifth instar larvae were selected for experimentation. The larvae were starved for 12-15 hours at room temperature prior to being inoculated with NeabNPV polyhedral inclusion bodies (PIBs) resuspended in a 10% pasteurized liquid honey solution. *N. abietis* test larvae were each inoculated by imbibing a 5 µl drop of honey containing an estimated 10,000 PIBs. Negative control larvae fed 5 µl of a 10% pasteurized liquid honey solution with no PIBs. Before harvesting, larvae were maintained on balsam fir foliage, which had been decontaminated with 5% bleach for 30 minutes and rinsed with water.

Larvae used in this experiment were sacrificed at 1, 2, 5, 8, 12, 24, 48, and 72 hours post inoculation (hpi). Ten (10) larvae were harvested at each time point and were histologically processed according to the methodology described in Chapter 4 Section 4.3.2.

Embedded samples were sectioned with a Leica Ultra-cut microtome to thin (500nm) and ultra-thin (70) thicknesses using a Diatom Histo and Diamond knife, respectively. Thin sections were stained with Richardson Stain (1% azure blue, 1% borax, 1% methylene blue) and visualized on a Zeiss Universal up-right compound microscope. Light micrographs were taken with a Spot CCD camera and Spot Software.

Ultra-thin sections were stained with uranyl acetate (5%) and lead citrate (5%), before viewing on a Hitachi H7100 Transmission Electron microscope, using a 75 kV beam. Electron micrographs were captured using Northern Eclipse software (v7.0) and a Qicam 1.4 megapixel digital camera. Calibrated scale bars were added to the digital images during image capturing.

5.3.3 Determination of Cytopathology

Measurements of the surface area of cells, microvilli and nuclei were taken using ScionImage software for samples at each time point. The presence of viral features, such as virogenic stroma, nucleocapsid assembly, polyhedra formation and polyhedra maturation, were tabulated manually from electron micrographs of samples at each time point. Changes in cellular structures, upon infection, were determined by calculating the ratio of either the microvillar (M) or nuclear (N) surface area to the total cellular (C) surface area, where:

M μm^2 / C μm^2 = proportional surface area of the microvillar border

N μm^2 / C μm^2 = proportional surface area of the nucleus.

By using the proportional surface areas of the microvilli and nuclei, differences in size due to instar and tissue development were eliminated. Hypertrophy of the cell was hypothesized to reduce the surface area of the microvilli, since the cytoplasmic membrane would be stretched to accommodate the increase cell size. Nuclear hypertrophy is a characteristic cytopathic effect occurring as viral DNA replication begins. These two effects were used to determine the infection of cells at very early phases. The presence of virogenic stroma and nucleocapsid assembly was used to determine the transition of NeabNPV infection into the late phases, while the formation and maturation of polyhedra defined the timing of very late infection. GraphPad Instat 3.05 software was used to calculate the p-values of cytopathic effects through Kruskal-Wallis non-parametric analyses and Dunn Multiple Comparison tests.

5.4 Results

The *in vivo* characterization of NeabNPV in third through fifth instar larvae was hindered by the high incidence of pre-existing viral disease. Approximately one third (3 of 10) of the larval samples from the negative control population exhibited very late stages of viral pathology (polyhedra formation) within the midgut tissues. Presence of pre-existing disease likely originated from the environment, even though larvae were collected from the leading front of the sawfly epidemic. A general time-line of cytopathic effects induced by NeabNPV in *N. abietis* larvae was determine with the aid of transcription analysis (Duffy, 2006) and studies of three other hymenopteran NPVs (Bird, 1952; Bird & Whalen, 1954). Samples of larval midguts that exhibited intact

polyhedra before 24 hpi were discarded since polyhedrin was not detected before this time by transcriptional and Western blot analysis (Duffy, 2006 and Chapter 6 of this dissertation). Of the 10 total larvae processed histologically for each time post inoculation, only half of the larval guts (5) were used for analysis of early samples (1-12 hpi) due to the pre-existing disease and all 10 were examined for 24-72 hpi .

Pathology of NeabNPV was restricted to the midgut epithelia of *N. abietis* larvae. No evidence of infection could be found in the foregut and hindgut tissues, nor the surrounding musculature, Malpighian tubules, and tracheal cells. Sloughing of midgut epithelium, however, was observed from 12 hpi through to 72 hpi, and became increasing more frequent during the later time periods. Also, the peritrophic membrane was often disrupted, especially in larvae with very late infection.

The first indication of pathology was hypertrophy of midgut epithelial cell nuclei and a reduction of the microvilli border at 5 hpi (Table 5-1 and Figure 5-1). Nuclear size increased by 20 to 65% over 72 hours. No significant difference was observed in nuclear size between the cells of uninfected controls and the initial two time points (1-2 hpi), nor did the microvillar surface area change. Increases in nuclear size and reduced microvillar surface areas were observed at 12 and 24 hpi and were greater than those changes observed at 5 and 8 hpi.

Virogenic stroma were first observed in 5 hpi samples, with approximately 55% of the observed cells showing a diffuse network of electron-dense material in the center of the nucleus (Table 5-2 and Figures 5-2 & Figure 5-3). By 8 hpi, size of the virogenic stroma increased and nucleocapsids were detected within the virogenic stroma (Figure 5-4). Although the number of cells exhibiting virogenic stroma continued to increase

Table 5-1. Determination of the reduction of microvilli and nuclear hypertrophy based on mean values of the proportional surface area of the cytopathic effect.

The proportion of microvillar and nuclear surface areas were calculated on the basis of the total surface area of the cell. Mean values were determined for each time point, as well as the standard deviation (SD). Kruskal-Wallis analysis was performed for each cytopathic effect, along with Dunn's multiple comparisons tests, to obtain a measure of the statistical significant of each trait over the course of infection. All Kruskal-Wallis tests revealed significant differences between the time points with a Statistic KW Value of 52.74 or greater

Cytopathic effects		NeabNPV infected *N. abietis* larvae								
		Uninfected	1 hpi	2 hpi	5 hpi	8 hpi	12 hpi	24 hpi	48 hpi	72 hpi
Microvillar reduction	Mean *	25.45	25.49	25.27	14.94	15.83	18.26	18.15	10.20	15.14
	Sample size	84	79	65	68	81	73	66	120	138
	SD	0.0717	0.0728	0.0763	0.0363	0.0407	0.0660	0.0532	0.0562	0.0790
	‡Uninfected		P>0.05	P>0.05	P<0.001	P<0.001	P<0.001	P<0.001	P<0.001	P<0.001
	‡ 1 hpi			P>0.05	P<0.001	P<0.001	P<0.001	P<0.001	P<0.001	P<0.001
	‡ 2 hpi				P<0.001	P<0.001	P<0.001	P<0.001	P<0.001	P<0.001
	‡ 5 hpi					P>0.05	P>0.05	P>0.05	P<0.01	P<0.05
	‡ 8 hpi						P>0.05	P>0.05	P<0.01	P<0.05
	‡ 12 hpi							P>0.05	P<0.01	P>0.05
	‡ 24 hpi								P<0.01	P>0.05
	‡ 48 hpi									P<0.01
	‡ 72 hpi									
Nuclear hypertrophy	Mean †	29.35	28.92	29.54	42.35	42.35	38.15	37.36	43.87	48.70
	Sample size	84	79	65	68	81	73	66	120	138
	SD	0.1160	0.1073	0.1127	0.1572	0.1572	0.1535	0.1127	0.6447	0.0871
	‡Uninfected		P>0.05	P>0.05	P<0.001	P<0.001	P<0.001	P<0.001	P<0.001	P<0.001
	‡ 1 hpi			P>0.05	P<0.001	P<0.001	P<0.001	P<0.001	P<0.001	P<0.001
	‡ 2 hpi				P<0.001	P<0.001	P<0.001	P<0.001	P<0.001	P<0.001
	‡ 5 hpi					P>0.05	P>0.05	P>0.05	P<0.05	P>0.05
	‡ 8 hpi						P>0.05	P>0.05	P<0.05	P>0.05
	‡ 12 hpi							P>0.05	P>0.05	P>0.05
	‡ 24 hpi								P>0.05	P>0.05
	‡ 48 hpi									P>0.05
	‡ 72 hpi									

* proportional surface area of the microvillar border compared to the surface area of the entire cell (%)
† proportional surface area of the nucleus compared to the surface area of the entire cell (%)
‡ Dunn's multiple comparison tests

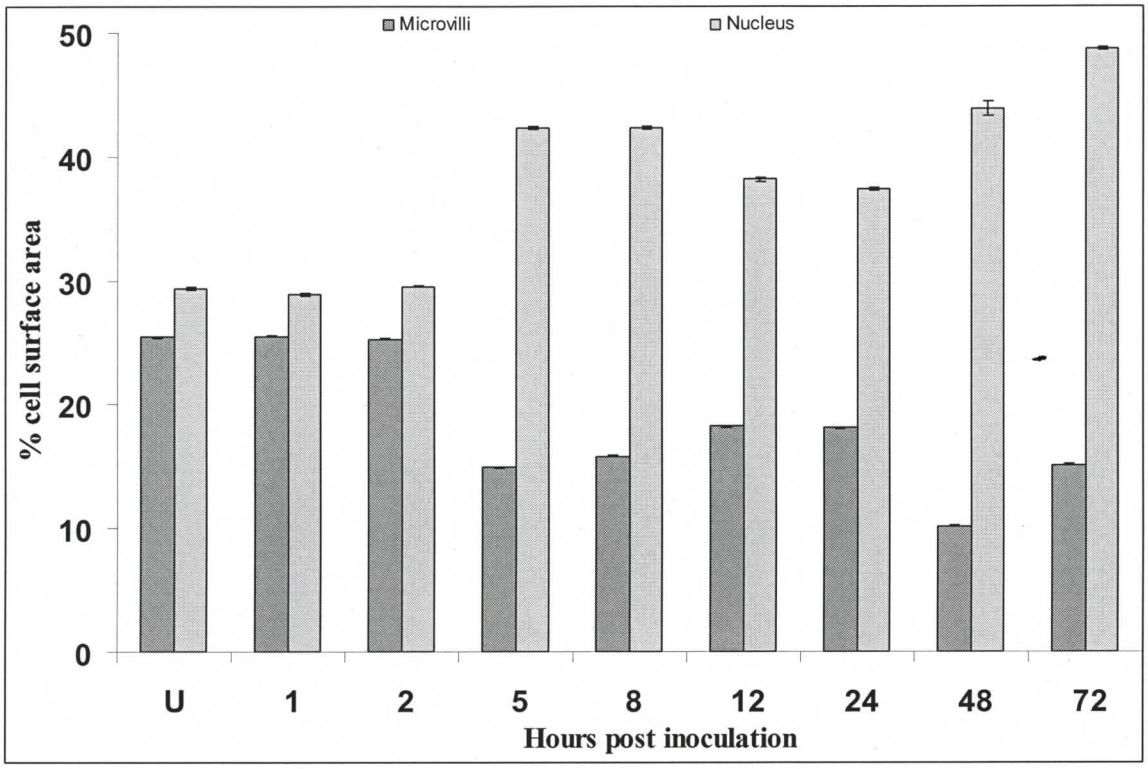

Figure 5-1. Reduction of midgut epithelial cell microvillar surface area and increase in size of nuclei during NeabNPV infection of *N. abietis* larvae.

Table 5-2. Analysis of significant of cytopathic effects observed over a 72 hour period of NeabNPV infection of *N. abietis* larvae.

The percentages of cells exhibiting each cytopathic effect were determined for each time point, as well as the standard deviations (SD). Kruskal-Wallis analysis was performed for each cytopathic effect, along with Dunn's multiple comparisons tests. All Kruskal-Wallis tests resulted in a Statistic KW value of 182.02 or greater.

Cytopathic effects		NeabNPV infected *N. abietis* larvae						
		Uninfected	5 hpi	8 hpi	12 hpi	24 hpi	48 hpi	72 hpi
Virogenic stroma	*% cells	0.00	55.88	60.98	76.71	81.82	91.66	94.59
	Sample size	84	68	81	73	66	120	138
	SD	0.0000	0.5040	0.4939	0.4256	0.3887	0.2787	0.2292
	‡Uninfected		P<0.001	P<0.001	P<0.001	P<0.001	P<0.001	P<0.001
	‡ 5 hpi			P>0.05	P>0.05	P>0.05	P<0.05	P<0.05
	‡ 8 hpi				P>0.05	P>0.05	P<0.05	P<0.05
	‡ 12 hpi					P>0.05	P>0.05	P>0.05
	‡ 24 hpi						P>0.05	P>0.05
	‡ 48 hpi							P>0.05
	‡ 72 hpi							
Nucleocapsid assembly	*% cells	0.00	0.00	31.71	54.79	68.82	91.66	94.59
	Sample size	84	68	81	73	66	120	138
	SD	0.0000	0.0000	0.4711	0.5011	0.4693	0.2787	0.2292
	‡Uninfected		P>0.05	P<0.05	P<0.001	P<0.001	P<0.001	P<0.001
	‡ 5 hpi			P>0.05	P<0.001	P<0.001	P<0.001	P<0.001
	‡ 8 hpi				P>0.05	P<0.01	P<0.001	P<0.001
	‡ 12 hpi					P>0.05	P<0.001	P<0.01
	‡ 24 hpi						P>0.05	P>0.05
	‡ 48 hpi							P>0.05
	‡ 72 hpi							
Polyhedra formation	*% cells	0.00	0.00	0.00	0.00	25.76	66.66	81.08
	Sample size	84	68	81	73	66	120	138
	SD	0.0000	0.0000	0.0000	0.0000	0.4497	0.4754	0.3971
	‡Uninfected		P>0.05	P>0.05	P>0.05	P<0.01	P<0.001	P<0.001
	‡ 5 hpi			P>0.05	P>0.05	P>0.05	P<0.001	P<0.001
	‡ 8 hpi				P>0.05	P<0.05	P<0.001	P<0.001
	‡ 12 hpi					P<0.01	P<0.001	P<0.001
	‡ 24 hpi						P<0.001	P<0.001
	‡ 48 hpi							P>0.05
	‡ 72 hpi							
Polyhedra maturation	*% cells	0.00	0.00	0.00	0.00	0.00	8.69	48.65
	Sample size	84	68	81	73	66	120	138
	SD	0.0000	0.0000	0.0000	0.0000	0.0000	0.6642	0.5067
	‡Uninfected		P>0.05	P>0.05	P>0.05	P>0.05	P>0.05	P<0.001
	‡ 5 hpi			P>0.05	P>0.05	P>0.05	P>0.05	P<0.001
	‡ 8 hpi				P>0.05	P>0.05	P>0.05	P<0.001
	‡ 12 hpi					P>0.05	P>0.05	P<0.001
	‡ 24 hpi						P>0.05	P<0.001
	‡ 48 hpi							P<0.001
	‡ 72 hpi							

* percentage of cells exhibiting cytopathic effects ‡ Dunn's Multiple comparison tests

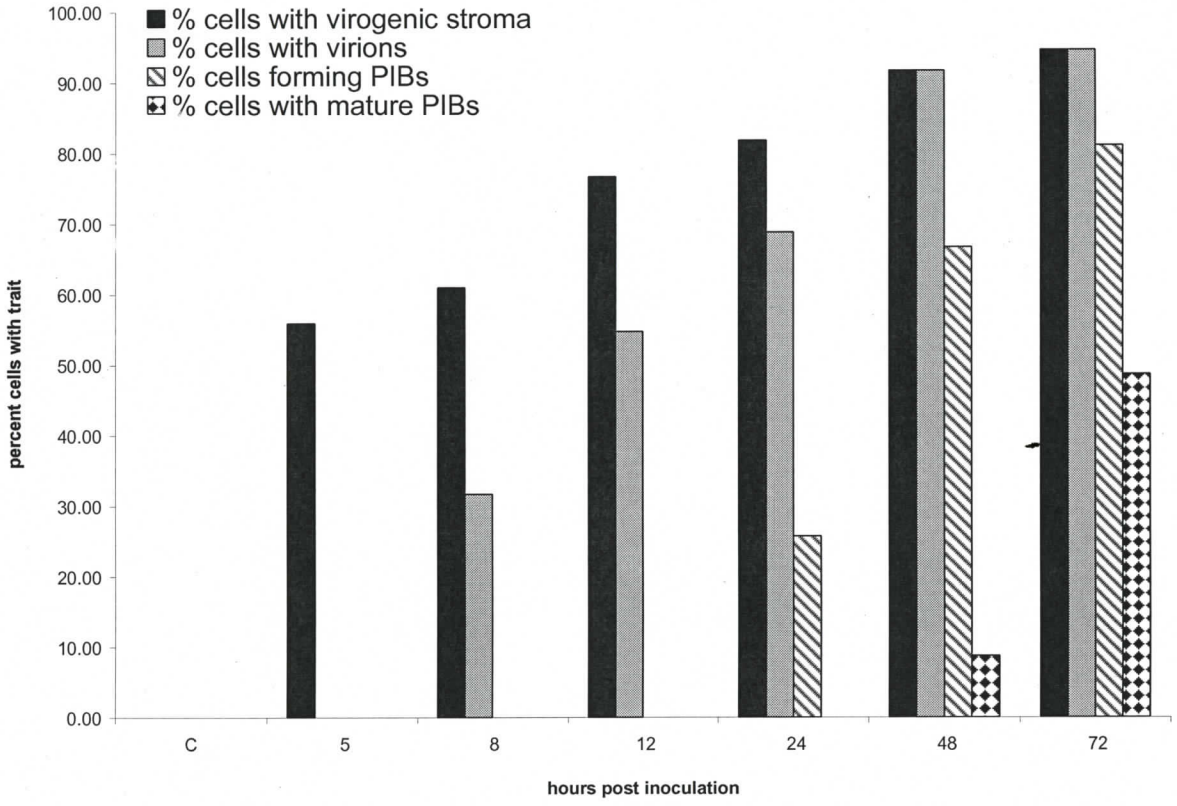

Figure 5-2. Accumulation of cytopathic effects exhibited in midgut epithelial cells infected with NeabNPV.

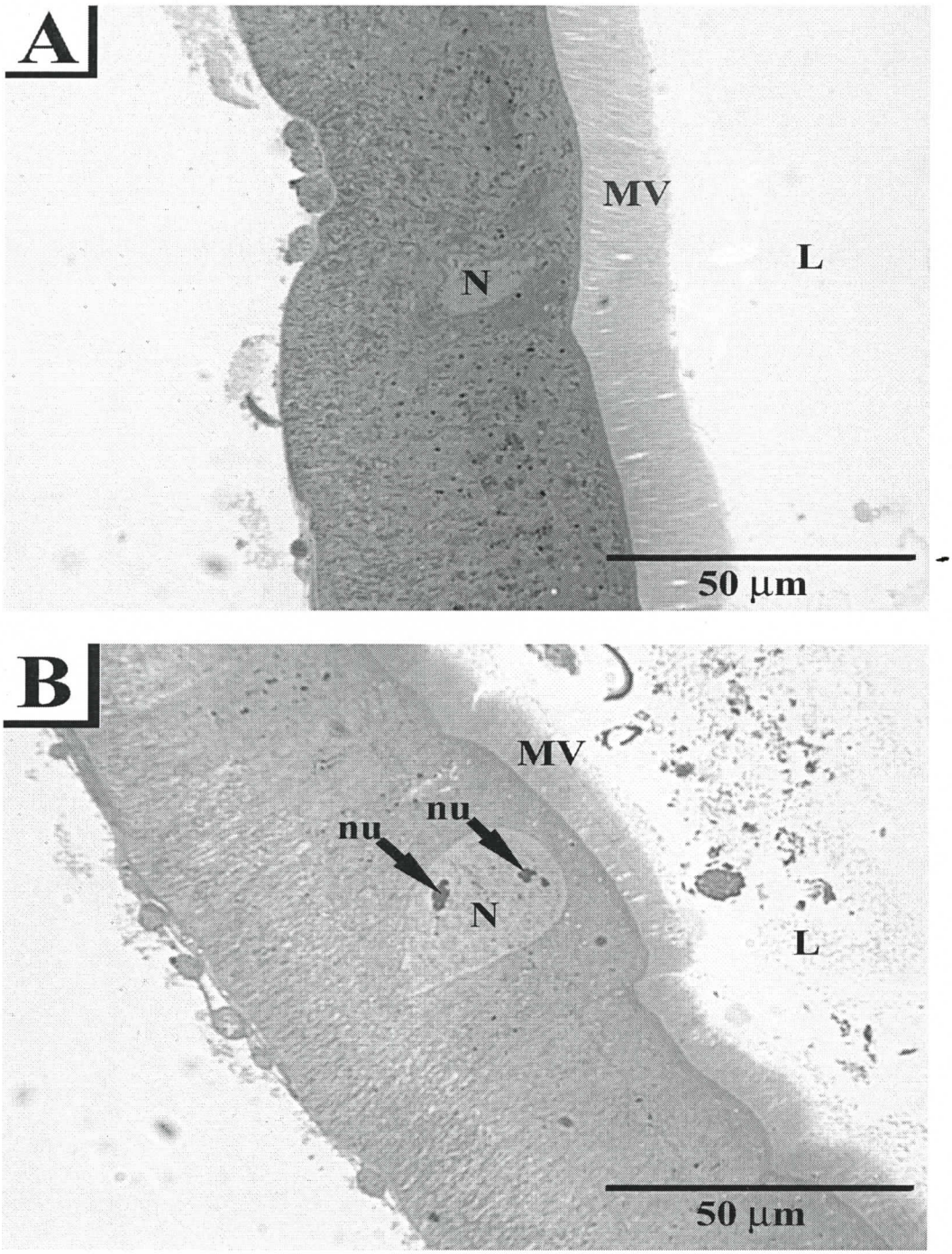

Figure 5-3. Light micrographs of *N. abietis* midgut epithelia infected with NeabNPV at 2 (A) and 5 (B) hpi.

A) The epithelial layer consisted of columnar epithelial cells with a thick microvillar border (MV) at the luminal (L) side. The nuclei (N) were relatively small in early infected tissue, but **B)** by 5 hpi the nuclei exhibited hypertrophy, once viral DNA replication began. nu, nucleoli.

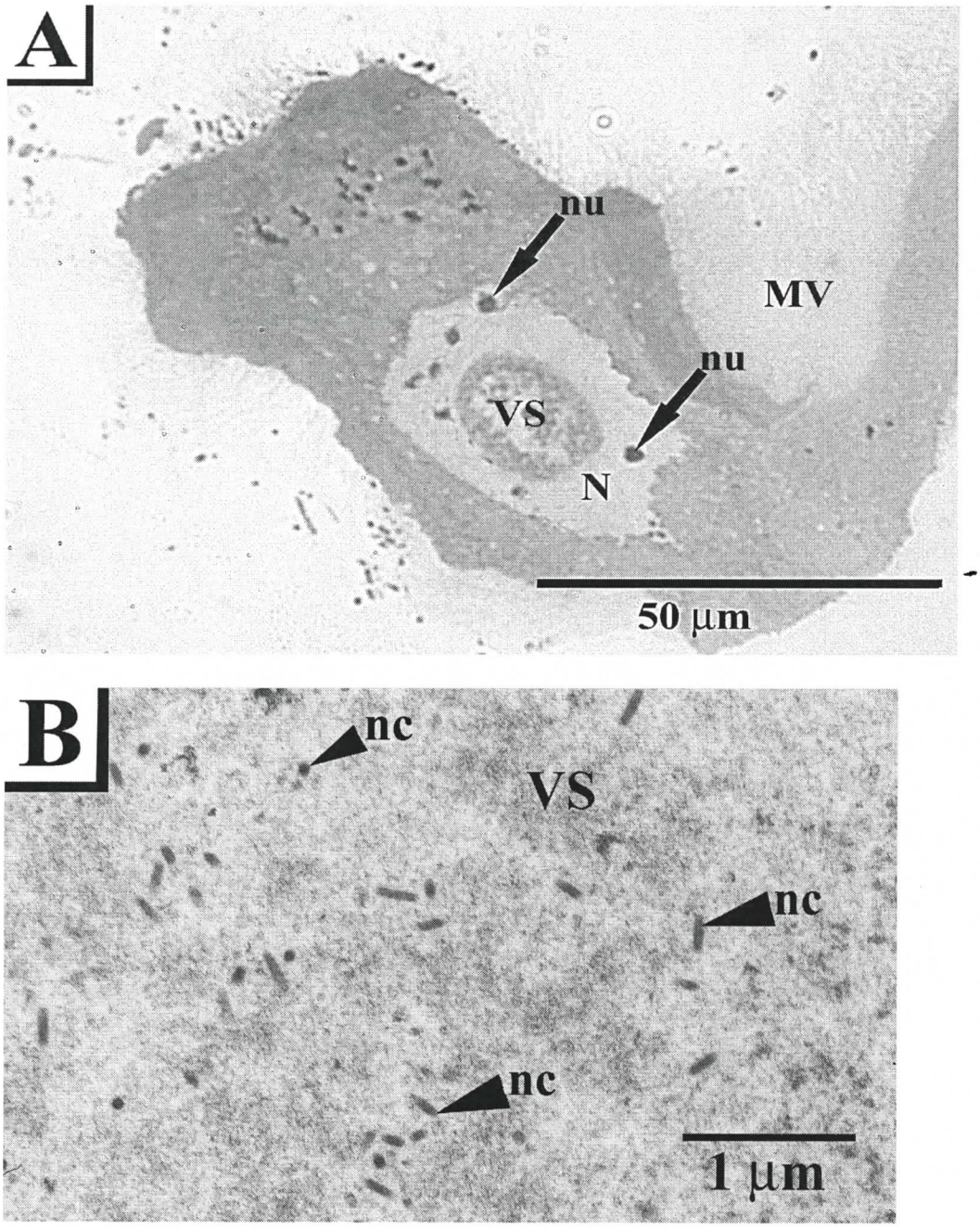

Figure 5-4. Light (A) and electron transmission (B) micrographs of *N. abietis* midgut epithelia infected with NeabNPV at 8 hpi.

A) By 8 hpi, the hypertrophied nucleus (N) had a prominent virogenic stroma (VS) in its central region, wherein **B)** nucleocapsids (nc) of NeabNPV were assembled (B). MV, microvilli; nu, nucleoli.

nucleocapsids were observed in only half of the cells. The matrix of the virogenic stroma continued to increase until 12 hpi and was often observed throughout 50% or more of the nucleus (Figure 5.5).

While nucleocapsids continued to be assembled within the virogenic stroma until 24 hpi, assembled nucleocapsids appeared to localize to the ring-zone, where they were enveloped, as early as 12 hpi (Figure 5.5 B). Polyhedra formation was first observed by 24 hpi (Figure 5.6). This process occurred in the ring zone where assembled virions accumulated. Averages of all larval tissues examined at 48 and 72 hpi suggested that polyhedra continued to be formed until the entire nucleus was filled (Figure 5.7 and 5.8). Calyx assembly was observed in 48% of the cells examined at 72 hpi (Figure 5.8B). During polyhedra assembly and maturation, the virogenic stroma condensed and fragmented, and by 72 hpi the virogenic stroma had almost disappeared.

5.5 Discussion

Infection of insect cells by baculoviruses is a complex process that requires the regulation of viral gene expression and induction of cytopathic effects into distinct temporal phases. Similar to the lepidopteran baculoviruses, hymenopteran NPV infection of primary tissues results in characteristic cytopathic effects and viral structures, such as the hypertrophy of the infected nucleus, development of a virogenic stroma, and the assembly of progeny virions into polyhedra (Bird & Whalen, 1954; Williams & Faulkner, 1997). In contrast to most lepidopteran baculoviruses, hymenopteran NPV infection is limited to the columnar epithelial tissue of the insect midgut. Due to this monorganotrophism, the entire infection cycle is completed in the midgut tissue,

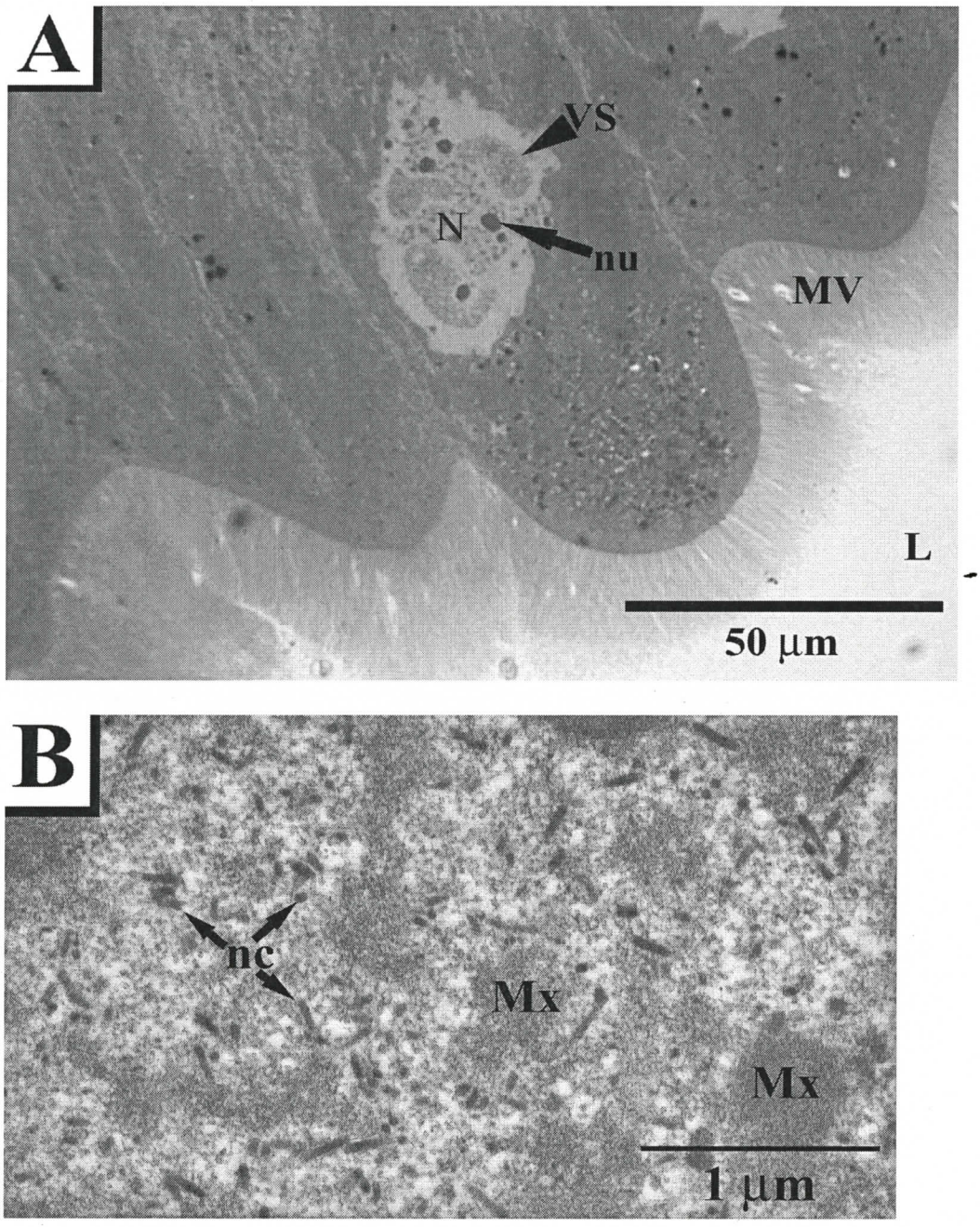

Figure 5-5. Light (A) and electron transmission (B) micrographs of *N. abietis* midgut epithelia infected with NeabNPV at 12 hpi.

A) By 12 hpi, the virogenic stroma (VS) had dispersed through nearly the entire hypertrophied nucleus (N). B) An increase in the number of nucleocapsids (nc) was observed, some of which localized to the intrastromal spaces where they acquired *de novo* envelopes. L, gut lumen; MV, microvilli; Mx, virogenic stromal matrix; nu, nucleoli.

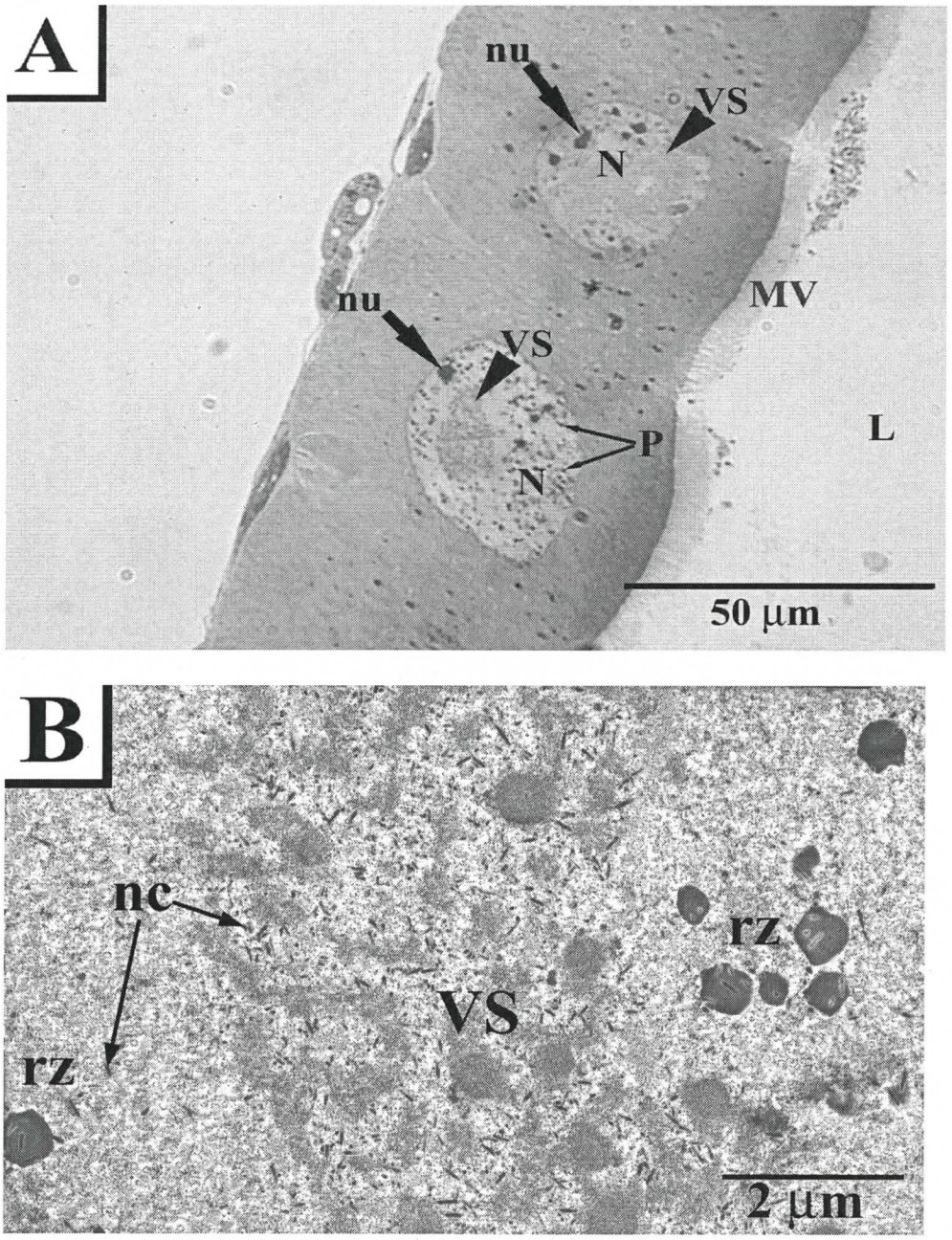

Figure 5-6. Light (A) and electron transmission (B) micrographs of *N. abietis* midgut epithelia infected with NeabNPV at 24 hpi.

A) By 24 hpi, the virogenic stroma (VS) had condensed to the central region of the hypertrophied nucleus (N), while immature polyhedra (P) were visible in the ring zone (rz), which borders the nuclear membrane. **B**) The virogenic stroma still contained several nucleocapsids, though many had localized to the ring zone where the formation of polyhedra occurs (rz). L, gut lumen; MV, microvilli; nu, nucleoli.

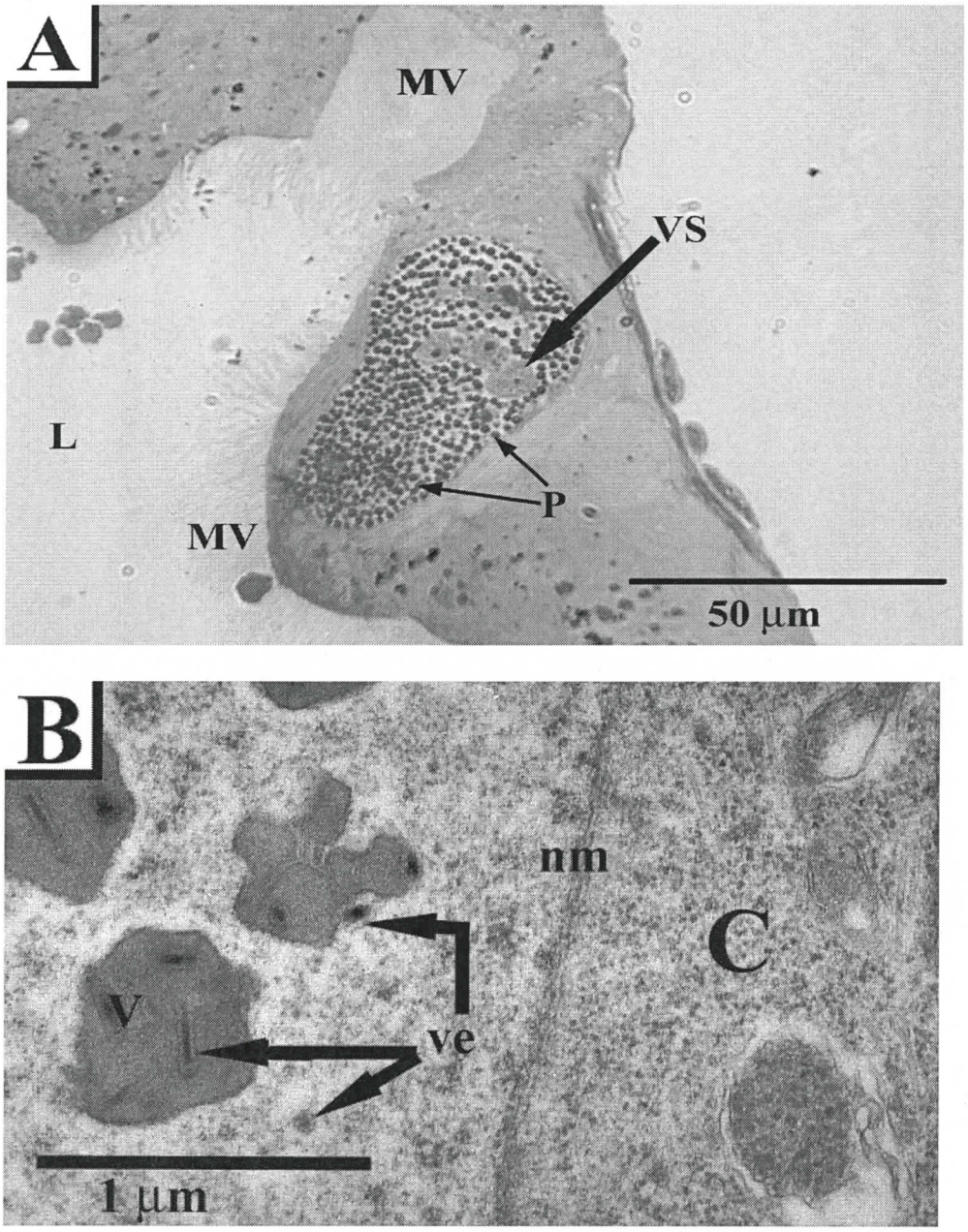

Figure 5-7. Light (A) and electron transmission (B) micrographs of *N. abietis* midgut epithelia infected with NeabNPV at 48 hpi.

A) By 48 hpi, the virogenic stroma (VS) had condensed further and was located within the central region of the hypertrophied nucleus, which was filled with immature polyhedra (P). **B**) The virions (V) were dispersed through the nucleoplasm or were embedded in the polyhedrin matrix. Virions had acquired a *de novo* envelope (ve). C, cytoplasm; L, gut lumen; MV, microvilli, nm, nuclear membrane.

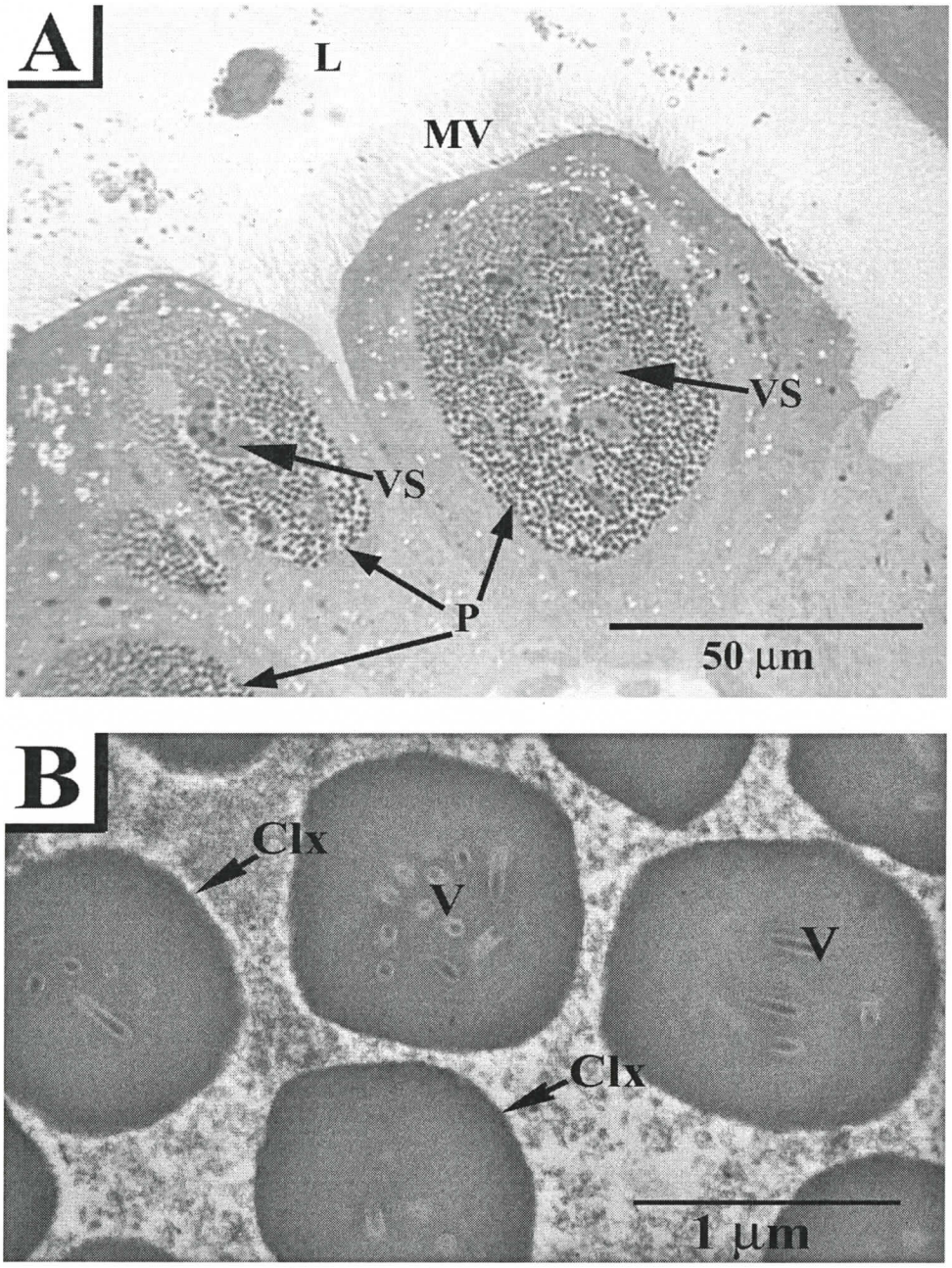

Figure 5-8. Light (A) and electron transmission (B) micrographs of *N. abietis* midgut epithelia infected with NeabNPV at 72 hpi.

A) The virogenic stroma (VS) was still visible within the central region of the hypertrophied nucleus, but was completely surround by maturing polyhedra (P). **B**) Most virions (V) were embedded in the polyhedrin matrix and the calyx (Clx) had form around the polyhedra. L, gut lumen; MV, microvilli.

including the embedding of virions into the polyhedrin matrix. Lepidopteran NPVs often lack inclusion of virions during primary tissue infection, but produce copious polyhedra in secondarily infected tissues such as the fat body and hemocytes (Federici, 1997). Three possible barriers to systemic infections may limit hymenopteran NPVs to monorganotrophism: the lack of the budded virus phenotype (Duffy, 2006; Duffy *et al.*, 2006; Garcia-Maruniak *et al.*, 2004; Lauzon *et al.*, 2004), the thick granular and fibrous basal lamina that surrounds the gut tissues (Chapter 4), and host defences. Haas-Stapleton *et al.* (2003; 2005) concluded that midgut infection is the primary barrier to systemic spread, particularly in insects that have a low foci-per-OB ratio. Unlike insects that exhibit active immunity to baculoviruses (Trudeau *et al.*, 2001), melanization and encapsulation of tracheae and haemocytes were not observed. However, sloughing of midgut cells was a common occurrence. Epithelial cells were often observed in the gut lumen, while an intact basal lamina and a thin layer of putative differentiating regenerative cells were observed. Disruption of the peritrophic membrane likely resulted from host defences in conjunction with sloughing of midgut cells rather than a viral infectivity factor, such as enhancins, since no homologues of the enhancin molecules described in lepidopteran baculoviruses (Derksen & Granados, 1988) have been found in NeabNPV (Duffy, 2006).

Entry of nucleocapsids and their translocation to the nucleus were not observed during early NeabNPV infection and likely occurred prior to the times points examined in this study. Transcriptional analyses of NeabNPV infected midgut tissue indicated that nucleocapsid uncoating had occurred by 0.5 hpi (Duffy, 2006), suggesting that very early pathogenesis occurs within the first few minutes post inoculation. While empty capsids

within the nucleus were not detected within the first 2 hpi, Western blot analysis showed that the ODV tegument glycoprotein, GP41, was present within this time period (Chapter 6). These results indicate that NeabNPV nucleocapsids had attached to and entered cells and that viral structural proteins were present by 2 hpi. Further investigation of very early pathogenesis is required to elucidate the mechanisms of entry, translocation, and uncoating. Techniques such as immunohistochemistry and *in situ* hybridization of samples collected within the first 10 to 30 minutes post inoculation are good candidates for determining these mechanisms.

The first microscopic evidence of NeabNPV pathology was the reduction of the microvilli and hypertrophy of the nucleus. As early expressed viral proteins accumulate in the nucleus, the nucleoplasm expands resulting in hypertrophy (Federici, 1997; Williams & Faulkner, 1997). The existing cytoplasm and organelles are redistributed and the cytoplasmic membrane expands in order to accommodate the increased nuclear size. Analysis of cellular hypertrophy has been studied using *in vitro* insect cells, allowing for the characterization of cells of near equivalent size (Federici, 1997). However, the size of larval midgut tissue varies between instars and the developmental stage within an instar (Chapman, 1985; Nation, 2002; Wigglesworth, 1972). Cellular hypertrophy was determined by the reduction of microvilli length, measured as the proportional surface area of the entire cell size (see pages 148-9 for definintion), since these structures are readily apparent compared to the invaginations of the basal membrane (Chapter 4). Thus, variations in cell size between larvae could be eliminated. The measurement of microvillar length, as a proportional value of total cell surface area, has also been used to

study the disease process of rotavirus infections in pigs and lambs (Pearson & McNulty, 1979; Snodgrass *et al.*, 1977).

The virogenic stroma was observd within 5 hpi. Several processes have been reported concurrent with stromal development in AcMNPV infected cells, including the onset of viral DNA replication, margination of host chromatin, and localization of late expression factors (LEFs) within the nuclear matrix that associate with the virogenic stroma. Amoung these factors, IE-1, DNA-binding protein (DBP), and LEF-3, as well as host proliferating cell nuclear antigen (PCNA), are directly involved in DNA synthesis (Iwahori *et al.*, 2004; Okano *et al.*, 1999), and LEF-4 and PP31 are associated with late gene expression (Durantel *et al.*, 1998; Guarino *et al.*, 1992). In AcMNPV infection, localization of LEFs to the virogenic stroma correlates with the timing of DNA replication and late gene expression, 6 and 10 hpi, respectively (Hefferon, 2004; Rapp *et al.*, 1998).

During the progression of infection to late and very late phases, the virogenic stroma enlarges as nucleocapsids are assembled. Capsids are typically found associated in an end-on configuration with the stromal network, where capsid shell formation and nucleocapsid maturation occurs within the intrastromal spaces. The presence of p6.9, a DNA-binding protein associated with the viral genome within capsids, and pp31 within the intrastromal regions may aid in viral DNA packaging (Guarino *et al.*, 1992; Wilson & Miller, 1986; Wilson & Price, 1988). Progeny nucleocapsids of AcMNPV are detectable within the stromal network by 10 hpi, two hours after the first nucleocapsids were observed within the virogenic stroma during NeabNPV infection. The continued expansion of the NeabNPV induced virogenic stroma to 12 hpi suggests that viral DNA

replication and nucleocapsids assembly are maximal during this time period. Duffy (2006) reported that a linear increase in NeabNPV DNA copy number between 4-72 hpi. This data correlates well with the cytopathic evidence that viral DNA accumulates within the stromal network, and is then packaged over an extended period of time after viral structural proteins are expressed.

Condensation of the virogenic stroma within the central region of the NeabNPV infected nuclei was observed at 24 hpi, when polyhedra formation started. This condensation process typically occurs between 16-18 hpi in AcMNPV infected cells (Williams & Faulkner, 1997). The condensation of the virogenic stroma in NeabNPV infected cells may have started as early as 14 hpi but was not observed due the time points used in our experiments. The formation of NeabNPV occlusion bodies occurred within the peristromal ring-zone. Virions were randomly oriented and occluded by the addition of polyhedrin between the particles. During the occlusion process, the *de novo* envelopes acquired by the nucleocapsids became readily apparent and the addition of the calyx membrane to polyhedra was only observed once the nucleus had filled will occlusion bodies. In AcMNPV infected cells, the calyx protein has been observed attaching to the outer surfaces of a subpopulation of POLH and a phosphorylated 34 kDa protein (PP34), while other occlusion bodies were being formed (Whitt & Manning, 1988). This suggests that NeabNPV polyhedrin formation may be more tightly regulated into distinct phases than in AcMNPV.

In summary, this study supports the observations of hymenopteran NPV pathology reported by Bird and Whalen (1954). The pathology of NeabNPV corresponds closely to pathogenesis exhibited by the model baculovirus AcMNPV. Although AcMNPV is not

occluded in primary infected midgut tissue, NeabNPV infection mimics the pathological effects observed in host tissues of secondary AcMNPV infection. Timing of pathology appears to occur more rapidly in the hymenopteran NPV, except for distinct delay in the formation and maturation of polyhedra.

Chapter 6 Analysis of temporally important transcripts and proteins defining transitional stages in the *N. abietis* nucleopolyhedrovirus life-cycle

6.1 Abstract

While lepidopteran NPVs have been well characterized due to the availability of *in vitro* systems of propagation, the temporal expression and molecular pathology of non-lepidopteran baculoviruses is almost unknown. *In vivo* investigations of NeabNPV replication kinetics and gene expression in the native larval host, *N. abietis* revealed that these processes undergo temporal patterns similar to those observed in lepidopteran NPVs. Duffy (2006) found that early gene expression commenced at approximately 2 hours post inoculation (hpi), followed by viral DNA replication between 4-6 hpi. Late gene expression initiated by 6 hpi and continued through to larval death. Preliminary results of very late gene expression indicated a significant delay in the detection of *vlf-1* and *polh* transcripts. Microscopic examination of infected larvae contradicted this result, suggesting that polyhedra formation occurs as early as 24 hpi (Chapter 5). To investigate late and very late gene expression further, RT-PCR of *vlf-1* and *polh* transcripts was performed, in addition to Western blot analysis of GP41 and POLH proteins. Transcripts of *vlf-1* and *polh* were detected at 12 and 24 hpi, respectively, while GP41 and polyhedrin proteins were observed by 6 and 24 hpi. These new results of late and very late gene expression fit better with the cytopathology observed by microscopy and are in greater accordance with published results of other NPVs.

6.2 Introduction

A temporal cascade regulates the transcription of lepidopteran baculovirus genes into immediate early, early, late, and very late phases, with viral DNA replication commencing between the early and late phases. Immediate early genes are transcribed upon uncoating of the baculovirus genome in the nucleus. This event has been shown to occur within the first 15 minutes post infection (Carstens *et al.*, 2002; Kovacs *et al.*, 1991; Wang *et al.*, 2004), using host cell RNA polymerase II and transcription factors (Hoopes & Rohrmann, 1991) and continues until 3 hours post infection (hpi).

Immediate early genes, ie0, ie1, ie2, pe38 and me-53, act as strong transactivators of early and late genes and up-regulate their expression. Baculovirus early genes encode for the DNA replication machinery and factors involved in the transcription of late genes (*lef*s). Genes essential for DNA replication, DNA polymerase (*dnapol*) and *lef-2*, are the first early genes to be transcribed (Ahrens & Rohrmann, 1995; Chaeychomsri *et al.*, 1995; Liu & Carstens, 1995; Passarelli & Miller, 1993b; Sriram & Gopinathan, 1998), at 2 hpi , followed by other early genes involved in RNA polymerase production and viral transcription , 3 and 4 hpi, respectively (Durantel *et al.*, 1998; Smith *et al.*, 1982). Early gene expression continues well past the initiation of the late gene expression and in some viral expression patterns is observed up to 18 hpi (Ahrens & Rohrmann, 1995; Sriram & Gopinathan, 1998). Late structural genes are expressed within 6 hpi and continue up to 24 hpi (Blissard *et al.*, 1989; Braunagel *et al.*, 1996; Rashidan *et al.*, 2005; Thiem *et al.*, 1989), while transcripts of transactivators of very late gene expression (*vlf-1*) first appear at 12 hpi and continue until cell death and lysis (McLachlin & Miller, 1994). Products of very late genes are primarily involved in the occlusion of the virus and dispersion by cell

lysis and disruption of the host integument. *Polh* encodes polyhedrin, the major component of the occlusion body matrix, is expressed during the very late phase of infection. *Polh* expression is dependent upon the expression of *vlf-1* and continues until cell lysis (McLachlin & Miller, 1994). Transcripts of some very late genes, whose products are involved in cell lysis and OB dispersal, have been observed up to 48 hours later.

Unlike the lepidopteran baculoviruses, hymenopteran and dipteran nucleopolyhedroviruses (NPVs) do not appear to have homologues of the immediate early class of genes (Afonso *et al.*, 2001; Duffy *et al.*, 2006; Garcia-Maruniak *et al.*, 2004; Lauzon *et al.*, 2004). (Afonso *et al.*, 2001; Duffy *et al.*, 2006; Garcia-Maruniak *et al.*, 2004; Lauzon *et al.*, 2004). In his Ph. D. dissertation, Duffy (2006) investigated the *in vivo* gene expression and replication kinetics of NeabNPV infected *N. abietis* larvae and demonstrated that hymenopteran NPVs follow a similar temporal regulation of expression as observed in lepidopteran NPVs. The replication kinetics of NeabNPV in *N. abietis* larvae indicated that viral DNA was present within the midgut tissue within the first 30 minutes post-inoculation (Figure 6-1). A rapid increase in NeabNPV copy number was observed from 0.5 - 4 hpi, followed by a slow linear increase in the number of viral genomic copies, between 4 and 72 hpi indicated the initiation of viral DNA replication. Transcriptional analysis of *dnapol*, *lef-1*, *lef-2*, *lef-8*, *lef-9*, *gp41*, and *p74* genes (Figure 6-2), as well as two putative immediate early genes, *Neab24* and *Neab52* (data not shown), indicated that NeabNPV expression occurs in a temporal cascade similar to lepidopteran baculoviruses (Duffy, 2006). The transcripts of the two putative immediate early NeabNPV genes (*Neab24* and *Neab52*) encode for predicted

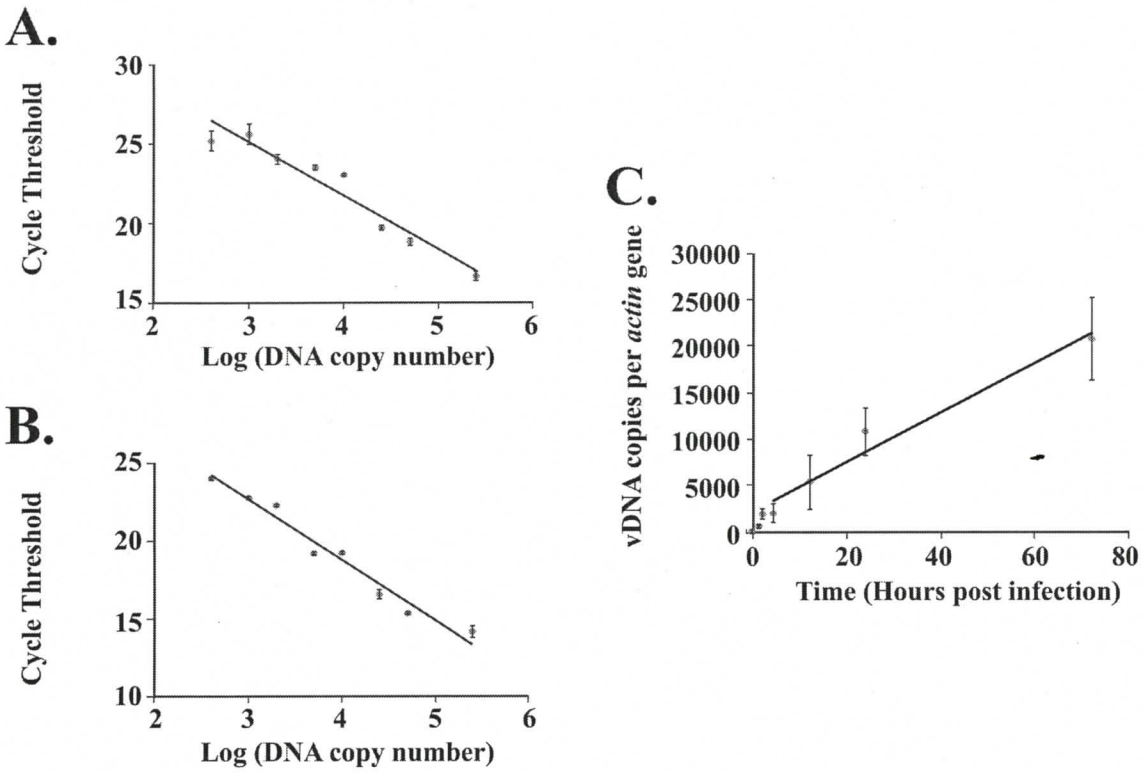

Figure 6-1. Quantification of NeabNPV DNA copy number in mid-guts of NeabNPV-infected *N. abietis* larvae.

Calibration curves were generated for A) the host *actin* gene and B) the NeabNPV polyhedrin (*polh*) gene. These two genes were amplified by PCR and cloned. Quantitative PCR was performed on the clones with gene-specific primers to generate the standard curves. C) Quantitative PCR was employed to determine the number of *polh* gene copies relative to the *actin* gene at various times following infection. The correlation coefficents (R^2-values) for the calibration curves are (A) 0.938 and (B) 0.935. The R^2-value NeabNPV replication between 4 and 72 hpi was 0.967. Modified from Duffy (2006) to normalize vDNA copy number against actin gene number.

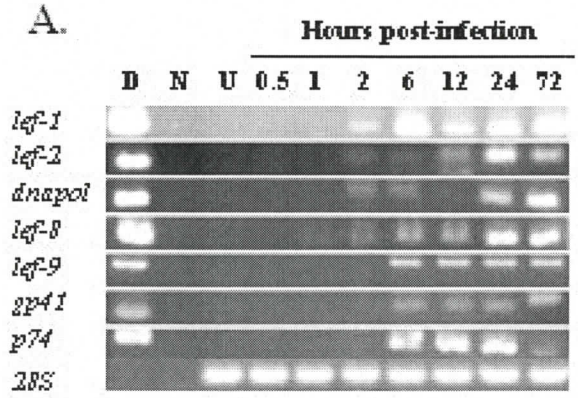

Figure 6-2. RT-PCR of selected NeabNPV genes with RNA extracted from mid-guts of NeabNPV-infected N. abietis larvae.

RT-PCR was performed to detect transcripts of NeabNPV genes orthologous to lepidopteran baculovirus genes known to be early- transcribed (*lef-1*, *lef-2*, *dnapol*), subunits of the viral RNA polymerase (*lef-8*, *lef-9*), or late-expressed (*gp41*, *p74*) at 0.5, 1, 2, 6, 12, 24, and 72 hours post infection; D, NeabNPV DNA, N, no template control, U, uninfected larvae. The host *28S* gene was used as a positive control for all RT-PCR reactions. Image taken from Duffy (2006).

DNA-binding proteins and were observed at 0.5 hpi and 2 hpi (respectively) (Duffy, 2006). NeabNPV early gene expression occurs rapidly after viral entry into the nucleus, with *lef-8* transcripts (the virally-encoded RNA-polymerase of late gene transcription), being observed within 1 hpi , while expression of components of the viral DNA replication machinery were observed within 2 hpi. Late structural genes were detected within 6 hpi *in vivo* (Duffy, 2006). Very late factor (*vlf-1*) was observed approximately 12 hpi later than would be predicted from the lepidopteran NPV models and *polh* transcription was not detected (Duffy, 2006).

This chapter expands upon the findings of Duffy (2006) by characterizing the expression of *gp41*, *vlf-1* and *polh*, within NeabNPV-infected *N. abietis* larvae. Reverse transcriptase (RT) PCR was used to determine the temporal expression of *vlf-1* and *polh*, while Western blot analysis allowed for the detection of GP41 and POLH proteins.

6.3 Materials and Methods

6.3.1 Virus Stock

The nucleopolyhedrovirus of *Neodiprion abietis* (NeabNPV) was collected from infected *N. abietis* larvae in Western Newfoundland in 1997. Polyhedra of NeabNPV were obtained from Dr. C. Lucarotti (Natural Resources Canada, Canadian Forest Services, Atlantic Forestry Center, Fredricton, New Brunswick, Canada) as a 5 X 10^9 polyhedra ml^{-1} suspension in water, which had been purified as per Moreau *et al.* (2005). A description of the purification is found in Chapter 3, Section 3.3.1.

6.3.2 Larval infection

Collection and infection of *N.* abietis larvae were conducted as described in Chapter 5 Section 5.3.1 and Section 5.3.2, except only second and third instar larvae were selected

for experimentation. After inoculation, larvae were sacrificed every half hour for the first 6 hours, then every hour until 12 hours post inoculation (hpi). Between 12 and 24 hours, larvae were sacrificed every three hours, and after 24 hpi larvae were sacrificed every 12 hours until 120 hpi. Each sacrificed larva was washed for 30 seconds 10% Bleach, rinsed in distilled deionized water (ddH_2O) for 30 seconds, then washed in 70% Ethanol for 1 minute and rinsed again in ddH_2O. The larvae were subsequently immersed in sterile Dulbecco's phosphate buffered saline (pH 7.4) (Invitrogen) (PBS), then the head and hind-end were removed immediately posterior to the head capsule and anterior of the 8th proleg. The larval gut was separated from the fat body and cuticle in fresh sterile PBS. The extracted gut was immediately placed into 1 ml of RNAlater (Ambion, Inc) and stored at -20°C.

6.3.3 Viral RNA and Protein Isolation

Excised guts of larvae, whose viral DNA content fit within the NeabNPVreplication kinetics determined by Duffy (2006), were collected from the RNAlater solution by centrifugation at 1000 x g, then the RNAlater solutions were filtered through a Micro-concentrator (Millipore YM-10) with a 10,000 kDa pore size to collect any solubilized RNA and protein. The gut tissues and concentrated retentates were each homogenized in 50µl TRIzol reagent (Invitrogen) containing sand (ignited and baked 4 hrs). The ground midgut suspensions were collected and TRIzol reagent was added to 1 mL. Debris was collected by centrifugation at 12,000 × g for 10 minutes at 4°C. RNA and protein of each homogenized sample were extracted following the manufacturer's protocol.

6.3.4 RNA Reverse Transcription PCR

Three different larval RNA samples, extracted using Trizol, were DNAse treated (3 U enzyme (Invitrogen); 20 mM Tris-Cl, pH 8.4; 50 mM KCl; 2 mM $MgCl_2$) for 15 minutes at 25°C. EDTA (to 2.5 mM) was added to the reaction, which was then incubated at 65°C for 10 minutes. First strand cDNAs were generated by incubating 50 ng DNAse-treated total RNA in 20 µl reaction buffer (50 mM KCl; 25 mM Tris- HCl, pH 8.3; 500 µM dNTP; 10 µM DTT; 10 U RNAse Inhibitor; 200 U Superscript II Reverse Transcriptase) at 25°C for 10 minutes, followed by a further incubation at 42°C for 50 minutes and inactivation at 70°C for 15 minutes. Synthesized cDNAs were stored at -20°C.

Three primer sets (*28S*, *vlf-1*, and *polh*), described in Chapter 3 Table 3.1, were used to amplify the cDNAs of infected larval midgut tissues at various time points. NeabNPV-genomic DNA positive controls, uninfected larval cDNA negative controls, and *28S* rRNA host insect control were included in each PCR set. The templates were amplified using Platinum Taq polymerase, following the manufacturer's protocol, with a hot-start cycle of 95°C (4 minutes), then 45 cycles of 95°C (30 seconds), 55°C (60 seconds), and 72°C (90 seconds). All products were resolved by gel electrophoresis in 2% agarose and stained with SYBR Green. Each PCR reaction was repeated three times.

6.3.5 SDS-PAGE and Western Blot Analysis of GP41 and POLH

Peptides were synthesized for the 17-34 amino acid region of NeabNPV POLH and the 68-84 amino acid region of NeabNPV GP41 by GeneScript, Inc. Peptides were conjugated to the KLH carrier peptide and polyclonal antibodies were raised in New Zealand white rabbits, following a 4-immunization schedule. Sera from both rabbits

were pooled and used for Western blot analysis. Preimmune sera from both rabbits were also pooled together and used in Western blots as negative control for the antibodies.

Larvae whose NeabNPV DNA content fit within the replication curve (Duffy, 2006) were selected for total protein extraction at each time point. The protein extracts, from three larvae at each time point, were pooled and resolved by discontinuous denaturing polyacrylamide gel electrophoresis (SDS-PAGE). Forty micrograms of each sample were combined with Laemmli's Sample buffer (62.5 mM Tris, pH 6.8; 2% SDS; 5% Beta-mercaptoethanol, 10% glycerol; 0.002% Bromophenol Blue) and incubated at 95°C for 5 minutes. Samples were loaded onto a 12.5% acrylamide resolving/ 4% acrylamide stacking gel and resolved by electrophoresis, using conventional methods. Protein bands were transferred to a PVDF membrane, using the Mini-Electroblot system (BioRad) and the manufacturer's protocols.

The blot was blocked in a solution of 5% skimmed milk in PBS with 0.1% Tween 20 (PBST), for 1 hour at 25°C. Thereafter, the blot was incubated with primary polyclonal antibody (Rabbit anti-GP41 and Rabbit anti-POLH) at a 1:5000 dilution in blocking solution, overnight at 4 °C. Six washes of the blot were performed over 1 hour, using 600 ml PBST. The blot was then incubated with goat-anti-rabbit horseradish-peroxidase-conjugated secondary antibody (Stressgen, Inc) at a 1:20,000 dilution in blocking solution. Following another six-wash series, as previously described, the blot was incubated with SuperSignal West-Pico Chemiluminescent Substrate (Pierce Co.) for 15 minutes at room temperature. The blot was exposed to MR film (Kodak), which was developed using a X-ray developer. The blot was subsequently stained with G-250 Colloidal Coomassie Stain (1.2% Coomassie Blue G-250; 4.9% Ethanol; 8.5%

phosphoric acid) for 24 hours, then destained in water until the background cleared. Blots were digitalized using a flat-bed Epson scanner and Photoshop 6 (Adobe).

6.4 Results

The atypical expression of the very late factor (*vlf-1*) and polyhedrin (*polh*) observed by Duffy (2006), as compared to the model AcMNPV expression, was re-examined. Transcriptional analysis of infected larvae harvested between 12 and 96 hpi, by RT-PCR, revealed that *vlf-1* expression initiated at 12 hpi (Figure 6.3). A very weak amplification signal of *polh* transcripts was detected at 24 hpi and had increased by 36 hpi. Both transcripts were observed until larval death started to occur at 96 hpi.

Expression of the late and very late structural proteins associated with ODV and the occlusion body, GP41 and POLH, were investigated by Western blot analysis (Figure 6-4). GP41 was detectable within 0.5 hour of inoculation and persisted at reduced levels until 2 hpi, suggesting that this protein originated from the ODV and was not synthesized by the infected cells. No GP41 protein was detected at 4 hpi but the protein was observed again from 6 hpi to 72 hpi, indicating that late gene expression commenced coincident with the re-appearance of GP41. POLH was first observed at 24 hpi and continued to be expressed until 96 hpi, when larvae started to die.

6.5 Discussion

Due to the lack of available tissue culture propagation systems for non-lepidopteran NPVs, replication kinetics and analysis of the temporal expression of 9 NeabNPV genes (*Neab24* and *Neab52*, *dnapol*, *lef-1*, *lef-2*, *lef-8*, *lef-9*, *gp41*, and *p74*), were investigated *in vivo* (Duffy, 2006). Seven of these genes (*dnapol*, *lef-1*, *lef-2*, *lef-8*, *lef-9*, *gp41*, and *p74*) are conserved in all completely sequenced lepidopteran baculoviruses and

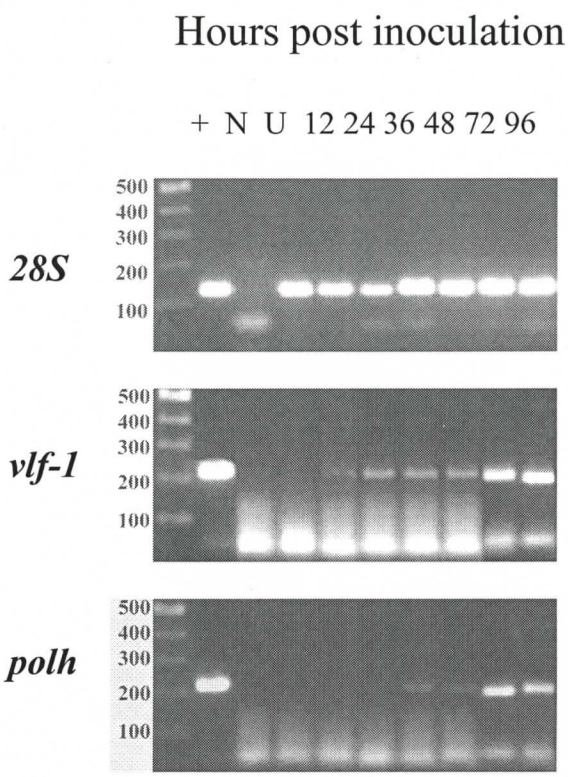

Figure 6-3. RT-PCR analysis of *vlf-1* and *polh* gene expression in NeabNPV-infected *N. abietis* larvae, harvested at various time points post inoculation.

cDNAs of extracted RNA samples from uninfected (U) and NeabNPV infected larvae (12-96), harvested at various times post inoculation, were amplified using gene-specific primers to the very late expression factor (*vlf-1*) and polyhedrin (*polh*). Amplification of NeabNPV genomic DNA represents the positive control reaction (+), while no-template (N) and cDNA of uninfected larvae (U) were used as negative controls. Ribosomal (*28S*) cDNA was amplified to demonstrate the integrity of the RNA samples.

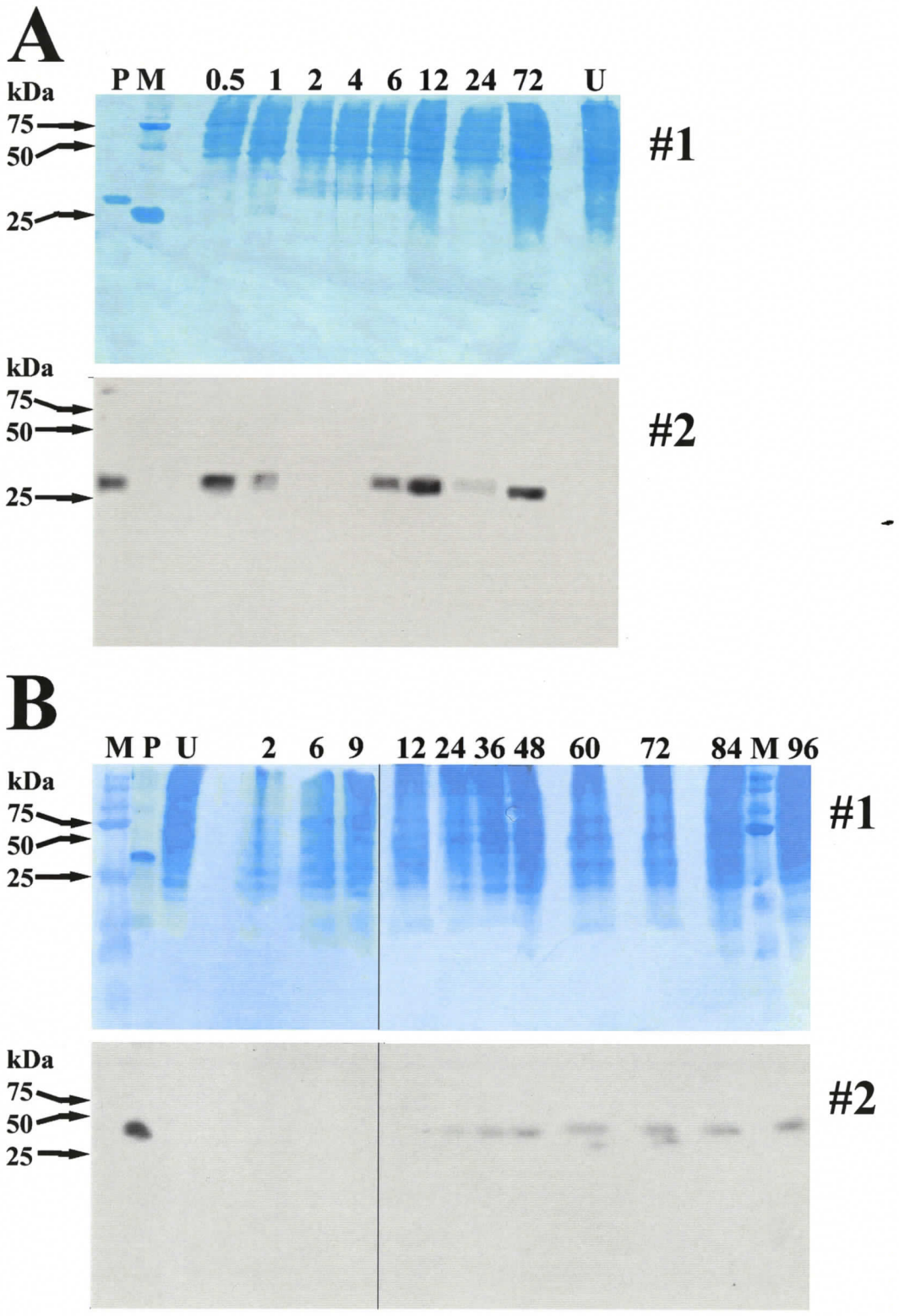
A
P M 0.5 1 2 4 6 12 24 72 U
kDa
75
50
25
#1
kDa
75
50
25
#2
B
M P U 2 6 9 12 24 36 48 60 72 84 M 96
kDa
75
50
25
#1
kDa
75
50
25
#2

Figure 6-4. Western blot analysis of NeabNPV GP41 (A) and POLH (B) expression. Total protein (40 μg) extracted from purified polyhedra (P), uninfected *N. abietis* larvae(U) and NeabNPV-infected larvae at various times (0.5 – 96 hpi) were electrophoresed on a 12.5% acrylamide resolving gel under denaturing conditions. PVDF membranes containing transferred proteins were stained with Colloidal Coomassie Blue G-250 (first image of each plate (#**1**)). Western blot of GP41 (A) and POLH (B), probed with protein specific rabbit polyclonal antibodies (second image of each plate (#**2**)). Arrows represent 25, 50, and 75 kDa protein molecular weight standards (M).

characterization of their expression patterns allowed for a comparison of the temporal cascades exhibited observed during hymenopteran and lepidopteran NPV pathology.

While investigating the replication kinetics of NeabNPV, Duffy (2006) noted that several uncontrollable factors associated with *per os* inoculation of *N. abietis* larvae were encountered. These factors include the inability to determine the actual amount of polyhedra ingested by each larva, the number of occlusion derived virions (ODV) released from the occlusion matrix, and the number of virions that penetrated into the host midgut epithelium. Neither the total number of midgut cells within the tissue nor the amount of cells infected could be determined (Duffy, 2006). Nevertheless, ultrastructural examination of infected larvae revealed that 56% of midgut cells exhibited virogenic stroma by 5 hpi (Chapter 5). This suggests that not all cells were infected at the same time and that the number of viral copies could not be quantified on a per cell basis. The nature of the host biology also confounds the quantification of viral copy number on a per cell basis since sawflies are arrhenotokous and midgut tissues often exhibits variant ploidy (1-16N), depending on the developmental stage within an instar (Hakim *et al.*, 2001). To overcome these concerns viral copy number was changed from Duffy's definition of the number of viral DNA copies per cell, to be normalized against the host actin gene and is now defined as the number of NeabNPV genomes per copy of host actin gene. A plot of virus genome copy number versus hours post inoculation was generated and samples that deviated from the predicted replication curve were discarded as outliers (Figure 6-1) and were not used in either the transcriptional analysis or Western blot.

Based on this new definition of viral copy number, the replication kinetics of NeabNPV, determined by Duffy, shows a similar pattern of DNA synthesis as observed

from lepidopteran NPVs (Duffy, 2006). A rapid increase in the number of viral copies (Figure 6.1) between 0.5 and 4 hpi suggests increasing amounts of virion penetration and uncoating, while the slow linear increase suggests viral DNA replication, which continued to 72 hpi,and levels off. Replication of AcMNPV DNA, in the *Spodoptera frugiperda* cell line, began at 6 hpi and continued until 20 hpi at a constant rate (Rosinski *et al.*, 2002), while *S. frugiperda* NPV replication, in the same cell line, was maximal between 8 to 20 hpi (Liu & Bilimoria, 1990). The extended period of NeabNPV DNA replication likely represents the infection of midgut epithelial cells over a range of several hours since microscopic examination at late time points (72 hpi) showed that approximately half of the infected cells exhibited phenotypic traits of the same viral phase (Chapter 5).

Transcriptional analyses of early and late NeabNPV genes suggest that a cascade of gene expression occurs in a similar temporal pattern as lepidopteran NPVs. Transcripts of two putative DNA binding proteins were detected within 0.5 hpi of inoculation, suggesting that viral entry and translocation of nucleocapsids occurs very rapidly. The immediate early gene, ie-1, is expressed within 1 hpi *in vitro*, suggesting that NeabNPV may initiate transcription slightly faster than lepidopteran viruses. Transcripts of early DNA replicative genes, *dnapol*, *lef-1*, and *lef-2*, were detected within 2 hours of inoculation. The rapid increase in viral copy number, observed by Duffy (2006) between 2-4 hpi, may be an accumulation of NeabNPV DNA from ingested polyhedra and/or early replication products, synthesized after the expression of the replicative genes at 2 hpi. NeabNPV early gene expression is similar to that observed in AcMNPV infected

cells; *lef-1* and *lef-2* transcripts have been detected between 2-3 hpi (Passarelli & Miller, 1993a; Passarelli & Miller, 1993b).

Expression of AcMNPV early genes is required for transcription of late genes, such as *lef*-4 and *lef*-7, typically occurs following the expression of replicative genes and is coincident with the initiation of viral DNA replication (Durantel *et al.*, 1998; Morris *et al.*, 1994). Since *lef-4* is a component of the virus-encoded RNA polymerase and *lef-7* has been proposed as a transactivator of late genes (Durantel *et al.*, 1998; Morris *et al.*, 1994), their expression occurs at the same time as the other AcMNPV RNA polymerase subunits, LEF-8 and LEF-9 (Guarino *et al.*, 1998). It is therefore likely that transcription of NeabNPV *lef-8* and *lef-9* occurs earlier than 6 hpi, since their products are also required as part of the virally-encode RNA polymerase that transcribes late structural proteins such as GP41. Both transcriptional (Duffy, 2006) and Western blot (Figure 6-4 A) analyses detected *gp41* RNA and protein, respectively, at 6 hpi, suggesting that late gene expression coincides with the later stages of viral DNA synthesis. The rapid translation of RNA transcripts indicates that temporal regulation of gene expression is at the transcriptional level (Durantel *et al.*, 1998; Rashidan *et al.*, 2005). While GP41 was initially detected within 0.5 hpi by Western blot analysis, the first appearance of *gp41* transcripts at 6 hpi suggests that the protein detected at earlier time points originated from the inoculating ODVs and was not synthesized within the midgut tissue examined.

Transcriptional analysis of the AcMNPV *gp41* gene revealed two consensus later transcription start sites and the generation of a possible bicistronic message (Whitford & Faulkner, 1992). This message was first detected at 12 hpi by Northern-blot hybridization and continued to be translated until 36 hpi. While Northern hybridization is

a powerful technique for showing the size and quantity of transcript, the limited amount of total RNA isolated from each larval sample precluded the use of this technique.

Contrary to the results obtained by Duffy (2006), the timing of transcription of the very late transactivator, *vlf-1*, and the very late expressed *polh* genes was in accordance with those observed for lepidopteran NPVs. Weak RT-PCR amplicons were first detected for NeabNPV *vlf-1* and *polh* transcripts at 12 and 24 hpi, respectively (Figure 6.3). In AcMNPV, VLF-1 transactivates very late genes, such as *polh* and *p10*, and expression of *vlf-1* typically occurs by 12 hpi (McLachlin & Miller, 1994). Expression of NeabNPV *polh* at 24 hpi was confirmed by Western blot analysis, which detected POLH from 24 to 96 hpi. POLH, which is the major component of the viral occlusion matrix, has been detected from 12 to 96 hpi (Choi *et al.*, 1998; Chou *et al.*, 1996; Rohel & Faulkner, 1984) and during late phases of lepidopteran infection POLH can constitute up to 50% of the total protein detected. The delayed expression of the NeabNPV *polh* gene may be due to insufficient levels of the VLF-1 protein, which may need to accumulate to a threshold level before acting (Yang & Miller, 1998a, b).

To confirm the integrity of the RNA isolated from each larval sample, RT-PCR of the *28S* rRNA was performed. RNA of this gene continues to be expressed even during late phases of infection when other host transcripts are reduced (Ooi & Miller, 1988). In AcMNPV infected cells, shutdown of host protein synthesis occurs due to the reduction of host transcripts (12-18 hpi) and appears to be a prerequisite for the transition from late to very late phases. Several host-nuclear RNAs are reduced, including actin, histone, and hsp70, although the mechanism by which this reduction occurs is unknown. Ribosomal *28S* gene is an ideal candidate of host RNA transcription as actin could not be used due to

the reduction of transcript levels beyond detection at 24 hpi (Ooi & Miller, 1988). However, normalization of viral copy number for replication kinetics with *28S* would result in a biased underestimation of viral quantity since multiple ribosomal RNA (rRNA) clusters exist in *N. abietis* genome (Rousselet *et al.*, 2000). An ancient chromosome fission event during Diprioninae evolution resulted in the generation of an eighth telocentric chromosome. A break point of the fission occurred at the rRNA cluster, leading to the duplication of ribosomal DNA on the largest pseudoacrocentric and smallest telocentric chromosomes (Rousselet *et al.*, 2000).

In conclusion, replication and expression of the sawfly NPV closely resembles analogous events in the well characterized lepidopteran baculoviruses. Except for the lack of homologues of immediate early and budded virus genes in the non-lepidopteran genomes, baculoviruses appear to have conserved a complex system of gene regulation throughout their evolution. The timing of transcription at each phase corresponds to the requirements of replication kinetics and viral occlusion and is in accordance to the phenotypic cytopathology observed by microscopy (Chapter 5). Characterization of the expression of *gp41*, *vlf-1* and *polh* concludes the initial analysis by Duffy (2006) and establishes a model of gene expression in non-lepidopteran baculoviruses.

Chapter 7 Summary and Conclusions

7.1 Revisiting hymenopteran NPV Pathology

Knowledge of baculovirus pathology has increased drastically over the last 20 years due to the availability of improved molecular techniques and the ability to culture insect cells *in vitro*. *Autographa californica* nucleopolyhedrovirus has become the best characterized baculovirus, most likely due to its broad host range, and knowledge about its pathology has exceeded that of the first discovered baculovirus, *Bombyx mori* nucleopolyhedrovirus (BmMNPV) (Benz, 1986). Due to the availability of sequence data from 30 baculovirus genomes, a set of 29 genes, conserved throughout the Baculoviridae, have been defined (Duffy *et al.*, 2006; Herniou *et al.*, 2003; Herniou *et al.*, 2004). Many of these genes have been shown to be important for viral DNA replication and late gene expression (Hefferon, 2004; Todd *et al.*, 1995), while others act as virulence factors. Since baculovirus genomes have between 90 and 180 predicted open reading frames, many of the potential viral genes are not conserved and may lead to various pathologies.

A recent proposal for the revision of the baculovirus classification and nomenclature system (Jehle *et al.*, 2006) suggests that the updated taxonomy include 4 genera. This classification is based on baculovirus phylogeny that follows host origin as opposed to morphological traits. The lepidopteran NPVs, GVs, hymenopteran NPVs, and dipteran NPVs would be separated into the Alpha, Beta, Gamma and Deltabaculovirus genera, respectively (Jehle *et al.*, 2006). This classification system will likely reflect the pathology of baculoviruses more accurately with regards to tissue trophism and cytopathology.

Regardless of taxonomy, cytopathology of baculoviruses appears to be dependent on the interaction between host and virus. In chapter 2 of this dissertation, the pathology of LafiNPV-W was examined in two lepidopteran cell lines. While much of the pathogenesis was identical, key events involved in very late infection were different. LafiNPV-W infection of *Malacosoma disstria* (Md108) cells resulted in the biased production of budded virions as opposed to ODVs. Infection of *Choristoneura fumiferana* (Cf70) cells, however, led to virion occlusion that yielded infectivity similar to *in vivo* propagated polyhedra. The pathology exhibited in Md108 cells more closely resembled that of primary infection of midgut tissues, while the Cf70 pathogenesis was more characteristic of infection of secondary targets. These differences in pathology are likely host induced and indicate that caution be used when characterizing baculovirus pathology in an artificial system.

The pathology described in chapter 2, however, indicates that tissue culture systems are well suited for defining key molecular events such as DNA replication and viral gene expression. Many studies of AcMNPV gene characterization have successfully used cell lines derived from *Spodoptera frugiperda* and *Trichoplusia ni* (Guarino *et al.*, 1992; Iwahori *et al.*, 2004; Lanier & Volkman, 1998), while the use of non- and semipermissive cultures have led to the discovery of important processes, including apoptosis and global protein synthesis shutdown (Du & Thiem, 1997a; Ishikawa *et al.*, 2003; Mazzacano *et al.*, 1999; Prikhod'ko & Miller, 1999). In chapter three, the semipermissive infection of NeabNPV in Cf70 cells demonstrated that early infection processes could be detected. The block to successful NeabNPV infection resulted in aborted late gene expression. This is the first time that a non-lepidopteran NPV has been characterized in an *in vitro*

system. The partial success in transmitting the virus between cultures was likely due to the encapsulation of viral DNA, though envelopment likely did not occur, and the subsequent lysis of cells undergoing apoptosis. Release of the "nucleocapsids" into the surrounding media and passage onto fresh cells possibly permitted viral entry in a subpopulation of the culture. Future studies, using this or other *in vitro* propagation systems, may help elucidate the function of the 11 unique genes found in NeabNPV (Duffy *et al.*, 2006) and possible determine whether functional analogues of immediate early genes exist or if these genes are required in all baculovirus infections.

At present, however, the use of *in vitro* culturing for the characterization of NeabNPV infection is not possible and *in vivo* propagation is necessary. Infection of NeabNPV in midgut tissues, with subsequent microscopic (Chapter 5), transcriptional (Duffy, 2006 and Chapter 6) and replication (Duffy, 2006; Appendix 1) analyses, have shown that hymenopteran pathology occurs in a temporally regulated manner similar to lepidopteran NPVs. Powerful techniques, including RT-PCR, qPCR, immunochemistry and advanced microscopy, enabled this characterization using very small amounts of tissue. Previous studies had the afforded ability to propagate large numbers of lab-reared specimens or use a culturing system (Federici, 1997). Therefore characterization of lepidopteran NPVs, whose techniques requiring copious amounts of material, such as Northern blot analysis, were possible.

It is only through use of both *in vitro* and *in vivo* techniques that the true pathology of baculoviruses can be accurately studied. This study provides a starting model for examining hymenopteran NPV pathology and shows subtle, but potentially significant, differences between lepidopteran and hymenopteran baculoviruses. Larval mortality

from hymenopteran NPVs is generally faster than that observed in the lepidopteran counterparts, 3-5 days versus 4-9 days, respectively (Granados & Williams, 1986; Lucarotti, Personal Communication). Recombination of lepidopteran NPVs to mimic hymenopteran NPV pathology may have profound implications for biological control of pest species. Moreover, the powerful and sensitive molecular and microscopic techniques used to study NeabNPV could serve well in studying other monorganotrophic NPVs.

7.2 Implications of NeabNPV Pathogenesis on Biocontrol

Interest in the use of sawfly baculoviruses as biological control agents has been stimulated by the most recent and persistent outbreak of the Balsam Fir Sawfly in western Newfoundland. The Canadian Pest Management Regulatory Agency (PMRA) licensed the use of NeabNPV for field trials, under the name Abietiv ™. Requirements for registration of the virus as a commercial insecticide include: genetic characterization, efficacy trials, and pathological studies. This study helps to complete the third requirement of registration, while an extensive study on the efficacy of NeabNPV aerial application (Moreau *et al.*, 2005) and the sequence analysis of the viral genome (Duffy *et al.*, 2006) has completed the first two components. Several difficulties with registration were encountered due to the inability to study and propagate NeabNPV in tissue culture (Lucarotti, Personal Communication), particularly those that necessitated new techniques for an accurate characterization of pathology in host and non-target organisms. Fortunately, registration is pending within the next year and commercial production and application of the NeabNPV should soon be available to control the spreading sawfly population.

Registration of the *Neodiprion lecontei* NPV (NeleNPV) occurred before strict requirements were introduced by PMRA (Arif, Personal Communication); therefore, less information is available about this virus. The successful registration of two diprionid NPVs will hopefully facilitate the registration of other non-lepidopteran baculoviruses since this method of biological control offers great advantages over traditional chemical pesticides. Hymenopteran baculoviruses have a very narrow host range, causing fatal infection in only a few species (Federici, 1997). No evidence of productive non-arthropod infection by baculoviruses exists, making these agents of control a desirable commodity in terms of health and environmental impact. Efficacy trials have shown that very low doses of polyhedra are required to induce fatal infection (Moreau *et al.*, 2005), which improve the cost effectiveness of producing the pathogen. Finally, the nature of hymenopteran NPV pathology, including the rapid mortality of the insect and epidemic spread through sloughing of infected cells increases their value as a biocontrol agent.

Bibliography

Abraham, W. R., Strompl, C., Meyer, H., Lindholst, S., Moore, E. R., Christ, R., Vancanneyt, M., Tindall, B. J., Bennasar, A., Smit, J. & Tesar, M. (1999). Phylogeny and polyphasic taxonomy of *Caulobacter* species. Proposal of *Maricaulis* gen. nov. with *Maricaulis maris* (Poindexter) comb. nov. as the type species, and emended description of the genera *Brevundimonas* and *Caulobacter*. International Journal of Systematic Bacteriology **49 Pt 3**, 1053-1073.

Ackermann, H. W. & Smirnoff, W. A. (1983). A morphological investigation of 23 baculoviruses. Journal of Invertebrate Pathology **41**, 269-280.

Adang, M. J. & Spence, K. D. (1981). Surface morphology of peritrophic membrane formation in the cabbage looper, *Trichoplusia ni*. Cell and Tissue Research **218**, 141-147.

Afonso, C. L., Tulman, E. R., Lu, Z., Balinsky, C. A., Moser, B. A., Becnel, J. J., Rock, D. L. & Kutish, G. F. (2001). Genome sequence of a baculovirus pathogenic for *Culex nigripalpus*. Journal of Virology **75**, 11157-11165.

Ahrens, C. H. & Rohrmann, G. F. (1995). Replication of *Orgyia pseudotsugata* baculovirus DNA: lef-2 and ie-1 are essential and ie-2, p34, and Op-iap are stimulatory genes. . Virology **212**, 650-662.

Arab, A. & Caetano, F. H. (2001). Functional ultrastructure of the midgut of the fire ant *Solenopsis saevissima* Forel 1904 (Formicidae: Myrmicinae). Cytobios **105**, 45-53.

Avery, O. T., MacLeod, C. M. & McCarty, M. (1944). Studies on the chemical nature of the substance inducing transformation of pneumococcal types. Induction of transformation by a desoxyribonucleic acid fraction isolated from Pneumococcus Type III. Journal of Experimental Medicine **79**, 137-158.

Ayres, M. D., Howard, S. C., Kuzio, J., Lopez-Ferber, M. & Possee, R. D. (1994). The complete DNA sequence of *Autographa californica* nuclear polyhedrosis virus. Virology **202**, 586-605.

Battu, G. S. (1986). Occurrence and influence of two baculovirus infections on larval growth, moulting and food consumption of *Achaea janata* (Linnaeus) (Noctuidae; Lepidoptera). Annals of Biology **2**, 51-57.

Bauer, S., Tholen, A., Overmann, J. & Brune, A. (2000). Characterization of abundance and diversity of lactic acid bacteria in the hindgut of wood- and soil-feeding termites by molecular and culture-dependent techniques. Archives of Microbiology **173**, 126-137.

Benz, G. A. (1963). Arthropoden-Viren. Vierteljahrsschrift der Naturforschenden Gesellshcaft in Zürich **108**, 1-35.

Benz, G. A. (1986). Historical Perspectives. In *The biology of Baculoviruses*, pp. 1-35. Edited by R. R. Granados & B. A. Federici. Boca Raton, Florida, USA: CRC Press.

Bergold, G. H. (1947). Die Isolierung des Polyeder-Virus und die Natur der Polyeder. Zeitschrift für Naturforschung B **2b**, 122-143.

Berridge, M. J. (1970). A structural analysis of intestinal absorption. Symposium of the Royal Entomological Society of London **5**, 135–150.

Bignell, D. E. (2000). Introduction to symbiosis. In *Termites: Evolution, Sociality, Symbioses, Ecology*, pp. 209-231. Edited by T. Abe, D. E. Bignell & M. Higashi. Dordrecht, Netherlands: Kluver Academic Publishers.

Billingsley, P. F. & Lehane, M. J. (1996). Structure and ultrastructure of the insect midgut. In *Biology of the midgut*, pp. 3-30. Edited by P. F. Billingsley & M. J. Lehane. London: Chapman and Hall.

Bird, F. T. (1952). On the multiplication of an insect virus. Biochimica et biophysica acta **8**.

Bird, F. T. (1955). Virus Diseass of Sawflies. Canadian Entomologist **87**, 124-127.

Bird, F. T. & Whalen, M. M. (1954). Stages in the development of two insect viruses. Canadian Journal of Microbiology **1**, 170-174.

Blissard, G. W. (1996). Baculovirus--insect cell interactions. Cytotechnology **20**, 73-93.

Blissard, G. W., Quant-Russell, R. L., Rohrmann, G. F. & Beaudreau, G. S. (1989). Nucleotide sequence, transcriptional mapping, and temporal expression of the gene encoding p39, a major structural protein of the multicapsid nuclear polyhedrosis virus of *Orgyia pseudotsugata*. Virology **168**, 354-362.

Blissard, G. W. & Rohrmann, G. F. (1990). Baculovirus diversity and molecular biology. Annual Review of Entomology **35**, 127-155.

Blissard, G. W. & Wenz, J. R. (1992). Baculovirus gp64 envelope glycoprotein is sufficient to mediate pH-dependent membrane fusion. Journal of Virology **66**, 6829-6835.

Bonning, B. C., Hoover, K., Duffey, S. & Hammock, B. D. (1995). Production of polyhedra of the *Autographa californica* nuclear polyhedrosis virus using the Sf21 and Tn5B1-4 cell lines and comparison with host-derived polyhedra by bioassay. Journal of Invertebrate Pathology **66**, 224-230.

Bordas, M. L. (1895). Appareil glandulaire des Hyménoptères. Annales des Sciences Naturelles Zoologie et Biologie Animale **19**, 1-362.

Boursaux-Eude, C. & Gross, R. (2000). New insights into symbiotic associations between ants and bacteria. Research in Microbiology **151**, 513-519.

Boyce, F. M. & Bucher, N. L. (1996). Baculovirus-mediated gene transfer into mammalian cells. Proceedings of the National Academy of Sciences of the United States of America **93**, 2348-2352.

Brauman, A., Dore, J., Eggleton, P., Bignell, D., Breznak, J. A. & Kane, M. D. (2001). Molecular phylogenetic profiling of prokaryotic communities in guts of termites with different feeding habits. FEMS Microbiology Ecology **35**, 27-36.

Braunagel, S. C., Elton, D. M., Ma, H. & Summers, M. D. (1996). Identification and analysis of an *Autographa californica* nuclear polyhedrosis virus structural protein of the occlusion-derived virus envelope: ODV-E56. Virology **217**, 97-110.

Brenner, D. J., Muller, H. E., Steigerwalt, A. G., Whitney, A. M., O'Hara, C. M. & Kampfer, P. (1998). Two new *Rahnella* genomospecies that cannot be phenotypically differentiated from *Rahnella aquatilis*. International Journal of Systematic Bacteriology **48 Pt 1**, 141-149.

Breznak, J. A. (2000). Ecology of prokaryotic microbes in the gut of wood- and litter-feeding termites. In *Termites: Evoltion, Sociality, Symbioses, Ecology*, pp. 209-231. Edited by T. Abe, D. E. Bignell & M. Higashi. Dordrecht, Netherlands: Kluver Academic Publishers.

Breznak, J. A. & Pankratz, H. S. (1977). *In situ* morphology of the gut microbiota of wood-eating termites [*Reticulitermes flavipes* (Kollar) and *Coptotermes formosanus* (Shiraki)]. Applied and Environmental Microbiology **33**, 406-426.

Broderick, N. A., Raffa, K. F., Goodman, R. M. & Handelsman, J. (2004). Census of the bacterial community of the gypsy moth larval midgut by using culturing and culture-independent methods. Applied and Environmental Microbiology **70**, 293-300.

Brune, A. (1998). Termite guts: the world's smallest bioreactors. Trends in Biotechnology **16**, 16-21.

Brune, A. & Friedrich, M. (2000). Microecology of the termite gut: structure and function on a microscale. Current Opinion in Microbiology **3**, 263-269.

Cann, A. J. (1997). Principles of molecular virology Second Edition edn. San Diego, CA: Academic Press.

Carbonell, L. F. & Miller, L. K. (1987). Baculovirus interaction with nontarget organisms: a virus-borne reporter gene is not expressed in two mammalian cell lines. Applied and Environmental Microbiology **53**, 1412-1417.

Carroll, W. J. (1962). Some Aspects of the *Neodiprion abietis* (Harr.) complex in Newfoundland. Ph.D. Dissertation. State University College of Forestry, Syracuse University. Syracuse, NY.

Carstens, E. B., Liu, J. J. & Dominy, C. (2002). Identification and molecular characterization of the baculovirus CfMNPV early genes: ie-1, ie-2 and pe38. Virus Research **83**, 13-30.

Castro, M. E., Souza, M. L., Araujo, S. & Bilimoria, S. L. (1997). Replication of *Anticarsia gemmatalis* nuclear polyhedrosis virus in four lepidopteran cell lines. Journal of Invertebrate Pathology **69**, 40-45.

Chaeychomsri, S., Ikeda, M. & Kobayashi, M. (1995). Nucleotide sequence and transcriptional analysis of the DNA polymerase gene of *Bombyx mori* nuclear polyhedrosis virus. Virology **206**, 435-447.

Chapman, R. F. (1985). Structure of the digestive system. In *Comprehensive insect physiology, biochemistry and pharmacology*, pp. 165-211. Edited by G. A. Kerkut & L. I. Gilbert. Oxford: Pergamon Press.

Charlton, C. A. & Volkman, L. E. (1991). Sequential rearrangement and nuclear polymerization of actin in baculovirus-infected *Spodoptera frugiperda* cells. Journal of Virology **65**, 1219-1227.

Charlton, C. A. & Volkman, L. E. (1993). Penetration of *Autographa californica* nuclear polyhedrosis virus nucleocapsids into IPLB Sf 21 cells induces actin cable formation. Virology **197**, 245-254.

Choi, J. Y., Kim, Y. L. & Yang, J. M. (1998). Molecular cloning and analysis of transcription initiation in the *Anaographa falcifera* multiple nucleocapsid polyhedrosis virus polyhedrin gene. Molecules and Cells **8**, 537-543.

Chou, C. M., Huang, C. J., Lo, C. F., Kou, G. H. & Wang, C. H. (1996). Characterization of *Perina nuda* nucleopolyhedrovirus (PenuNPV) polyhedrin gene. Journal of Invertebrate Pathology **67**.

Cioffi, M. (1979). The morphology and fine structure of the larval midgut of a moth (*Manduca sexta*) in relation to active ion transport. Tissue Cell **11**, 467-479.

Croizier, G., Croizier, L., Argaud, O. & Poudevigne, D. (1994). Extension of *Autographa californica* nuclear polyhedrosis virus host range by interspecific replacement of a short DNA sequence in the p143 helicase gene. Proceedings of the National Academy of Sciences of the United States of America **91**, 48-52.

Cruden, D. L. & Markovetz, A. J. (1984). Microbial aspects of the cockroach hindgut. Archives of Microbiology **138**, 131-139.

Cunningham, J. C. (1970a). Pathogenicity tests of nuclear polyhedrosis viruses infecting the Eastern Hemlock Looper, *Lambdina fiscellaria fiscellaria* (Lepidoptera: Geometridae). Canadian Entomologist **102**, 1534-1539.

Cunningham, J. C. (1970b). Strains of nuclear polyhedrosis viruses displaying different inclusion body shapes. Journal of Invertebrate Pathology **16**, 299-330.

Cunningham, J. C. (1971). Ultrastructural study of the development of a nuclear polyhedrosis virus of the Eastern Hemlock Looper, *Lambdina fiscellaria fiscellaria*. Canadian Journal of Microbiology **17**, 69-72.

da Cruz-Landim, C. & Cavalcante, V. M. (2003). Ultrastructural and cytochemical aspects of metamorphosis in the midgut of *Apis mellifera* L. (Hymenoptera: Apidae: Apinae). Zoological Science **20**, 1099-1107.

Davies, I. (1977). The effect of diet on the ultrastructure of the mid-gut cells of *Nasonia vitripennis* (Walk.) (Insecta: Hymenoptera) at various ages. Cell and Tissue Research **184**, 529-538.

Davies, I. & King, P. E. (1977a). The effect of age on the ultrastructure of the mid-gut cells of the hymenopteran *Nasonia vitripennis* (Walk.) (Hymenoptera, Pteromalidae). Cell and Tissue Research **177**, 239-245.

Davies, I. & King, P. E. (1977b). The ultrastructure of the mid-gut cells of *Nasonia vitripennis* (Walker) (Hymenoptera, Pteromalidae). Cell and Tissue Research **177**, 227-238.

Derksen, A. C. G. & Granados, R. R. (1988). Alteration of a lepidopteran peritrophic membrane by baculoviruses and enhancement of viral infectivity. Virology **167**, 242-250.

Dillon, R. & Charnley, K. (2002). Mutualism between the desert locust *Schistocerca gregaria* and its gut microbiota. Research in Microbiology **153**, 503-509.

Dillon, R. J. & Dillon, V. M. (2003). The gut bacteria of insects: nonpathogenic interactions. Annual Review of Entomology **49**, 71-92.

Dimitriadis, V. K. & Papamanoli, E. (1992). Functional morphology of the crop of *Drosophila auraria*. Cytobios **69**, 143-152.

Dockray, G. J. (1988). Comparative biochemistry and physiology of gut hormones. Annual Review of Physiology **41**, 83-95.

Dreschers, S., Roncarati, R. & Knebel-Morsdorf, D. (2001). Actin rearrangement-inducing factor of baculoviruses is tyrosine phosphorylated and colocalizes to F-actin at the plasma membrane. Journal of Virology **75**, 3771-3778.

Du, X. & Thiem, S. M. (1997a). Characterization of host range factor 1 (hrf-1) expression in *Lymantria dispar* M nucleopolyhedrovirus- and recombinant *Autographa californica* M nucleopolyhedrovirus-infected IPLB-Ld652Y cells. Virology **227**, 420-430.

Du, X. & Thiem, S. M. (1997b). Responses of insect cells to baculovirus infection: protein synthesis shutdown and apoptosis. Journal of Virology **71**, 7866-7872.

Dubreuil, R. R. (2004). Copper cells and stomach acid secretion in the *Drosophila* midgut. International Journal of Biochemistry and Cell Biology **36**, 745-752.

Duffy, S. (2006). Genomics and transcriptional analysis of the *Neodiprion abietis* nucleopolyhedrovirus. Ph.D. Dissertation. Department of Biology, University of Victoria. Victoria, British Columbia, Canada.

Duffy, S. P., Young, A. M., Morin, B., Lucarotti, C. J., Koop, B. F. & Levin, D. B. (2006). Sequence Analysis and Organization of the *Neodiprion abietis* Nucleopolyhedrovirus Genome. Journal of Virology **80**, 6952-6963.

Durantel, D., Croizier, G., Ravallec, M. & Lopez-Ferber, M. (1998). Temporal expression of the AcMNPV lef-4 gene and subcellular localization of the protein. Virology **241**, 276-284.

Eason, J. E., Hice, R. H., Johnson, J. J. & Federici, B. A. (1998). Effects of substituting granulin or a granulin-polyhedrin chimera for polyhedrin on virion occlusion and polyhedral morphology in *Autographa californica* multinucleocapsid nuclear polyhedrosis virus. Journal of Virology **72**, 6237-6243.

Egert, M., Stingl, U., Bruun, L. D., Pommerenke, B., Brune, A. & Friedrich, M. W. (2005). Structure and topology of microbial communities in the major gut compartments of *Melolontha melolontha* larvae (Coleoptera: Scarabaeidae). Applied and Environmental Microbiology **71**, 4556-4566.

Erickson, R. D. (1984). Western hemlock looper. pp. 1-4. Victoria, British Columbia: Pacific Forestry Research Centre.

Escasa, S. R., Lauzon, H. A., Mathur, A. C., Krell, P. J. & Arif, B. M. (2006). Sequence analysis of the *Choristoneura occidentalis* granulovirus genome. Journal of General Virology **87**, 1917-1933.

Federici, B. A. (1997). Baculovirus Pathogenesis. In *The Baculoviruses*, pp. 33-60. Edited by L. K. Miller. New York: Plenum Press.

Flipsen, J. T., Martens, J. W., van Oers, M. M., Vlak, J. M. & van Lent, J. W. (1995). Passage of *Autographa californica* nuclear polyhedrosis virus through the midgut epithelium of *Spodoptera exigua* larvae. Virology **208**, 328-335.

Flower, N. E. & Filshie, B. K. (1976). Goblet cell membrane differentiations in the midgut of a lepidopteran larva. Journal of Cell Science **20**, 357-375.

Frederick, B. A. & Caesar, A. J. (2000). Analysis of Bacterial Communities Associated with Insect Biological Control Agents using Molecular Techniques. Proceedings of the 10th International Symposium on Biological Control of Weeds, 261-267.

Garcia-Maruniak, A., Maruniak, J. E., Zanotto, P. M., Doumbouya, A. E., Liu, J. C., Merritt, T. M. & Lanoie, J. S. (2004). Sequence analysis of the genome of the *Neodiprion sertifer* nucleopolyhedrovirus. Journal of Virology **78**, 7036-7051.

Gartner, L. P. (1970). Submicroscopic morphology of the adult *Drosophila* midgut. Journal of the Baltimore College of Dental Surgery **25**, 64-76.

Gartner, L. P. (1987). The fine structural morphology of the midgut of aged *Drosophila*: a morphometric analysis. Experimental Gerontology **22**, 297-304.

Gemetchu, T. (1974). The morphology and fine structure of the midgut and peritrophic membrane fo the adult female, *Phlebotomus longipes* Parrot and Martin (Diptera: Psychodidae). Annals of Tropical Medicine and Parasitology **68**, 111-124.

Gomi, S., Zhou, C. E., Yih, W., Majima, K. & Maeda, S. (1997). Deletion analysis of four of eighteen late gene expression factor gene homologues of the baculovirus, BmNPV. Virology **230**, 35-47.

Gonin, M., Quardokus, E. M., O'Donnol, D., Maddock, J. & Brun, Y. V. (2000). Regulation of stalk elongation by phosphate in *Caulobacter crescentus*. Journal of Bacteriology **182**, 337-347.

Granados, R. R. & Lawler, K. A. (1981). *In vivo* pathway of *Autographa californica* baculovirus invasion and infection. Virology **108**, 297-308.

Granados, R. R. & Williams, K. A. (1986). *In vivo* infection and replication of Baculoviruses. In *The biology of baculoviruses*, pp. 89-108. Edited by R. R. Granados & B. A. Federici. Boca Raton, Florida: CRC Press, Inc.

Granados, R. R. & Williams, K. A. (2000). In vivo infection and replication of baculoviruses. In *The biology of baculoviruses*, pp. 89-108. Edited by R. R. Granados & B. A. Federici. Boca Raton, Florida, USA: CRC Press, Inc.

Gratia, A., Brachet, J. & Jeener, R. (1945). Etude histochimique et microchimique des acides nucléiques au cours de la grasserie du ver à soie. Bulletin de l'Académie Royale de Médecine de Belgique **10**, 72-81.

Gross, C. H. & Shuman, S. (1998). RNA 5'-triphosphatase, nucleoside triphosphatase, and guanylyltransferase activities of baculovirus LEF-4 protein. Journal of Virology **72**, 10020-10028.

Guarino, L. A., Dong, W., Xu, B., Broussard, D. R., Davis, R. W. & Jarvis, D. L. (1992). Baculovirus phosphoprotein pp31 is associated with virogenic stroma. Journal of Virology **66**, 7113-7120.

Guarino, L. A., Xu, B., Jin, J. & Dong, W. (1998). A virus-encoded RNA polymerase purified from baculovirus-infected cells. Journal of Virology **72**, 7985-7991.

Gul, N., Sayar, H., Ozsay, N. & Ayvali, C. (2001). A study on endocrine cells in the midgut of *Agrotis segetum* (Denn. and Schiff.) (Lepidoptera: Noctuidae). Turkish Journal of Zoology **25**, 193-197.

Haas-Stapleton, E. J., Washburn, J. O. & Volkman, L. E. (2003). Pathogenesis of *Autographa californica* M nucleopolyhedrovirus in fifth instar *Spodoptera frugiperda*. Journal of General Virology **84**, 2033-2040.

Haas-Stapleton, E. J., Washburn, J. O. & Volkman, L. E. (2005). *Spodoptera frugiperda* resistance to oral infection by *Autographa californica* multiple nucleopolyhedrovirus linked to aberrant occlusion-derived virus binding in the midgut. Journal of General Virology **86**, 1349-1355.

Hakim, R. S., Baldwin, K. M. & Loeb., M. (2001). The role of stem cells in midgut growth and regeneration. In Vivo Cellular and Developmental Biology - Animal **37**, 338-342.

Hashidoko, Y., Itoh, E., Yokota, K., Yoshida, T. & Tahara, S. (2002). Characterization of five phyllosphere bacteria isolated from *Rosa rugosa* leaves, and their phenotypic and metabolic properties. Bioscience Biotechnology and Biochemistry **66**, 2474-2478.

Hayakawa, T., Ko, R., Okano, K., Seong, S. I., Goto, C. & Maeda, S. (1999). Sequence analysis of the *Xestia c-nigrum* granulovirus genome. Virology **262**, 277-297.

Hecker, H. (1977). Structure and function of midgut epithelial cells in culicidae mosquitoes (insecta, diptera). Cell and Tissue Research **184**, 321-341.

Hefferon, K. L. (2003). Characterization of HCF-1, a determinant of *Autographa californica* multiple nucleopolyhedrovirus host specificity. Insect Molecular Biology **12**, 651-658.

Hefferon, K. L. (2004). Baculovirus late expression factors. Journal of Molecular Microbiology and Biotechnology **7**, 89-101.

Hefferon, K. L. & Miller, L. K. (2002). Reconstructing the replication complex of AcMNPV. European Journal of Biochemistry **269**, 6233-6240.

Hennigan, B. B., Wolfersberger, M. G., Parthasarathy, R. & Harvey, W. R. (1993). Cation-dependent leucine, alanine, and phenylalanine uptake at pH 10 in brush-border membrane vesicles from larval *Manduca sexta* midgut. Biochimica et biophysica acta **1148**, 209-215.

Herniou, E. A., Luque, T., Chen, X., Vlak, J. M., Winstanley, D., Cory, J. S. & O'Reilly, D. R. (2001). Use of whole genome sequence data to infer baculovirus phylogeny. Journal of Virology **75**, 8117-8126.

Herniou, E. A., Olszewski, J. A., Cory, J. S. & O'Reilly, D. R. (2003). The genome sequence and evolution of baculoviruses. Annual Review of Entomology **48**, 211-234.

Herniou, E. A., Olszewski, J. A., O'Reilly, D. R. & Cory, J. S. (2004). Ancient coevolution of baculoviruses and their insect hosts. Journal of Virology **78**, 3244-3251.

Herrera-Alvarez, L., Fernández, I., Benito, J. & Pardos, F. (2000). Ultrastructure of the midgut and hindgut of *Derocheilocaris remanei* (Crustacea, Mystacocarida). Journal of Morphology **244**, 177-189.

Herz, A., Kleespies, R. G., Huber, J., Chen, X. & Vlak, J. M. (2003). Comparative pathogenesis of the *Helicoverpa armigera* single-nucleocapsid nucleopolyhedrovirus in noctuid hosts of different susceptibility. Journal of Invertebrate Pathology **83**, 31-36.

Hongoh, Y., Ohkuma, M. & Kudo, T. (2003). Molecular analysis of bacterial microbiota in the gut of the termite *Reticulitermes speratus* (Isoptera; Rhinotermitidae). FEMS Microbiology Ecology **44**, 231-242.

Hoopes, R. R. & Rohrmann, G. F. (1991). In vitro transcription of baculovirus immediate early genes: accurate mRNA initiation by nuclear extracts from both insect and human cells. Proceedings of the National Academy of Sciences of the United States of America **88**.

Hoy, M. A. & Jeyaprakash, A. (2005). Microbial diversity in the predatory mite *Metaseiulus occidentalis* (Acari: Phytoseiidae) and its prey, *Tetranychus urticae* (Acari: Tetranychidae). Biological Control **32**, 427-441.

Huang, J. & Levin, D. B. (2001). Expression, purification and characterization of the *Spodoptera littoralis* nucleopolyhedrovirus (SpliNPV) DNA polymerase and interaction with the SpliNPV non-hr origin of DNA replication. Journal of General Virology **82**, 1767-1776.

Huang, J., Liu, X. & Levin, D. B. (1999). Characterization of *Spodoptera littoralis* type B nucleopolyhedrovirus infection in selected insect cell lines. Archives of Virology **144**, 935-955.

Hughes, K. M. (1953). The development of an insect virus within cells of its host. Hilgardia **22**, 391.

Hung, C., Lin, T. & Lee, W. (2000). Morphology and ultrastructure of the alimentary canal of the Oriental fruit fly, *Bactrocera dorsalis* (Hendel) (Diptera: Tephritidae) (2): The structure of the midgut. Zoological Studies **39**, 387-394.

Ishikawa, H., Ikeda, M., Alves, C. A., Thiem, S. M. & Kobayashi, M. (2004). Host range factor 1 from *Lymantria dispar* Nucleopolyhedrovirus (NPV) is an essential viral factor required for productive infection of NPVs in IPLB-Ld652Y cells derived from *L. dispar*. Journal of Virology **78**, 12703-12708.

Ishikawa, H., Ikeda, M., Yanagimoto, K., Alves, C. A., Katou, Y., Lavina-Caoili, B. A. & Kobayashi, M. (2003). Induction of apoptosis in an insect cell line, IPLB-Ld652Y, infected with nucleopolyhedroviruses. Journal of General Virology **84**, 705-714.

Iwahori, S., Ikeda, M. & Kobayashi, M. (2004). Association of Sf9 cell proliferating cell nuclear antigen with the DNA replication site of *Autographa californica* multicapsid nucleopolyhedrovirus. Journal of General Virology **85(Pt) 10**, 2857-2862.

Izumi, H., Anderson, I. C., Alexander, I. J., Killham, K. & Moore, E. R. (2006). Endobacteria in some ectomycorrhiza of Scots pine (Pinus sylvestris). FEMS Microbiology Ecology **56**, 34-43.

Jehle, J. A., Blissard, G. W., Bonning, B. C., Cory, J. S., Herniou, E. A., Rohrmann, G. F., Theilmann, D. A., Thiem, S. M. & Vlak, J. M. (2006). On the classification and nomenclature of baculoviruses: A proposal for revision. Archives of Virology **151**, 1257-1266.

Kasman, L. M. & Volkman, L. E. (2000). Filamentous actin is required for lepidopteran nucleopolyhedrovirus progeny production. Journal of General Virology **81**, 1881-1888.

Katou, Y., Ikeda, M. & Kobayashi, M. (2001). Characterization of *Bombyx mori* nucleopolyhedrovirus infection of *Spodoptera frugiperda* cells. Journal of Insect Biotechnology and Sericology **70**, 137-147.

Kocan, K. M., Bezuidenhout, J. D. & Hart, A. (1987). Ultrastructural features of *Cowdria ruminantium* in midgut epithelial cells and salivary glands of nymphal *Amblyomma hebraeum*. The Onderstepoort Journal of Veterinary Research **54**, 87-92.

Koot, H. P. (1994). Western hemlock looper Victoria, BC, Canada: Canadian Forest Service, Forest Insect and Disease Survey, Pacific Forestry Centre.

Kovacs, G. R., Guarino, L. A. & Summers, M. D. (1991). Novel regulatory properties of the IE1 and IE0 transactivators encoded by the baculovirus *Autographa californica* multicapsid nuclear polyhedrosis virus. Journal of Virology **65**, 5281-5288.

Kumar, S., Tamura, K. & Nei, M. (2004). MEGA3: Integrated software for Molecular Evolutionary Genetics Analysis and sequence alignment. Briefings in Bioinformatics **5**, 150-163.

Lanier, L. M., Slack, J. M. & Volkman, L. E. (1996). Actin binding and proteolysis by the baculovirus AcMNPV: the role of virion-associated V-CATH. Virology **216**, 380-388.

Lanier, L. M. & Volkman, L. E. (1998). Actin binding and nucleation by *Autographa california* M nucleopolyhedrovirus. Virology **243**, 167-177.

Lauzon, H. A., Garcia-Maruniak, A., Zanotto, P. M., Clemente, J. C., Herniou, E. A., Lucarotti, C. J., Arif, B. M. & Maruniak, J. E. (2006). Genomic comparison of *Neodiprion sertifer* and *Neodiprion lecontei* nucleopolyhedroviruses and identification of potential hymenopteran baculovirus-specific open reading frames. Journal of General Virology **87**, 1477-1489.

Lauzon, H. A., Lucarotti, C. J., Krell, P. J., Feng, Q., Retnakaran, A. & Arif, B. M. (2004). Sequence and organization of the *Neodiprion lecontei* nucleopolyhedrovirus genome. Journal of Virology **78**, 7023-7035.

Levin, D. B., Laitinen, A. M., Clarke, T., Lucarotti, C. J., Morin, B. & Otvos, I. S. (1997). Characterization of nuclear polyhedrosis viruses from three subspecies of *Lambdina fiscellaria*. Journal of Invertebrate Pathology **69**, 125-134.

Levy, S. M., Falleiros, A. M., Gregorio, E. A., Arrebola, N. R. & Toledo, L. A. (2004). The larval midgut of *Anticarsia gemmatalis* (Hubner) (Lepidoptera: Noctuidae): light and electron microscopy studies of the epithelial cells. Brazilian Journal of Biology **64**, 633-638.

Li, H., Medina, F., Vinson, S. B. & Coates, C. J. (2005). Isolation, characterization, and molecular identification of bacteria from the red imported fire ant (*Solenopsis invicta*) midgut. Journal of Invertebrate Pathology **89**, 203-209.

Li, S. Y. (2005). Virulence of a Nucleopolyhedrovirus to *Neodiprion abietis* (Hymenoptera: Diprionidae). Journal of Economic Entomology **98**, 1870-1875.

Li, S. Y. & Otvos, I. S. (1999a). Differential mortality between male and female *Choristoneura occidentalis* (Lepidoptera: Tortricidae) larvae exposed to a baculovirus with or without optical brighteners. Canadian Entomologist **131**, 65-70.

Li, S. Y. & Otvos, I. S. (1999b). Laboratory rearing of the Eastern Hemlock Looper (Lepidoptera: Geometridae) on artifical diet and Grand Fir foliage. Journal of Entomological Society of British Columbia **96**, 25-27.

Lipovsek, S., Novak, T., Janzekovic, F., Sencic, L. & Pabst, M. A. (2004). A contribution to the functional morphology of the midgut gland in phalangiid harvestmen *Gyas annulatus* and *Gyas titanus* during their life cycle. Tissue Cell **36**, 275-282.

Liu, H. S. & Bilimoria, S. L. (1990). Infected cell specific protein and viral DNA synthesis in productive and abortive infections of *Spodoptera frugiperda* nuclear polyhedrosis virus. Archives of Virology **115**, 101-113.

Liu, J. J. & Carstens, E. B. (1995). Identification, localization, transcription, and sequence analysis of the *Choristoneura fumiferana* nuclear polyhedrosis virus DNA polymerase gene. Virology **209**, 538-549.

Lu, A. & Miller, L. K. (1995a). Differential requirements for baculovirus late expression factor genes in two cell lines. Journal of Virology **69**, 6265-6272.

Lu, A. & Miller, L. K. (1995b). The roles of eighteen baculovirus late expression factor genes in transcription and DNA replication. Journal of Virology **69**, 975-982.

Lu, A. & Miller, L. K. (1996). Species-specific effects of the hcf-1 gene on baculovirus virulence. Journal of Virology **70**, 5123-5130.

Lung, O., Westenberg, M., Vlak, J. M., Zuidema, D. & Blissard, G. W. (2002). Pseudotyping *Autographa californica* multicapsid nucleopolyhedrovirus (AcMNPV): F proteins from group II NPVs are functionally analogous to AcMNPV GP64. Journal of Virology **76**, 5729-5736.

Machesky, L. M., Insall, R. H. & Volkman, L. E. (2001). WASP homology sequences in baculoviruses. Trends in Cell Biology **11**, 286-287.

Martin, G. G. & Chiu, A. (2003). Morphology of the midgut trunk in the penaeid shrimp, *Sicyonia ingentis*, highlighting novel nuclear pore particles and fixed hemocytes. Journal of Morphology **258**, 239-248.

Maruniak, J. E., Brown, S. E. & Knudson, D. L. (1984). Physical maps of SfMNPV baculovirus DNA and its genomic variants. Virology **136**, 221-234.

Maxwell, D. E. (1955). The comparative internal larval anatomy of sawflies (Hymenoptera:Symphyta). Canadian Entomologist **87**, 1-132.

Mazzacano, C. A., Du, X. & Thiem, S. M. (1999). Global protein synthesis shutdown in *Autographa californica* nucleopolyhedrovirus-infected Ld652Y cells is rescued by tRNA from uninfected cells. Virology **260**, 222-231.

McClintock, J. T., Dougherty, E. M. & Weiner, R. M. (1986). Semipermissive Replication of a Nuclear Polyhedrosis Virus of *Autographa californica* in a Gypsy Moth Cell Line. Journal of Virology **57**, 197-204.

McClintock, J. T., Guzo, D., Guthrie, K. P. & Dougherty, E. M. (1991). DNA-binding proteins of baculovirus-infected cells during permissive and semipermissive replication. Virus Research **20**, 133-145.

McIntosh, A. H. & Ignoffo, C. M. (1986). Restriction endonuclease cleavage patterns of commercial and serially passaged isolates of *Heliothis* baculovirus. Intervirology **25**, 172-176.

McLachlin, J. R. & Miller, L. K. (1994). Identification and characterization of vlf-1, a baculovirus gene involved in very late gene expression. Journal of Virology **68**, 7746-7756.

Mikhailov, V. S. & Rohrmann, G. F. (2002). Binding of the baculovirus very late expression factor 1 (VLF-1) to different DNA structures. BMC Molecular Biology **3**, 14.

Miller, H. K. & Fisk, F. W. (1971). Taxonomic implication of the camparative morphology of cockroach preventriculi. Annals of the Entomological Society of America **64**, 671-687.

Montasser, A. A. (2005). Gram-negative bacteria from the camel tick *Hyalomma dromedarii* (Ixodidae) and the chicken tick *Argas persicus* (Argasidae) and their antibiotic sensitivities. Journal of the Egyptian Society of Parasitology **35**, 95-106.

Moreau, G., Lucarotti, C. J., Kettela, E. G., Thurston, G. S., Holmes, S., Weaver, C., Levin, D. B. & Morin, B. (2005). Aerial application of nucleopolyhedrovirus induces decline in increasing and peaking populations of *Neodiprion abietis*. Biological Control **33**, 65-73.

Morris, O. N. (1962). Quantitative infectivity studies on the nuclear polyhedrosis virus of the Western Oak Looper, *Lambdina fiscellaria somniaria* (Hulst). Journal of Insect Pathology **4**, 207-215.

Morris, O. N. (1964). Susceptibility of *Lambdina fiscellaria somniaria* (Hulst) (Geometridae) and *Lambdina fiscellaria lugubrosa* (Hulst) (Geometridae) to viruses from several species of lepidopterous insects. Canadian Journal of Microbiology **10**, 273-280.

Morris, T. D. & Miller, L. K. (1992). Promoter influence on baculovirus-mediated gene expression in permissive and nonpermissive insect cell lines. Journal of Virology **66**, 7397-7405.

Morris, T. D. & Miller, L. K. (1993). Characterization of productive and non-productive AcMNPV infection in selected insect cell lines. Virology **197**, 339-348.

Morris, T. D., Todd, J. W., Fisher, B. & Miller, L. K. (1994). Identification of lef-7: a baculovirus gene affecting late gene expression. Virology **200**, 360-369.

Moser, B., Becnel, J., White, S., Afonso, C., Kutish, G., Shanker, S. & Almira, E. (2001). Morphological and molecular evidence that *Culex nigripalpus* baculovirus is an unusual member of the family Baculoviridae. Journal of General Virology **82**, 283-297.

Murakami, R. & Shiotsuki, Y. (2001). Ultrastructure of the hindgut of *Drosophila* larvae, with special reference to the domains identified by specific gene expression patterns. Journal of Morphology **248**, 144-150.

Nation, J. L. (2002). Digestion. In *Insect physiology and biochemistry*, pp. 27-64. Edited by J. L. Nation. Boca Raton, Florida: CRC Press LLC.

Neves, C. A., Peixoto, E. B. & Serrao, J. E. (2000). Histochemistry of the cuticle from proventriculus in stingless bee, *Melipona quadrifasciata anthidioides* (Hymenoptera, Apidae). Folia Histochemica et Cytobiologica **38**, 193-196.

Nòbel, U., Englen, B., Felske, A., Snaidr, J., Wieshber, A., Amann, R. I., Ludwig, W. & Backhaus, H. (1996). Sequence heterogeneities of genes encoding 16S rRNAs in Paenibacillus polymyxa detected by temperature gradient gel electrophoresis. Journal of Bacteriology **178**, 5636-5643.

Nobiron, I., O'Reilly, D. R. & Olszewski, J. A. (2003). *Autographa californica* nucleopolyhedrovirus infection of *Spodoptera frugiperda* cells: a global analysis of host gene regulation during infection, using a differential display approach. Journal of General Virology **84(Pt) 11**, 3029-3039.

Noirot, C. & Noirot-Timothee, C. (1969). The digestive system. In *Biology of Termites*, pp. Edited by K. Krishna & F. M. Weesner. New York: Academic Press.

O'Brien, V. (1998). Viruses and apoptosis. Journal of General Virology **79 (Pt 8)**, 1833-1845.

O'Reilly, D. R., Miller, L. K. & Luckow, V. A. (1992). Baculovirus expression vectors: A laboratory manual. New York: W. H. Freeman.

Ohkawa, T., Rowe, A. R. & Volkman, L. E. (2002). Identification of six *Autographa californica* multicapsid nucleopolyhedrovirus early genes that mediate nuclear localization of G-actin. Journal of Virology **76**, 12281-12289.

Ohkawa, T. & Volkman, L. E. (1999). Nuclear F-actin is required for AcMNPV nucleocapsid morphogenesis. Virology **264**, 1-4.

Okano, K., Mikhailov, V. S. & Maeda, S. (1999). Colocalization of baculovirus IE-1 and two DNA-binding proteins, DBP and LEF-3, to viral replication factories. Journal of Virology **73**, 110-119.

Olszewski, J. & Miller, L. K. (1997). A role for baculovirus GP41 in budded virus production. Virology **233**, 292-301.

Ooi, B. G. & Miller, L. K. (1988). Regulation of Host RNA levels during baculovirus infection. Virology **166**.

Paillot, A. (1924). Sur l'étiologie et l'épidémiologie de al grasserier due ver à soie. Comptes rendus de l'Académie des sciences **179**, 229.

Parfett, N., Otvos, I. S. & Van Sickle, A. (1995). Historical western hemlock looper outbreaks in British Columbia: input and analysis using a geographical information system. pp. 1-36. Victoria, British Columbia: Canadian Forest Service.

Passarelli, A. L. & Miller, L. K. (1993a). Identification and characterization of lef-1, a baculovirus gene involved in late and very late gene expression. Journal of Virology **67**, 3481-3488.

Passarelli, A. L. & Miller, L. K. (1993b). Three baculovirus genes involved in late and very late gene expression: ie-1, ie-n, and lef-2. Journal of Virology **67**, 2149-2158.

Pearson, G. R. & McNulty, M. S. (1979). Ultrastructural changes in small intestinal epithelium of neonatal pigs infected with pig rotavirus. Archives of Virology **59**, 127-136.

Pearson, M. N., Groten, C. & Rohrmann, G. F. (2000). Identification of the lymantria dispar nucleopolyhedrovirus envelope fusion protein provides evidence for a phylogenetic division of the Baculoviridae. Journal of Virology **74**, 6126-6131.

Pidiyar, V. J., Jangid, K., Patole, M. S. & Shouche, Y. S. (2004). Studies on cultured and uncultured microbiota of wild *Culex quinquefasciatus* mosquito midgut based on 16s ribosomal RNA gene analysis. American Journal of Tropical Medicine and Hygiene **70**, 597-603.

Prikhod'ko, E. A. & Miller, L. K. (1999). The baculovirus PE38 protein augments apoptosis induced by transactivator IE1. Journal of Virology **73**, 6691-6699.

Rapp, J. C., Wilson, J. A. & Miller, L. K. (1998). Nineteen baculovirus open reading frames, including LEF-12, support late gene expression. Journal of Virology **72**, 10197-10206.

Rashidan, K. K., Nassoury, N., Giannopoulos, P. N. & Guertin, C. (2005). Transcription, translation, and immunolocalization of ODVP-6E/ODV-E56 and p74 proteins:

two highly conserved ODV-associated envelope proteins of *Choristoneura fumiferana* Granulovirus. Journal of Biochemistry and Molecular Biology **38**, 65-70.

Reed, L. J. & Muench, H. (1938). A simple method of estimating 50 percent end-points. American Journal of Hygiene, **27:** , 493-497.

Relman, D. (1993). The identification of uncultured microbial pathogens. Journal of Infectious Diseases **168**, 1-8.

Rohel, D. Z. & Faulkner, P. (1984). Time course analysis and mapping of *Autographa californica* Nuclear Polyhedrosis Virus Transcripts. Journal of Virology **50**.

Roncarati, R. & Knebel-Morsdorf, D. (1997). Identification of the early actin-rearrangement-inducing factor gene, arif-1, from *Autographa californica* multicapsid nuclear polyhedrosis virus. Journal of Virology **71**, 7933-7941.

Rosinski, M., Reid, S. & Nielsen, L. K. (2002). Kinetics of baculovirus replication and release using real-time quantitative polymerase chain reaction. Biotechnology and Bioengineering **77**.

Roulston, A., Marcellus, R. C. & Branton, P. E. (1999). Viruses and apoptosis. Annual Review of Entomology **53**, 577-628.

Rousselet, J., Monti, L., Auger-Rozenberg, M.-A., Parker, J. S. & Lemeunier, F. (2000). Chromosome fission associated with growth of ribosomal DNA in *Neodiprion abietis* (Hymenoptera: Diprionidae). Proceedings of the Royal Society of London - B: Biological Sciences **267**, 1819-1823.

Santos, A. V., Dillon, R. J., Dillon, V. M., Reynolds, S. E. & Samuels, R. I. (2004). Ocurrence of the antibiotic producing bacterium *Burkholderia sp.* in colonies of the leaf-cutting ant *Atta sexdens rubropilosa*. FEMS Microbiology Letters **239**, 319-323.

Sauer, C., Dudaczek, D., Holldobler, B. & Gross, R. (2002). Tissue localization of the endosymbiotic bacterium "Candidatus *Blochmannia floridanus*" in adults and larvae of the carpenter ant *Camponotus floridanus*. Applied and Environmental Microbiology **68**, 4187-4193.

Schroder, D., Deppisch, H., Obermayer, M., Krohne, G., Stackebrandt, E., Holldobler, B., Goebel, W. & Gross, R. (1996). Intracellular endosymbiotic bacteria of *Camponotus species* (carpenter ants): systematics, evolution and ultrastructural characterization. Molecular Microbiology **21**, 479-489.

Sehnal, F. & Zitnan, D. (1996). Midgut endocrine cells. In *Biology of the midgut*, pp. 55-85. Edited by P. F. Billingsley & M. J. Lehane. London: Chapman and Hall.

Shannon, A. L., Attwood, G., Hopcroft, D. H. & Christeller, J. T. (2001). Characterization of lactic acid bacteria in the larval midgut of the keratinophagous lepidopteran, *Hopmannophila pseudospretella*. Letters in Applied Microbiology **32**, 36-41.

Simón, O., Williams, T., López-Ferber, M. & Caballero, P. (2004). Virus entry or the primary infection cycle are not the principal determinants of host specificity of *Spodoptera spp*. nucleopolyhedroviruses. Journal of General Virology **85(Pt) 10**, 2845-2855.

Smith, G. E. & Summers, M. D. (1978). Analysis of baculovirus genomes with restriction endonucleases. Virology **89**, 517-527.

Smith, G. E., Vlak, J. M. & Summers, M. D. (1982). *In Vitro* Translation of *Autographa californica* Nuclear Polyhedrosis Virus Early and Late mRNAs. Journal of Virology **44** 199-208.

Snodgrass, D. R., Angus, K. W. & Gray, E. W. (1977). Rotavirus infection in lambs: pathologenesis and pathology. Archives of Virology **55**, 263-274.

Sohi, S. S. & Cunningham, J. C. (1972). Replication of a nuclear polyhedrosis virus in serially transferred insect hemocyte cultures. Journal of Invertebrate Pathology **19**, 51-61.

Sproer, C., Mendrock, U., Swiderski, J., Lang, E. & Stackebrandt, E. (1999). The phylogenetic position of *Serratia*, *Buttiauxella* and some other genera of the family Enterobacteriaceae. International Journal of Systematic Bacteriology **49 Pt 4**, 1433-1438.

Sriram, S. & Gopinathan, K. P. (1998). The potential role of a late gene expression factor, lef2, from *Bombyx mori* nuclear polyhedrosis virus in very late gene transcription and DNA replication. Virology **251** 108-122.

Struble, G. R. (1957). Biology and control of the white-fir sawfly. Forest Science **3**, 306-313.

Summers, M. D. (1971). Electron microscopic observations on granulosis virus entry, uncoating and replication processes during infection of the midgut cells of *Trichoplusia ni*. Journal of Ultrastructure Research **35**, 606-625.

Takahashi, Y., Uno, T., Furuki, J., Yamada, S. & Araki, T. (1988). The morphology of *Trichinella spiralis*: ultrastructural study of the mid- and hindgut of the muscle larvae. Parasitology Research **75**, 19-27.

Tang, Y. & Ward, R. D. (1998). Stomodaeal valve ultrastructure in the sandfly *Lutzomyia longipalpis* (Diptera: Psychodidae). Medical and Veterinary Entomology **12**, 132-135.

Terra, W. R., Ferreira, C. & Baker, J. E. (1996). Compartmentalization of digestion. In *Biology of the midgut*, pp. 206-235. Edited by M. J. Lehane & P. F. Billingsley. London: Chapman and Hall.

Thiem, S. M., Miller, L. K. & (1989). Identification, sequence, and transcriptional mapping of the major capsid protein gene of the baculovirus *Autographa californica* nuclear polyhedrosis virus. Journal of Virology **63**, 2008-2018.

Todd, J. W., Passarelli, A. L., Lu, A. & Miller, L. K. (1996). Factors regulating baculovirus late and very late gene expression in transient-expression assays. Journal of Virology **70**, 2307-2317.

Todd, J. W., Passarelli, A. L. & Miller, L. K. (1995). Eighteen baculovirus genes, including lef-11, p35, 39K, and p47, support late gene expression. Journal of Virology **69**, 968-974.

Tompkins, G. J., Vaughn, J. L., Adams, J. R. & Reichelderfer, C. F. (1981). Effects of propagating *Autographa californica* nuclear polyhedrosis virus and its *Trichoplusia ni* variant in different hosts. Environmental Entomology **10**, 801-806.

Trager, W. (1935). Cultivation Of The Virus Of Grasserie In Silkworm Tissue Cultures. Journal of Experimental Medicine **61**, 501-514.

Trinadha Babu, B., Shyamasundari, K. & Hanumantha Rao, K. (1989). Observations on the morphology and histochemistry of the midgut and hindgut of *Portunus sanguinolentus* (Herbst) (Crustaceans: Brachyura). Folia morphologica **37**, 373-381.

Trudeau, D., Washburn, J. O. & Volkman, L. E. (2001). Central role of hemocytes in *Autographa californica* M nucleopolyhedrovirus pathogenesis in *Heliothis virescens* and *Helicoverpa zea*. Journal of Virology **75**, 996-1003.

Turnquist, R. (1991). Western hemlock looper in British Columbia. Forestry Canada Pacific and Yukon Region, . pp. 91-98. Victoria: Canadian Forest Services.

Ulrich, R. G., Buthala, D. A. & Klug, M. J. (1981). Microbiota associated with the gastrointestinal tract of the Common House Cricket, *Acheta domestica*. Applied and Environmental Microbiology **41**, 246-254.

van Borm, S., Billen, J. & Boomsma, J. J. (2002a). The diversity of microorganisms associated with *Acromyrmex* leafcutter ants. BMC Evolutionary Biology **2**, 9.

van Borm, S., Buschinger, A., Boomsma, J. J. & Billen, J. (2002b). *Tetraponera* ants have gut symbionts related to nitrogen-fixing root-nodule bacteria. Proceedings of the Royal Society of London - B: Biological Sciences **269**, 2023-2027.

Villaro, A. C., Garayoa, M., Lezaun, M. J. & Sesma, P. (1999). Light and electron microscopic study of the hindgut of the ant (Formica nigricans, hymenoptera): I. Structure of the ileum. Journal of Morphology **242**, 189-204.

Volkman, L., Storm, K., Aivazachvili, V. & Oppenheimer, D. (1996). Overexpression of actin in AcMNPV-infected cells interferes with polyhedrin synthesis and polyhedra formation. Virology **225**, 369-376.

Wang, W., Davison, S. & Krell, P. J. (2004). Identification and characterization of a major early-transcribed gene of *Trichoplusia ni* single nucleocapsid nucleopolyhedrovirus using the baculovirus expression system. Virus genes **29**, 19-29.

Washburn, J. O., Kirkpatrick, B. A. & Volkman, L. E. (1995). Comparative pathogenesis of *Autographa californica* M nuclear polyhedrosis virus in larvae of *Trichoplusia ni* and *Heliothis virescens*. Virology **209**, 561-568.

Washburn, J. O., Trudeau, D., Wong, J. F. & Volkman, L. E. (2003). Early pathogenesis of *Autographa californica* multiple nucleopolyhedrovirus and *Helicoverpa zea* single nucleopolyhedrovirus in *Heliothis virescens*: a comparison of the 'M' and 'S' strategies for establishing fatal infection. Journal of General Virology **84(Pt) 2**, 343-351.

Wei, N. & Volkman, L. E. (1992). Hyperexpression of baculovirus polyhedrin and p10 is inversely correlated with actin synthesis. Virology **191**, 42-48.

Whitford, M. & Faulkner, P. (1992). Nucleotide sequence and transcriptional analysis of a gene encoding gp41, a structural glycoprotein of the baculovirus *Autographa californica* nuclear polyhedrosis virus. Journal of Virology **66**, 4763-4768.

Whitt, M. A. & Manning, J. S. (1988). A phosphorylated 34-kDa protein and a subpopulation of polyhedrin are thiol linked to the carbohydrate layer surrounding a baculovirus occlusion body. Virology **163**, 33-42.

Wigglesworth, V. B. (1972). Digestion and Nutrition. In *The principles of insect physiology*, 7th edn, pp. 476-536. London: Chapman and Hall.

Williams, G. V. & Faulkner, P. (1997). Cytological changes and viral morphogenesis during baculovirus infection. In *The Baculoviruses*, pp. 61-108. Edited by L. K. Miller. New York, NY: Plenum Press.

Wilson, M. E. & Miller, L. K. (1986). Changes in the nucleoprotein complexes of a baculovirus DNA during infection. Virology **151**, 315-328.

Wilson, M. E. & Price, K. H. (1988). Association of *Autographa californica* nuclear polyhedrosis virus (AcMNPV) with the nuclear matrix. Virology **167**, 233-241.

Yang, S. & Miller, L. K. (1998a). Control of baculovirus polyhedrin gene expression by very late factor 1. Virology **248**, 131-138.

Yang, S. & Miller, L. K. (1998b). Expression and mutational analysis of the baculovirus very late factor 1 (vlf-1) gene. Virology **245**, 99-109.

Yang, S. & Miller, L. K. (1999). Activation of baculovirus very late promoters by interaction with very late factor 1. Journal of Virology **73**, 3404-3409.

Young, A. M. (2002). Molecular characterization of the *Neodiprion abietis* nucleopolyhedrovirus M.Sc. Thesis. Department of Biology, University of Victoria. Victoria, British Columbia, Canada.